THE
PHYSICAL REVIEW

A journal of experimental and theoretical physics established by E. L. Nichols in 1893

SECOND SERIES, VOL. 80, NO. 1 OCTOBER 1, 1950

The Molecular Spectrum of He^3

G. H. DIEKE
The Johns Hopkins University, Baltimore, Maryland*

AND

EUGENE SANT ROBINSON
Los Alamos Scientific Laboratory, Los Alamos, New Mexico

(Received May 29, 1950)

The band spectrum of the molecule $(He^3)_2$ has been studied in the region from 3000A to longer wavelengths. The present paper treats the band system $3p^3\Sigma \rightarrow 2s^3\Sigma$. The rotational and vibrational molecular constants have been determined.

I. INTRODUCTION

IT is well known that excited helium atoms form a diatomic molecule emitting a well-developed band spectrum which lies chiefly in the visible and the neighboring parts of the ultraviolet and infra-red.[1] It formed the subject of a large number of investigations and its structure is fairly well known. Nevertheless it presents still a number of problems which can be studied with improved facilities now that the lighter isotope He^3 is available for spectroscopic studies.

The structure of the band spectrum of helium is in many ways analogous to that of the spectrum of the hydrogen molecule. Its regularities are, however, much more easily unraveled and may thus often serve as a guide for the much more difficult study of the molecular spectrum of hydrogen. This parallelism is much more direct now that the two isobaric molecules, He_2^3 and $H_2^3(T_2)$ may be compared. A study of the band spectrum of He^3 seemed, therefore, highly desirable. Such a study would give as one immediate result a reliable determination of the nuclear spin of He^3.

II. EXPERIMENTAL PROCEDURE

A Pyrex tube of conventional design with aluminum electrodes and a capillary of 8 mm outer diameter was filled at Los Alamos to a pressure of 25 mm with He^3 obtained from the decay of tritium. The tube was intended for end-on observation. It is usually stated that the He_2 spectrum appears best in a wide tube with a mildly condensed discharge when the helium is very pure. We found no difficulty in obtaining it with great intensity in the capillary by excitation with an ordinary neon sign transformer with currents of about 20 to 200 ma. The appearance of the He_2 spectrum in such discharges has been reported previously.[2] It was found that even with a fair amount of impurities the principal He_2 bands appear with considerable strength. In the first tube filled with He^3 we did not succeed in eliminating traces of argon, nitrogen, oxygen, carbon, and hydrogen. In the beginning the bands caused by such molecules as N_2^+, CH, and CO obliterated the He_2 bands completely. After running the tube for some time, however, the impurity gases cleaned up, and, although the atomic lines of the elements mentioned were still much in evidence, the He_2 bands were not interfered with seriously. It turned out that the gas was entirely free from any detectable traces of He^4.

A second tube was prepared with the walls and electrodes more carefully outgassed. The He^3 gas was passed into the tube through a coil immersed in liquid helium. This froze out all impurities, and none showed spectroscopically except small traces of oxygen, hydrogen, and mercury. These did not interfere appreciably with the molecular spectrum of He^3.

Between 3000 and 5000A the spectrum was photo-

* The spectroscopic work was carried out under a contract between the AEC and the Johns Hopkins University.

[1] W. E. Curtis, Proc. Roy. Soc. A89, 146 (1913); E. Goldstein, Verh. d. D. Phys. Ges. 15, 402 (1913). Many other papers particularly between 1922 and 1930.

[2] Y. Fujioka, Zeits. f. Physik 52, 657 (1928); W. F. Meggers and G. H. Dieke, Bur. Stand. J. Research 9, 121 (1932).

TABLE I.[a] The $3p^3\Pi \rightarrow 2s^3\Sigma$-system of He_2^3.

K	P branch ν	P branch I	Q branch ν	Q branch I	R branch ν	R branch I	
			0→0 band at 4650A				
0	—	—	—	—	21 518.42	134	
1	—	—	21 498.60	69.1	535.78	64.2	
2	21 458.17	78.0	496.38	318	551.72	289	
3	435.46	42.4	493.08	132	566.26	82.2	
4	411.44	171	488.70	481	579.41	262	
5	386.18	125	483.23	186	591.11	83.8	
6	359.73	214	476.66	465	601.35	229	
7	332.07	72.8	469.06	143	610.16	67.2	
8	303.32	196	460.37	396	617.52	178	
9	273.45	71.4	450.68	106	623.44	51.3	
10	242.52	161	439.91	280	627.91	119	
11	—	—[b]	428.17	71.4	630.95	64	
12	177.70	90	415.38	164	632.58	97	s
13	143.85	28.8	401.63	48.3	632.58	97	s
14	109.14	61	386.98	125	631.50	64	
15	073.64	12.8	371.38	27.2			
16	037.35	32	354.85	56.7	624.85	24.3	
17	000.37	6.1	337.48	14.4	619.56	6.4	
18	20 962.74	21.6	319.22	30.3	612.88	13.0	
19	924.46	3.8	300.11	12.3	604.93	4.1	
20	885.64	7.0	280.20	13.8	595.62	5.6	
21	846.28	2.4	259.56	4.4	585.12		
22	806.58	3.0	238.12		573.33	3.2	
23	766.47	1.9			560.38		
24	726.04	2.3			546.41		

Intensities are quantitative photoelectric measurements at a current of 117 ma through the tube, except P 12 to P 24 which are estimates from microphotometer curve.

				0→1 band near 5122A				
0	—	—		—	—	19 536.47	70	s
1	—	—		19 517.40	60	554.63	103	s y
2	19 478.45	44	s	516.83	170	s 572.04	115	x s
3	457.83	26		515.57	70	588.84	46	
4	436.97	180	s	514.15	145	605.41	102	
5	415.28	36		512.36	73	s 620.26	45	
6	393.29	85		510.24	140	634.98	98	
7	370.81	35		507.76	63	648.96	38	
8	347.98	77		505.05	120	662.22	71	
9	324.74	29	(s)	501.97	51	674.76	27	
10	301.22	70		498.66	100	686.69	58	
11	277.56	20	c	495.07	32	697.99	16	
12	253.53	41		491.24	70	708.41	26	
13	229.37	11		487.21	18	718.07	11	x s
14	205.13	24		482.98	44	727.47	21	
15	180.75	6		478.45	44	s 736.04	9	
16	156.54	23		474.00	24	744.05	14	
17				469.39	6	751.43	6	
18				464.66	17	758.36	8	
19				460.03	3	764.42	28	x y
20				455.17	6	770.58	2	x

Intensities are photographic densities multiplied by 100.

				1→0 band near 4274A				
0	—	—		—	—	23 407.89	1	
1	—	—		23 388.07	00	423.87	0	
2	23 347.66	00		384.44	4	437.82	3	
3				379.09	1	449.53	1	
4	297.48	2		371.96	5	459.29	3	
5	269.56			363.04	2			
6	239.54	3		352.38	4	472.29	3	
7	207.74	0		339.86	2	475.69	1	s
8	174.22	3		325.72	4	476.80	3	
9				309.78	2	475.69	1	s
10				292.26	3	472.84	2	
11				272.86	0			
12				251.88	3	460.31	1	
13					4			
14				204.89	1			

Intensities are eye estimates.

graphed in the second order of a 21-ft. grating Paschen spectrograph with a dispersion of about 0.6A/mm, between 5000 and 9000A in the first order of the same spectrograph (dispersion 1.2A/mm) and beyond 9000A in the first order of a 21-ft. Wadsworth mounting (dispersion 5.01A/mm). The exposure times ranged from 20 min. for the stronger bands to 48 hr. for the weaker

TABLE I.—*Continued.*

K	P branch ν	P branch I	Q branch ν	Q branch I	R branch ν	R branch I	
			1→1 band near 4670A				
0	—	—	—	—	21 425.88	7.0q	
1	—	—	21 406.75	3.6q	442.56	4.2q	
2	21 367.83	3.6q	404.66	16.3q	458.17	s	
3	345.96	2.7	401.64	s	472.01	5.6q	
4	322.84	9.9	397.33	24.9q	484.65		
5	298.51	3.4	392.07	9.3q	495.81		
6	273.05	12.6	386.08	y	505.77	16.0q	
7	246.50		378.62	9.3q	514.30		
8	218.99	s	370.37		521.41	13.6q	
9	189.91		361.10	7.9	527.11	3.2	
10	160.45		350.92	23.4	531.48	8.1	
11	129.79		339.75	4.3	534.32		y c
12	098.31	5.0	327.67	11.0			c
13	065.96	2.5	314.67	3.2	535.21		c
14	032.79	3.4	300.78	6.5	532.96	15.3	
15	20 998.91	2.1	286.09		529.34	4.0	
16	964.39	2.7	270.50	4.5	524.38	6.5q	
17	929.66		254.13				
18		2.3	236.99		510.18		
19	857.16		218.99	s			
20	820.51		199.99				

Intensities: Those marked q are quantitative photoelectric measurements on the same scale as for the 0→0 band. The rest are estimates from a microphotometer curve.

				1→2 band near 5119A				
0	—	—		—	—	19 547.42		c
1	—	—		19 529.18	3	564.91	4	
2	19 491.88	2		528.59	18	582.06	60	s
3	472.16	2		527.72	6	597.49	5	x
4	452.13		c	526.59	23	613.90	12	
5	431.61	3		525.22	9	628.97	5	
6	410.78	12		523.54	26	643.54	14	
7	389.66	6	c	521.62	10	657.20	6	x
8	368.12	17		519.52	23	670.62	12	
9	546.36	4		(517.20)	c	s 683.34	4	
10	324.60	29	s	514.71	20	c 695.34	10	
11	302.53	5		(512.19)	73	s 706.97	3	
12	279.89	8		509.22	18	c 717.90	11	s
13				506.26	3			
14	234.21	5		503.16	8			
15				500.08	5	c		
16				496.98	5			

Intensities same as for 0→1 band.

				2→2 band near 4688A				
0	—	—		—	—	21 344.05	2	
1	—	—						
2	21 288.42	1		21 323.75	3	374.96	4	
3				320.77	1	388.13	8	y
4	245.10	3		316.84	4	400.71	5	
5				311.96	2	409.47	2	
6				306.15	5	421.32	4	
7				299.45	3			
8	145.80	4		291.67	3	436.67	4	
9	118.50	0		283.06	2			
10	090.30	4		(273.50)		446.89	3	
11				263.29	2			
12	031.31	2		251.97	3	451.70	4	

Intensities are eye estimates.

[a] The letters in the column after the intensities have the following meaning: c = line confused with a neighboring one, no reliable intensity measurement possible. x = line diffuse, probably blend. y = line too strong for the classification, probably blend. s = line coincides with another classified line.

[b] Covered by the atomic line 4713A.

ones. A general continuous background particularly in the region below 5000A sets the limit for the weakest lines that can be observed. Possibly the background is due, at least partly, to traces of impurities left in the tube. An attempt will be made to remedy this with an even more carefully purified tube. Weak molecular lines in the vicinity of the greatly overexposed atomic helium lines are obscured by the irradiation and ghosts from the atomic lines.

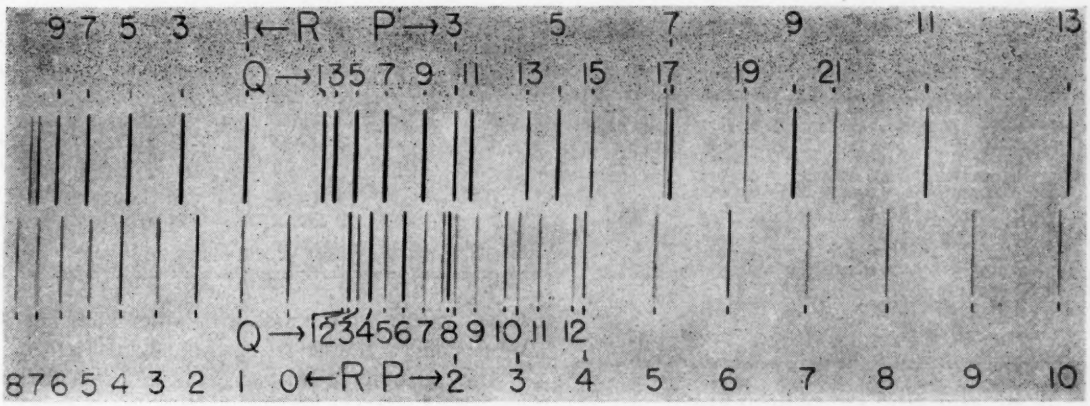

FIG. 1. The 4650 bands of He_2^4 (above) and He_2^3 (below).

The dispersion obtained for the He_2^3 bands is in general considerably better than that with which the analogous He_2^4 data in the literature[3] were obtained. Accordingly the constants for He_2^3 can be regarded as more accurate than the accepted He_2^4 constants. An increase in resolving power and dispersion is, of course, always desirable because of the higher accuracy that can be achieved. For He_2^3 this is essential in the denser parts of the spectrum because the average spacing of the lines is only two-thirds that of the He_2^4 lines.

III. RESULTS

The present paper contains one of the principal band systems, $3p^3\Sigma \rightarrow 2s^3\Sigma$, the 0→0 band of which near 4650 is possibly the strongest band in the spectrum. The analogous data for He_2^4 were given by Curtis[4] (0→0 band), Weizel and Füchtbauer[5] (0→1, 1→1 bands), and Dieke, Takamine, and Suga[6] (1→0, 1→2, 2→2 bands). Table I gives the wave numbers and intensities of the six bands comprising the system. These are exactly the same bands that are also known for He_2^4. There may be additional weak bands of this system hidden among the stronger lines which may be found when the spectrum is more completely classified.

TABLE II. The $3p^3\Pi \rightarrow 2s^3\Sigma$-system of He_2^4.

K	P branch ν	P branch I	Q branch ν	Q branch I	R branch ν	R branch I
			0→0 band near 4648A			
1	——		21 506.42	298	21 534.68	280
3	21 458.88	182	502.28	552	558.08	360
5	421.92	319	494.80	716	577.41	389
7	381.39	314	484.06	632	592.67	319
9	337.41	282	470.11	536	603.74	237
11	290.18	222	452.99	382	610.66	160
13	239.91	164	430.13	238	613.50	40
15	186.79		409.57	143	612.19	
17			383.98	84	606.94	
19					597.71	

The intensities are photoelectric measurements at a current of 84.5 ma (d.c.) through the tube.

Table II gives the 0→0 band of He_2^4 obtained under the same circumstances as the He_2^3 bands. We believe that these data are considerably more accurate than the original measurements of Curtis.[4]

The intensities listed in Table I and II are partly photoelectrically measured values obtained at a current of 110 ma through the discharge tube. These values should be quite accurate. The other intensities are estimates from microphotometer traces. No attempts were made to obtain a completely consistent intensity scale for the weaker lines. More data on the intensities will be given in a subsequent paper (see also Section V of the present paper). As a general guide it may be stated that under the conditions under which we worked the strong molecular lines are about 1000 times weaker than the strong atomic lines and that the 1→1 band is about 19 times weaker than the 0→0 band.

Figure 1 gives a reproduction of the 0→0 band taken in the second order of a 21-ft. Wadsworth mounting together with the 0→0 band of He_2^4. It shows that the qualitative differences between the two bands are as they must be expected. (1) The origin of the He_2^3 band (in the vicinity of the Q_1 line) is displaced to longer wave-lengths because of the increased zero-point vibrational energy. (2) In He_2^4 the even-numbered rotational lines are absent because of the zero nuclear spin of He^4. These lines are present in He_2^3 and actually stronger than the odd-numbered lines. This is in accordance with the fact that He^3 possesses a nuclear spin and because it has an odd number of nucleons, and, therefore, different statistics from that of He^4. (3) The spacing of the rotational lines is wider in He_2^3 because of the smaller moment of inertia.

[3] In the original work of Curtis (reference 4) only the 4650 band was obtained in the third order of a 10-ft. grating spectrograph with a dispersion of 1.7A/mm, the rest with 2.5 and 5.0A/mm, respectively. The maximum dispersion achieved for the stronger bands in the later work was 1.4A/mm [Dieke, Takamine, and Suga, (reference 6)].

[4] W. E. Curtis, Proc. Roy. Soc. **A103**, 315 (1923).

[5] W. Weizel and C. Füchtbauer, Zeits. f. Physik **44**, 431 (1927).

[6] Dieke, Takamine, and Suga, Zeits. f. Physik **49** 637 (1928).

TABLE III.

	He_2^3		He_2^4	
	$2s^3\Sigma$	$3p^3\Pi^-$	$2s^3\Sigma$	$3p^3\Pi^-$
B_0	10.046	9.495	7.587	7.170
B_1	9.678	9.151	7.351	6.889
B_2	9.289	8.798	7.096	
D_0	0.000976	0.000908	0.000547	0.000505
D_1	0.000974	0.000916	0.000567	0.000435
D_2	0.000938	0.000855	0.000552	
ω_0	1 981.99	1 890.08	1 732.8	1 652.5
ω_1	1 878.33	1 797.21	1 654.4	1 580.4
(B_e) Y_{01}	10.222	9.664	7.698	
α Y_{11}	−0.3465	−0.3346	−0.217	
Y_{21}	−0.0106	−0.0047	−0.0095	
Y_{10}	2 085.65	1 982.95	1 811.2	1 724.6
Y_{20}	51.83	46.44	39.2	36.0
ν_e	21 549.79		21 549.54	

IV. MOLECULAR CONSTANTS

The constants occurring in the rotational and vibrational energies are listed in Table III. The constants are those occurring in the expression for the vibrational and rotational energy

$$E(K, V)=\Sigma Y_{m,n}K^n(K+1)^n(V+\tfrac{1}{2})^m, \qquad (1)$$

and the usual abbreviations are used for

$$B_v=\Sigma_m Y_{m,1}(V+\tfrac{1}{2})^m, \quad D_v=\Sigma_m Y_{m,2}(V+\tfrac{1}{2})^m.$$

The rotational constants were obtained in the usual way with a least-square method from the first eight rotational differences for $2s^3\Sigma$ for which (1) can be regarded as a good enough approximation with only two terms ($n=1, 2$). The constants for $3p^3\Pi^-$ were obtained from the first eight lines of the Q branches. It is known that the rotational constants for the $3p^3\Pi^+$-levels which give rise to the P and R branches have a less simple theoretical interpretation. The band origins of He_2^3 and He_2^4 are given in Table IV.

In the calculation of the constants, care was taken that in the weaker bands lines that obviously were blends (marked z in Table I) were not used. When the frequencies of the lines or differences were recalculated with the constants so obtained, the agreement between calculated and observed values was within the limits of experimental errors in all cases. For the 0⟶0 band the maximum deviation was 0.02 cm^{-1}. For the weaker, bands where interference with other lines has a more serious effect, the deviations are slightly larger.

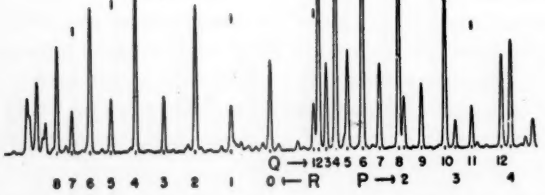

FIG. 2. Photoelectric intensity traces of the 4650 band of He_2^3. The tops of the short vertical lines indicate the intensity of the weak rotational lines multiplied by 3.

TABLE IV. Band origins.

$V'/\pm V''$	0	1	2
	He_2^3		
0	21 499.69	19 517.76	
1	23 389.83	21 407.78	19 529.45
2			21 326.66
	He_2^4		
0	21 502.26	19 773.97	
1	23 159.22	21 427.09	19 772.34
2			21 352.78

The constants of He_2^3 and He_2^4 in Table III have the numerical relations expected from the theory of band spectra of isotopic molecules. A precise comparison is not useful at this point because of the less accurate values for He_2^4 which moreover often were calculated by different methods.

V. NUCLEAR SPIN

While the work on this paper was under way a note by Douglas and Herzberg[7] appeared in which the nuclear spin of He^3 was determined as $\frac{1}{2}\hbar$. The results of this section are, therefore, a confirmation of their work. As our results were obtained from different bands by a different method they may be of interest even though the nuclear spin is already known.

The rotational lines in the band of a homonuclear diatomic molecule are alternately strong and weak. The intensities of the strong lines lie on one continuous curve, the weak ones on another one and, if I is the nuclear spin (expressed in units of $\hbar$), the ratio of the ordinates of the two curves is $(I+1)/I$. This ratio is 3:1, 2:1, 5:3, ⋯ if the nuclear spin is $\frac{1}{2}$, 1, $\frac{3}{2}$, ⋯ respectively.

Figure 2 shows a trace of the 4650A band obtained by scanning the spectrum with an electron multiplier photo-tube. The spectrograph used for this purpose was a plane grating monochromator with two off-axis parabolic mirrors of two meters focal length. Entrance and exit slits are fixed and the wave-lengths are changed by rotating the grating. The amplitudes of the traces in Fig. 2 are strictly proportional to the intensities.

The tops of the short vertical lines indicate the amplitudes of the alternate weaker band lines multiplied by a factor of three. It is evident that they lie now on a continuous curve with the strong lines which indicates that the intensity ratio is 3:1 which is characteristic for a nuclear spin $\frac{1}{2}$. It is quite evident that any of the other possible ratios (2:1, 5:3, etc.) would not have brought the two curves to coincidence.

Figure 3 shows a different representation of these data which allows a better quantitative evaluation. As the intensity of a line is

$$I_{n,m}=A_{nm}N_n,$$

[7] A. E. Douglas and G. Herzberg, Phys. Rev. **76**, 1529 (1949).

where A_{nm} is the transition probability (which contains also the factor ν^4) and N_n the number of molecules in the upper state. From this

$$\ln(I_{nm}/A_{n,m}) = \ln N_n = \text{const} - E_n/kT$$

if there is statistical equilibrium and therefore

$$N_n = N_0 e^{-E_n/kT}.$$

The $I_{n,m}$ values are measured, the $A_{n,m}$ for a $\Pi \rightarrow \Sigma$-transition are known. If, therefore, $\ln(I/A)$ is plotted against the empirically known E_n a straight line should result with slope $-1/kT$ and furthermore the points for all lines of a band, whether they be P, Q, or R lines should lie on this one straight line.

Figure 3 shows such a plot for the Q lines of the $0 \rightarrow 0$ band. The weak lines, however, were first multiplied by a factor of three. The fact that they lie then on the same curve as the strong lines shows again that the nuclear spin of He^3 is $\frac{1}{2}$.

The P and R lines have not been entered in order not to confuse the picture. They fall, however, on the same curve as the Q lines, within the limits of experimental errors.

Intensities in the corresponding He_2^4 band were published by Childs.[8] He called attention to several discrepancies between his measurements and the theory, in particular that the points for the three branches did not lie on the same curve. A part of these discrepancies arose from the fact that the proper interpretation of the structure of the bands was not known, but some remain even if Childs' data are treated according to modern views. We believe that the difficulty of obtaining reliable intensities with the photographic method of intensity measurements was responsible for this. All these difficulties disappear if the intensities are obtained photoelectrically. This was confirmed in our laboratory by Mr. Riesz, who made the corresponding measurements for the He_2^4 band.

From this one can conclude that the transition probabilities obtained from the simple theory represent the results adequately.

[8] W. H. J. Childs, Proc. Roy. Soc. A118, 296 (1928).

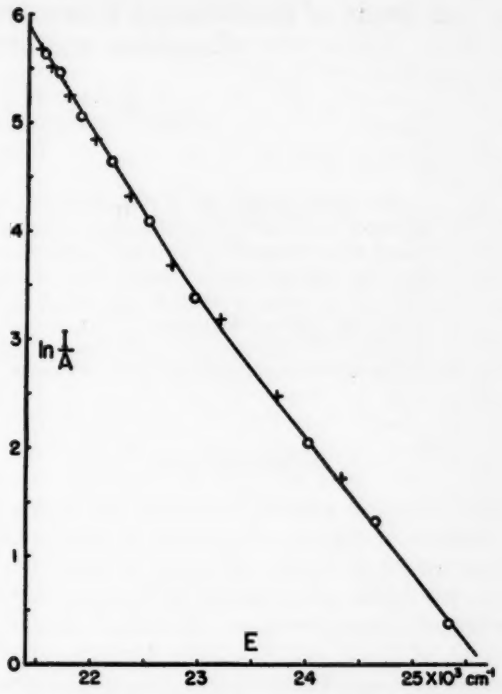

FIG. 3. $\text{Ln}I_{nm}/A_{nm}$ against E_n plot of the intensities in the Q branch of the 4650 band. Circles represent the strong lines, crosses the weak ones multiplied by 3.

Figure 3 shows that there is a slight curvature to the line representing the intensity points. This curvature is different for different currents and may represent a real deviation from thermal equilibrium. Additional measurements which are being undertaken now probably will clear up this point.

The temperatures obtained from the $\ln I/A$ plot range from 580 to 820°K for currents from 20 to 115 ma through the tube. The temperatures obtained in He^4 in a tube of similar construction under equivalent conditions also are of this order of magnitude.

The authors are glad to acknowledge the aid of Mr. F. T. Byrne who photographed the spectrum and made the intensity measurements and of Mrs. Dorothy McVay who made the wave-length measurements.

A Study of the Slowing Down Distribution of Sb^{124}-Be Photo-Neutrons in Graphite, and of the Use of Indium Foils*

L. D. Roberts, J. E. Hill, and G. McCammon
Oak Ridge National Laboratory, Oak Ridge, Tennessee

(Received May 1, 1950)

The spatial density distribution of indium resonance neutrons (1.44 ev resonance) has been measured around a point Sb^{124}—Be photo-neutron source in a graphite slowing down medium. This distribution was found to be in agreement with appropriate theory. The source energy of the photo-neutrons was calculated from the measured neutron distribution and a value of 20 ± 4 kev was obtained in fair agreement with values obtained by other methods. It was found that there is a quite appreciable capture cross section in In^{115} above the 1.44-ev resonance extending in energy to at least several kev. It is shown that this capture of neutrons with energies above 1.44 ev can introduce an error into neutron slowing down measurements which can be important under some circumstances, and it is shown how this error can be corrected.

I. INTRODUCTION

FAST neutrons, emitted from a point source in a medium of infinite extent and of atomic weight large compared with the neutron mass, slow down in such a way as to give a spatial neutron density distribution of slower neutrons (of 1.44 ev energy, for example) which is approximately gaussian. It seems that this first approximation to the spatial neutron density distribution was first used some time ago by Bethe, Korff, and Placzek[1] in their investigation into the slowing down of cosmic-ray neutrons in the atmosphere. More recently, Placzek[2] and Marshak[3] have obtained theoretically the next approximation to this neutron density distribution. Although many neutron slowing down density distribution measurements have been made, the experimental conditions in all of these have always been so complex that this theoretical treatment was not directly applicable. We have performed an experiment under such conditions that the theoretical treatment applies quite well. Our measurement served the following purposes. First, by fitting the measured neutron density distribution to Placzek's theoretical distribution a parameter was obtained from which we calculated the energy of the photo-neutrons produced by the interaction of Sb^{124} gamma-rays with Be. Second, it was possible to study the errors in the use of indium foils for epithermal neutron flux measurements. One possible error, pointed out to us by Dr. G. Goertzel, may arise as follows. From the work of Havens *et al.*[4] and Segrè[5] it is known that indium has a total cross section of the order of thirty barns extending up into the kilovolt energy region with an appreciable fraction of this due to capture. On the other hand it is usually assumed that only the 1.44-ev indium resonance contributes appreciably to the indium foil activity when the latter is used for epithermal neutron flux measurements, as in the measurement of a neutron slowing down distribution. Considering the fact that the 1.44-ev resonance will be quite strongly self-protected in a foil of usual thickness ($\sim$0.1 g/cm^2), it is clear that any part of the above 30 barns caused by capture may be relatively important in the interpretation of the foil activity as a neutron flux at resonance energy.

In the course of the following discussion we shall show that, for gaussian slowing down, and with a neutron source energy as low as ours, about 24 kev, neutron capture at energies above 1.44 ev does contribute to the indium foil activity, and if this additional activity should be interpreted as due to the 1.44-ev resonance, an appreciable error would result in the spatial neutron density distribution. Another case in which capture above 1.44 ev would be important would be that in which the neutron energy spectrum contained a high proportion of neutrons in the kilovolt energy region relative to the proportion in the 1 to 10 volt energy region. We shall not treat this case, however.

II. EXPERIMENTAL EQUIPMENT AND TECHNIQUE

(A) The Neutron Source

From the recent work of Meyerhof and Scharff-Goldhaber,[6] it is found that Sb^{124} has but one gamma-ray capable of producing photo-neutrons in beryllium, neglecting a small percentage of cross-over transitions. Wattenberg,[7] and Hanson and Hemmendinger[8] have found Sb^{124}+Be to be a very satisfactory source of photo-neutrons of about 24 kev energy. Because of the low monochromatic energy of the neutrons, which would emphasize the effect of capture in the kilovolt energy region; and because there has been some disagreement in the literature concerning the energy of Sb^{124}—Be photo-neutrons (which energy our experiment would measure) we selected this combination as our neutron source.

* This document is based on work performed for the Atomic Energy Project at Oak Ridge National Laboratory.

[1] Bethe, Korff and Placzek, Phys. Rev. **57**, 573 (1940).
[2] G. Placzek, Manhattan Project Report A-25 (unpublished).
[3] R. E. Marshak, Rev. Mod. Phys. **19**, 212–213 (1947).
[4] Havens, Wu, Rainwater, and Meaker, Phys. Rev. **71**, 165 (1947).
[5] E. Segrè, Rev. Mod. Phys. **19**, 283 (1947).
[6] W. E. Meyerhof and G. Scharff-Goldhaber, Phys. Rev. **72**, 273 (1947).
[7] A. Wattenberg, Phys. Rev. **71**, 497 (1947).
[8] A. O. Hanson and A. Hemmendinger, Phys. Rev. **75**, 1794 (1949).

The source consisted of a sphere of normal antimony about 1.59 cm in diameter and weighing 13.6 g enclosed in a spherical beryllium shell with an over-all diameter of about 2.5 cm and weighing 9.24 g. The antimony sphere was activated in the Oak Ridge National Laboratory pile.

Because of their smaller mass, beryllium atoms are more effective than are carbon atoms in slowing down neutrons. The amount of beryllium in our source, however, was too small to perturb the neutron flux distribution in the slowing down medium detectably. This was demonstrated by measuring two neutron flux distributions, one with the neutron source described above, and one with a source containing approximately 0.1 as much beryllium, i.e., (0.963 g). The ratio between the two distributions, shown in Table I, columns 4 and 5, was independent of the distance from the source, being constant to within one percent, thus demonstrating the fact that the beryllium in the neutron source did not perturb the measured neutron distribution.

(B) The "Slowing-Down" Medium

The slowing-down medium which we selected was graphite. This was used because graphite has a constant and fairly small scattering cross section from 1 ev to ~100 kev. This is illustrated by Table II. A simple average of these values gives $\bar{\sigma}_s = 4.59 \times 10^{-24}$ cm². Also, the ratio of the mass of C^{12} to the neutron mass is sufficiently large that one might expect the Placzek distribution to apply.

The graphite column in which the experiments were made had an average density of 1.652 g/cm³ and the dimensions were 6 ft.×6 ft.×11 ft. The neutron source was located at the center of this column and the neutron flux measurements were made along the central 11 ft. or principal axis. The graphite column dimensions were such that it was effectively infinite in size for our neutron source and detection energies.

(C) Neutron Flux Measurements

We were interested in measuring the isotropic component of the neutron flux at a particular resonance energy and at a number of positions along the principal axis of the graphite column. To do this, indium foils suitably protected from the thermal flux by cadmium, or from the thermal and slightly higher energy flux by B^{10} or from thermal and resonance energy flux by cadmium plus indium self-protection, were activated at the desired positions in the column for approximately eight half-lives and then counted on both sides. During the activation the foils were oriented in the plane perpendicular to the principal axis of the column. The saturated activity, i.e., the foil activity immediately after an infinite time of activation, was then calculated for each side of the foil using 54 min. as the half-life of indium and the average of these two values, $A_s(r, u)$, (Section IIIA) was obtained. It is this average saturation activity $A_s(r, u)$ which is proportional to the isotropic component of the neutron flux.[9] The foils were usually counted one or two half-lives to obtain the best possible statistics. Also, the results reported in Table III represent the average of many experiments. The counting was done on a thin-wall glass β-ray counter connected to a scale of 64.

All of the foils were 4 cm×6.35 cm in area, the indium foils being 0.094 ± 0.0005 g/cm² thick. The cadmium boxes in which the foils were encased were about 2.9 g/cm² thick. When B^{10} was used, it was in the form of a powder assaying 98 percent in boron of which 90 percent was B^{10}. The boron powder was used by packing it in a box of such design that the foil was completely enclosed with a uniform layer of boron, but of such a shape that the boron was essentially undisturbed from one experiment to another. The thickness of the boron layer was either 0.338 g/cm² or 1.334 g/cm².

We were not interested in the absolute value of the neutron flux but only in quantities proportional to this. Hence, we report simply the saturated activity of the foil $A_s(r, u)$ and not the corresponding neutron flux which produced the activity.

It should be mentioned that an experiment was made to see whether the antimony gamma-rays would activate the foils. No activity was found.

(D) Geometrical Corrections

It is an interesting fact that if the spatial distribution to be measured has a Gaussian form, a spherical shell source of finite size will appear as a point source if the detector is close to the source. Similarly, a detector of finite size will appear as a point detector. This will perhaps be made clear by the following discussion.

Consider a source which is a spherical shell of radius α with a point detector on the r axis at position r_0. Then, with τ a constant defined in Section IIIA, the flux at r_0 will be approximately proportional to the integral

$$nv(r_0, \tau) \sim 2\pi \int_0^{\tau} \sin\theta d\theta \exp(-\rho^2/4\tau). \qquad (1)$$

Substituting $\rho^2 = \alpha^2 + r_0^2 - 2r_0\alpha\cos\theta$ and integrating we find

$$nv(r_0, \tau) \sim 4\pi\alpha \left(\frac{2\tau}{\alpha r_0}\right) \sinh\left(\frac{\alpha r_0}{2\tau}\right) \exp\left[-\frac{\alpha^2 + r_0^2}{4\tau}\right]. \qquad (2)$$

TABLE I. Neutron flux distributions with different sources.

r (cm)	A_s (9.241 g source)	A_s' (0.963 g source)	$A_s' \times (17.506)$	$100(A - A_s' \times 17.506)/A_s$ percent dev.
7.78	3081	176.0	3081	——
12.86	2358	134.8	2360	+0.08
17.94	1654	94.34	1652	−0.12
23.02	1123	63.95	1120	−0.27

[9] W. Bothe, Zeits. f. Physik **120**, 437–449 (1943).

TABLE II. The scattering cross sections of graphite from 1.10 ev to 95 kev.

Energy	Scattering cross section	Reference
1.10 ev	4.45 barns	a
1.44	4.84	b
2.00	4.50	a
5.00	4.43	a
24 kev	4.6	c
35	4.63±0.19	d
95	4.65±0.14	d
	Av. 4.59 barns	

[a] Goldsmith, Ibser, and Feld, Rev. Mod. Phys. 19, 266 (1947), see Fig. 11.
[b] J. Marshall, Phys. Rev. 70, 107 (1946).
[c] Wattenberg, Fields, Russell, and Sachs, Phys. Rev. 71, 508 (1947).
[d] D. H. Frisch, Phys. Rev. 70, 589 (1946).

If $\alpha r_0/2\tau \leqslant 0.25$, $\sinh(\alpha r_0/2\tau) \cong \alpha r_0/2\tau$ to within 1 percent. Making this substitution we get

$$nv(r_0, \tau) \sim 4\pi\alpha \exp[-(\alpha^2+r_0^2)/4\tau], \qquad (3)$$

which is Gaussian in r_0. In this experiment $\tau = 147$ cm^2, $\alpha \cong 1.25$ cm, so that the maximum value of r_0 allowed by the above criterion would be $r_0(\max) = 60$ cm. Our measurements lie within this range. The proof that a detector of finite size will appear as a point detector in a Gaussian flux distribution is similar to the above. The deviation of the theoretical distribution[2,3] from a Gaussian form is small and does not need to be taken into account in the above considerations of geometry corrections. Thus, our experimental conditions correspond very closely to an ideal point geometry.

III. EXPERIMENTAL RESULTS

(A) Fit of Data to the Theoretical Distribution

In our experiment, we have measured the saturation activity of an indium foil $A_s(r, u)$ measured in β counts/min. as a function of distance r of the foil from the neutron source and corresponding to the logarithmic neutron energy u. The major part of the indium foil activity will be due to the narrow region of logarithmic energy, u, at the 1.44-ev indium resonance. This measured function, A_s, should be proportional to the theoretical slowing down density distribution and thus we write,[2,3]

$$A_s(r, u)_{(\text{measured})} = c\frac{\exp(-r^2/4\tau)}{E_d\tau^{\frac{1}{2}}}\left[1+\frac{F(r^2/\tau)}{4u}\right], \qquad (4)$$

where r is the source to foil distance in cm, c is a constant, the logarithmic energy $= u = \ln(E_s/E_d)$, E_s is the source energy in volts, E_d is the energy in volts at which the neutrons are detected, i.e., captured, and $\tau = \lambda_s^2 u/K$ where λ_s is the neutron scattering mean free path in graphite and K is a constant depending on the masses of C^{12} and of the neutron.[2,3] The coefficients in $F(r^2/\tau)$ below also depend simply on the masses of C^{12} and of the neutron.[2,3]

$$F(r^2/\tau) = 2.68599 - 1.16432(r^2/\tau) + 0.071665(r^2/\tau)^2.$$

The function $A_s(r, u)$ measured with cadmium covered indium detectors is given in Table III, column A. The graph, Fig. 1, shows a plot of these experimental points on the coordinates $\ln_{10}A_s$ *vs.* r^2 which for a

TABLE III. Neutron flux measurements.

Distance of foil from neutron source		A: Measured saturated activity of In foil covered with Cd only		B: Measured saturated activity of In foil covered with Cd and with three different thicknesses of In. Thickness in cm			C: Column A saturated activities corrected for high energy components by use of column B for the three In thicknesses in cm			D: Average of column C (corrected)	
r	r^2	$A_s(r, u)$	$\ln_{10}A_s(r, u)$	0.0127	0.0254	0.0508	0.0127	0.0254	0.0508	$A_s(r, u)$	$\ln_{10}A_s(r, u)$
3.551	12.61	3529	3.54770	1650	1308	1052	3155.3	3035.4	2972.2	3054.4	3.48493
6.091	37.10	3162	3.50001	1411	1101	839.5	2940.4	2816.7	2787.1	2848.1	3.45455
8.631	74.49	2836	3.45271	1220	935.0	679.6	2713.7	2598.05	2587.8	2633.2	3.42065
11.171	124.79	2563	3.40870			585.2			2373.5	2373.5	3.37535
13.71	187.96	2240	3.35017			486.5			2104.3	2104.3	3.32311
16.25	264.06	1906	3.28007								
18.79	353.06	1581	3.19896	630.6	440.4	316.1	1596	1558.8	1517.9	1557.6	3.19246
21.33	454.97	1276	3.10584								
23.02	529.9	1122.8	3.05030								
23.82	567.4	1051.2	3.02168			178.87			1046.8		3.01987
28.10	789.6	711.3	2.85205								
28.90	835.20	656.3	2.81713			109.85			655.8		2.81677
33.18	1100.9	410.8	2.61363								
33.98	1154.6	373.8	2.57262			57.74			379.3		2.57898
38.26	1463.8	217.0	2.33646								
39.04	1524.1	197.4	2.29542	79.85	52.97	34.54			195.4		2.29092
43.34	1878.4	113.3	2.05423								
48.42	2344.5	52.09	1.71675								
49.27	2427.5	47.67	1.67822								
53.50	2862.3	26.65	1.42570								
54.35	2953.9	21.50	1.33245								
58.58	3431.6	12.08	1.08207								
59.43	3531.9	10.17	1.00746								
63.66	4052.6	4.84	0.68485								

simple Gaussian form on these coordinates would be a straight line. The best fitting straight line, $\tau = 147$ cm², is dotted in Fig. 1, to show the departure of the experimental data from this first approximation. The deviation is about a factor of 2 at our largest value of r. The solid curve drawn through the experimental points is the best fit of the second theoretical approximation, Eq. (4), using $\tau = 147$ cm². From $r^2 = 400$ cm² to $r^2 = 4000$ cm², the fit is seen to be quite good, but between $r^2 = 0$ and $r^2 \cong 400$ cm² the experimental points fall significantly above the theoretical curve. These two regions of r will be discussed separately below.

(B) Calculation of the Energy of Sb^{124}-Be Photo-Neutrons

We have taken the value of the carbon scattering cross section in the relevant energy range as 4.59×10^{-24} cm², Table II. For our graphite density of 1.652 g/cc, this gives $\lambda_s = 2.63$ cm. Referring to the definition of τ, Eq. (4), one can then calculate the logarithmic energy u. Taking the 1.44-ev line $= E_d$ and $\tau = 147$ cm², one obtains the source energy, $E_s = 20$ kev. The probable error of τ/λ_s^2 is perhaps of the order of 2 percent. This leads to an error of about 20 percent in E_s. Within this error there is agreement with the previous result of ~24 kev found by Wattenberg, and by Hansen and Hemmendinger (see reference b, Table II). Due to self-protection the effective value of E_d is somewhat less than 1.44 ev but considering the above error it is not worthwhile to make this refinement.

(C) Activation of Indium in the Energy Range Above 1.44 ev and the Effect of This Activation on Foil Measurements

As was noted above, Eq. (4) fits the experimental data very well from $r^2 = \sim 400$ cm² to $r^2 = 4000$ cm² (Fig. 1), but, as is shown clearly upon examination of the graph, the experimental points fall far above this theoretical curve near the origin. The first point at $r^2 = 12.61$ cm² is about 16 percent higher than the theoretical value, (Eq. (4)). Since one would expect the theory to be best in the region of small r, it would seem that there must be some additional phenomenon occurring. As mentioned earlier, although beryllium has a greater slowing down effect than graphite, we were able to show that the quantity of beryllium used even if reduced by almost a factor of 10 made no measurable change in the distribution in Table III. Thus the anomaly could not be due to the neutron source.

Also, this anomalous distribution could not be due to geometrical corrections or to γ-ray activation of the indium, as was mentioned earlier.

This additional activity at small r can be understood, however, when one recalls that indium has an appreciable total cross section[4,5] up to several kev, and that an appreciable part of this is due to capture. In Section IIIB we noted that the value of $\tau = 147$ cm² was equivalent to an energy, $E_d = 1.44$ ev, at which the majority of the neutrons were captured by the foil over the distribution of A_s *vs.* r. Close to the neutron source, however, the neutron flux is especially rich in neutrons with energies in the kilovolt region, and these higher energy neutrons may be captured by the detecting foil. Now capture at energies higher than 1.44 ev will correspond to $\tau < 147$ cm² causing $\exp(-r^2/4\tau)$ to fall off faster than for the principal value of τ, 147 cm². If then a theoretical $A_s(r, u)$ be composed of two parts, a major part caused by the function (Eq. (4)) with $\tau = 147$ cm², and a second smaller part consisting of a suitable integral over this function for a spectrum of $\tau < 147$ cm², our experimental data may be fitted. The correctness of this explanation that the additional activity is due to neutron capture by the foil at energies above 1.44 ev may be demonstrated by using indium self-absorption and boron absorption experiments.

(D) Self-Absorption Experiments

These measurements were made by enclosing the detecting indium foil with the usual cadmium box and with a box made from indium in addition. Three different wall thicknesses of the indium were used in experiments with the additional indium box, 0.005 inch, 0.010 inch, and 0.020 inch. Reference to Fig. 1 shows that the measured points, cadmium covering only, fit the theoretical curve with but a single $\tau = 147$ cm² beyond $r^2 \cong 350$ cm². It is assumed then that the foil activity is essentially due to the 1.44-ev resonance at and beyond this value of r^2. Thus a self-absorption experiment made at r^2, about 353 cm², would correspond to the 1.44-ev line only. The 3.8-ev and 8.6-ev lines do not lead to the 54-min. activity.[10] On the other hand, a self-absorption measurement made at r^2 about 12 cm² would consist of two parts, the higher energy part in which the indium cross section is small compared with the 1.44-ev resonance, and for which essentially no self-absorption would occur, plus the activity of the 1.44-ev line, which would be self-absorbed in the same

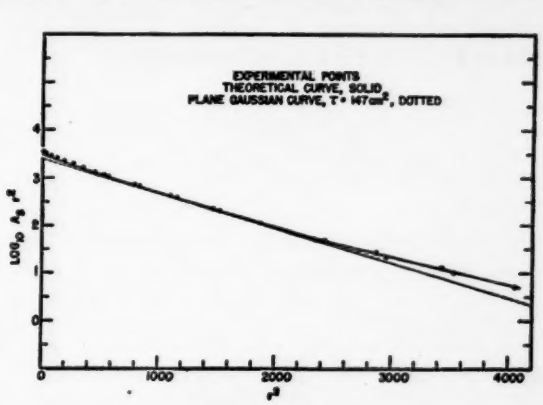

FIG. 1. Data on the neutron density distribution from a spherical shell source.

[10] M. Goldhaber (private communication).

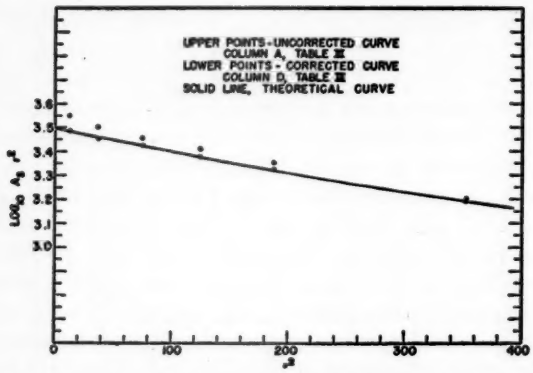

FIG. 2. Comparison of the corrected experimental values with the theoretical distribution.

way as at $r^2=353$ cm^2. Then the saturated activities for foils covered only with cadmium, are

$$A_{\text{Cd}}(12.61\text{ cm}^2)=A_s(r_1,u)+A(\text{high energy}), \quad (5)$$
(1.44 ev line)

$$A_{\text{Cd}}(353.1\text{ cm}^2)=A_s(r_2,u) \quad (6)$$
(1.44 ev line)

and the saturated activities for foils covered with both camium and indium

$$A_{\text{Cd+In}}(12.61\text{ cm}^2)=A_s(r_1,u)\cdot F+A(\text{high energy}), \quad (7)$$
(lines)

$$A_{\text{Cd+In}}(353.1\text{ cm}^2)=A_s(r_2,u)\cdot F, \quad (8)$$
(lines)

where F is the factor of self-absorption assumed independent of r of the 1.44-ev line by the indium.

By measuring A_{Cd} and $A_{\text{Cd+In}}$ in (5), (6), (7) and (8), one can solve these simultaneously and obtain F, $A_s(r,u)$, and A(high energy). We are primarily interested in calculating $A_s(r,u)$; i.e., in correcting the experimental curve for the high energy component. This has been done at ten foil positions and for three thicknesses of indium absorber. The same Cd thickness was used in all cases. Note, in column C, Table III, the good agreement for the three indium thicknesses. The agreement between the theory (Eq. (4)), and this corrected experimental A_s, column D, Table III, is shown in Fig. 2 and is seen to be very good.

TABLE IV. Boron absorption measurements.

r	0.338 g/cm^2 boron	1.334 g/cm^2 boron
3.551	309.1	191.6
6.091	169.0	98.9
8.631	100.2	59.5
11.171	66.4	35.1
13.71	27.4	14.5
16.25	20.5	8.9
18.79	13.0	

Thus, it is shown that the anomalous activity is due to a comparatively low cross section in the indium of comparatively high mean energy, and it is clear that, in some types of In foil measurements, such as ours, this additional A_s(high energy) is important and should be taken into account. On the other hand, it is seen that Eq. (4) is valid throughout the range of r over which we have measured.

(E) Boron Absorption Measurements

The above work on self-absorption gives a technique for correcting the activity of an indium foil to correspond to the 1.44-ev line, but provides little information concerning the high energy activity. In an effort to learn something of the character of this high energy indium cross section, distributions of indium foil activity *vs.* the distance r under two boron thicknesses were made (Table IV). These thicknesses of boron, 0.338 g/cm^2 and 1.334 g/cm^2, 88 percent B^{10}, were each sufficient to remove effectively the 1.44-ev line.

Interpretation of these distributions in a conclusive way turned out to be impossible since there is no theory, such as Eq. (4), applicable in the relevant detecting energy range, i.e., from perhaps 100 ev to 3 kev. However, it may be stated qualitatively that the high energy activity is not due to a single or narrow group of lines since the two boron covered distributions are not proportional to each other.

The authors are happy to acknowledge their appreciation to Dr. A. M. Weinberg and to Dr. G. Goertzel for numerous helpful theoretical discussions in connection with this experiment.

Neutron Penetration and Slowing Down at Intermediate Distances through Medium and Heavy Nuclei*

H. A. BETHE,** L. TONKS, AND H. HURWITZ, JR.
Knolls Atomic Power Laboratory, Schenectady, New York

(Received February 2, 1950)

This paper reports new theoretical results and numerical calculations of neutron slowing down and penetration to fairly large distances from the source assuming constant mean free path and no absorption. The Placzek one-velocity problem which results from a Laplace transformation of the Boltzmann equation is solved approximately by keeping only a finite number of harmonic terms in the Laplace transform of the scattering function but not restricting the expansion of the neutron density. The Laplace inversion is carried out by the method of steepest descent. Numerical results are given for nuclei of mass infinity and 9, carried out to three orders of approximation, namely zeroth, first, and second. They show the expected transition behavior between age theory and the asymptotic exponential behavior. The accuracy of the method is high, being greater than that of the numerical work over the useful range of the calculations. Rough agreement with Wick's asymptotic results for $M=12$ is found.

I. INTRODUCTION

IN many problems it is necessary to know the distribution of neutrons in a moderating material at large distances from a source. If the distance expressed in mean free paths is not small compared with $u'=(M/2)u$, where $u=\ln(E_0/E)$ the customary age theory breaks down, and improvements on this theory, such as the spherical harmonics method, are also inadequate. (In our notation E_0 is the energy of the neutrons as they are emitted from the source, E is the energy of the neutrons whose spatial distribution is to be found, and M is the mass number of the moderator. The quantity u' is a measure of the number of collisions required to reduce the neutron energy from E_0 to E.) On the other hand, "asymptotic" theories in which the neutrons are assumed to move very nearly in the forward direction are not valid until $z\gg u'^3$, which, even for moderate values of u' is far outside the practical range. It is the purpose of this paper to bridge the gap between "age theory" and the "asymptotic theory." The methods which we employ are similar to those which have been developed independently by Wick.[1] The numerical results which we shall present are for moderators of fairly large M (say $M\geqq 9$), whereas Wick and his collaborators have paid particular attention in their numerical work to the case of hydrogen ($M=1$).

We shall use the notation of Marshak[2] except where otherwise mentioned. All distances are measured in units of the mean free path, which is assumed to be independent of the velocity of the neutron. The slowing-down medium is assumed to be non-absorbing and infinite. We assume that the neutrons are emitted isotropically from a monoenergetic infinite plane source with unit strength per unit area located at the position $z=0$.

The theory we present here is a development of Placzek's "one-velocity theory" which is described by Marshak. Our formalism will give results accurate to 10 or 20 percent for *any* distance, provided only that the number of collisions u' is large. (For any practical problem with materials as heavy as Be or heavier, u' is at least about 20.) This is in contrast, for example, to the spherical harmonics method (Marshak, reference 2, p. 222), which breaks down at distances z of the order $u'^{\frac{1}{2}}$, or at attenuations of the order $\exp(-u'^{\frac{1}{2}})$ which is insufficient for many shielding problems. Placzek's extension of the spherical harmonics method (Marshak, Eq. (146a)) extends this to attenuations of the order $\exp(-u'^{\frac{1}{3}})$ which is often valuable; it represents a second approximation toward our theory.

II. TRANSPORT EQUATION. DEFINITIONS

We start from the transport equation (Marshak's Eq. (140)):

$$(1-i\nu\mu)\phi(\nu,\eta,\mu)=\int d\Omega'\phi(\nu,\eta,\mu')g(\eta,\mu_0)+1/(4\pi), \quad (1)$$

where ϕ is the Fourier-Laplace transform of the collision density (number of collisions per unit volume, unit time and unit u), that is,

$$\phi(\nu,\eta,\mu)=\int_{-\infty}^{\infty}e^{i\nu z}dz\int_0^{\infty}due^{-\eta u}\psi(z,u,\mu). \quad (2)$$

The notation is the same as Marshak's: z is the distance from the plane source in units of the mean free path,

* *Note added June 14, 1950:* This paper is based on the Atomic Energy Commission report, KAPL-256, which was declassified on January 16, 1950. Since its submission for publication it has come to the authors' attention that report A.E.R.E. T/R 523, April, 1950, of the Atomic Energy Research Establishment, Harwell, Berks., entitled "Calculation of the Functions Used for Determining Neutron Diffusion at Large Distances from the Source" by J. P. Price was issued. This report covers very much the same ground as the present paper but gives about half the number of values. It uses the fact that the function ψ can be expanded as a Taylor series in increasing powers of $1/M$, of which the first two terms are given. This is equivalent in our case to linear-in-$1/M$ interpolation between ψ_∞ and ψ_9. J. P. Price's results agree with those of the present authors when the sign of her $1/M$ term is reversed.

** Permanently at Cornell University, Ithaca, New York.

[1] G. C. Wick, Phys. Rev. 75, 738 (1949).

[2] R. E. Marshak, Rev. Mod. Phys. 19, 185 (1947).

$u=\ln(E_0/E)$, μ is the direction cosine of the motion of the neutron, y is the parameter of the Fourier transform and η is that of the Laplace transform. The function g in (1) is given by Marshak's (140b), (see also his definition of α, Eq. (17a)) *viz.*,

$$g(\eta, \mu)=\alpha F(\mu, \eta)=\int_0^\infty e^{-\eta u} f(\mu, u)du, \tag{3}$$

where $f(\mu, u)$ is the transfer function in Marshak's Eq. (7).

It is advantageous to discuss first the range of parameters η and y which will be of importance. It will be shown that by far the main contribution to the Fourier inverse of ϕ comes from the pole of ϕ, i.e. from that value of y for which the *homogeneous* Eq. (1) has a solution. This is the case for some purely imaginary value of y; we therefore set

$$iy=\nu. \tag{4}$$

Positive values of ν are relevant for positive z; ν will lie between 0 and 1, with small values of ν corresponding to age theory and ν near 1 corresponding to large attenuation.

It turns out further that the relevant values of η are of order M. It is therefore not permissible to expand in powers of η as is done in the spherical harmonics method. Instead, we expand the function g in spherical harmonics as does Wick,[4] except that our $g_l(\eta)$ are $(2l+1)$ times his. Thus

$$g(\eta, \mu)=(1/4\pi)\sum g_l(\eta)P_l(\mu). \tag{5}$$

It may be noted that the evaluation of the g_l's becomes simple if the double integration on $f(\mu, u)$ is carried out first with respect to the angular distribution before the Laplace transformation is performed.

If in Wick's equations, modified by $2l+1$, the transformation

$$\eta=\tfrac{1}{2}Mx-1 \tag{6}$$

is made for the transform parameter, and the resulting functions be denoted by $g_l(x)$, then

$$g_0(x)=\left(\frac{M+1}{M}\right)^2\frac{1-[(M-1)/(M+1)]^{Mx}}{2x}, \tag{7a}$$

$$g_1(x)=\frac{3}{2}\left(\frac{M+1}{M}\right)^2\frac{x-1+(x+1)[(M-1)/(M+1)]^{Mx}}{x^2-1/M^2}, \tag{7b}$$

$$g_2(x)=\frac{5}{2}\left(\frac{M+1}{M}\right)^2\frac{x^2-3x+3-M^{-2}-[x^2+3x+3-M^{-2}][(M-1)/(M+1)]^{Mx}}{x(x^2-4/M^2)}, \tag{7c}$$

etc.

When M is large, then putting

$$G_l(x)=[M/(M+1)]^2 g_l(x) \tag{8}$$

we find

$$G_0=(1/2x)[1-e^{-2x}], \tag{9a}$$

$$G_1=(3/2x^2)[x-1+(x+1)e^{-2x}], \tag{9b}$$

$$G_2=(5/2x^3)[3-3x+x^2-(3+3x+x^2)e^{-2x}]. \tag{9c}$$

The G_l are essentially Bessel functions[3] of ix.

For reasonable values of x (up to about unity), the G_l decrease with increasing l; for small x,

$$G_l\sim x^l/[1\cdot 3\cdot 5\cdot\cdots\cdot(2l-1)]. \tag{10}$$

Inserting (5) into (1), we get

$$(1-iy\mu)\phi(y, x, \mu)=\sum_l g_l(x)\phi_l(y, x)P_l(\mu)+1/(4\pi), \tag{11}$$

where

$$\phi_l(y, x)=\tfrac{1}{2}\int_{-1}^{1} d\mu\phi(y, x, \mu)P_l(\mu). \tag{12}$$

The relation (2) can be rewritten, introducing (6) and inverting the Fourier transformation:

$$(2/M)\int_0^\infty du'\psi(z, u', u)e^{-u'(x-2/M)} = (1/2\pi)\int_{-\infty}^{\infty} dy\phi(y, x, \mu)e^{-iyz}, \tag{13}$$

where u' is approximately the average number of collisions and is given by

$$u'=Mu/2. \tag{14}$$

It should be noted that the factor in (14) is $M/2$, not $1/\xi$, which differs from it in the relative order $1/M$.

III. SOLUTION. RELATION BETWEEN ν AND x

As previously indicated, we shall first seek a solution of the homogeneous Eq. (11), postponing consideration of the complete equation until the next section. Such a solution exists for some real value of iy. We therefore consider the equation

$$(1-\nu\mu)\phi(\nu, x, \mu)=\sum_l g_l(x)\phi_l(\nu, x)P_l(\mu) \tag{15}$$

and try to determine the eigenvalue ν, for a given x.

[3] Gegenbauer's Integral. See Watson, *Bessel Functions*, p. 50.

[4] Reference 1, Eqs. (2) to (5).

The right-hand side of (15) is a rapidly converging series in l for any reasonable value of x (let us say, not much greater than unity), because the g_l are rapidly decreasing. (At this point, our assumption differs from that of Wick,[2] who considers the case in which many g_l's are about equal in magnitude.) Therefore it is permissible to consider only a small number of l's on the right-hand side of (11). Indeed, our numerical calculations which are reported below, show that in all cases of practical importance, the eigenvalue ν is given with sufficient accuracy by taking only the terms through $l=2$. Since g_1 contains the anisotropy of scattering due to the finite mass of the target nucleus, it is understandable that in all but the $M=\infty$ case both $l=0$ and $l=1$ terms must be included even for the smallest ν. In terms of age theory the omission of $l=1$ amounts to neglecting $\langle\cos\theta\rangle_{Av}$ in the transport cross section in age theory.

The error incurred by omitting $l=2$, 3, etc. terms will be indicated in Section VII.

We have considered as of possible practical importance all elements from Be up ($M\geqslant 9$) and all values of u from 3 up so that $u'\geqslant 13$, and any attenuation up to $10^{17}\approx e^{40}$.

While the right-hand side of (11) is rapidly convergent, an expansion of ϕ itself in spherical harmonics of μ would converge exceedingly slowly. In fact, the most important dependence of ϕ on μ is given by the factor $1/(1-\nu, u)$ in which ν may be as large as 0.9 or even closer to unity (see Table III). The expansion of ϕ in spherical harmonics will therefore converge very slowly, and the spherical harmonics method as used by Marshak[2] cannot give a good approximation. In other words, φ_l does not decrease rapidly with l, but $g_l\varphi_l$ does.

With any finite number $N+1$ of terms on the right-hand side of (15), the dependence of ϕ on μ is determined:

$$\phi(\nu, x, \mu)=\sum_{l=0}^{N} g_l(x)\phi_l(\nu, x)P_l(\mu)/(1-\nu\mu). \tag{16}$$

From this we obtain

$$\phi_l(\nu, x)=\sum_{n=0}^{N} g_n(x)A_{ln}(\nu)\phi_n(\nu, x), \tag{17}$$

where

$$A_{ln}(\nu)=\tfrac{1}{2}\int_{-1}^{1}\frac{P_l(\mu)P_n(\mu)}{1-\nu\mu}d\mu. \tag{18}$$

With the abbreviation

$$f(\nu)=\frac{1}{\nu}\tanh^{-1}\nu=\frac{1}{2\nu}\ln[(1+\nu)/(1-\nu)], \tag{19}$$

the first A_{ln} are

$$\begin{aligned}
&A_{00}=f,\\
&A_{01}=(f-1)/\nu,\\
&A_{11}=(f-1)/\nu^2,\\
&A_{02}=(3/(2\nu^2))[f(1-\nu^2/3)-1],\\
&A_{12}=A_{02}/\nu,\\
&A_{22}=A_{02}[3/(2\nu^2)-\tfrac{1}{2}].
\end{aligned} \tag{20}$$

Equation (17) is the fundamental system of equations of our theory. It is a system of $N+1$ ordinary linear homogeneous equations for the $N+1$ unknowns $\phi_0, \phi_1, \cdots\phi_N$. The system is soluble only if the determinant of the coefficients vanishes, and this condition determines the eigenvalue ν for any given x. Thus, the condition is

$$\begin{vmatrix} g_0A_{00}-1 & g_1A_{01} & \cdots & g_NA_{0N}\\ g_0A_{01} & g_1A_{11}-1 & \cdots & g_NA_{1N}\\ \cdots & \cdots & \cdots & \cdots\\ g_0A_{0N} & g_1A_{1N} & \cdots & g_NA_{NN}-1 \end{vmatrix}=0. \tag{21}$$

Note that all g's are known functions of x, and the A's are known functions of ν.

In the "zero-order" approximation we have, for instance,

$$\begin{aligned}
A_{00}(\nu)\equiv f(\nu)&\equiv\frac{1}{2\nu}\ln\frac{1+\nu}{1-\nu}=\frac{1}{g_0}\\
&=\left(\frac{M}{M+1}\right)^2\frac{2x}{1-[(M-1)/(M+1)]M^x}
\end{aligned} \tag{22}$$

as in the equation succeeding Marshak's Eq. (149). From this equation it is easy to determine ν as a function of x, or, conversely, x as a function of ν.

It is not, in general, permissible to expand Eq. (21) in powers of ν or x or both. Such an expansion is unsatisfactory especially because the power series for $f(\nu)$ is very slowly convergent except for very small ν. *If* an expansion is made, and M is assumed large, equating the lowest powers of ν and x gives

$$\nu=(3x)^{\frac{1}{2}} \tag{23}$$

which corresponds to the age theory. Further results of expansion will be given at the end of Section V.

The "first-order" approximation, in which g_0 and g_1 are taken into account, gives for ν the relation

$$f(\nu)=\frac{1}{g_0}-\frac{f(\nu)-1}{\nu^2}\left(\frac{1}{g_0}-1\right)g_1. \tag{24}$$

It is convenient to determine an approximate value of ν from (22), then insert this into the right-hand side of (24), determine a more accurate value of ν, etc. Equation (24) is equivalent to the equation below (151) in Marshak's paper.

In principle, the relation between ν and x can be obtained to any desired accuracy by numerical calculation. This will be done in Sections IV and V for infinite mass of the slowing atoms and for $M=9$; the results for any "practical" value of M can then be estimated by interpolation. Once the relation $\nu(x)$ is known and tabulated, the neutron density can be obtained without difficulty, as will be shown in the following.

IV. FOURIER INVERSION

To calculate the Fourier transform (13) of ϕ for positive z, the path of integration can be deformed from the real axis into the negative imaginary plane. The function ϕ is regular in this plane except for a pole at $y=-i\nu$, corresponding to the solution of the homogeneous equation found in the last section, and a branch line extending from $-i$ to $-i\infty$ along the imaginary axis. As will be justified below (see also Marshak's remarks after Eq. (149)), the contribution of the branch line is unimportant. Therefore, the integral on the right of (13) will be $-2\pi i$ times the residue at the pole.

Thus we need the solution of the inhomogeneous Eq. (11) for $iy=\nu'$ in the neighborhood of the eigenvalue ν. We have then in the "Nth approximation"

$$\phi(\nu', x, \mu)=\sum_{l=0}^{N} g_l(x)\phi_l'\nu', x)\frac{P_l(\mu)}{1-\nu'\mu}+\frac{1}{4\pi(1-\nu'\mu)}. \quad (25)$$

Multiplying by P_l and integrating we find

$$\phi_l(\nu', x)=\sum_{n=0}^{N} g_n\phi_n A_{ln}+A_{0l}/(4\pi). \quad (26)$$

While it is possible to obtain all of the ϕ's, we are interested mostly in the total neutron intensity moving in all directions, which is given by

$$\int \phi(y, x, \mu)d\Omega=4\pi\phi_0(y, x). \quad (27)$$

The "residue" of this quantity near the pole ν can be obtained in the same numerical process as the eigenvalue ν itself, as follows:

Introducing the quantity

$$\varphi=g_0\phi_0+1/(4\pi), \quad (28)$$

and dividing Eqs. (26) for $l\neq 0$ by this quantity, one gets

$$(\phi_l/\varphi)-\sum_{n=1}^{N} g_n(x)A_{ln}(\nu')(\phi_n/\varphi)=A_{0l}(\nu'). \quad (29)$$

For any x and ν' these equations can be solved for the unknowns ϕ_l/φ for $l=1, 2, \cdots N$. The result can then be inserted into the equation for $l=0$. If this equation is also divided by φ and (26) used, we get

$$-\frac{1}{4\pi g_0\varphi}=A_{00}(\nu')+\sum_{l=1}^{N} g_l(x)A_{0l}(\nu')(\phi_l/\varphi)-1/g_0 \quad (30)$$
$$\equiv\Lambda(x, \nu').$$

Since the ϕ_l/φ can be determined as functions of x and ν' from (29), the middle member of (30) is a calculable function of x and ν' for which the abbreviation Λ is introduced. For general values of x and ν', (30) determines the remaining unknown φ. However, the *eigenvalue* ν of ν' is determined by the condition that the homogeneous equation (1) has a solution, so that φ is infinite and

$$\Lambda(x, \nu)=0. \quad (31)$$

Thus this can replace Eq. (21) in the actual calculation of $x(\nu)$.

In the process of determining x numerically from Eq. (31) one also obtains automatically the derivative

$$\lambda=-\left(\frac{\partial}{\partial x}\Lambda(x, \nu)\right) \quad (32a)$$

which will be useful in the numerical calculation. In the analysis we need

$$\Lambda'=[(\partial/\partial\nu')\Lambda(x, \nu')]_z. \quad (32b)$$

It is easily seen that Λ' and λ are positive.

For ν' near ν we find from Eqs. (28) and (30), since the last term of the former is negligible near the pole,

$$4\pi\phi_0=4\pi\varphi/g_0=-1/(g_0^2(\nu'-\nu)\Lambda') \quad (33)$$

and the Fourier inversion of (13) gives

$$L(z, x)=(2/M)\int_0^\infty du'\psi_0(z, u')e^{-u'(x-2/M)}$$
$$=1/(2\pi)\int_{-\infty}^{\infty} dy 4\pi\phi_0(y, x)e^{-iyz}=e^{-\nu z}/g_0^2\Lambda', \quad (34)$$

where ψ_0 is the total collision density integrated over all directions of neutron motion,

$$\psi_0(z, u')=\int d\Omega\psi(z, u', \mu). \quad (35)$$

The parameters ν and x in (34) are connected by the relation derived in Section III.

Equation (34) is exact (insofar as the relation between ν and x is correct) except for the neglect of the integral along the branch line from $y=-i$ to $-i\infty$. In the "zero order" approximation, this integral is given explicitly in Marshak's Eq. (149). Except for a numerical factor depending on x which is of order unity (in general smaller), this integral is proportional to e^{-z}. Its ratio to (41) is therefore,

$$\text{branch/pole}\sim e^{-z(1-\nu)}. \quad (36)$$

For moderately small ν, this is of order e^{-z}; we can therefore neglect the branch integral at distances large compared to a mean free path, which are the only ones of interest to us. As was pointed out by Marshak, the branch integral represents the direct effect of the source which is of no interest for our purposes. One might be afraid that $(1-\nu)z$ is no longer large when ν is nearly unity, which is the case for large attenuation. However, as we shall see in Section VI, $(1-\nu)z$ is in this case about $u'/4$ which we have assumed to be large. Therefore in spite of the smallness of $1-\nu$, the product $(1-\nu)z$ stays

large, and the contribution of the branch integral is always negligible.

This conclusion remains true in spite of the fact that the numerical factor of the pole contribution (especially the factor $1/\Lambda'$) is small for ν close to unity. This only gives a factor of order $1/z$, which is unimportant compared to the *exponential* factor $(\exp(-u'/4)$.

For the numerical work it is not convenient to keep x fixed and to calculate the function Λ for various values of ν', but it is preferable to calculate Λ as a function of x, for fixed ν. Equation (31) for the eigenvalue $\nu(x)$ then implies, using Eqs. (32a) and (32b), that

$$\Lambda' \equiv (\partial\Lambda/\partial\nu)_x = -(\partial\Lambda/\partial x)(dx/d\nu) \equiv \lambda dx/d\nu. \quad (37)$$

The derivative $\partial\Lambda/\partial x$ must be evaluated at the eigenvalue of x as defined by (31). The quantity λ is then a function of ν only, but through $\nu(x)$ it can also be regarded as a function of x.

Another convenient modification is the introduction of the slowing-down density,

$$q = \xi\psi_0. \quad (38)$$

Using this and (37), we get from (34)

$$L(z, x) = 2/(M\xi)\int_0^\infty du' q(z, u') e^{-u'(x-2/M)} = (d\nu/dx)(1/g_0^2\lambda)e^{-\nu z}. \quad (39)$$

The slowing-down density has the advantage that it remains finite for $M\to\infty$, whereas ψ_0 would become infinite (proportional to M). In the limit $M\to\infty$, the factor $2/(M\xi)$ in (39) tends to unity.

TABLE I. Functions of ν, Eqs. (20).

ν	$A_{00}(\nu)$	A_{01}	A_{11}	A_{02}	A_{12}	A_{22}
0	1.0000000	0	0.3333	0	0	
0.05	1.0008346	0.01669	0.3338	0.00054	0.01080	0.32373
0.10	1.003354	0.03354	0.3354	0.00140	0.01400	0.20930
0.15	1.007603	0.05069	0.3379	0.00306	0.02040	0.20247
0.20	1.013663	0.06830	0.3415	0.00554	0.02772	0.20498
0.25	1.021651	0.08660	0.3464	0.00881	0.03524	0.20704
0.30	1.031732	0.1058	0.3527	0.01300	0.04333	0.2102
0.35	1.044125	0.1261	0.3603	0.01824	0.05211	0.2142
0.40	1.0591	0.1478	0.3695	0.02452	0.06130	0.2176
0.45	1.0771	0.1713	0.3807	0.03256	0.07236	0.2249
0.50	1.0986	0.1972	0.3944	0.04230	0.08460	0.2327
0.55	1.1244	0.2260	0.4109	0.05466	0.09938	0.2437
0.575	1.1390	0.2417	0.4204	0.06113	0.10628	0.2467
0.60	1.1552	0.2587	0.4312	0.06908	0.11513	0.2533
0.625	1.1730	0.2768	0.4429	0.07784	0.12454	0.2600
0.65	1.1928	0.2966	0.4563	0.08808	0.13554	0.2687
0.675	1.2146	0.3179	0.4710	0.09919	0.14695	0.2770
0.70	1.2390	0.3414	0.4877	0.11213	0.16018	0.2872
0.725	1.2663	0.3673	0.5066	0.12705	0.17524	0.2990
0.75	1.2973	0.3964	0.5285	0.14416	0.19221	0.3124
0.775	1.3326	0.4292	0.5538	0.16433	0.21204	0.3282
0.80	1.3733	0.4666	0.5833	0.18827	0.23534	0.3471
0.825	1.4210	0.5103	0.6185	0.21732	0.26342	0.3703
0.85	1.4778	0.5621	0.6613	0.25307	0.29773	0.3989
0.875	1.5475	0.6257	0.7151	0.29891	0.34161	0.4362
0.90	1.6358	0.7064	0.7849	0.35950	0.39944	0.4860
0.925	1.7542	0.8154	0.8815	0.44509	0.48118	0.5577
0.95	1.9282	0.9771	1.0285	0.57861	0.60906	0.6724

V. LAPLACE INVERSION; MAIN FORMULA

Having calculated $L(z, x)$ in Eq. (39) we now wish to obtain its Laplace inverse $q(z, u')$.

According to the general method for this we get from (39):

$$q(z, u') = \frac{1}{2\pi i}\frac{M\xi}{2}e^{-2u'/M}\int_{-i\infty}^{+i\infty} dx L(z, x)e^{u'z} = -\frac{M\xi}{2}e^{-2u'/M}\frac{1}{2\pi i}\int_{-i\infty}^{+i\infty}\frac{d\nu}{dx}\frac{1}{g_0^2\lambda}e^{-\nu z+u'z}dx. \quad (40)$$

In this expression, ν, g_0, and λ should, at this point, be regarded as functions of x, determined by the theory of the preceding sections. Equation (40) is exact except for the neglect of the branch-line integral [see Eq. (36)].

To evaluate (40) we remember that we are interested only in large values of u' and/or z. In this case, the exponential varies far more rapidly with x than do any of the other factors. The exponential has a saddle point at a certain value of x determined by the condition

$$z(d\nu/dx)_{x_0} = u'. \quad (41)$$

Since ν is a given function of x, this determines x_0 (or ν_0,

TABLE II. Functions of x for $M=\infty$, Eqs. (9).

x	$G_0^{-1}(x)$	$G_1(x)$	$G_2(x)$
0	1.000000	0	0
0.05	1.050833	0.047573	0.0015776
0.10	1.103331	0.090574	0.0060365
0.15	1.157489	0.129397	0.012931
0.20	1.213298	0.164402	0.021897
0.25	1.270747	0.195920	0.032595
0.30	1.329822	0.224267	0.044735
0.35	1.390504	0.249674	0.058055
0.40	1.4528	0.272447	0.07232
0.45	1.5166	0.292793	0.08733
0.50	1.5820	0.310914	0.10291
0.55	1.6489	0.327025	0.11889
0.60	1.7172	0.341292	0.13514
0.65	1.7870	0.353887	0.15153
0.70	1.8582	0.364943	0.16797
0.75	1.9308	0.374608	0.18437
0.80	2.0048	0.383004	0.20063
0.85	2.0800	0.390238	0.21671
0.90	2.1565	0.396422	0.23254
0.95	2.2342	0.401651	0.24807
1.00	2.3130	0.406010	0.26327
1.05	2.3931	0.409530	0.27810
1.10	2.4741	0.412420	0.29252
1.15	2.5563	0.414621	0.30652
1.20	2.6394	0.416230	0.32010
1.25	2.7236	0.417303	0.33323
1.30	2.8086	0.417896	0.34589
1.35	2.8945	0.418053	0.35819
1.40	2.9813	0.417814	0.36986
1.45	3.0689	0.417223	0.38116
1.50	3.1572	0.416313	0.39197
1.55	3.2462	0.415115	0.40233
1.60	3.3360	0.413661	0.41228
1.65	3.4264	0.411979	0.42169
1.70	3.5174	0.410090	0.43074
1.75	3.6090	0.408022	0.43933
1.80	3.7011	0.405790	0.44749
1.85	3.7938	0.403416	0.45527

i.e. the corresponding value of ν) for any given ratio z/u'.

In Eq. (40) the factors multiplying the exponential are slowly variable functions of x and may be replaced by their values at x_0 (or ν_0). For the exponential we need its value at ν_0 which we write in the form

$$e^{-u'\varphi(\nu_0)}, \tag{42}$$

where

$$\varphi(\nu)=\nu dx/d\nu-x. \tag{43}$$

In addition, we need the second derivative of the exponent,

$$\frac{\partial^2}{\partial x^2}(u'x-\nu z)=-z\frac{\partial^2\nu}{\partial x^2}=u'\left(\frac{d\nu}{dx}\right)^2\frac{\partial^2 x}{\partial\nu^2}, \tag{44}$$

where Eq. (41) has been used in the elimination of z. This is easily seen to be positive so that the steepest descent from the saddle point is for purely imaginary changes of ν or x. The slowing-down density is then easily calculated to be

$$q(z,u')=\frac{K_M(\nu)}{\sqrt{u'}}e^{-u'\psi_M(\nu)} \tag{45}$$

with

$$K_M(\nu)=\frac{M\xi}{2g_0^2\lambda}\frac{1}{(2\pi)^{\frac{1}{2}}}\frac{1}{(d^2x/d\nu^2)^{\frac{1}{2}}} \tag{46A}$$

and

$$\psi_M(\nu)=\varphi(\nu)+2/M, \tag{46B}$$

where all functions of ν must be determined at the value of ν defined by (41), i.e., by

$$(dx/d\nu)=z/u'. \tag{41'}$$

TABLE III. Functions in slowing-down density Eq. (45) for $M=\infty$.

ν	x	$\frac{dx}{d\nu}=\frac{z}{u'}$	ψ	$\psi/(z/u')$	$-\frac{\partial\Lambda}{\partial x}=\lambda$	$\frac{d^2x}{d\nu^2}$	K_∞
0	0						
		0.0167	0.0002097	0.0126	(1.001)	0.667	0.4886
0.05	0.0008346						
		0.0504	0.001897	0.0376	(1.003)	0.679	0.4859
0.10	0.0033535						
		0.085	0.005366	0.0631	(1.0035)	0.705	0.4797
0.15	0.0076029						
		0.1213	0.010814	0.0892	(1.004)	0.744	0.4713
0.20	0.0136637						
		0.1600	0.018552	0.1160	(1.0045)	0.802	0.4594
0.25	0.0216537						
		0.2017	0.029056	0.1441	(1.006)	0.881	0.4454
0.30	0.0317402						
		0.2484	0.04301	0.1731	(1.008)	0.983	0.4302
0.35	0.0441573						
		0.3008	0.06147	0.2044	(1.0125)	1.1215	0.4124
0.40	0.05920						
		0.3610	0.08562	0.2372	(1.0175)	1.302	0.3938
0.45	0.07725						
		0.4346	0.11883	0.2734	(1.022)	1.550	0.3737
0.50	0.09898						
		0.5248	0.16404	0.3126	(1.027)	1.899	0.3513
0.55	0.1252				1.03		
		0.6320	0.22318	0.3531	(1.035)	2.413	0.3264
0.60	0.1568						
		0.774	0.3095	0.3999	(1.045)	3.311	0.2947
		0.732	0.2826	0.3861	(1.042)	3.04	0.3029
0.625	0.1751						
		0.816	0.3352	0.4108	(1.048)	3.614	0.2878
0.650	0.1955						
		0.916	0.4002	0.4369	(1.055)	4.35	0.2711
0.675	0.2184						
		1.036	0.4813	0.4646	(1.062)	5.31	0.2544
0.70	0.2443						
		1.184	0.5850	0.4941	(1.07)	6.52	0.2398
0.725	0.2739						
		1.374	0.7229	0.5261	(1.075)	8.068	0.2269
0.75	0.3080				1.08		
		1.596	0.8898	0.5575	(1.085)	10.32	
0.775	0.3479						
		1.892	1.1195	0.5917	(1.095)	14.14	
0.80	0.3938						
0.825	0.4506	2.53	1.63	0.6443	(1.11)		
0.850	0.5217	3.23	2.23	0.6904	(1.12)		
0.875	0.6154	4.36	3.20	0.7339	(1.14)		
0.900	0.7460	7.26	5.79	0.7975	1.16		
0.925	1.0260	16.27	14.02	0.8617			
0.950	1.7582						

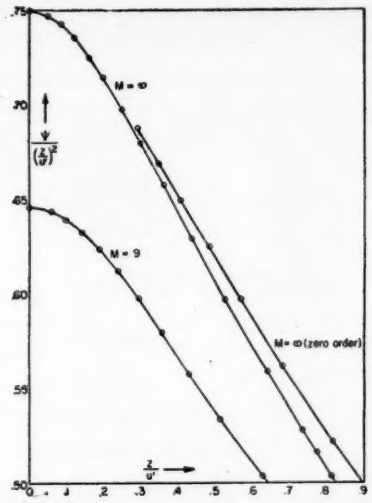

FIG. 1. Slowing-down density exponent in Eq. (47) for $M=\infty$ and $M=9$ for small z/u'.

Equation (45), with (43), (46), and (41′), is the principal result of our theory. In using it, one first has to determine x as a function of ν by solving (21) or (31). In doing this, one also finds λ [Eq. (32a)]. Having the relation $x(\nu)$, one also has $dx/d\nu$ and ψ [Eqs. (43) and (46B)] as functions of ν, as well as $d^2x/d\nu^2$ and g_0. Equation (41) then yields z/u' as a function of ν, or, conversely, ν as a function of the ratio z/u' which embodies the conditions of the experiment. Thus ψ and K are also determined as functions of z/u', and finally q is found from (45) as a function of z and u'; hence q can be expressed in the form:

$$q(z,u')=\frac{K_M(z/u')}{\sqrt{u'}}\exp[-u'\psi_M(z/u')]. \quad (47)$$

The exponent, which is the most important part of the expression, can also be written as

$$-z[\psi_M/(z/u')]. \quad (47')$$

It can be shown that in the case of infinite M, ψ is determined correctly to order $(z/u')^6$ by taking only g_0 and g_1 into account. We find:

$$\psi=\frac{3}{4}\left(\frac{z}{u'}\right)^2-\frac{81}{80}\left(\frac{z}{u'}\right)^4+\frac{20613}{5600}\left(\frac{z}{u'}\right)^6. \quad (48)$$

For finite M, the coefficients of $(z/u')^4$ and $(z/u')^6$ are affected slightly by g_2 but not by g_3 which is zero for $\eta=0$. For Be($M=9$) and C($M=12$), ψ is given to order $(z/u')^6$ by the following expressions:

$$\text{Be:}\quad \psi=0.6456(z/u')^2-0.6972(z/u')^4+2.046(z/u')^6, \quad (49)$$

$$\text{C:}\quad \psi=0.6705(z/u')^2-0.7659(z/u')^4+2.372(z/u')^6. \quad (50)$$

Neglecting g_2, one obtains instead

$$\text{Be:}\quad \psi=0.6456(z/u')^2-0.6964(z/u')^4+2.048(z/u')^6, \quad (49')$$

$$\text{C:}\quad \psi=0.6705(z/u')^2-0.7654(z/u')^4+2.374(z/u')^6. \quad (50')$$

The effect of g_2 is thus very small. The values of ψ obtained by the numerical procedure described below agree with Eq. (49) to within 2 percent up to $(z/u')=0.35$. The "exponential" theory of Placzek[5] is equivalent to using only the first two terms in the expansion of ψ in $(z/u')^2$. For $M=1$, using Wick[1]

$$\text{H:}\quad \psi=\frac{1}{4}\left(\frac{z}{u}\right)^2-\frac{11}{240}\left(\frac{z}{u}\right)^4+\frac{73}{4032}\left(\frac{z}{u}\right)^6.$$

The power series for K_∞ and K_9 have been worked out to $(z/u')^4$. They are:

$$K_\infty=[3/(4\pi)]^{\frac{1}{2}}[1-(14/5)(z/u')^2+19.20(z/u')^4\cdots],$$
$$K_9=0.4533[1-2.225(z/u')^2+12.39(z/u')^4\cdots]. \quad (51)$$

The age theory approximation is equivalent to using only the first terms in the expansions of ψ and K,

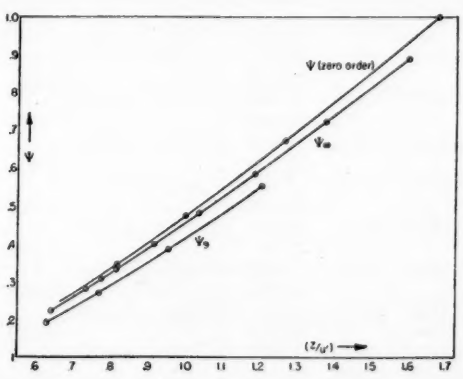

FIG. 2. Slowing-down density exponent in Eq. (47) for $M=\infty$ and $M=9$ for larger z/u'.

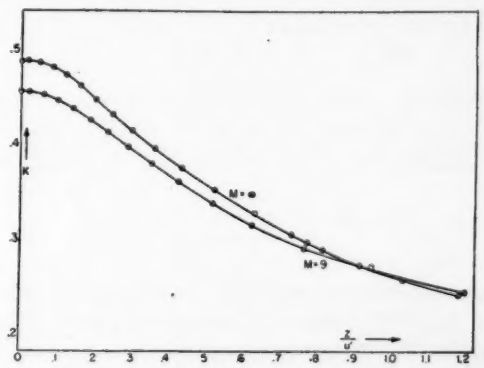

FIG. 3. Slowing-down density coefficient in Eq. (47) for $M=\infty$ and $M=9$.

[5] G. Placzek, *"The Spatial Distribution of Neutrons Slowed Down by Elastic Collisions."* Declassified Report A-25 (1941). The author has given explicit formulas for the first two terms in ψ for any M.

specifically

$$\psi=\tfrac{3}{4}\cdot\tfrac{1}{2}M\xi[1-\tfrac{2}{3}M]\cdot(z/u')^2, \tag{52}$$

$$K=\left[\frac{4\pi}{\tfrac{3}{2}\xi M(1-2/3M)}\right]^{\frac{1}{3}}. \tag{53}$$

VI. CALCULATIONS FOR NUCLEI OF INFINITE MASS, $M=\infty$

Calculations have been made in accordance with the procedure outlined below Eq. (47). They were carried through the second order approximation. ν was used as the independent, x as the dependent variable.

Table I contains a tabulation of the necessary A's, and Table II covers the G's.

Equation (21) with $N=2$ was expanded to give Eq.

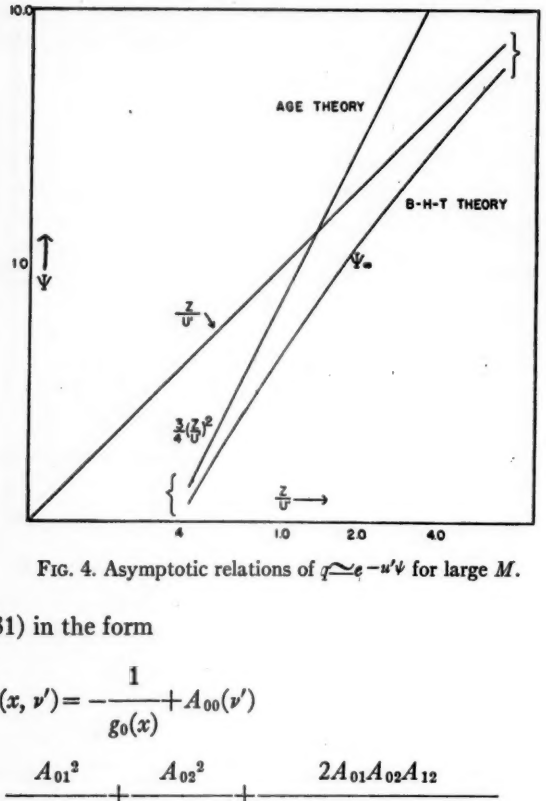

FIG. 4. Asymptotic relations of $q\simeq e^{-u'\psi}$ for large M.

(31) in the form

$$\Lambda(x,\nu')=-\frac{1}{g_0(x)}+A_{00}(\nu')$$
$$+\frac{\dfrac{A_{01}^2}{g_1^{-1}-A_{11}}+\dfrac{A_{02}^2}{g_2^{-1}-A_{22}}+\dfrac{2A_{01}A_{02}A_{12}}{(g_1^{-1}-A_{11})(g_2^{-1}-A_{22})}}{1-\dfrac{A_{12}^2}{(g_1^{-1}-A_{11})(g_2^{-1}-A_{22})}}. \tag{54}$$

The zero-order approximation is obtained by retaining g_0 and A_{00} only. A pair of these values, x and ν, from the zero-order calculations were used as x and ν' in the second and third terms of the right member and an improved g_0^{-1} found, since $\Lambda(x,\nu)=0$. From this a better value of x was found and this iterative process was continued until no further change in x occurred. Since each approximate value of x gave a non-vanishing value of Λ, this process furnished $\lambda\equiv-\partial\Lambda/\partial x$. The

TABLE IV. Functions of x for $M=9$, Eqs. (7).

x	$g_{00}^{-1}(x)$	$g_{10}(x)$	$g_{20}(x)$
0.20	0.979472	0.20433	0.01003
0.25	1.026030	0.243449	0.01600
0.30	1.073910	0.278597	
0.35	1.123097	0.310127	
0.40	1.173575	0.338347	
0.45	1.225325	0.363551	0.05102
0.50	1.278324	0.386002	0.06083
0.55	1.332549	0.405931	0.07099
0.575	1.360114		0.07608
0.60	1.387976	0.423575	0.08123
0.625	1.416131		0.08638
0.65	1.444577	0.439132	0.09155
0.675	1.473309		0.09672
0.70	1.502325	0.452786	0.10189
0.725	1.531619		0.10705
0.75	1.561189	0.464708	0.11218

first two columns of Table III tabulate $x(\nu)$ in the second-order approximation.

From a table such as III we had to calculate ψ in the exponent of e in the slowing-down density, Eq. (45). The variable part of ψ is φ, Eqs. (43) and (46B), and it is desirable to have this as a function of $dx/d\nu$. This can be done by well-known methods using differences. For much of the work we used a method that gave $\nu dx/d\nu-\nu$ as a function of $dx/d\nu$ more accurately than usual methods but this led to later unfortunate computational complications because it required forsaking the established tabular points which are equally spaced in ν. The interlining of the results of this calculation in

TABLE V. Functions in slowing-down density Eq. (45) for $M=9$.

ν	x	$-\frac{\partial\Lambda}{\partial x}$	$\frac{dx}{d\nu}=\frac{z}{u'}$	ψ	$\psi/(z/u')$	$\frac{d^2x}{d\nu^2}$	K_9
0	0.22222	0.9298					0.4533
			0.0194	0.00024	0.0124	0.776	0.4532
0.05	0.22319	0.930					
			0.0586	0.00221	0.0377	0.792	0.4499
0.10	0.22612	0.931					
			0.0988	0.00624	0.0632	0.820	0.4444
0.15	0.23106	0.933					
			0.1412	0.01262	0.0894	0.876	0.4342
0.20	0.23812	0.934					
			0.1868	0.02176	0.1165	0.948	0.4231
0.25	0.24746	0.936					
			0.2364	0.03419	0.1446	1.036	0.4118
0.30	0.25928	0.938					
			0.2914	0.05073	0.1741	1.168	0.3961
0.35	0.27385	0.942	0.3211	0.06076	0.1892		
			0.3544			1.356	0.3775
0.40	0.29157	0.945	0.3895	0.08645	0.2220		
			0.4284			1.600	0.3552
0.45	0.31299	0.951	0.4694	0.12044	0.2566		
			0.5168			1.968	0.3349
0.50	0.33883	0.956	0.5691	0.16792	0.2951		
			0.6260			2.476	0.3123
0.55	0.37031	0.963	0.6930	0.23305	0.3363		
			0.766			3.200	0.2884
0.60	0.4087	0.970	0.8508	0.3240	0.3808		
			0.950			4.316	0.2690
0.65	0.4564	0.978	1.069	0.4607	0.4309		
			1.204			6.160	0.2425
0.70	0.5172	0.988	1.385	0.6743	0.487		
0.75	0.5978	1.003					
0.80	0.7109						

columns 3, 4, 5, etc. of Table III recognizes that values calculated in this way apply to points intermediate between the tabulated ν and x values.

As ν approaches unity there is difficulty because $dx/d\nu$ and x both increase indefinitely there. But there we used

$$-x^2\frac{d}{d\nu}\left(\frac{\nu}{x}\right)=dx/d\nu-x=\varphi, \tag{55}$$

whence

$$dx/d\nu=(\varphi+x)/\nu \tag{56}$$

and

$$d^2x/d\nu^2=-\frac{1}{\nu}\frac{d\varphi}{d\nu}. \tag{57}$$

All of the above material appears in Table III. Plots essentially of ψ against z/u' appear in Figs. 1, 2, and 5. The first is of $\psi/(z/u')^2$ to make the comparison with age theory which gives a constant for this quantity. The second and third are appropriate to Eqs. (47) and (47′), respectively.

Next, $K_\infty(\nu)$ had to be calculated. The calculation of $x(\nu)$ led quite naturally to a value for λ and the other quantities presented no difficulties. $K_\infty(\nu)$ is tabulated in column 8 of Table III and is plotted in Fig. 3.

We now had everything necessary to evaluate Eq. (45):

$$q(z,u')=\frac{K_\infty(z/u')}{\sqrt{u'}}\exp[-u'\psi_\infty(z/u')]$$

for M very large. Here the functional dependence on the physical quantities z and u', instead of ν, is indicated.

Figure 4 compares the present results with age theory on the one hand and with the asymptotic form e^{-z} for large z/u' on the other. The comparison is based on the exponential factor only. The agreement with age theory at low z/u' is apparent, and at $z/u'\simeq 7$ the approach to e^{-z} is evident.

VII. CALCULATION FOR NUCLEUS OF MODERATE MASS, $M=9$

The difference between this and the previous case is that the functions $g_0(x)$, g_1, g_2 of Eqs. (7) were used in place of the functions G_0 of Eqs. (9). In these functions only the region $x\geq 2/M=2/9$ is of interest [see Eq. (6)] since $\eta\geq 0$. For purposes of calculation, however, the g's were tabulated from $x=0.20$. Values of g_0^{-1}, g_1, g_2 are given in Table IV for $M=9$ and are accordingly designated as g_{09}^{-1}, g_{19}, g_{29}, respectively.

The calculations of $x(\nu)$, ψ, etc. were carried out just as for $M=\infty$, noting that here $2/M$ must be added to φ to get ψ and that $M\xi/2=1.080$. The results are tabulated in Table V and in Figs. 1, 2, 3, and 5.

It was of immediate concern to know what the accuracy of the present approximation is. Using Eq. (54) it was possible to segregate (approximately) the various orders of approximation. In the calculations

$$0=\Lambda=-2.3542+1.7542+0.4557+0.1443 \quad \text{for } M=\infty,\ \nu=0.925,$$

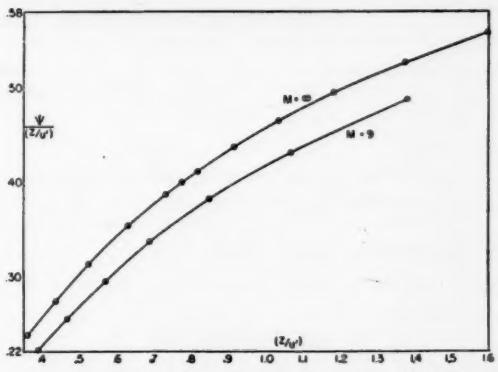

FIG. 5. Slowing-down density exponent as in Eq. (47′) for $M=\infty$ and $M=9$ for larger z/u'.

$$0=\Lambda=-1.5206+1.4210+0.0934+0.0062 \quad \text{for } M=\infty,\ \nu=0.825,$$

$$0=\Lambda=-1.5150+1.3733+0.1351+0.0066 \quad \text{for } M=9,\ \nu=0.80,$$

where, in turn, the two zero-order terms, the first- and the second-order appear. The first expression applies well beyond the range of z/u' for which we have made accurate calculations, yet the convergence is not very bad. In the second expression the corrections amount, successively, to 6 percent and 0.4 percent, thus predicting an error of well under 0.1 percent. The consequent error in x is less than 4×10^{-4} since $\lambda\sim 1$. A little analysis shows that, for the same $dx/d\nu$, ψ would decrease somewhat less than x increases, that is by less than 0.025 percent. The third expression indicates about the same accuracy as the second although we are here outside the tabulated range of ψ.

Another matter of interest concerns the error caused by using ψ_∞ instead of ψ_9 for Be. The comparison must, of course, be made at the same z (relative distance) and the same u' (relative slowing down). From 1 Mev. to thermal in Be, $u'=79$. If we choose $z=79$, a distance of about 130 cm in Be, the difference in $\psi/(z/u')$ from Fig. 5 is 0.04, the ψ_∞ giving too low a value of q by the factor

$$e^{-0.04\times 79}=0.043.$$

Finally, we can make a comparison of asymptotic results obtained by Marshall, a student of G. C. Wick,[6] for $M=12$ with our results. Marshall's results can be expressed as

$$\psi_{12}=z/u'-0.587(z/u')^{\frac{1}{2}}+0.0417.$$

From $z/u'=1$ to 16 both ψ_{12} and $\psi_{12}-z/u'$ agree within better than 10 percent with our ψ_∞ results, and this seems to be better than is to be expected.

We wish to acknowledge the services of Mrs. Dorothy Guy and Miss Bernice Warr in performing the calculations.

[6] By letter communication. Wick (see reference 1) has shown that the behavior of ψ for large z/u' can be studied by means of a Schroedinger-type differential equation for the transform of the neutron angular distribution. This approach was suggested independently by J. A. Wheeler.

Neutron Scattering Cross Sections of the Noble Gases

SIGMUND P. HARRIS
Argonne National Laboratory, Chicago, Illinois
(Received May 5, 1950)

The neutron scattering cross sections of five noble gases were measured using a neutron beam and an annular BF_3 proportional counter. Boron absorption and self-indication techniques were used to detect resonances. A strong neutron resonance was found in xenon and indications of resonances in argon and krypton were obtained.

I. INTRODUCTION

AN examination of the literature reveals relatively little data on the neutron scattering cross sections of the noble gases,[1] especially of those other than helium. One expects this since the noble gases can only be measured conveniently in the gaseous state. In addition two of them, krypton and xenon, are scarce. A neutron beam from the Argonne heavy water reactor, used with a 4π-solid angle annular BF_3 proportional neutron counter,[2,3] affords a method of measuring the scattering cross sections of the noble gases. Their total cross sections can also be measured if they are sufficiently large. The general method is similar to that described in references 2 and 3 for materials in solid foil form.

II. APPARATUS AND PROCEDURE

The apparatus consists of a collimator, shield block, annular BF_3 neutron counter and containers for the gas samples. Figure 1 of reference 3, is a schematic diagram of the general arrangement. A container for the gases (Fig. 1) is placed in the beam in the center of the annular counter. The gas fillings serve as scattering detectors (labeled "scattering foil" in Fig. 1, reference 3). The gas pressure is limited to two atmospheres because the detector gas would be lost should one of the aluminum windows 2 mil thick and 3 cm in diameter burst. The spaces in front of and behind the gas detector cell are evacuated to reduce neutron scattering by air.

For each reading the annular counter is allowed to count for 100 units of 512 counts on the fission counter pile monitor (see Fig. 1, reference 3), after which both counters shut off automatically. Counting rates are corrected for background and for the annular counter dead time.

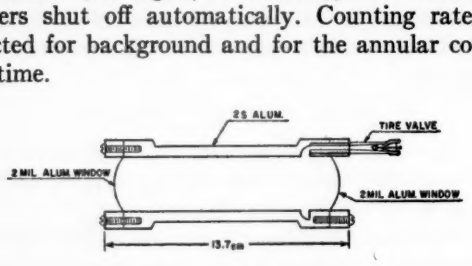

FIG. 1. Gas detector cell.

To calculate the scattering cross section, σ_s, counting rates are compared with those from a thin graphite disk using formula (1) of Section III. The graphite disk used as a standard detector (i.e., one of known scattering cross section) is very thin, 0.0915 g/cm^2, and therefore no geometrical sensitivity correction need be made to the counting rates obtained with it. The fact that the length of the gas samples is not negligible compared with that of the annular counter reduces the sensitivity of the counter to neutrons scattered from the gas. The net counting rates obtained for the gas samples in the cell must be multiplied by a factor of 1.03. This corrects for the lower efficiency of the annular counter away from its center. The figure of 1.03 was determined from a graph of counting rate *vs.* position of graphite detector in the annular counter.

For a material possessing resonances, a much higher cross section is obtained when its transmission is measured using the same material as the detector than when another material (e.g., graphite) is used as the detector. This method of detecting resonances is known as self-indication. In measuring the total cross section of a gas by self-indication an aluminum pressure cylinder one foot long and of inside diameter one inch is used to contain the gas acting as the filter. This cylinder has a Pyrex glass side arm for freezing out the gas. The transmitted neutron intensity is measured with the gas in the cylinder and with the gas frozen out in the side arm. The same kind of gas is used as the detector in the above described cell. For all measurements background is measured with the empty detector cell, (valve core removed) in the beam, and is subtracted from the corresponding gross counting rate. In the case of the graphite detector, backgrounds are measured with only its holder in the beam.

III. THEORY

In the following relation the various symbols are defined as follows:

σ_s = the effective scattering cross section of the detector sample,
σ_c = the effective scattering cross section of the graphite detector (see Table I),
N = the net corrected counting rate from the detector sample,

[1] H. Carroll, Phys. Rev. **60**, 702 (1941); H. Carroll and J. R. Dunning, Phys. Rev. **54**, 541 (1938).
[2] Harris, Langsdorf, and Seidl, Phys. Rev. **72**, 866 (1947).
[3] C. T. Hibdon and C. O. Muehlhause, Phys. Rev. **76**, 100 (1949).

TABLE I. Scattering cross sections used for graphite standard.[a]

Neutron spectrum	Cross section in barns
Thermal[b]	5.0
Epi-cadmium	4.60
Transmitted by B^{10} absorber No. 2	4.55
Transmitted by B^{10} absorber No. 3	4.50
Transmitted by B^{10} absorber No. 5	4.47
Transmitted by B^{10} absorber No. 6	4.46

[a] All values except the thermal value were determined at this Laboratory by transmission measurements on graphite.
[b] Goldsmith, Ibser, and Feld, Rev. Mod. Phys. 19, 266 (1947). The thermal cross-section curve for carbon is quite irregular because of crystal effects. It is therefore somewhat uncertain just what value to use. There is some evidence that this whole curve is too low. See Havens and Rainwater, Phys. Rev. 75, 1296(A) (1949). K. Way and G. Haines, *Themal Neutron Cross Sections for Elements and Isotopes, H–Bi* (Technical Information Division, AEC Oak Ridge, Tennessee, 1948), p. 5.

N_c = the net corrected counting rate from the graphite detector,
A = the number of atoms/cm² of the detector sample,
A_c = the number of atoms/cm² of the graphite detector,

$$\sigma_s/\sigma_c = NA_c/N_cA. \quad (1)$$

This relation holds only if the sample is sufficiently thin that its transmission is close to unity. In most cases the error introduced by formula (1) because of the approximation involved in it is less than one percent.

To determine the self-indication total cross section the exponential relation

$$I/I_0 = \exp(-A_f\sigma_t) \quad (2)$$

is used where I = net corrected counting rate with the filter in, I_0 = net corrected counting rate with the filter out, A_f = the number of atoms/cm² of filter and σ_t = the total cross section in cm²/atom.

When B^{10} absorbers of various thicknesses (see Table II) are inserted in the beam, the energy spectrum is modified from $1/E$ to $E^{-1}\exp(-C/E^{\frac{1}{2}})$ so that the mean energy of the neutrons is higher. Here C is proportional to the B^{10} thickness. If there is a resonance in the element under investigation, the cross section will increase markedly as Cd and then B^{10} are inserted in the beam. If the resonance is at a sufficiently low energy the cross section will begin to fall for the greater thicknesses of B^{10}.

The relative sensitivity function of the annular counter with its paraffin reflector is given by the expression[5]

$$1-0.0587\ln 2E.$$

Using this to calculate the difference in sensitivity of the counter for neutrons scattered by He (ξ, the average logarithmic decrement per collision, is 0.425) and for those scattered by carbon ($\xi=0.158$), it is found that the sensitivity is about two percent higher for helium scattered neutrons than for carbon scattered, if $E=1000$ ev initially, and slightly more than one percent higher if $E=0.5$ ev initially. Even for helium then, this effect does not change the cross sections appreciably and no correction is made for it.

TABLE II. B^{10} absorbers.

Number	B^{10}	Energy for $1/e$ transmission
2	0.157 g/cm²	27.8 ev
3	0.315	110
5	0.635	455
6	1.267	1670

If the resonance energy is low a rough estimate of the energy can be made by the following graphical method. The counting rates found for filter-in and filter-out in the self-indication measurements are subtracted. These differences (corrected for scattering in the B^{10} absorbers) are plotted on a semilog plot against the corresponding B^{10} thicknesses. If all the neutrons thus counted are of one energy, a straight line is obtained. This simple situation is not achieved in practice because of the potential scattering and scattering in the wings of the resonance, and thus the line always curves at least a little. If more than one resonance is effective, the plot becomes still more curved. Since the energy is determined in effect from the slope, the method is good only to an order of magnitude in this case.

Figure 2 is the boron absorption curve for Xe plotted in the above described way. The best straight line through the first three points gives a Xe resonance energy of about 11 ev. The fourth point lies off the straight line, showing that the line is beginning to curve.

IV. RESULTS

The results of the various cross-section measurements are given in Tables III–V. Helium and neon have low, constant cross sections for scattering. Argon has the lowest thermal scattering cross section of any of the gases measured. The data with B^{10} absorbers indicate a resonance at fairly high energy. Krypton and xenon also indicate resonances via boron absorption. The greatest resonance effect is in xenon. Its highest effective scattering cross section is 20.1 barns by comparison with

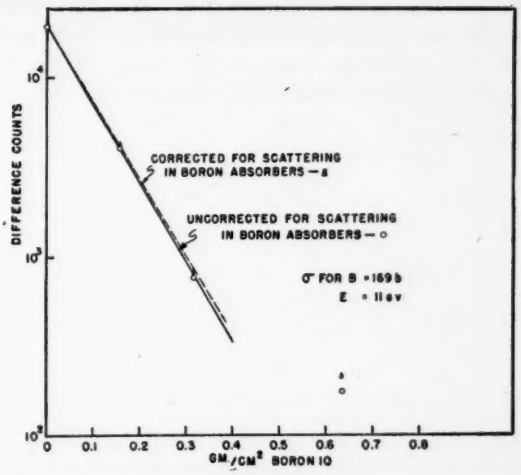
DIFFERENCE COUNTS
CORRECTED FOR SCATTERING IN BORON ABSORBERS — s
UNCORRECTED FOR SCATTERING IN BORON ABSORBERS — o
σ FOR B = 189 b
E = 11 ev
GM/CM² BORON 10

FIG. 2. Boron absorption of xenon in and out differences with xenon detection.

TABLE III. Measured cross sections.

Element	Thermal σ_s	Epi-Cd σ_s	Thermal σ_{self}	Epi-Cd σ_{self}	Detector g/cm²	Filter g/cm²
He	1.4 b[a]	1.50 b			0.00309	
Ne	2.4	2.4			0.0130	
A	0.8	0.95			0.0272	
Kr	7.2	8.8	36 b	103 b	0.0481	0.207
Xe	4.3	20.1	18	540	0.0685	0.333

[a] Corrected for Doppler effect. See J. Schwinger, Phys. Rev. 58, 1004 (1940).

TABLE IV. Scattering cross sections.

B^{10} absorber number	Scattering cross section in barns He	Ne	A	Kr	Xe
None—Cd only	1.50	2.4	0.95	8.8	20.1
2	1.60	2.6	1.28	9.7	13.1
3	1.45	2.7	1.5	9.5	9.0
5			1.6	9.6	7.6
6				7.3	

TABLE V. Self-indication cross sections.

B^{10} absorber number	Self-indication total cross section in barns Kr	Xe
None—thermal	36	18
None—Cd only	103	540
2	93	330
3	70	110
5	29	40

graphite with only cadmium in the beam. Under the same conditions the self-indication transmission cross section is 540 barns. This xenon resonance appears to have a considerable portion of scattering in the energy region of ~11 ev.

A comparison of the thermal σ_s for He, Ne, A, and Kr with the thermal σ_{total} of Carroll[1] is possible. The cross section obtained for helium is 0.15 barn higher than that of Carroll. The neon cross sections differ by about 0.4 barn, which is just outside the experimental errors, if negligible absorption is assumed. For argon, assuming an absorption cross section as high as 1.2 barns, the scattering cross section found is 0.4 barn lower and definitely outside the experimental error. The value of 0.8 barn agrees with that of Melkonian.[4] The values shown in Table IV also give an indication of the high energy resonance shown in Melkonian's curve. The value of 7.2 barns for the thermal σ_s of krypton when compared with Carroll's σ_{total} of 27.3 barns indicates large absorption and/or influence of the result by the resonance near the thermal region (see Table V).

Using the thermal scattering cross section as the potential scattering cross section, σ_p, for xenon (see Table III) and the following relation,[5] the resonance scattering integral, Σ_s, can be found.

$$\Sigma_s = 8.4(\sigma_{epi\text{-}Cd} - \sigma_p)\left(\frac{1}{1-0.0587\ \ln 2E_0}\right),$$

$$\Sigma_s = 8.4(20.1-4.3)\left(\frac{1}{1-0.0587\ \ln 2(11)}\right).$$

This gives $\Sigma_s = 162$ b.

V. DISCUSSION OF ERRORS

The values of σ_s given in Table III have a probable error of about ±5 percent, except for the thermal values which have about ±10 percent, partly due to the uncertainty in the graphite cross section. The probable error in the values in Table IV varies from about ±5 percent for no B^{10} to about ±10 percent for the thickest B^{10} absorber. The values of the total cross section in Table V are based in general on transmissions close to unity and thus have a probable error varying from ±5 percent for high σ_t to ±50 percent for low σ_t. These errors arise mainly from the statistical error in the counting rates which may be multiplied a number of times by various background corrections and subtractions. The percentage error may be increased by a factor of 2 to 4 in the case of σ_s, and by as much as a factor of 10 in the case of σ_t for transmissions very close to one.

The helium used had a purity of 99.8 percent. The other gases were those available commercially in glass containers and were of high purity.

[4] E. Melkonian, Phys. Rev. 76, 1750 (1949).
[5] Harris, Muehlhause, and Thomas, Phys. Rev. 79, 11 (1950).

Total Cross Sections of Nuclei for 280-Mev Neutrons*

R. Fox, C. Leith, and L. Wouters
Radiation Laboratory, Department of Physics, University of California, Berkeley, California

and

K. R. MacKenzie
Department of Physics, University of California at Los Angeles, California

(Received June 16, 1950)

The measurement of 280-Mev neutron cross sections of various nuclei is described. The neutron beam used results from 340-Mev protons in the 184-in. cyclotron striking a 2-in. Be target. The neutron detector consists of a double-coincidence anthracene scintillation counter telescope which counts recoil protons scattered at 15° from a paraffin cylinder placed in the collimated neutron beam. A 2-in. Cu absorber placed between the counters assures that only protons of energy greater than 250 Mev are counted. The cross sections for all nuclei measured from Li to Pb are smaller than the corresponding cross sections measured at 85 Mev by factors between 0.5 and 0.6.

I. INTRODUCTION

WHEN the total cross sections of various elements for 85-Mev neutrons were measured a year ago[1] it was noticed that elements of low atomic weight behaved as if they were at least partially transparent. Therefore, when the 280-Mev neutron beam became available after conversion of the 184-in. cyclotron, it was considered advisable to examine this effect at the higher energy. The measurements also would add to our knowledge of the fundamental properties of nuclei; a correct theory should be able to predict these cross sections and their functional dependence upon energy and atomic number in an unambiguous manner. Conversely, knowledge of these values may furnish additional clues leading to the correct nuclear model. These measurements were made using two independent detection methods. In this paper measurements made using scintillation counters are described, and in an accompanying paper[2] measurements made using bismuth fission counters are described.

II. SOURCE OF NEUTRONS

The neutron beam used for these measurements was produced by bombarding a 2-in. thick beryllium target in the cyclotron vacuum chamber with 350-Mev protons. Charge exchange leads to the production of a neutron beam of about 270-Mev mean energy and angular width at half-maximum intensity of about 58°. The central forward section of this beam was selected by a collimating system, consisting first of a $\frac{1}{2}$-in. hole through a 7-ft. cube of concrete placed between the cyclotron and the surrounding concrete shielding wall, and second by means of an exchangeable steel plug with any desired aperture inserted into a 3-in. hole in the 10-ft. shielding wall itself. In this experiment, a $2\frac{5}{8}$-in.$\times 1\frac{3}{8}$-in. aperture was employed.

The energy distribution of the neutron beam was obtained by measuring the range distribution, and hence deducing the energy distribution, of recoil protons from hydrogen, at a fixed angle with respect to the beam. The range-energy curves used were calculated from the theoretical formula of Livingston and Bethe[3] $I=11.5Z$ ev. Paraffin and carbon scatterers were used alternately to obtain the hydrogen difference. The range distribution was determined by varying the absorber thickness between two scintillation counters in coincidence counting the recoil protons as illustrated in Fig. 1. To each thickness there corresponds a minimum proton energy E_{p1} for penetration, so that all protons with energy $E_p > E_{p1}$ passing through both counters were counted. This number is proportional to the number of neutrons of energy $E_n > E_{n1} = E_{p1}/\cos^2\theta$, θ being the laboratory scattering angle with respect to the forward direction.

There is one serious difficulty. At these energies the absorber thickness required is an appreciable fraction of a mean free path for a nuclear encounter, so that a fraction of the protons of energy $E_p > E_{p1}$ are not

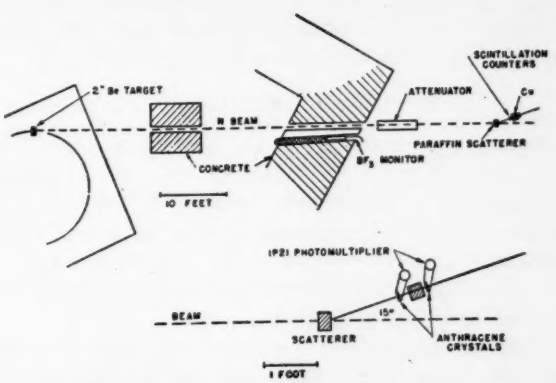

FIG. 1. Experimental arrangement for measurement of total cross sections. For measurement of neutron beam energy distribution, the scatterer is alternately carbon and paraffin, the copper absorber thickness is varied, and there is no attenuator.

* The work was carried out under the auspices of the AEC.

[1] Cook, McMillan, Peterson, and Sewell, Phys. Rev. **75**, 7 (1949).

[2] J. DeJuren, Phys. Rev. **80**, 27 (1950), following paper.

[3] H. A. Bethe, Rev. Mod. Phys. **9**, 263 (1937), Eq. (749).

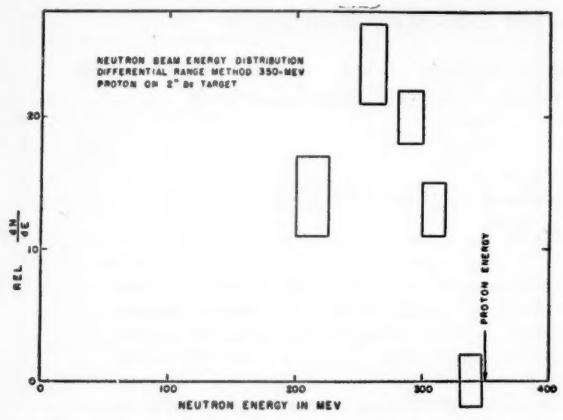

FIG. 2. Energy distribution of neutron beam produced by 340-Mev protons bombarding a ½-in. beryllium target.

counted. If the cross section for these processes which remove protons were known, an accurate correction could be made; however, only an estimated correction is possible at present.

Incorporating this estimated correction and differentiating the resulting distribution, it is found to have a peak of 270 Mev (±15 Mev) with an estimated width of 30 Mev as shown in Fig. 2.

III. EXPERIMENTAL METHOD

A. Principle

To measure the total cross sections of various elements for high energy neutrons, use is made of the exponential decrease in intensity of a monoenergetic beam in the forward direction as the thickness of matter traversed (X) is increased:

$$I(X)=I(0)\exp(-X/\lambda),$$

where λ is the mean free path, related to the total cross section by the formula

$$1/\lambda=(N\rho/A)\sigma_t,$$

N being Avogadro's number, ρ the density, and A the atomic weight. Then the total cross section is:

$$\sigma_t=(A/N\rho X)\ln[I(0)/I(X)].$$

Numbers proportional to the beam intensities $I(0)$, $I(X)$ are obtained by counting the recoil protons generated at a fixed angle (usually 15°) by a small paraffin cylinder placed in the neutron beam behind the samples. The recoil protons were counted by means of two scintillation counters in coincidence, in much the manner described above.

This paraffin proton generator was placed in the neutron beam 12 ft. from the last collimator; the sample, about one mean free path in length and 3 in. in diameter, was placed in the beam 2 ft. from the last collimator. A BF_3 slow-neutron counter was located in a hole in the concrete wall adjacent to that collimator for monitoring purposes. With these arrangements the ratio $R(X)$ of detector to monitor counting rates is proportional to $I(X)$, a second ratio $R(0)$, proportional to $I(0)$, is obtained by removing the sample. When these ratios are corrected for background, we get new ratios $R'(0)$, $R'(X)$. Then,

$$I(0)/I(X)=R'(0)/R'(X).$$

B. Counter

(See also Fig. 1.) The individual scintillation counters consisted of uniform anthracene crystals $\frac{3}{16}$ in. thick and 1 sq. in. in area mounted in light-tight polished aluminum boxes, each in turn facing a 1P21 photomultiplier tube. Two such units were mounted as a coincidence telescope looking at the paraffin recoil proton generator at 15° laboratory angle. In order to confine coincidences to protons generated by high energy neutrons, a 2-in. Cu absorber was placed between the crystals, thus providing an equivalent neutron threshold[3] of 250 Mev.

The geometry was arranged so that the path of the counted recoil protons passes normally through the crystals and through a uniform, known thickness of aluminum. Fast (10^{-8} sec.) light pulses were produced due to the excitation and subsequent fluorescence induced in the anthracene by the protons. The photomultipliers convert these into electric signals which are further amplified and mixed in a coincidence circuit. The system has a 0.25-μsec. resolving time. The output was counted by a standard scaler.

When plotting counting rate *versus* photo-multiplier voltage (or gain), a plateau is observed as shown in Fig. 3, corresponding to the detection of virtually all protons, but no other particles. Above this proton plateau γ-rays, β-particles, noise, etc., begin to be counted. Since the plateau width is 300 volts (corresponding to a gain ratio of about 8), constant detector efficiency is assured by setting the photo-multiplier voltage at its center.

C. Monitor

The BF_3 monitor counted slow neutrons leaking through the concrete from the collimator. Since the

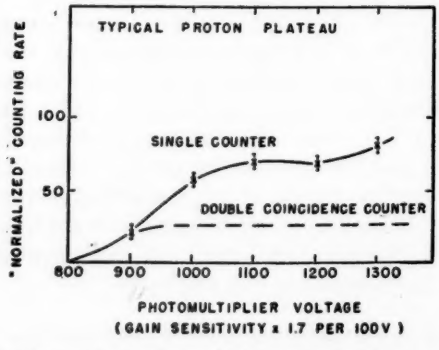

FIG. 3. Plateau for counting high energy protons. ——— line is for a single counter, – – – – line is for two counters in coincidence.

background flux was several orders of magnitude smaller than the slow neutron flux originating at the collimator, its counting rate was satisfactorily proportional to the latter. This monitor was shielded from backscattering by a 2-ft. Cu plug between it and the sample. The chief problem with such a monitor is the finite slope and narrow width of its plateau, in contrast to the wide, flat plateau of the scintillation counters. Accordingly, very good voltage regulation must be provided or the efficiency will vary. Any significant variations due to this or other causes affecting the entire experiment can be checked by a statistical analysis of groups of counts.

D. Technique

1. *Alignment*

The equipment was mounted in such manner as to permit accurate centering of the paraffin generator in the neutron beam. This alignment was checked by means of a cathetometer previously aligned with the inner collimator and the central point of emergence of the neutron beam at the vacuum tank. Likewise the alignment of the samples could be similarly checked, to see that no neutron path could reach the generator without passing through the sample.

In operation, the counting rate is maximized as a function of cyclotron target position to ensure that the beam is not emerging obliquely. The entire alignment was further checked by exposing film in the beam, at the generator.

2. *Geometry*

The beam area was 3.6 sq. in. and the sample-to-generator distance varied from 7 to 9 ft. depending on sample length. This gives a solid angle of from 3×10^{-4} to 5×10^{-4} steradian, which is sufficiently "good" to avoid scattering correction in case of the light elements. For the heavy elements, a small scattering correction is necessary.

3. *Accidental Coincidences. Background*

During early runs, the coincidence counting rate was of the order of 3 c/sec. with single counting rates of $N_1\sim800$ c/sec. in the first counter and $N_2\sim150$ c/sec. in the second counter. Calling the accidental coincidence rate N_c and using the relation $N_c=2N_1N_2\tau A$, where τ is the resolving time of 0.25 μsec. and A (~300) is the reciprocal beam duty factor, we get $N_c\sim0.06$ c/sec. This is about two percent of the observed total coincidence rate. Therefore, for later runs, N_c was measured experimentally by placing sufficient absorber between the crystals to eliminate true coincidences. The beam intensity was then reduced until N_c was less than 0.5 percent of the total coincidence rate.

The principal source of background arose from diffracted neutrons reaching the first crystal directly and there producing recoil protons which were counted. With the sample in place, these neutrons came from the sample. With the sample removed, they came from the iron collimator. This background was measured directly before and after all runs by removing the paraffin proton generator and determining the coincidence rate. This was done with the sample in place and with the sample removed. Detector to monitor ratios thus obtained were subtracted from the ratios $R(X)$ and $R(0)$ to yield $R'(X)$ and $R'(0)$.

In order to check for other sources of background, the following experiment was performed. First, a run was made with one mean free path of carbon and 24 in. of lead as the sample and with the paraffin in place. A second run was made with the paraffin removed. Then a third run was made with both paraffin and lead removed. Normalizing the coincidence counts to equal monitor counts, the following numbers were obtained: 1st run, 12 counts; 2nd run, 6 counts; 3rd run, 92 counts.

The first set-up detects diffracted neutrons which pass through several mean free paths of sample to the first crystal, neutrons scattered by air around the sample into the first crystal, neutrons scattered by air around the sample into the paraffin, and neutrons from the beam which reach the paraffin through about seven mean free paths of sample. The second set-up detects only the first and second of these. The third set-up detects neutrons scattered by air around the sample into the first crystal and diffracted neutrons which have

TABLE I. Total cross sections at 280 Mev with those at 85 Mev included for comparison.* Errors are calculated from counting statistics alone.

Element	A	$A^{\frac{1}{3}}$	280 Mev $\sigma\times10^{24}$ cm^2	280 Mev $(\sigma/2\pi)^{\frac{1}{2}}\times10^{13}$ cm	85 Mev $\sigma\times10^{24}$ cm^2	85 Mev $(\sigma/2\pi)^{\frac{1}{2}}\times10^{13}$ cm
H^1	1.008	1.00	0.033±0.003	0.725±0.04	0.083±0.004	1.15
H^2	2.015	1.26	0.049±0.005	0.884±0.04	0.117±0.005	1.36
Li	6.940	1.91	0.164±0.007	1.62 ±0.04	0.314±0.006	2.24
Be	9.02	2.08	0.225±0.004	1.89 ±0.02	0.431±0.008	2.26
C	12.01	2.29	0.279±0.004	2.11 ±0.01	0.550±0.011	2.96
O	16.00	2.52	0.380±0.008	2.46 ±0.03	0.765±0.020	3.49
Al	26.97	3.00	0.566±0.018	3.00 ±0.05	1.12 ±0.02	4.22
Cu	63.57	3.98	1.19 ±0.02	4.35 ±0.04	2.22 ±0.04	5.95
Sn	118.7	4.92	1.83 ±0.03	5.40 ±0.11	3.28 ±0.06	7.23
Hg	200.6	5.85	2.80 ±0.03	6.69 ±0.11		
Pb	207.2	5.92	2.89 ±0.03	6.79 ±0.10	4.53 ±0.09	8.49
U	238.1	6.20	3.14 ±0.05	7.02 ±0.21	5.03 ±0.10	8.95

* Later considerations have shown that the mean detection energy was actually 85 Mev and not 90 Mev as stated in reference 1.

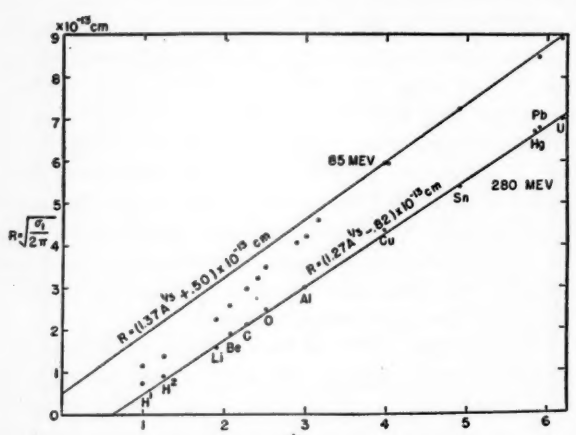

FIG. 4. "Effective radius" $R=(\sigma t/2\pi)^{\frac{1}{2}}$ plotted against $A^{\frac{1}{3}}$. 85-Mev results shown also for comparison.

passed through less than a mean free path of sample on the average and then reach the first crystal of the counter.

While the difference between the first two runs is not statistically significant, it is about what one would expect due to attenuation of the beam in the sample. Comparison of these runs with the third one shows that the background due to beam neutrons scattered around the sample into the paraffin is negligible compared with that due to diffracted neutrons reaching the first crystal. The latter is just the background measured for all runs.

The background correction thus measured ranged from less than one percent for light elements up to 10 percent for heavy elements. It was proportional to the total cross section of the sample used as would be expected if it were due to diffracted neutrons.

Another check on the accidental coincidence rate was made at the beginning of all runs by checking the linearity of the counting rate with beam intensity. This also proved to be a critical check on equipment performance and in addition showed that the factors of proportionality $R'(X)/I(X)$ and $R'(0)/I(0)$ must be the same.

4. *Counting*

Since long runs were needed to obtain cross-section values with reasonable accuracies, it was not feasible to repeat each run many times. Instead, they were broken up into short equal periods, so that any significant drifts could be noticed. $R(0)$ and $R(X)$ were calculated, both for each short run and for the entire group, together with their statistical error and standard deviation. In only one case did the fraction of short runs lying outside the standard error of the mean exceed the expected 30 percent. In that case, a monitor voltage drift was found, and the run discarded.

5. *Samples*

With the exception of lithium and uranium, all samples were 3 in. in diameter and about one mean free path long. Liquids were held in brass cylinders 3 in. in diameter of appropriate length, having $1\frac{1}{16}$-in. walls; empty cylinders were used for the blank run. In the case of lithium, the 2-in. square blocks already available were employed.[1] The uranium cylinder was about 2 in. in diameter, so that a smaller beam collimator was used, and an individual film exposure made to insure that it intercepted all of the beam.

Hydrogen was measured by a difference method, using pentane and carbon; this gave both σ_H and σ_C. The deuteron cross section was done by a similar method using water and heavy water; this gave σ_D and σ_O, using σ_H determined above. Such procedures lead to reduced accuracy, so that the purity, density, and dimensions of all these materials were checked. For all samples used, the thickness (in g/cm²) was established to better than one percent, in most cases to 0.2 percent.

6. *Scattering Correction*

For elements of high atomic weight, a small correction for neutron scattering is necessary. This was calculated in the manner of Cook *et al.*[1]

The values of the various constants are:

$$a=1.5 \text{ in.}, \quad k=3.94\times10^{13} \text{ cm}^{-1},$$
$$x_1=100 \text{ in.}, \quad x_2=480 \text{ in.}$$

It turns out fortuitously that the correction to the cross section in percent is just the value of the cross section in "barns," except for uranium, for which the correction was 1.5 percent.

IV. DISCUSSION OF RESULTS

The results are tabulated in Table I together with the 85-Mev results[1] for comparison. The errors are those computed from counting statistics alone.

At present, no nuclear model theories fit these data very well. The results of Cook *et al.* at 85-Mev show a nuclear transparency in terms of a[4] "mean free path within the nucleus." They also show agreement with the consequent prediction that the transparency should be greatest for elements of low atomic weight, as shown by the deviation from a straight line in Fig. 4. However, at 280 Mev, the transparent nucleus theory predicts a higher cross section for elements of high atomic weight than is actually observed.

The group wishes to thank Professor E. O. Lawrence for suggesting and encouraging the work, and members of the Laboratory for assistance.

[4] Fernbach, Serber, and Taylor, Phys. Rev. **75**, 1352 (1949).

Nuclear Cross Sections for 270-Mev Neutrons*

JAMES DEJUREN
Radiation Laboratory, Department of Physics, University of California, Berkeley, California
(Received June 16, 1950)

The total cross sections of eleven different elements were measured for the neutrons resulting from the bombardment of a 2-in. Be target by the 350-Mev protons of the 184-in. cyclotron. Bismuth fission ionization chambers served as the neutron detectors and had an estimated mean neutron detection energy of 270 Mev for the measurements. The attenuating materials were placed inside the concrete shielding and the monitor was placed to one side of the attenuators. The detector was placed about 30 ft. from the attenuators in line with the target and the attenuators. Collimators in the concrete shielding and a concrete block immediately behind the attenuating materials limited the detection of neutrons scattered through small angles to 20 min. "Poor" geometry cross sections of carbon, copper, and lead were measured by placing a shallow fission chamber behind attenuators of large cross-sectional area over which the neutron flux was uniform. The inelastic cross section is at least half the total for all three elements.

I. INTRODUCTION

NUCLEAR collision cross sections for 95-Mev neutrons[1] have been measured using bismuth fission ionization chambers for neutron detection. Since the chambers have excellent operating characteristics for high energy neutron detection, they were employed again in attenuation measurements of nuclear cross sections for the neutrons produced by the bombardment of a 2-in. beryllium target with the 350-Mev protons of the 184-in. cyclotron.

Measurements of the ratio of the cross section for bismuth fission relative to the $(n,2n)$ cross section for carbon show an increase by a factor of 3.5 in the energy interval between the two sets of measurements. The $C(n,2n)$ cross section is expected to be fairly flat in this interval, decreasingly by less than a factor of two; hence the fission chambers are more efficient neutron detectors for the 270-Mev neutrons than for the 90-Mev neutrons of the previous experiments.

These new measurements were undertaken to shed further light on the transparency of nuclei to neutrons of high energy. The model of the transparent nucleus,[2] developed by Fernbach, Serber, and Taylor, for nuclear cross-section measurements in the vicinity of 90 Mev gave consistent interpretations for the total cross sections[3] using $C(n,2n)$ and bismuth fission[1] for detection, which have estimated mean detection energies of 84 and 95 Mev, respectively, for the neutrons produced by "stripping" 190-Mev deuterons with a 0.5-in. Be target. Both sets of data, when interpreted by this model, gave as the relation of best fit for the radii: $R=1.38A^{\frac{1}{3}}\times10^{-13}$ cm.

Inelastic cross sections for four nuclei were measured in the earlier experiments employing bismuth fission detection at 95 Mev, and the ratios of inelastic to total cross sections obtained were in approximate agreement with the values predicted by the transparent model. The nuclear cross sections measured using "poor" geometry for the 270-Mev neutrons will represent lower limits to the true inelastic values, since inelastically scattered neutrons can lose large amounts of energy and still be above the bismuth fission threshold.

II. AVERAGE ENERGY OF DETECTION

The energy distribution of the neutrons knocked out of the 2-in. Be target by the 350-Mev protons has been measured by Hadley and by Fox *et al.*[4] The distribution of neutrons is peaked around 270 Mev with a width at half-maximum of 60 Mev. The ratio of the bismuth fission cross section to the $(n,2n)$ cross section of carbon for the 270-Mev neutrons relative to the ratio for the 90-Mev neutrons was measured by placing an $\frac{1}{8}$-in. thick, $1\frac{11}{16}$-in. diameter polystyrene disk in front of a fission chamber mounted in the collimated neutron flux outside the shielding. The number of fission pulses in the chamber was recorded for steady, 10-min. bombardments and the beta-activity resulting from the $(n,2n)$ reaction of carbon was counted on a standard Geiger-Müller counter. Bombardments were also made with brass plugs in the collimator to eliminate background effects at both energies. The ratio of the bismuth fission cross section to the $(n,2n)$ cross section of carbon increased by 3.56 ± 0.11 when the mean neutron energy was changed from 90 to 270 Mev.

Measurements were made inside the shielding of the ratio of the two cross sections by varying the radius of the 0.5-in. Be target and therefore the energy of the incident protons. A fission chamber and polystyrene disk were placed near the cyclotron tank wall behind 4 in. of lead which absorbed stray protons but allowed the neutrons to reach the two detectors. The results indicated that the ratio of the bismuth fission to the $C(n,2n)$ cross section increased almost linearly with proton energy and presumably, therefore, linearly with the average energy of the ejected neutrons. Since the carbon $(n,2n)$ cross section is theoretically fairly flat in

* This work was carried out under the auspices of the AEC.
[1] J. DeJuren and N. Knable, Phys. Rev. 77, 606 (1950).
[2] Fernbach, Serber, and Taylor, Phys. Rev. 75, 1352 (1949).
[3] Cook, McMillan, Peterson, and Sewell, Phys. Rev. 75, 7 (1949).
[4] Fox, Leith, Wouters, and MacKenzie, Phys. Rev. 80, 23 (1950), preceding paper.

the interval between 90 and 270 Mev, decreasing by less than a factor of two,[5] the bismuth fission cross section increases slowly over the energy spectrum of the neutrons obtained by bombarding the 2-in. Be target with 350-Mev protons. The energy distribution of neutrons detected by bismuth fission should correspond very closely to the measured distribution which peaks at 270 Mev and the contribution from any low energy tail that may exist in the distribution will be further depressed by the decrease of the fission cross section with lowered neutron energy.

III. COUNTER CHARACTERISTICS

The bismuth fission chambers employed in these measurements were used previously and described in the report containing the 95-Mev results[1] and by Wiegand.[6] The counting rates were, in general, between 10 and 20 c/sec. using the 270-Mev neutrons, roughly half the rate at 95 Mev. Operation was essentially equivalent at both energies as regards pile-ups, distribution of fission pulse heights, and stability of counters.

The effect of background on the chambers at 270 Mev was checked by placing brass plugs in the collimator through the concrete shielding. Without the plugs 24,000 fission counts were obtained on the detector, and none with the plugs inserted for steady 10-min. runs. Repeated measurements of cross sections gave differences that appear to be statistical and the errors assigned to the cross-section values are expressed in standard deviations.

IV. EXPERIMENTAL ARRANGEMENT

The diffraction scattering of 270-Mev neutrons by nuclei is peaked so strongly in the forward direction that considerable distance must be placed between absorber and detector in order to obtain good geometry with negligible corrections for the total cross sections

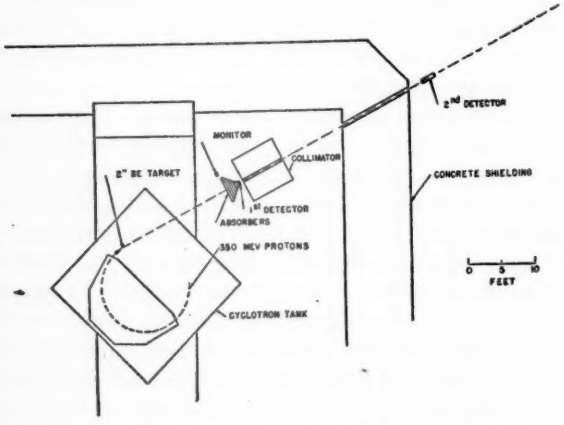

FIG. 1. Plan view of experimental arrangement.

[5] L. Baumhoff (private communication).
[6] C. Wiegand, Rev. Sci. Inst. 19, 790 (1948).

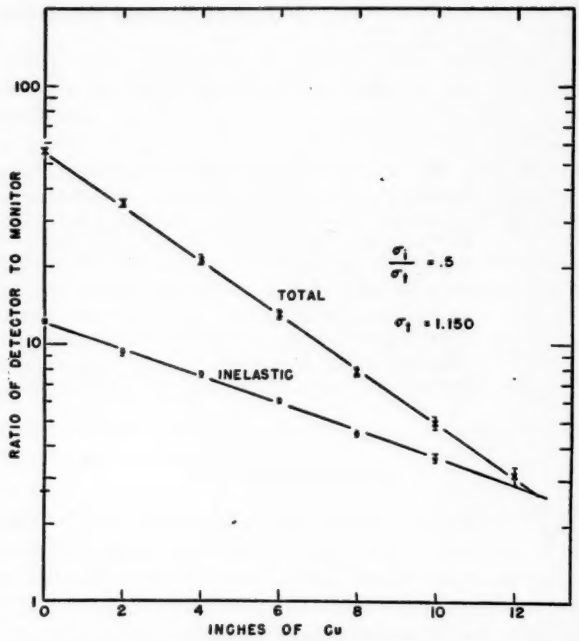

FIG. 2. Attenuation of 270-Mev neutrons in copper for "good" and "poor" geometries.

measured. Accordingly the monitor and absorber were placed inside the concrete shielding of the 184-in. cyclotron and the detector was placed outside the 10-ft. thick shielding in line with the target (Fig. 1). The distance between the absorber and the detector was 30 ft. An 8-ft. thick concrete block, in front of which the attenuating materials were placed, collimated the neutron beam to a 2-in. diameter (equal to the diameter of the bismuth-coated plates inside the fission chamber detector). Neutrons scattered through an angle greater than 20 min. could not activate the detector. The corrections for detection of neutrons diffracted into small angles, even for the heavy nuclei, are less than one-half of one percent of the measured cross sections.

The ratios of inelastic to total cross sections were measured with the "poor" geometry arrangement[1] used at 95 Mev. Slabs of attenuating material were placed in tront of a detector which was centered at the peak of the angular distribution of neutrons emerging through the cyclotron tank wall, in line with the collimator in fhe concrete block mentioned above. The detector placed ouside the concrete shielding simultaneously measured total cross sections as described above.

The neutron angular distribution from proton bombardment of the 2-in. Be target is much broader than the distribution resulting from "stripping" 190-Mev deuterons; the total angular width at half-maximum is about 50° for the 270-Mev neutrons (measured with bismuth fission detection). Thus it was possible to employ absorbers of greater cross-sectional area than in the former experiment and still have uniformity of neutron flux over the faces of the absorbers.

V. TEST MATERIALS

Practically the same attenuating materials used at 95 Mev were employed for the present measurements, except that longer lengths of absorber were used (because of the smaller cross sections) at 270 Mev. The hydrogen cross section was measured using pentane-carbon difference and the difference between the deuterium and hydrogen cross sections was measured directly by D_2O-H_2O difference. For most of the materials the ratios of detector to monitor were taken for several thicknesses of absorber. For both "good" and "poor" geometry the logarithm of the ratio decreased linearly as a function of absorber thickness, with no transition effects, over several mean free paths of length. Figure 2 contains the experimental data for copper.

VI. RESULTS

Table I contains the experimentally measured total cross sections. Comparison with the 95-Mev values[1] reveals a surprising constancy in the ratio of

$$\sigma_t(270\text{ Mev})/\sigma_t(95\text{ Mev})$$

for the elements from deuterium to tin.

Although the "poor" geometry cross sections measured at 270 Mev may not represent true inelastic cross sections, since neutrons may lose energy inelastic collisions and still be above the bismuth fission threshold, the ratios of inelastic to total cross section for the nuclei studied were higher than the ratios obtained at 95 Mev (Table II).

The values of σ_i/σ_t at 270 Mev indicate that the inelastic cross sections are at least half of the total cross sections.

Secondary or inelastic neutrons resulting from the interaction of an incident neutron with a nucleus would have lower energies and presumably a greater attenuation in matter than the primary neutrons. Consequently the logarithm of the attenuation should not be linear as a function of absorber thickness if neutrons degraded in energy comprise a large fraction of the detected neutrons. For lead the logarithm of the attenuation was linear through 3.5 mean free paths of absorber, but since the measured inelastic cross section is a slowly varying function of neutron energy this evidence is not a conclusive argument for calling the "poor" geometry measurement the inelastic collision cross section. But it is possible to state for lead that at 270 Mev the inelastic cross section is at least 80 percent of its value at 95 Mev. This is a smaller reduction than that observed for the total cross section.

VII. CONCLUSIONS

The total neutron collision cross sections measured by scintillation counters and bismuth fission chambers in

TABLE I. Total cross sections for 270-Mev neutrons measured with bismuth fission chambers.

Element	Atomic number Z	Mass number A	$A^{\frac{1}{3}}$	270 Mev total cross section $\sigma_t \times 10^{24}$ cm^2	$\frac{\sigma_t(270\text{ Mev})}{\sigma_t(95\text{ Mev})}$	Density g/cm^3
Hydrogen	1	1	1.00	0.037±0.002	0.52 ±0.03	
				0.039±0.002		
				0.038±0.0015(av.)		
Deuterium	1	2	1.26	0.057±0.003	0.55 ±0.03	
Beryllium	4	9	2.08	0.229±0.003	0.58 ±0.01	1.847
Carbon	6	12	2.29	0.287±0.007		1.580
				0.293±0.005		
				0.277±0.005		
				0.290±0.009		
				0.288±0.003(av.)	0.58 ±0.01	
Oxygen	8	16	2.52	0.372±0.007	0.56 ±0.01	
Aluminum	13	27	3.00	0.555±0.010		2.714
				0.552±0.019		
				0.561±0.024		
				0.555±0.008(av.)	0.56 ±0.01	
Copper	29	63.57	3.99	1.14 ±0.02		8.90
				1.15 ±0.02		
				1.145±0.0015(av.)	0.57 ±0.01	
Tin	50	118.7	4.92	1.87 ±0.003	0.59 ±0.01	7.28
Tungsten	74	183.9	5.69	2.56 ±0.07		19.3
				2.66 ±0.07		
				2.61 ±0.05(av.)		
Lead	82	207.2	5.92	2.83 ±0.04		11.34
				2.81 ±0.06		
				2.91 ±0.06		
				2.84 ±0.03(av.)	0.635±0.01	
Uranium	92	238.1	6.20	3.32 ±0.07		18.88
				3.30 ±0.07		
				3.35 ±0.08		
				3.31 ±0.07		
				3.28 ±0.12		
				3.12 ±0.09		
				3.29 ±0.03(av.)	0.67 ±0.01	
Deuterium-hydrogen	0	1	1.00	0.019±0.002	0.61 ±0.10	

TABLE II. Ratios of "poor" geometry to total cross section measured with bismuth fission chambers.

Element	σ_i/σ_t (270 Mev)	σ_i/σ_t (95 Mev)
Carbon	0.505±0.02	0.46±0.015
Copper	0.50 ±0.02	0.39±0.005
Lead	0.51 ±0.01	0.40±0.01
	0.49 ±0.02	

the neighborhood of 270 Mev agree well with each other from beryllium to lead. To obtain a reasonable fit with the data in terms of the transparent model of the nucleus,[2] the potential change experienced by the bombarding neutron when entering a nucleus must be dropped to zero. New measurements, to be published later, indicate the total cross sections for these elements are flat in the vicinity of 270 Mev.

The experimentally measured value of the total $n-p$ cross section for the 270-Mev neutrons is $38\pm1.5\times10^{-27}$ cm^2. The value predicted[7] by the model proposed by Christian and Hart, in which tensor forces are combined with a Yukawa potential, is 37×10^{-27} cm^2 at 280 Mev.[8]

The author wishes to express his appreciation to Dr. Burton J. Moyer, who sponsored the work; to Messrs. N. Knable and W. Knox, who assisted with the measurements involving beta-counting; and to the cyclotron crew for their cooperation in performing the experiments.

[7] R. S. Christian, private communication.

[8] The value published by R. S. Christian and E. W. Hart, Phys. Rev. 77, 441 (1950), is erroneous.

PHYSICAL REVIEW VOLUME 80, NUMBER 1 OCTOBER 1, 1950

Measurement of Absolute Electron Capture Rates with an Application to the Decay of Ni^{57}*

G. FRIEDLANDER, M. L. PERLMAN, D. ALBURGER, AND A. W. SUNYAR
Chemistry Department and Physics Department, Brookhaven National Laboratory, Upton, Long Island, New York

(Received June 9, 1950)

Observation of radiations from 36-hour Ni^{57} with a proportional counter and pulse-height analyzer shows that cobalt x-rays are emitted. Decay is divided equally between K-capture and emission of 845-kev positrons. The positron spectrum has the allowed shape. Coincidence measurements involving the comparison of Ni^{57} and Na^{22} give the result that both K-capture and positron emission in Ni^{57} are followed by emission of a 1.9-Mev gamma-quantum. In the K branch there are some 120-kev gamma-rays and possibly others of energy less than 0.5 Mev in cascade with the hard gammas.

I. INTRODUCTION

PULSE analyzers and proportional counters suitable for the detection and identification of x-rays[1,2] have recently been developed. With the aid of such an instrument, the quantitative investigation of electron capture processes is being undertaken. The first case studied is that of 36-hour Ni^{57}, which, it has been reported, emits 0.67- to 0.72-Mev positrons, 1.97-Mev gamma-rays, and some softer gamma-rays.[3,4] The observation[5] that the apparent yield of the reaction $Ni^{58}(\gamma, n)Ni^{57}$ as measured by β-counting was lower than expected from (γ, n) yields in neighboring elements led to the suspicion that Ni^{57} might decay by electron capture.

The Ni^{57} was produced by bombardment of iron with 30-Mev alpha-particles in the cyclotron of the Department of Terrestrial Magnetism of the Carnegie Institution. With the aid of carriers the nickel activity was chemically separated from the target and purified from other activities, especially those of cobalt, manganese, and copper, which may have been produced by alpha-particles, deuterons, or neutrons either in the iron or in its supporting materials. The treatment involved dissolution of the iron target in 12N HCl; oxidation of the iron to the ferric state and its removal from the solution by ether extractions; and precipitation then of nickel dimethylglyoxime in the presence of tartrate ion to keep ferric ion in solution and of carriers to "hold back" cobalt, manganese, and copper. The nickel precipitate was dissolved and reprecipitated under the above conditions twice more. The Ni^{57} with its 0.1 to 4 milligrams of nickel carrier was finally converted to NiS and mounted on thin aluminum foil.

II. X-RAY MEASUREMENTS

It was found that cobalt K x-rays are emitted in the decay of Ni^{57}. The counter for measurements of the energy and intensity of the x-rays was made from a four-inch diameter brass tube, 12 inches long, in which

* Work carried out under the auspices of the AEC.

[1] Curran, Cockroft, and Angus, Phil. Mag. 40, 53, 522, 631, 929 (1949).

[2] Bernstein, Brewer, and Rubinson, Nucleonics 6, No. 2, 39 (1950).

[3] G. T. Seaborg, and I. Perlman, Rev. Mod. Phys. 20, 585 (1948).

[4] F. Maienschein and J. L. Meem, Jr., Phys. Rev. 76, 899 (1949).

[5] M. L. Perlman, Phys. Rev. 75, 988 (1949).

was placed a coaxial tungsten wire 0.004 inch in diameter. Gas composition was 90 percent argon and 10 percent methane; the total pressure was one atmosphere. Radiations entered the sensitive space through a beryllium window 20 mg/cm² in thickness. This instrument was operated as a proportional counter, and it demonstrated a voltage plateau in total number of pulses above noise level. The sliding channel analyzer used to measure the pulse spectrum from the counter has been described.[2]

If monochromatic x-rays are allowed to enter the counter and if the number of pulses observed in each pulse height interval is plotted *versus* the pulse height, two maxima are observed in the resultant curve; one whose position corresponds in pulse height to the energy of the incident quanta and the other, much less pronounced, to an energy lower by the K x-ray energy of the principal counter gas. The observed peak position for Ni^{57} was compared with the peak positions for K radiations of manganese, copper, and cobalt produced in the decays of Fe^{55}, Zn^{65}, and Ni^{59}, respectively. It is clear (Fig. 1) that cobalt x-rays are emitted in the decay of Ni^{57}.

For one sample the decay of the x-ray peak was followed over a period of 12 days. Day-to-day corrections for rather small drifts of channel width and peak position were made by measurement of an Fe^{55} standard. After subtraction of a long-lived contribution amounting to approximately one percent of the original peak activity, the x-ray half-life was found to be 38 ± 2 hours.

The absolute electron capture rate for a sample was determined in the following manner. The area under the pulse height distribution curve was measured. A background originating probably from Compton electrons in the counter was subtracted. The net area remaining is equal to the K x-ray counting rate multiplied by the size of the pulse-height acceptance interval or channel width. The latter quantity was obtained by two independent methods. One was essentially to put

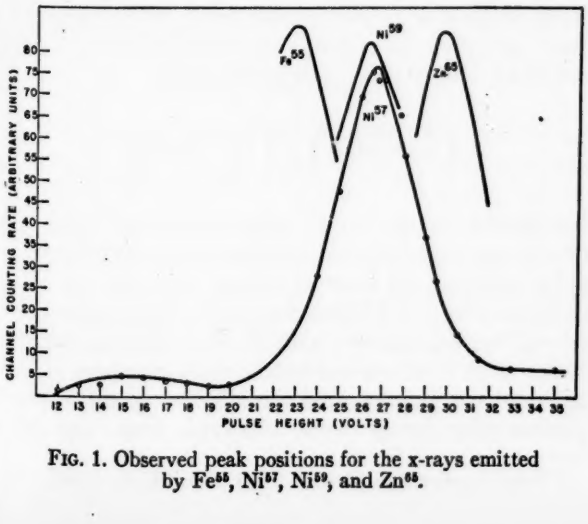

FIG. 1. Observed peak positions for the x-rays emitted by Fe^{55}, Ni^{57}, Ni^{59}, and Zn^{65}.

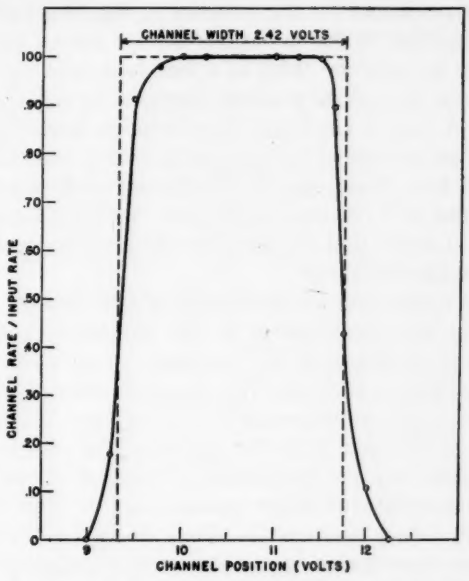

FIG. 2. Measurement of channel width of pulse-height analyzer.

into the analyzer pulses of uniform height from a generator and to see over what range in channel position the pulses were accepted. Figure 2 shows the ratio of the observed channel rate to input rate as a function of channel position. The channel width was taken as the width of a rectangle having the same height and area as the curve. The second method was to set the measured area under a curve for Fe^{55} (no gamma-rays) equal to the total counting rate observed; i.e., all pulses above noise, multiplied by the channel width. The two width measurements agreed within one percent. For the Ni^{57} sample the counting rate thus calculated was converted to an absolute capture rate by corrections for geometrical efficiency, absorption in air and in the beryllium window, fluorescence yield,[6] and counter efficiency. The last quantity, about 0.90 for the counter used, is simply the fraction of the x-rays absorbed by the counter gas in the average path. For quanta in this energy range absorbed in argon, processes other than photoelectric ones may be neglected.

III. BETA- AND GAMMA-RAY MEASUREMENTS

Absorption of the radiations with detection by end-window and windowless counters demonstrated the presence of a component, probably Auger electrons, completely removed by aluminum 0.2 mg/cm² thick. The aluminum end point of the positron activity was at 263 mg/cm², equivalent to 0.78 Mev as determined by Feather analysis[7] with Na^{22} (0.55 Mev) as the standard. A small x-ray contribution to the Geiger counting rate was corrected for with the aid of the result of a beryllium absorption experiment. Measurements with a mica-window counter in a magnetic field

[6] Steffen, Huber, and Humbel, Helv. Phys. Acta 22, 167 (1949).
[7] Macklin, Lidofsky, and Wu, Phys. Rev. 78, 318A (1950).

gave no evidence for the presence of negative electrons. Examination of the radiations from a source approximately 0.5 mg/cm² thick in a lens-type beta-ray spectrometer showed the positron energy to be 0.845±0.010 Mev. A line of electrons, very weak in intensity (less than one percent of the positron activity) was observed at 114 kev; these may be interpreted as K-conversion electrons of a 120-kev gamma-ray. A Fermi-Kurie plot (Fig. 3) shows that the positron spectrum is simple and has an allowed shape.

The source was not sufficiently active to allow detection in the spectrometer of the gamma-rays accompanying the decay of Ni^{57} by means of photo-electrons ejected from a radiator. The energy of some of the Ni^{57} gamma-rays was determined to be between 1.7 and 2.2 Mev by the facts that they produce photo-neutrons in beryllium but not in deuterium. The half-thickness for the absorption of these gamma-rays in lead is 15.7 g/cm², which corresponds to an energy of 2.0 Mev. Measurements were made also with a variably biased scintillation counter; by comparison of the bias curves for the hard gamma-rays of Ni^{57}, Pr^{144} (2.19 Mev),[8] Sb^{124} (1.7 Mev),[3] and Co^{60} (1.17 and 1.33 Mev),[3] the energy of the Ni^{57} gamma-rays was determined to be 1.9±0.1 Mev, in agreement with an earlier measurement.[4] Absorption in lead of the Ni^{57} gamma-rays with scintillation counter detection demonstrated that, in addition to the 1.9-Mev gamma-rays and annihilation radiation, softer radiations are also present whose absorption characteristics are compatible with an energy of 120 kev. The presence of still another low energy component cannot be excluded.

The beta- and gamma-activities were followed separately for 10 to 15 days. They decayed with half-lives of 36.2±1 and 36.6±1 hours, respectively. In the spectrometer it was determined that the 114-kev line decays with approximately the same half-life as the positron activity.

For the same Ni^{57} sample for which the electron capture rate was measured, an absolute beta-disintegration rate was determined by correction[9] of the measured Geiger activity for solid angle, absorption in air and counter window, backscattering, coincidence loss, and x- and gamma-activities. The ratio of positron decay rate to the simultaneous K-capture rate is 1.0±0.1.

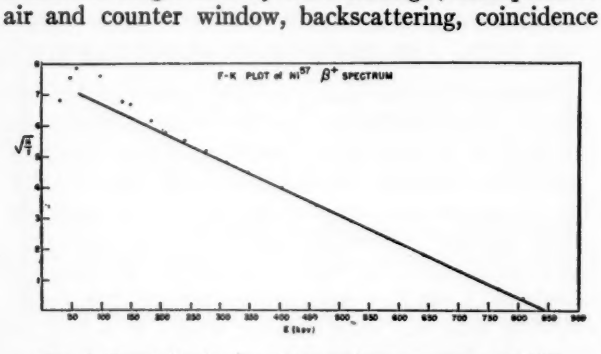

FIG. 3. Fermi-Kurie plot of the positron spectrum of Ni^{57}.

IV. COINCIDENCE MEASUREMENTS

Coincidences were observed from Ni^{57} between counts in a mica-window G-M tube and in a scintillation counter biased so as not to register annihilation radiation. These coincidences, corrected for chance events, confirm the observation of Maienschein and Meem[4] that a hard gamma-ray follows positron emission. This is presumably the 1.9-Mev ray previously mentioned. The coincidence rate per hard gamma for Ni^{57}, corrected for a few $X-\gamma_h$-coincidences, was compared in a fixed geometry with the same quantity for Na^{22}, which decays by emission of a positron followed by one 1.3-Mev gamma-quantum.[10] The ratio

$$\left(\frac{\beta-\gamma_h}{\gamma_h}\mathrm{Na}^{22}\right)\Big/\left(\frac{\beta-\gamma_h}{\gamma_h}\mathrm{Ni}^{57}\right)$$

is 1.95. Here γ_h represents the hard gamma-counting rate, and $\beta-\gamma_h$ the positron-hard gamma-coincidence rate. The result indicates that in the decay of Ni^{57} there is a hard gamma-quantum following both the positron emission and the electron capture processes.

Coincidences were measured between a scintillation counter biased as above and one whose bias was set close to noise level. The ratio

$$\left(\frac{\gamma-\gamma_h}{\gamma_h}\mathrm{Na}^{22}\right)\Big/\left(\frac{\gamma-\gamma_h}{\gamma_h}\mathrm{Ni}^{57}\right)$$

was found to be 1.2; it should have been approximately 2.0 if the only gammas other than the hard ones were from the annihilation of the positrons. This observation of gammas in cascade is in agreement with the work previously cited.[4] The number of gamma-rays in cascade was not determined because the efficiency of the scintillation counter for the softer gammas was not known. An increase in the bias of the lower biased counter made it possible to cut off the softer nuclear gamma-rays, although sensitivity to annihilation radiation remained. Under this condition the ratio

$$\left(\frac{\gamma-\gamma_h}{\gamma_h}\mathrm{Na}^{22}\right)\Big/\left(\frac{\gamma-\gamma_h}{\gamma_h}\mathrm{Ni}^{57}\right)$$

was found to be 2.0 in good agreement with the $(\beta-\gamma_h)/\gamma_h$ experiment. It is thus established that the softer gamma-rays have an energy less than 0.5 Mev, as Maienschein and Meem suggested. The results of the $(\gamma-\gamma_h)/\gamma_h$ experiments with the two different counter biases show that approximately equal numbers of soft gamma-hard gamma- and annihilation quantum-hard gamma-coincidences were observed from the Ni^{57}

[8] D. E. Alburger *et al.*, Brookhaven National Laboratory Report 39 (AS-3), 17 (1949).
[9] B. P. Burtt, Nucleonics 5, No. 2, 28 (1949).
[10] Good, Peaslee, and Deutsch, Phys. Rev. 69, 313 (1946).

sample at the lower bias. Thus, since the counting efficiency for the soft nuclear gammas certainly does not exceed that for annihilation radiation, it may be concluded that Ni^{57} emits at least as many soft gamma-quanta as it does positrons. Some of these soft gamma-rays observed may be the 120-kev gammas whose conversion electrons were observed in the beta-ray spectrometer.

In an attempt to ascertain whether gamma-rays are in cascade in the positron branch of the Ni^{57} decay, coincidences were measured for Ni^{57} and for Na^{22} between a G-M tube and a scintillation counter biased just above noise level. The counters were shielded from each other by a one-inch thickness of lead. Measurements were made both with and without a beryllium absorber for the positrons in front of the mica window of the G-M tube, so that it was possible to correct for gamma- and x-ray counts in the G-M tube and for $X-\gamma$-coincidences. The ratio

$$\left(\frac{\beta-\gamma}{\beta}\mathrm{Ni}^{57}\right)\Big/\left(\frac{\beta-\gamma}{\beta}\mathrm{Na}^{22}\right)$$

was found to be 1.1. The $(\gamma-\gamma_A)/\gamma_A$ result shows that the annihilation quanta and softer gammas of Ni^{57} contribute about equally to the $\gamma-\gamma_A$ coincidence rate and therefore equally to the single rate in the low biased counter. It would thus appear from the value 1.1 for the ratio

$$\left(\frac{\beta-\gamma}{\beta}\mathrm{Ni}^{57}\right)\Big/\left(\frac{\beta-\gamma}{\beta}\mathrm{Na}^{22}\right)$$

that relatively few of the soft gammas of Ni^{57} are in the positron branch of the decay. In fact, because the 1.9-Mev Ni^{57} quanta are counted approximately 5 percent more efficiently than the 1.3-Mev Na^{22} quanta, the ratio should be greater than 1.0 even if no gammas are in cascade in the positron branch of the Ni^{57} decay. Thus it may be concluded that very few, if any, of the positrons are followed by a gamma-ray cascade; this result agrees with the simple shape of the Fermi-Kurie plot for the positrons.

IV. DISCUSSION

For a beta-transition of total energy $m_0c^2+0.84$ Mev the ratio of K-capture to positron emission processes should be 0.8 according to the Fermi theory.[6,11] The experimental value for the over-all ratio of K-capture to positron emission is 1.0. This difference, which we believe to be significant, together with the observation of gamma-gamma-coincidences outside of the main positron branch in the Ni^{57} decay, points to the existence of a low energy transition occurring principally by electron capture. This transition would need to account for approximately one-sixth of all the transitions in order to bring theory and experiment into agreement. From the fact that the number of gamma-hard gamma-coincidences approximately equals the number of annihilation quantum-hard gamma-coincidences it may be inferred that several soft gamma-quanta are in cascade following the low energy K-capture transition.

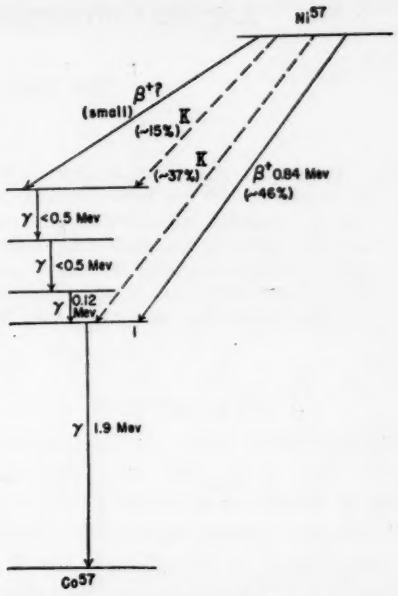

FIG. 4. Partial decay scheme of Ni^{57}. In the cascade, the relative position of the 0.12-Mev gamma-ray is not fixed and the number of low energy gamma-rays may be greater than three.

The data are in agreement with the partial decay scheme given in Fig. 4. This scheme, however, does not seem to be compatible with the assignment of spins and parities in accordance with the selection rules. Additional work on details of the Ni^{57} decay is needed for the determination of a complete scheme.

We are indebted for the cyclotron irradiations to Dr. D. Cowie and Dr. P. Abelson. The gamma-ray energy determinations by the photo-neutron and the biased scintillation counter methods were carried out by Mr. E. der Mateosian. Miss Elizabeth Wilson gave valuable assistance in making some of the measurements.

[11] C. Møller, Physik. Zeits. Sowjetunion 11, 9 (1937).

Angular Correlation in the Reaction $F^{19}(p,\alpha)O^{16*}(\gamma)O^{16}$

WAYNE R. ARNOLD*
State University of Iowa, Iowa City, Iowa
(Received June 12, 1950)

The angular correlation of alpha-particles and gamma-rays from the 340-kev resonance in the reaction $F^{19}(p,\alpha)O^{16*}(\gamma)O^{16}$ has been observed. This correlation is very strong and allows a unique identification with a correlation calculated for this transition by the method of Hamilton. If we assume even parity and zero spin for the ground state of O^{16}, even parity and spin ½ for the ground state of F^{19}, this experiment allows the following assignments of spin and parity: 13.24-Mev excited state of Ne^{20}, spin 1, even parity; 6.14-Mev excited state of O^{16}, spin 3, odd parity. Since no pairs have been observed from this resonance reaction, we can also assign even parity to the 6.0-Mev pair producing state of O^{16}.

I. INTRODUCTION

THE 340-kev resonance in the reaction $F^{19}(p,\alpha)O^{16*}(\gamma)O^{16}$ has a high yield and a spherically symmetric angular distribution of the 1.8-Mev alpha-particles and 6.14-Mev gamma-rays.[1] There is also strong evidence that there is no branching in the decay of the excited state of Ne^{20} formed, so that each alpha-particle has an associated gamma-ray.[1,2] For these reasons R. E. Holland suggested that this would be a good reaction to use in an attempt to extend to nuclear reactions the theory which Hamilton[3] applied to gamma-gamma cascade transitions and Falkoff[4] to beta-gamma transitions. A similar application to nuclear reactions has been made by Feld[5] and by Rose and Wilson[6] on the reaction $B^{10}(n,\alpha)Li^{7*}(\gamma)Li^{7}$.

The measured angular correlation in the fluorine reaction was very strong, so the shape of the resulting intensity *vs.* angle curves were compared with the theoretically expected curves instead of the usual procedure of calculating coefficients of $\cos^n\theta$.

II. THEORY

The spherically symmetric angular distribution of both alpha- and gamma-particles with respect to the beam means that one of the following possibilities is true: (1) the reaction proceeds with S-wave protons; (2) the compound nucleus Ne^{20*} has spin zero; (3) the alpha-particles are emitted with zero angular momentum. The last possibility is ruled out by the fact that the angular correlation of alpha-particles in coincidence with gamma-particles is not symmetric. Cases 1 and 2 are covered by the theory outlined below, which requires random orientation of the spin axes of the Ne^{20*}.

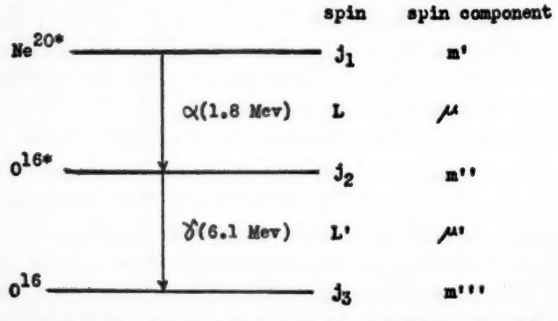

FIG. 1. Decay scheme of the excited state of Ne^{20} produced from F^{19} bombarded by 340-kev protons. The notations to the right are the ones used in the text.

The decay scheme of the Ne^{20*} is shown in Fig. 1, with the notation to be used. It will also be convenient to define $\Delta j = j_1 - j_2$ and $\Delta j' = j_2 - j_3$.

If we start with a given state of Ne^{20*}, i.e. given j_1 and m' values, and go by alpha-emission to a particular state of O^{16*} with given j_2 and m'', then the probability function $f_\mu{}^L(\theta_1)$ for finding an alpha-particle at an angle θ_1 with respect to the direction of m' and m'' will be given by the spherical harmonic $|Y_\mu{}^L|^2$. If we now have a transition by photon emission from the j_2, m'' state to the O^{16} state with j_3 and m''', the probability of finding the photon at an angle θ_2 with respect to the m', m'' direction can be shown from Hamilton's work[3] to be given by $F_\mu{}^{L'}(\theta_2)$ defined by

$$F_\mu{}^{L'}(\theta)=\left|\frac{\partial}{\partial\theta}Y_\mu{}^{L'}(\theta,\varphi)\right|^2+\left|\frac{1}{\sin\theta}\frac{\partial}{\partial\varphi}Y_\mu{}^{L'}(\theta,\varphi)\right|^2.$$

(This function is denoted by f in Hamilton's paper.) The functions F for L' up to 5 are given in Table I. The probability function, W, for the transition involving only the particular m values, and for the alpha- and gamma-particles being found at θ_1 and θ_2 will be the product of the individual probabilities. If we now take into account the fact that the Ne state may have several values of m' possible, and each may decay to one or more states with different m'', the probability functions, f, for the alpha-particle to be found at a particular angle must be multiplied by weighting factors, g, corresponding to the relative probabilities of decay from and to the states involved and then summed over all m-values. The same will be true of the gamma-ray transition. Because there is no preferred direction in the laboratory for the orientation of the Ne spin axes, and

* Now at Los Alamos Scientific Laboratory, Los Alamos, New Mexico.

[1] Van Allen and Smith, Phys. Rev. 59, 501 (1941).
[2] Bureham and Devons, Proc. Roy. Soc. 173, 555 (1939).
[3] D. R. Hamilton, Phys. Rev. 58, 122 (1940).
[4] D. L. Falkoff, Thesis, University of Michigan, April 1948.
[5] B. T. Feld, Phys. Rev. 75, 1618 (1949).
[6] B. Rose and A. R. W. Wilson, Phys. Rev. 78, 68 (1950).

TABLE I. Coefficients of powers of $\cos\theta$ for the functions $F_\mu{}^L(\theta)$.

$F_\mu{}^L$	const.	$\cos^2\theta$	$\cos^4\theta$	$\cos^6\theta$	$\cos^8\theta$	$\cos^{10}\theta$
1/0	2	−2				
1/1	1	1				
2/0	0	6	−6			
2/1	1	−3	4			
2/2	1	0	−1			
3/0	12	−132	420	−300		
3/1	1	111	−305	225		
3/2	10	−30	110	−90		
3/3	15	−15	−15	15		
4/0	0	180	−1020	1820	−980	
4/1	9	−153	885	−1463	784	
4/2	2	98	−450	742	−392	
4/3	7	−7	105	−217	112	
4/4	14	−28	0	28	−14	
5/0	180	−5220	47880	−148680	185220	−79380
5/1	6	4878	−42420	128268	−156114	66150
5/2	168	−3528	28560	−79632	92232	−37800
5/3	63	1827	−11970	32382	−36477	14175
5/4	126	378	1260	−7308	8694	−3150
5/5	315	−945	630	630	−945	315

These unnormalized functions have the proper relative weights within each L group.

because the same state m'' is involved in both transitions, we can simplify the expression for W by choosing either θ_1 or θ_2 as the preferred direction and expressing W as a function of $\theta=|\theta_1-\theta_2|$. This will eliminate interference terms, and give us the two expressions:

$$W(\theta)=\sum_{m''}\Big(\sum_{m'} {}^{\Delta jL}g_{m'm''}f_\mu{}^L(0)\Big)\Big(\sum_{m'''} G^{\Delta j'L'}_{m''m'''}F_{\mu'}{}^{L'}(\theta)\Big), \quad (1)$$

$$W(\theta)=\sum_{m''}\Big(\sum_{m'} {}^{\Delta jL}g_{m'm''}f_\mu{}^L(\theta)\Big)\Big(\sum_{m'''} G^{\Delta j'L'}_{m''m'''}F_{\mu'}{}^{L'}(0)\Big), \quad (2)$$

where the functions g and G are weighting factors for transitions between different m values and are given by

$$ {}^{\Delta jL}g_{m'm''}=|(\psi_{m'}\hat{\imath}_1|\psi_\mu{}^L\psi_{m''}\hat{\imath}_2)|^2,$$
$$G^{\Delta j'L'}_{m''m'''}=|(\psi_{m''}\hat{\imath}_2|\psi_{\mu'}{}^{L'}\psi_{m'''}\hat{\imath}_3)|^2.$$

Limited tables of these matrix elements g and G can be found in books on atomic spectra[7] but those for high L values must be calculated.

Equations (1) and (2) can be simplified further for the special conditions of the $Ne^{20*}-O^{16*}-O^{16}$ transitions. For Eq. (1): $f_\mu{}^L(0)=\delta_{m'm''}$; j_3 is assumed to be zero, so $m'''=0$ and the factors $G=1$. This gives

$$W(\theta)=\sum_{m'} {}^{\Delta jL}g_{m'm'}F_{m'}{}^{L'}(\theta). \quad (1a)$$

The simplification for Eq. (2) arises because $F_{\mu'}{}^{L'}(0)$ $=\delta_{m'',\pm1}$ for $m'''=0$ and the factors G are again equal to unity. This gives

$$W(\theta)=\sum_{m'} ({}^{\Delta jL}g_{m',+1}f^{L}_{m'-1}(\theta)+{}^{\Delta jL}g_{m',-1}f^{L}_{m'+1}(\theta)). \quad (2a)$$

TABLE II. Unnormalized correlation coefficients for $W(\theta)$.

$j_1-j_2-j_3$	L	const.	$\cos^2\theta$	$\cos^4\theta$	$\cos^6\theta$	$\cos^8\theta$	$\cos^{10}\theta$
0−1−0	1	1	−1				
0−2−0	2	0	1	−1			
0−3−0	3	1	−11	35	−25		
0−4−0	4	0	9	−51	91	−49	
0−5−0	5	1	−29	266	−826	1029	−441
1−1−0	0	1					
	1	1	1				
1−2−0	1	1	1				
	2	1	−3	4			
1−3−0	2	5	6	5			
	3	1	111	−305	225		
1−4−0	3	9	−9	39	−7		
	4	9	−153	855	−1463	784	
1−5−0	4	13	44	−210	364	−147	
	5	1	813	−7070	21378	−26019	11025

Since Eqs. (1a) and (2a) involve different g values and different functions f and F, the correlations $W(\theta)$ were calculated both ways as a check on the numerical computations. In the calculations constant factors in $W(\theta)$ were neglected since they do not affect the usefulness of the results and the final functions may be normalized, if desired, by integration. The unnormalized coefficients of the various powers of $\cos\theta$ for the different $W(\theta)$ are given in Table II, and the corresponding normalized curves in Figs. 5–7, where they are compared with the experimental results. There is a separate $W(\theta)$ for each value of the angular momentum L possible in a transition between states of given j values, however parity considerations separate these L values into even and odd groups, and rapidly decreasing barrier penetrabilities for higher annular momenta means that only the lowest even and odd angular momenta need be considered. The different $W(\theta)$ curves are distinguished by the notation $j_1-j_2-j_3$. The transitions for $j_1=0$ have only one value of L possible for each value of j_2 and are plotted together in Fig. 5. Transitions for $j_1=1$ have both even and odd values of L possible, and are separated into two groups in Figs. 6 and 7 corresponding to even and odd L. Only values of j_1 equal to 0 or 1 were used since the spin of F^{19} is $\frac{1}{2}$, the spin of the proton is $\frac{1}{2}$, and as has been indicated, the symmetric angular distribution means that $j_1=0$ or only S-wave protons are involved.

III. APPARATUS

The 350-kev protons used were obtained from the 500-kev Cockcroft-Walton linear accelerator recently constructed at the University of Iowa and described

[7] E. U. Condon and G. H. Shortley, *The Theory of Atomic Spectra* (Macmillan Company, New York, 1935), p. 76.

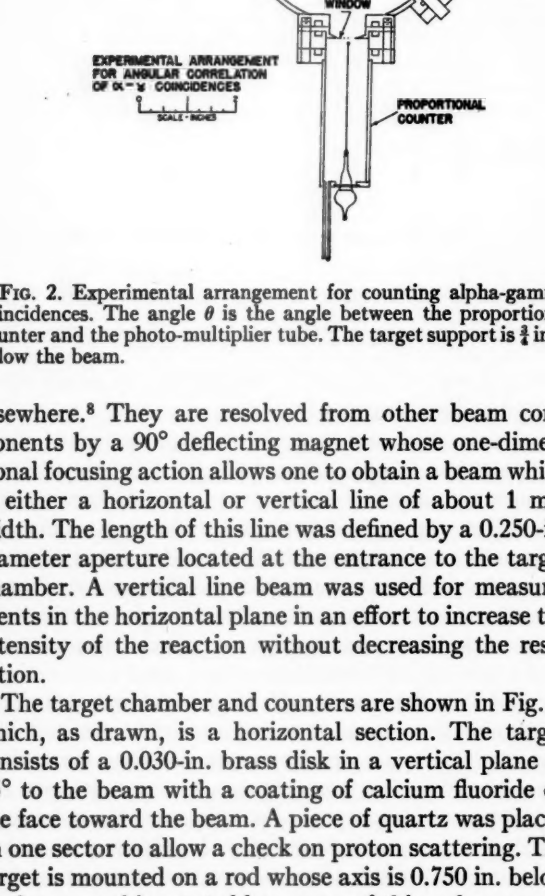

FIG. 2. Experimental arrangement for counting alpha-gamma coincidences. The angle θ is the angle between the proportional counter and the photo-multiplier tube. The target support is $\frac{3}{4}$ inch below the beam.

elsewhere.[8] They are resolved from other beam components by a 90° deflecting magnet whose one-dimensional focusing action allows one to obtain a beam which is either a horizontal or vertical line of about 1 mm width. The length of this line was defined by a 0.250-in. diameter aperture located at the entrance to the target chamber. A vertical line beam was used for measurements in the horizontal plane in an effort to increase the intensity of the reaction without decreasing the resolution.

The target chamber and counters are shown in Fig. 2, which, as drawn, is a horizontal section. The target consists of a 0.030-in. brass disk in a vertical plane at 45° to the beam with a coating of calcium fluoride on the face toward the beam. A piece of quartz was placed on one sector to allow a check on proton scattering. The target is mounted on a rod whose axis is 0.750 in. below the beam, and is rotated by means of this rod to expose a new area of calcium fluoride whenever the carbon deposited by the beam action becomes thick enough to interfere with alpha-particles escaping from the target. The walls of the chamber are of 0.125-in. brass which scatters about 15 percent of the 6.14-Mev gamma-rays. The top of the chamber is made of Lucite. The alpha-detector is a proportional counter with a 0.005-in. tungsten wire in the center of a 0.874-in. I.D. brass tube. It was operated using Iowa City illuminating gas (which is 80 percent methane, nine percent nitrogen, six percent ethane, and the rest are hydrocarbons of higher molecular weight) at a pressure of 2.6 cm of mercury, and with a voltage of 1050 volts positive on the center wire.

Between the proportional counter and the target chamber, and 6.2 cm from the target, is a 1.12-cm diameter window covered with cast films of Formvar lacquer. This window was made of such a thickness that the alpha-particles from the reaction could penetrate it while the scattered protons were for the most part excluded. Two films whose thickness was tested by use of polonium alphas were used in the window, as it was easier to find a combination of two films which would have the proper stopping power. These films were slightly irregular in thickness, and allowed a few protons to get into the propertional counter; however it was possible to discriminate electrically against almost all of the proton pulses.

The gamma-ray detector used was an RCA 5819 photo-multiplier tube with a 2-cm cube of anthracene taped to the front surface. Aluminum foil was used to shield the tube from room light. This detector is capable of rotation in two planes. In Fig. 2 it is rotating in a horizontal plane by means of a support pivoted on an axis on the bottom of the target chamber. An auxiliary bracket mounts on the bottom of the chamber and provides an axis of rotation coaxial with the beam. This allows an angular correlation to be taken in a plane through the target and proportional chamber, and perpendicular to the beam. When rotated in the horizontal plane the anthracene is 5.6 cm from the beam spot on the target, and when rotated in the vertical plane it is 7.2 cm away.

The photo-multiplier tube is in the stray field from the 90° magnet and its gain is sensitive to small magnetic fields. This change in gain is different for different orientations of the tube with respect to the stray field. For a constant pulse height discriminator setting this leads to an over-all efficiency for the gamma counter, ϵ_γ, which is a function of angle. This effect was reduced by magnetic shielding around the photo-multiplier tube, and between the tube and the magnet. In an attempt to keep ϵ_γ independent of angle the discriminator bias was set at different values for the different angles. The values used for the discriminator setting were obtained by the following procedure: for each setting of θ a Co^{60} source was placed in front of the counter and the change in discriminator bias found which would give the same counting rate with the magnet on as was obtained with the magnet off. The final results were then calculated so that the effect of efficiency changes in the gamma-counter were eliminated.

Pulses from each of the detectors were fed through cathode-follower circuits into amplifiers which give output pulses of uniform height and shape. These output pulses were used to drive a scaling circuit for each amplifier, and also to drive a channel in the coincidence circuit.

The coincidence circuit is similar to Atomic Instrument Model 502 Coincidence Analyzer, except that it has only two channels. The output of the coincidence circuit drives a third scalar. Since the alpha-particle pulses come at varying times after the alpha-particle has entered the proportional counter (due to varying collection times for the electrons formed in the ion's path) the formed pulse for the gamma-ray (in the coin-

[8] Submitted to Rev. Sci. Inst.

TABLE III. Experimental data.

Angle	N_α $\times 10^{-3}$	N_γ $\times 10^{-3}$	N_γ/N_α	N_c	N_a	N_{ct}	N_{ct}/N_γ $\times 10^4$
			Horizontal plane				
220	1923	499	0.259	140	34	106	21
210	1692	487	0.288	143	29	114	23
200	1586	456	0.288	160	25	135	30
190	1966	552	0.282	300	38	262	47
180	4545	1543	0.339	779	85	694	45
170	2845	880	0.309	462	53	409	46
165	1444	434	0.303	209	22	187	43
160	1996	627	0.314	214	26	188	30
150	5324	1664	0.313	377	72	305	18
145	1476	415	0.281	109	21	88	21
140	3765	1065	0.283	273	70	203	19
135	3787	1113	0.294	271	62	209	18
130	5626	1671	0.297	415	100	315	19
120	6822	2153	0.316	537	108	429	20
110	4387	1364	0.312	322	70	252	18
105	1271	424	0.333	74	19	55	13
100	3184	1009	0.317	154	57	97	10
90	6492	1998	0.308	211	101	110	6
			Vertical plane				
180	4248	732	0.172	438	109	329	45
170	4037	668	0.165	429	94	335	50
160	4037	711	0.176	357	100	257	36
150	4009	626	0.156	211	88	123	20
140	3659	552	0.151	168	71	97	18
130	4027	636	0.158	216	90	126	20
120	4210	698	0.166	266	103	163	23
110	3801	662	0.174	228	88	140	21
100	3633	640	0.176	187	81	106	17
90	2734	475	0.174	82	45	37	8

cidence circuit) was made almost three times as long as that for the alpha-particle so that true coincidences would be sure to overlap in time. The resolving time of the coincidence circuit was measured by counting accidental coincidences between gamma-rays from a Co^{60} source and pulses from the alpha-counter amplifier driven by a pulse generator.

IV. PROCEDURE

The energy of the proton beam was set by slowly increasing the high voltage until it was just above the value for which gamma-rays appeared from the 340-kev resonance. The target was then rotated until the small quartz plate was in the path of the beam. The bias on the alpha-counter amplifier was then set so that pulses from the scattered protons entering the chamber were almost entirely discriminated against. The beam was then allowed to strike the calcium floride. The intensity of the beam was adjusted so that the alpha-counting rate was 500–700 counts/sec. The discriminator on the photo-multiplier tube amplifier was set at the predetermined value for the angle being used, and a run of 200–300 sec. made. The angle θ, the time, and the total number of alpha-, gamma-, and coincidence counts were recorded. Runs were made at 5° to 10° intervals, and measurements between 90° and 180° in the horizontal plane of Fig. 2 were repeated several times. A single set of runs was made in the plane perpendicular to the beam. Since the theory predicts only even powers of $\cos\theta$, one quadrant is sufficient to determine the shape of the curve. Runs were made for angles up to 220° in the horizontal plane to check the predicted symmetry of the curve about 180°.

V. RESULTS

The measured value of the resolving time (0.52 μsec.) for the coincidence circuit was used to calculate the number of random coincidences that would be expected in each individual run. The value obtained for these random coincidences is too low as they depend upon the instantaneous product of the counting rates in the two counters and these counting rates varied with time due to changes in beam strength and beam location on the defining aperture. However, the ratio of true to accidental coincidences was greater than unity for all angles except 90° and the uncertainty due to fluctuations up to a factor of two in beam intensity will be less than the statistical probable error.

The number of scattered protons counted as alpha-particles was about one percent of the alpha-particles counted, and this percentage was almost a constant for all runs. Since this, in effect, gives a small and almost constant factor in the efficiency of the alpha-counter, the effect it has upon the shape of the correlation curve was negligible.

The following were each totaled for all the runs at a given angle: N_α, the total number of alpha-counts; N_γ, total gamma-counts; N_c, total coincidence counts; and N_a, total calculated accidental coincidences for each individual run. These totals, and values obtained from

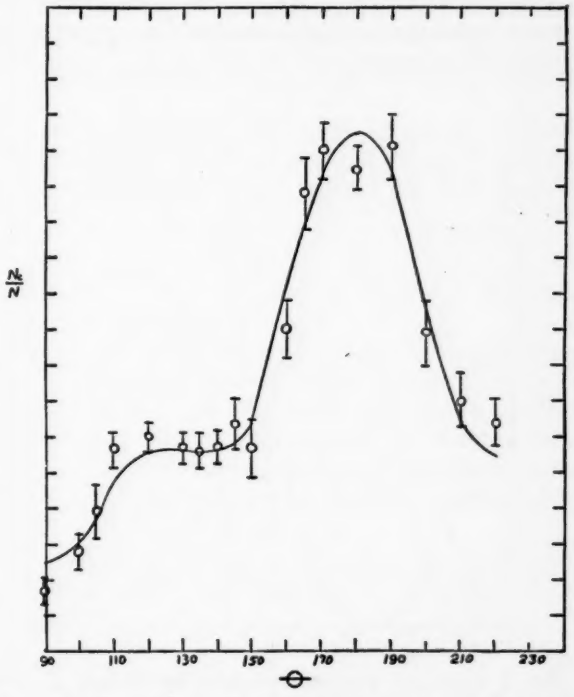

FIG. 3. Observed angular correlation for θ, the angle between alpha and gamma counted in coincidence, lying in a plane containing the beam. The solid line is the curve 1—3—0 from Fig. 7 modified for 40° resolution.

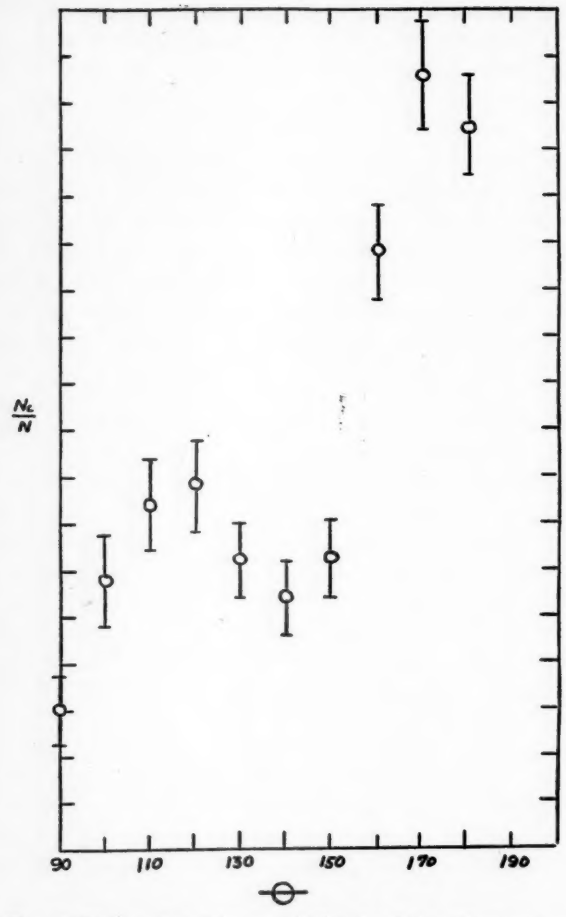

FIG. 4. Observed angular correlation for θ in a plane perpendicular to the proton beam. The low point at 180° is due to finite resolution in the dimension perpendicular to the plane of θ.

them are shown in Table III. The total number of coincidences minus the total number of accidental coincidences gives the number of true coincidences N_{ct}. If ϵ_α and ϵ_γ are the over-all efficiencies of the two counters, and N is the total number of disintegrations in the target in the time interval considered, then:

$$N_{ct}=N\epsilon_\alpha\epsilon_\gamma W(\theta)=N_\alpha\epsilon_\gamma W(\theta)=N_\gamma\epsilon_\alpha W(\theta).$$

The ratio N_{ct}/N_γ will then give a number proportional to the desired $W(\theta)$ regardless of changes in ϵ_γ provided only that ϵ_α remains constant. A constant ϵ_α was assumed in the calculation of the data. An indication of the changes in efficiencies is obtained from the ratio of $N_\gamma/N_\alpha=\epsilon_\gamma/\epsilon_\alpha$. With the exception of the data for angles of 220°, 105°, and 180° this ratio did not differ by more than six percent from the average and even if the change had been due partly to a change in the shape of the curve obtained (Fig. 3) would not have been radically different from the curve that would have resulted if the proper correction for efficiencies could have been made. Six runs were taken at 180° and the r.m.s. deviations in the values of N_{ct}/N_γ for the individual runs was 0.0006 compared to the expected statistical deviations of 0.0002.

The angular correlation was measured again in a plane perpendicular to the beam, and is shown in Fig. 4. This curve was taken with about 5° better resolution than the curve of Fig. 3, and the presence of a minimum at around 140° is a little more apparent.

Comparison of the experimental results as shown in Figs. 3 and 4 with the theoretical correlations as shown in Figs. 5–7 shows that only one theoretical curve (1−3−0, odd L, Fig. 7) corresponding to Ne^{20*} having spin 1, O^{16*} spin 3, the ground state of O^{16} spin zero, with odd angular momentum L for the alpha-particles, has the same shape as the experimental curves. Since the shape of the theoretical curves is modified by the finite resolution of the apparatus, the curve 1−3−0, odd L, modified for 40° resolution, is drawn in on Fig. 3

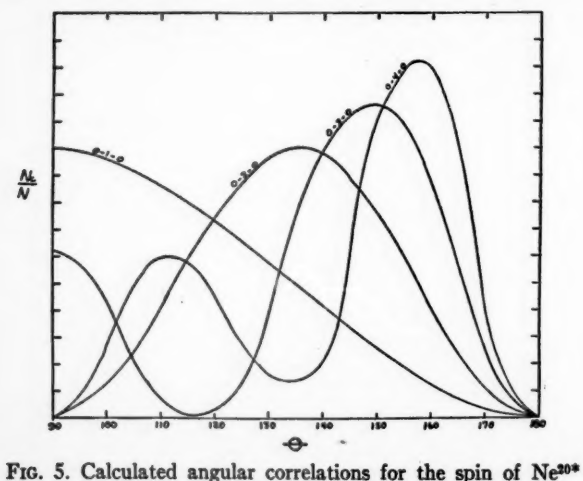

FIG. 5. Calculated angular correlations for the spin of Ne^{20*} equal to 0. The curves are labeled $j_1-j_2-j_3$ corresponding to the spins of $Ne^{20*}-O^{16*}-O^{16}$. Since only even powers of $\cos\theta$ are involved the correlation for θ between 90° and 180° is sufficient for identification. Note the value of zero for N_c/N at 180° for all of these curves.

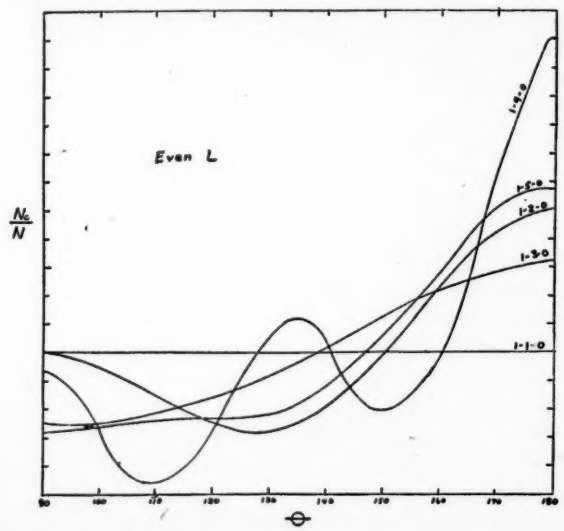

FIG. 6. Calculated angular correlations for the spin of Ne^{20*} equal to unity, and for the alpha-particle being emitted with even angular momentum L. Curves are labeled $j_1-j_2-j_3$ corresponding to the spins of $Ne^{20*}-O^{16*}-O^{16}$

for comparison. A $2\frac{1}{2}$ degree center of mass correction on θ was neglected.

VI. CONCLUSIONS

From the unique correlation between the experimental data and the one theoretical curve it appears that the spin of Ne^{20*} is unity, the spin of O^{16*} (6.14 Mev) is 3, and that the alpha-particles are emitted with angular momentum 3 (the only odd value of L possible in this transition). The spin of O^{16*} is thought not to be 6 or greater (for which theoretical curves were not calculated) because of general trends in the shape of the curves for spins below 6, and also because higher values for the spin of the excited state would lead to a lifetime for this state, which should be long enough to observe experimentally.

The spherically symmetric angular distribution of alpha-particles, combined with the measured spin of unity for Ne^{20*}, and a measured $L=3$ for the alpha-particle means that only S-wave protons are involved in the reaction. Therefore Ne^{20*} has the same parity as F^{19}, since the protons have even parity. The odd angular momentum of the alpha-particle means that O^{16*} has opposite parity from Ne^{20*} and hence opposite parity from F^{19}. Since F^{19} and O^{16} are both thought to have even parity[9] the parity of the 6.14-Mev excited state of O^{16} is probably odd. This would lead to electric octopole radiation for the γ-ray. This assumption of even parities for F^{19} and O^{16} is consistent with the fact that all of the atoms of Ne^{20*} formed in the 340-kev resonance decay by short range alpha-particles to the 6.14-Mev excited state of O^{16*} instead of emitting long range alphas and going directly to the ground state. The latter transition would be between states of even parity with a spin difference of unity, however, alpha-particles with angular momentum unity would require odd parity for either Ne^{20*} or O^{16}.†

Just below the 6.14-Mev excited state of O^{16} is a 6.0-Mev excited state which decays by pair emission,[10] and is therefore thought to have a spin of zero. The absence of pair production in the $F^{19}(p,\alpha)$ reaction at the 340-kev resonance, combined with the fact that the pair producing level is lower than the gamma-level involved, indicates even parity for this 6.0-Mev pair producing state. This spin and parity would indicate

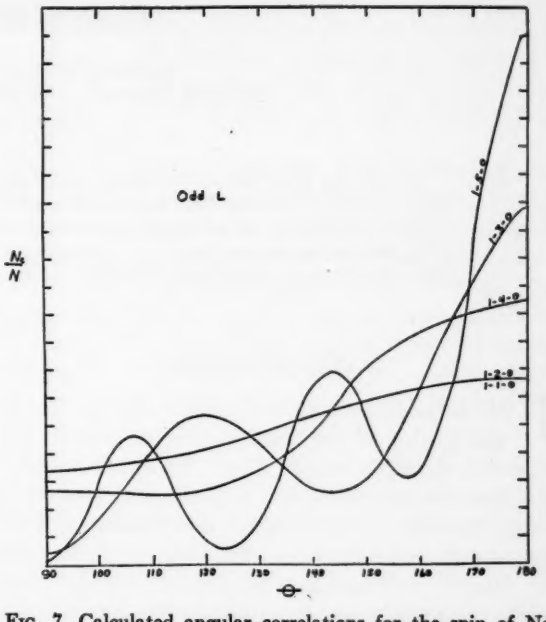

FIG. 7. Calculated angular correlations for the spin of Ne^{20*} equal to unity, and for the alpha-particle being emitted with odd angular momentum L. Curves are labeled $j_1-j_2-j_3$ corresponding to the spins of $Ne^{20*}-O^{16*}-O^{16}$.

that, in the absence of any other selection rules, any state which decays by particle emission to the ground state of O^{16} would also decay to the pair level, although perhaps by a low branching ratio. One such case is N^{16} which decays by beta-emission to the ground state of O^{16} and also to the 6.14- and 7.0-Mev excited state of O^{16}. This radioactive isotope was studied by Sommers and Sherr[11] whose data on the presence or absence of pairs is somewhat inconclusive. They suggest that N^{16} has a high spin value which makes it prefer the transition to the 6.14-Mev level of O^{16} in preference to transitions to states with zero spin, although the higher energy involved allows transitions to the ground state of O^{16} to compete. The gamma-rays from N^{16} have also recently been measured by Millar, Cameron, and Glicksman,[12] whose experiments were such that pairs would not have been observed.

This work was done as part of the research program at the University of Iowa under the direction of Professor James A. Jacobs. Dr. R. E. Holland, who suggested this problem, had previously modified the theory of Hamilton and Falkoff for use on alpha-gamma-transitions. Mr. J. Zijacek helped with the apparatus and the operation of the generator.

[9] Table VI of E. Feenberg and K. Hammack, Phys. Rev. **75**, 1877 (1949).

† *Note added in proof:* Identical conclusions as to the spin and parity of this O^{16*} state were obtained from a similar experiment reported by Barnes, French, and Devons [Nature **166**, 145 (1950)].

[10] V. K. Rasmussen *et al.*, Phys. Rev. **77**, 617 (1950).

[11] H. S. Sommers, Jr., and R. Sherr, Phys. Rev. **69**, 21 (1946).

[12] Millar, Cameron, and Glicksman, Phys. Rev. **77**, 742 (1950).

Cascade Showers in Lead*

KENNETH M. CROWE AND EVANS HAYWARD
Radiation Laboratory, University of California, Berkeley, California
(Received June 14, 1950)

A study has been made of the energy and angular distributions of the electrons produced when the x-ray beam from the 322-Mev Berkeley synchrotron falls on a slab of lead one-half inch in thickness. A cloud chamber containing the piece of lead was in a magnetic field of 1800 gauss. Measurements were made on 1286 electron secondaries having energies greater than three Mev. The energy and angular distributions of these electrons are in satisfactory agreement with the theory.

I. INTRODUCTION

THE diffusion equations of cascade theory[1] describe the course of an electron-photon shower as it progresses through matter. When the initial boundary conditions are introduced these equations determine the average number of the electrons and gamma-rays of a given energy as a function of thickness in the material. The lateral[2] development of the shower has been studied extensively and in particular the lateral spread and angular distributions of shower particles have been obtained under different simplifying assumptions. Other properties of cascade showers that have also been studied theoretically are the fluctuations in the number of particles as a function of thickness resulting from a single primary of a given energy.

Before the advent of high energy electron accelerators the experimental investigation of these shower problems was restricted to experiments on the soft component of cosmic rays. Many experiments[3] have been performed which measured the counting rate or ionization as a function of thickness of material. The transition (or shower) curves that are obtained rise rapidly to a maximum and then decrease more slowly as the thickness of absorber is increased. These results are in qualitative agreement with the theory but suffer from a number of difficulties: (1) it is necessary to integrate over the not too well-known primary spectrum in order to compare with the theory; (2) the experiments are subject to various large geometrical corrections; and (3) the hard component must be separated out.

A more direct comparison with experiment may be obtained from cloud-chamber data. From a study of fifty showers, Hazen[4] has been able to compare with the theory the number of particles at the maximum of the shower as a function of the total number of particles under eight 0.7 cm lead plates. Nassar and Hazen[5]

TABLE I. The observed number of tracks in 10 Mev and 10° intervals. These numbers have been corrected for the omission of tracks having dip angles greater than 45°. The lowest energy group has been normalized relative to the second to correct for the omission of electrons between three and ten Mev in the second half of the experiment. This group has also been corrected for the fact that the interval includes only seven Mev instead of ten.

E(Mev)\θ	0–9	10–19	20–29	30–39	40–49	50–59	60–69	70–79	80–89	Total
3–9	43.5	95.0	79.2	155	55.5	65.5	48.7	7.52		548±33
10–19	42	82	76	63	42	30.5	24.3	11.5	2.0	373±20
20–29	47	69	51	29	12	16.5	5.8			230±15
30–39	42	43	32	8	3	4.5		1.9		134±12
40–49	36	24	12	4	1					77±9
50–59	21	17	7	1						46±7
60–69	21	16	7		1					45±7
70–79	26	7	2							35±6
80–89	19	8	1							28±5
90–99	11	4	5							20±4.5
100–109	13	7								20±4.5
110–119	11	4								15±4
120–129	12	1								13±4
130–139	9	1								10±3
140–149	8	0								8±3
>150	13	1								14±4

* This work was performed under the auspices of the AEC.

[1] H. S. Snyder, Phys. Rev. **76**, 1563 (1949); B. Rossi and K. Greisen, Rev. Mod. Phys. **13**, 240 (1941).

[2] G. Molière in W. Heisenberg, *Cosmic Radiation* (Dover Publications, New York, 1946); S. Z. Belenky, J. Phys. U.S.S.R. **8**, 347 (1944); J. Roberg and L. W. Nordheim, Phys. Rev. **75**, 444 (1949).

[3] J. C. Street and R. T. Young, Phys. Rev. **46**, 823 (1934); **47**, 572 (1935); C. G. Montgomery and D. D. Montgomery, Phys. Rev. **48**, 786 (1935).

[4] W. E. Hazen, Phys. Rev. **66**, 254 (1944).

[5] S. Nassar and W. E. Hazen, Phys. Rev. **69**, 298 (1946).

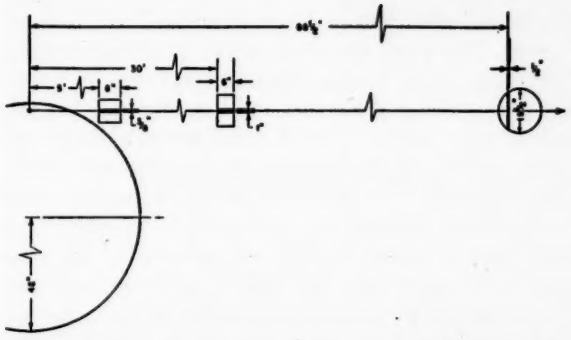

FIG. 1. The geometry of the experiment. Two lead collimators were used between the synchrotron and the cloud chamber.

have also determined the shape of the shower curve but in addition they have measured the energy spectrum of the electrons at the maximum of the shower as well as the fluctuations in the number of particles. Their results are certainly consistent with the theory but are unsatisfactory in two ways: (1) the energy of the incident electron is never experimentally determined, and (2) the number of showers observed is rather small.

When the 322-Mev Berkeley synchrotron began to operate, the systematic and controlled measurement of these quantities became possible. Blocker *et al.*[6] have determined the shape of the shower curve for lead, copper, aluminum, and carbon. They have measured the current from an ionization chamber as a function of thickness of material and have obtained the transition curves with extreme accuracy. We have sought to measure the energy spectrum at the maximum of the shower in lead; i.e., at the point where the maximum ionization occurs which is under approximately one-half inch of lead.

II. EXPERIMENTAL DETAILS

A cloud chamber, described in a previous paper,[7] in a magnetic field of 1800 gauss was located in the x-ray beam of the Berkeley synchrotron and 88½ feet from its target. Two collimators were used. The first was a ⅛ in.×⅜ in. horizontal slot located five feet from the synchrotron target, and the second was a 1/16 in.×¾ in. slot, 30 feet from the target and at the same vertical height as the center of the illuminated region of the cloud chamber. These produced a spray of electrons emerging from the lead and occupying an area about ¼×2 in. The x-ray beam traversed the ¾ in. quartz wall of the synchrotron donut, 88½ feet of air and the ¼ in. glass wall of the cloud chamber before impinging on a half-inch lead plate inside the chamber. (See Fig. 1.)

The energy and angular distributions of the electrons which emerge from the ½-in. thick lead plate have been measured by reprojection.[7] Besides the radius of curvature ρ, two angles, α and β, were measured. α is the dip angle or the angle that the start of the track makes with the horizontal. β is the angle that the start of the track makes with the plane defined by the beam direction and the vertical. The energy of the electron is then given by $E=300\ H\rho\cos\alpha$ and the scatter angle $\theta=\cos^{-1}(\cos\alpha\cos\beta)$.

The photographs measured were selected on the basis of quality and population. For example, a photograph that contained fifteen tracks was easy to measure, whereas one having twenty-five was measurable only in cases in which the photography was exceptional. Each photograph represented, of course, a single pulse from the synchrotron and, indeed, a single pulse of extremely low intensity. The tracks have in all cases been selected and measured by two independent observers and from their reproducibility we believe that the errors in the angles are about ±2° and in the radii of curvature, ±5 percent. Multiple scattering by the gas (a mixture of argon and helium) at the magnetic field used (1800 gauss) produces a standard error of approximately ±6 percent over the whole energy range.

In the first part of the experiment all of the tracks corresponding to electrons above three Mev were

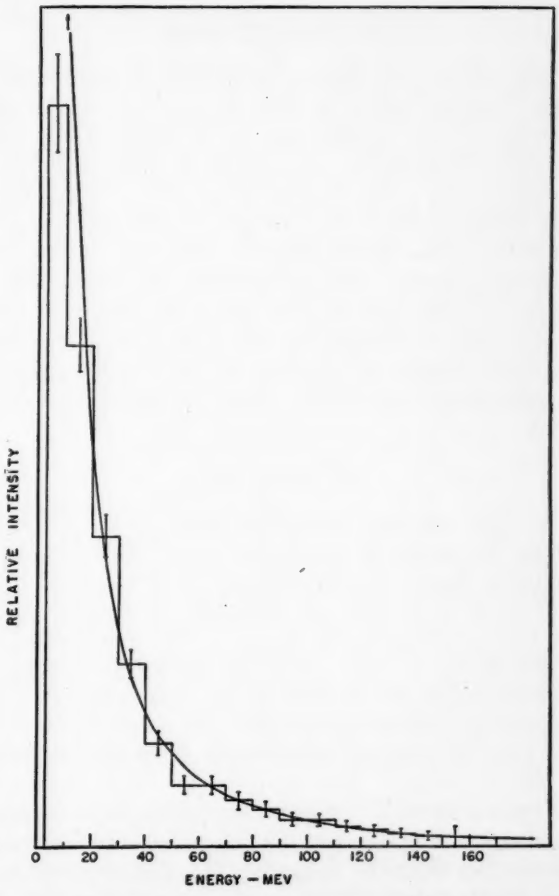

FIG. 2. The differential energy spectrum of the electrons. The standard deviations on the histogram are based only on the number of tracks measured. The smooth curve is the theoretical result obtained from Approximation *B* of Rossi and Greisen and has been normalized for the best fit with the experimental points.

[6] Blocker, Kenney, and Panofsky, Phys. Rev. **79**, 419 (1950).
[7] Brueckner, Hartsough, Hayward, and Powell, Phys. Rev. **75**, 1274 (1949).

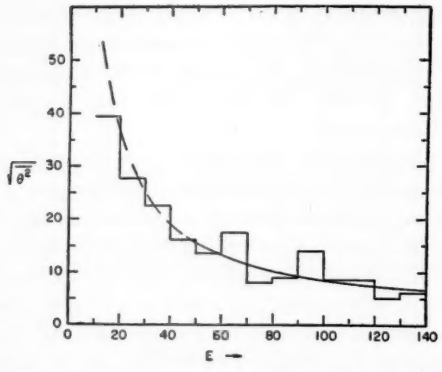

FIG. 3. The root mean square angle *versus* energy of the electrons. The smooth curve is taken from the paper by Roberg and Nordheim.

included; later, because of the preponderance of low energy electrons, we set the lower limit at 10 Mev and have normalized the data accordingly. With these limitations all tracks were measured if their dip angles were less than 45°; a geometrical correction based on the assumption of azimuthal symmetry was made for the omitted tracks:

$$\pi/[2\sin^{-1}(\sin 45°/\sin\theta)].$$

Since the scatter angles of the electrons result from their Coulomb scattering in the lead, they are a strong function of the energies of the electrons. Thus, for example, the geometrical correction mentioned above is necessary only below 40 Mev and is really important only below 20 Mev. Another result of this energy dependence is that it has effectively extended the upper limit of the energies that could be measured, for the high energy electrons come out from the lead plate essentially in the forward direction and traverse the diameter of the cloud chamber giving about 30 cm of track on which to make an otherwise very difficult curvature measurement.

III. RESULTS

We have measured a total of 1286 tracks. Table I shows the numbers of tracks in 10 Mev and 10° intervals. These numbers have been corrected for the omission of tracks with dip angles greater than 45° and the lowest energy group has been normalized relative to the second to correct for the omission of electrons between three and 10 Mev in the second half of the experiment. This group has also been corrected for the fact that the interval includes only seven Mev instead of 10.

Figure 2 shows a histogram of the measured energy distribution. The standard deviations are based only on the number of tracks measured. Mr. Walter Aron has very kindly calculated for us the energy spectrum of the electrons by applying the initial condition of a $1/E$ gamma-ray spectrum in Approximation B of Rossi and Greisen. The x-ray spectrum of the synchrotron differs from thin target bremsstrahlung spectrum because of pair production in the target and the differential absorption of the x-rays, by the synchrotron's target and quartz donut, the air between the synchrotron and the cloud chamber, as well as the quarter-inch glass wall of the chamber. Powell[8] has shown that the effect of all these corrections is to reduce the intensity of the x-rays almost uniformly over the whole spectrum, and since we are interested in relative intensities only, the corrections to the theory are unnecessary. The limitation of the Rossi and Greisen representation is that the asymptotic cross sections, which break down at low energies, are used. Aron has corrected this difficulty by increasing the shower unit to 0.783 cm from the asymptotic value 0.5 cm. This value was obtained from the analysis of the curves of Blocker *et al.*[6] The theoretical curve has been normalized for best fit with the experimental one. The agreement is really more than satisfactory. The low energy group is expected to be low due to the large fraction of shower particles which travel backwards as is apparent from the shape of the angular distribution.

Figure 3 shows a plot of the r.m.s. angle of scattering as a function of the energy. The rather large deviations from a smooth curve above 50 Mev result from the limited number of events at high energies. (See Table I.) The fluctuations in the number of particles in the shower are themselves large and have a large effect on the r.m.s. angle for all energies.

The smooth curve results from the calculations of Roberg and Nordheim.[2] They have calculated the mean square angle of scattering as a function of energy from the lateral spread of the shower, taking into account the Coulomb scattering of the emergent electron and its ancestors. Although the calculation was intended primarily for small scattering angles in which the angular distribution is taken to be gaussian, the extrapolation to large angles appears to fit the observations.

A calculation by Belenky[2] does not include the small angle approximation and should, therefore, be more applicable to the case of lead. We have compared our results with the distribution function of Belenky and find them to be consistent, though the number of events observed in the experiment is not great enough to permit any definite conclusion concerning the various available calculations.

The authors wish to thank Drs. E. M. McMillan, W. M. Powell, and R. Serber for their very helpful advice. Walter Aron, Leonard Eyges, and Sindney Fernbach contributed greatly by their discussions with us of the theory. We are also very much indebted to the synchrotron crew for their cooperation.

[8] W. M. Powell (to be published).

Note on the Li^7 Quadrupole Moment*

R. D. PRESENT
University of Tennessee, Knoxville, Tennessee
(Received June 2, 1950)

Recent measurements unexpectedly determine the sign of the quadrupole moment as positive, although the magnitude is uncertain. On the quasi-atomic model the ground state is $1s^2 2p^3\ ^2P_{\frac{1}{2}}$ and of symmetry [3] in Wigner's "first approximation." The corresponding quadrupole moment is -6 in units of $\langle r^2\rangle_{2p}/25$. The explanation of the discrepancy is sought in configuration interaction. A variational calculation of the moment has been made taking into account the P states of symmetry [3] from the low configurations $1s^2 2p^2 3p$ and $1s^2 2p^2 4f$. The maximum value of the moment is $+2.32$ in the above units; this value is increased by including other configurations. The admixture of [3] P states from excited configurations has no effect on the magnetic moment nor on the matrix element for Be^7 K-capture into the ground state of Li^7; this is satisfactory since the quasi-atomic model agrees reasonably well with experiment in these instances. When the [3] D states from the above configurations are included in the variational calculation, the maximum is raised to 8.03. The configuration interaction need not be large in this case to produce a positive moment; however the inclusion of the [3] D states does impair the agreement with the magnetic moment and the K-capture data. Considering the wide margin of uncertainty in the estimated experimental quadrupole moment, we find that all the data are adequately explained without assuming large spin-orbit interaction or large departures from partition symmetry.

I. INTRODUCTION

RECENT measurements[1] of the nuclear quadrupole interaction with the molecular fields in Li_2 and the lithium halides indicate a positive quadrupole moment for the Li^7 nucleus. The estimated magnitude (2×10^{-26} cm^2) is uncertain, however, because of lack of resolution in the Li_2 experimental line and the uncertain value of the electric field gradient. The quasi-atomic nuclear model predicts a negative quadrupole moment for the ground state ($1s^2 2p^3\ ^2P_{\frac{1}{2}}$) of Li^7. A value of -2.7×10^{-26} cm^2 was calculated by Welles[2] using a wave function determined from energy calculations on the quasi-atomic central force model[3] together with a reasonable estimate of $\langle r^2\rangle_{2p}$ (the mean square radius of a $2p$ nucleon in Li^7). Nearly the same wave function and quadrupole moment are obtained in the first approximation of Wigner's theory,[4] which is based on a central-force symmetric Hamiltonian with spin-exchange terms and Coulomb forces neglected. In this approximation the orbital wave function is characterized by a definite symmetry with respect to permutations of the nucleons. The orbital wave function belongs to an irreducible representation of the symmetric group and is labeled by a partition. It is then possible to determine the coefficients in the wave function from the quantum numbers and symmetry considerations, without having recourse to the usual perturbation theory procedure which entails the calculation of energy matrix elements and the solution of secular equations.[5] Assume first that Wigner's approximation is valid and that the partitions make good quantum numbers. The completed shell of $1s$ particles has no effect on the symmetry, makes no contribution to the quadrupole moment, and is therefore omitted. The partitions for Li^7 are then [3], [2+1] and [1+1+1] in the order of decreasing symmetry of the orbital wave function and increasing energy of the nuclear state. The ground state orbital wave function, belonging to the partition [3], is symmetric in the coordinates of the three particles outside the s-shell. Assuming the ground state to be $1s^2 2p^3\ ^2P_{\frac{1}{2}}$, the wave function is simply determined (see Table I) and the quadrupole moment found to be -6 in units[6] of $\langle r^2\rangle_{2p}/25$.

The discrepancy with the result inferred from Kusch's experiments may be resolved in several possible ways: (a) by configuration interaction (admixture of wave functions for higher configurations), (b) by spin-orbit interaction (admixture of D states), (c) by the breakdown of partition symmetry (admixture of [2+1] and [1+1+1]). These possibilities, of course, are not independent; furthermore, combinations of (a), (b), and (c) are possible. We denote, e.g., by "Case (bc)," the case in which configuration interaction is absent, but in which $L-S$ coupling and partition symmetry both break down.

Case (a): Partition symmetry and $L-S$ coupling are both preserved. Configuration interaction introduces an admixture of ^2P functions of symmetry [3] from low odd-parity configurations. A positive quadrupole moment may arise from the non-diagonal matrix elements of the quadrupole moment operator. This case is considered below in detail.

Case (b): It is impossible for D states to be admixed without either configuration interaction or a breakdown

* Presented at the 1950 Annual New York Meeting of the American Physical Society.

[1] P. Kusch, Phys. Rev. **76**, 138 (1949).

[2] S. Welles, Phys. Rev. **62**, 197 (1942).

[3] E. Feenberg and E. Wigner, Phys. Rev. **51**, 95 (1937); M. Rose and H. Bethe, Phys. Rev. **51**, 205 (1937).

[4] E. Wigner, Phys. Rev. **51**, 106, 947 (1937); F. Hund, Zeits. f. Physik **105**, 202 (1937).

[5] E. Feenberg and M. Phillips, Phys. Rev. **51**, 597 (1937).

[6] This unit, which is used in the following, is roughly estimated to be 0.3×10^{-26} cm^2.

TABLE I. Symmetric wave functions.*

$$\Phi_{2p^3}(P^i)=(2/3)\psi_{P^i}(P_\pi D_\nu)+(\sqrt{5}/3)\psi_{P^i}(P_\pi S_\nu)$$

$$\Phi_{2p^24f}(P^i)=(1/\sqrt{3})\psi_{P^i}(F_\pi D_\nu)+\sqrt{2}/\sqrt{3}\psi_{P^i}(P_\pi \mathfrak{D}_\nu)$$

$$\Phi_{2p^23p}(P^i)=(2\sqrt{5}/3\sqrt{7})\psi_{P^i}(P_\pi{}^*D_\nu)+(2\sqrt{6}/3\sqrt{7})\psi_{P^i}(P_\pi \mathbf{P}_\nu)$$
$$-(1/3\sqrt{7})\psi_{P^i}(P_\pi{}^*S_\nu)+\sqrt{2}/\sqrt{7}\psi_{P^i}(P_\pi \mathbf{S}_\nu)$$

$$\Phi^{\times}_{2p^23p}(P^i)=(1/3\sqrt{7})\psi_{P^i}(P_\pi{}^*D_\nu)+(\sqrt{7}/3\sqrt{2})\psi_{P^i}(P_\pi \mathbf{D}_\nu)$$
$$-\sqrt{5}/\sqrt{42}\psi_{P^i}(P_\pi \mathbf{P}_\nu)+(2\sqrt{5}/3\sqrt{7})\psi_{P^i}(P_\pi{}^*S_\nu)$$
$$+(\sqrt{10}/3\sqrt{7})\psi_{P^i}(P_\pi \mathbf{S}_\nu)$$

$$\Phi(D)=-(1/\sqrt{5})\Phi(D^1)\cdot{}^2\chi_{\frac{1}{2}}+(2/\sqrt{5})\Phi(D^2)\cdot{}^2\chi_{-\frac{1}{2}}$$

$$\Phi_{2p^24f}(D^i)=(1/\sqrt{3})\psi_{D^i}(F_\pi D_\nu)+(2/3)\psi_{D^i}(P_\pi \mathfrak{D}_\nu)$$
$$+(\sqrt{2}/3)\psi_{D^i}(P_\pi \mathfrak{F}_\nu)$$

$$\Phi_{2p^23p}(D^i)=(1/\sqrt{3})\psi_{D^i}(P_\pi{}^*D_\nu)-(1/\sqrt{6})\psi_{D^i}(P_\pi \mathbf{D}_\nu)$$
$$+(1/\sqrt{2})\psi_{D^i}(P_\pi \mathbf{P}_\nu)$$

* See footnote 13.

of partition symmetry, since the $2p^3$ configuration gives rise to no D state of symmetry [3].

Case (c): A large departure from partition symmetry is unlikely without a large spin-orbit interaction. The spin-exchange and Coulomb forces do not cause large departures from symmetry [3] in Li^7. This case has been investigated by Avery and Blanchard.[7] Taking into account the three P states of symmetry [2+1], they are unable to fit the quadrupole moment and other ground state properties of Li^7.

Case (ab): Both ^2P and ^2D functions of symmetry [3] from low odd-parity configurations are mixed in. The admixture of D states implies spin-orbit interaction and this breaks down the partition symmetry. Thus it is somewhat artificial to take into account the above D states and to omit the [2+1]D states from $2p^3$. However, one may reasonably inquire to what extent the properties of light nuclei can be accounted for without assuming a large departure from partition symmetry. This case is also considered below in detail.

Case (bc): This case has been investigated completely by Avery and Blanchard.[7] Using the eight independent functions of the $2p^3$ configuration, they find it possible to secure reasonable agreement with the quadrupole moment and magnetic moment of Li^7 and with the Be^7 K-capture data. A fairly unique wave function is determined in this way; it appears impossible to fit the data with any very different choice of coefficients. In order to obtain a positive quadrupole moment and retain good agreement with the other data, the wave function is required to be predominantly of symmetry [2+1]. Their final wave function,[8] which corresponds to a quadrupole moment of 3.5 in the above units, is 6 percent [3] and 94 percent [2+1].

Case (ac): In this case there is an admixture of P states of all partition symmetries from all low odd-parity configurations. This is somewhat artificial for the reason given under Case (c), and has not been considered.

Case (abc): The discrepancy is here attributed to a combination of all three explanations. This last alternative, while probably the most nearly correct, is so general and provides so many adjustable constants that it can be reasonably expected to explain all the experimental results without, however, providing much insight into the reliability of the various nuclear approximations.

II. CONFIGURATION INTERACTION

In the following it is assumed that all terms in the wave function are of symmetry [3]. Configurations that interact with $1s^42p^3$ must be of odd-parity; the lowest of these are $1s^42p^23p$, $1s^42p^24f$, $1s^32s2p^3$, and $1s^32p^33d$. If the individual nucleons are assumed to move independently in zero-order in a suitable "auxiliary potential," the zero-order energy is the sum of the eigenvalues for the individual particle states. In the case of the isotropic space oscillator potential, the four excited configurations listed above are lowest in energy and have all the same zero-order energy. Since the approximation of the auxiliary potential (Hartree) is not very suitable for the type of force found in nuclei, the description in terms of single configurations is correspondingly inaccurate and an appreciable interaction between neighboring configurations of the same parity is expected. For simplicity we consider only the $2p^23p$ and $2p^24f$ configurations. Quartet states are excluded by the symmetry [3] requirement; since the total nuclear angular momentum J is $\frac{3}{2}$, this excludes S and F states. The enumeration of the states of symmetry [3] arising from each configuration is elementary. For example, in the case of $2p^23p$ there is only one way to write a symmetric function corresponding to an orbital angular momentum component $M_L=\sum m_l=3$, hence one F state; there are two linearly independent symmetric functions with $M_L=2$, hence one D state; and, since there are four such functions with $M_L=1$, this configuration gives two P states. The number of linearly independent symmetric functions for each value of $\sum m_l$ is just the number of different ways in which values of m_l can be assigned to the individual nucleons. As noted in the previous section, the configuration $2p^3$ gives rise to no D states of symmetry [3] and to but one [3] P state. In the case of $2p^24f$ there is one P state and one D state of this

TABLE II. Matrix elements of Q in units of $\langle r^2\rangle_{2p}/25$.

$2p^3$ P	$2p^24f$ P	$2p^23p$ P	$2p^23p$ $P^\times$	$2p^24f$ D	$2p^23p$ D
-6	$2\sqrt{14}/\sqrt{5}$	$2\sqrt{2}/3\sqrt{7}$	$-34\sqrt{2}/3\sqrt{35}$	$4\sqrt{7}/\sqrt{15}$	$2\sqrt{2}/\sqrt{15}$
	$-46/15$	$8/\sqrt{5}$	$4/5$	$28\sqrt{6}/15$	$4\sqrt{21}/15$
		$-38/21$	$-32\sqrt{5}/35$	$8\sqrt{2}/\sqrt{15}$	$16\sqrt{3}/\sqrt{35}$
			$-748/105$	$4\sqrt{2}/5\sqrt{3}$	$-46/5\sqrt{21}$
				$22/15$	$-4\sqrt{14}/5$
					$28/15$

[7] R. Avery and C. Blanchard, Phys. Rev. **77**, 756A (1950); **78**, 704 (1950). A detailed article describing this work was kindly sent to the writer by R. G. Sachs.

[8] This function does not conform to any nuclear model hitherto proposed. The breakdown of partition symmetry through large axial dipole interaction should lead to comparable proportions of [3] and [2+1]. The above function preserves the partition symmetry, but the symmetry is not that appropriate to the Li^7 ground state.

symmetry. Taking into account all the P and D states arising from $2p^3$, $2p^23p$, and $2p^24f$, there are six symmetric wave functions to be calculated. Details of the calculation are to be found in Appendix I and the results are given in Table I.

The notation in Table I is conventional or self-explanatory except in the following respects: P_π is a $2p$ function and P_π^* a $3p$ function for the proton; D_ν represents a D state for equivalent $2p$ neutrons, $\mathbf{D}_\nu$ a non-equivalent $2p3p$ pair and $\mathfrak{D}_\nu$ a $2p4f$ pair. The two linearly independent P state functions for $2p^23p$ are denoted by Φ and $\Phi^\times$. In calculating the matrix elements of the quadrupole moment operator, the functions ψ are expanded in terms of product functions for the protons and neutrons each with its own magnetic quantum number, e.g.,

$$\psi_P{}^1(P_\pi D_\nu)=(1/\sqrt{10})\{P_\pi{}^1 D_\nu{}^0-\sqrt{3}P_\pi{}^0 D_\nu{}^1 +\sqrt{6}P_\pi{}^{-1}D_\nu{}^2\}.$$

The functions in Table I are orthogonal and normalized.

III. THE QUADRUPOLE MOMENT

The quadrupole moment, q, is defined as the expectation value of $Q=\sum_\pi(3z^2-r^2)$, summed over the protons, for the ground state eigenfunction with $M=J$. The $1s$ shell protons make no contribution to q and the sum reduces to one term.[9] The matrix elements of Q are to be calculated with respect to the set of normalized, symmetrized, orthogonal wave functions given in Table I. The radial integrals which occur in the matrix elements require for their evaluation some explicit assumption about the $2p$, $3p$, and $4f$ radial eigenfunctions. Assuming isotropic oscillator functions, these integrals have been expressed in terms of $\langle r^2\rangle_{2p}$. Some details of the evaluation of the matrix elements are given in Appendix II; the results are in Table II.

We seek the greatest possible values of q under the assumptions of Case (a) and of Case (ab) of Section I. The maximum of q is given by the largest root of the secular equation: $|Q_{ij}-\lambda\delta_{ij}|=0$. In Case (a) only the P states are taken into account and the maximum value of the moment is 2.32 in units of $\langle r^2\rangle_{2p}/25$. The coefficients of the normalized wave function for this value of q are 0.344, 0.630, 0.670 and -0.190 in the order: $2p^3\,P$, $2p^24f\,P$, $2p^23p\,P$, and $2p^23p\,P^\times$. The maximum quadrupole moment, while positive, is not large and since the corresponding eigenfunction is only 12 percent $2p^3$, very large configuration interaction is indicated. However the P states from other excited configurations have not been taken into account; their inclusion in the variational calculation can only increase the maximum above 2.32. We conclude that a positive quadrupole moment is consistent with a pure P ground state of symmetry [3], provided that there is large configuration interaction.

The inclusion of the D states helps materially to increase the moment. In contrast to the P states, the diagonal matrix elements for the D states are positive, and the two D functions together give a maximum q of 4.67. If all six functions of the set given in Table I are taken in combination, the maximum moment is raised to 8.03. The corresponding coefficients of the normalized wave function in the order of Tables I and II are: 0.276, 0.502, 0.523, -0.111, 0.542, and 0.304. This function is 38.6 percent D state and only 7.6 percent $2p^3$. It is interesting to note that a fair-sized positive moment can be obtained from a combination of the functions of Table I which is predominantly $2p^3$. Thus, a function which is 60 percent $2p^3$ and 10 percent each of $2p^24f\,P$, $2p^23p\,P$, $2p^24f\,D$, and $2p^23p\,D$, if the phases are all the same, yields a quadrupole moment of 2.55. We conclude that Case (ab) of the Introduction provides a possible explanation of Kusch's results.

IV. CONCLUSIONS

As a further test of the adequacy of the wave functions discussed in the preceding section, one can use them to calculate the magnetic moment of Li^7 and the matrix element for Be^7 K-electron capture leading to the ground state of Li^7. The symmetry [3] of the space wave functions makes the magnetic moment calculation very simple. The admixture of P states from excited configurations has no effect on the magnetic moment, essentially because the magnetic moment is given by the vector model and depends only on the quantum numbers. More explicitly, the non-diagonal terms in the spin part of the moment vanish through orthogonality of the space functions and the diagonal terms are all the same because all states have the same quantum numbers. The orbital part of the moment is unaffected by P state admixture since the symmetry of the wave function permits l_z for the proton to be replaced by $L_z/3$ and M_L is a good quantum number. The magnetic moment in Case (a) remains at the value predicted by the quasi-atomic model: $\mu_P+(1/3)=3.123$ nuclear magnetons, in reasonable agreement with the experimental value[10] of 3.253. Admixture of symmetry [3] D states can only decrease the magnetic moment. All cross terms vanish and the moment is the weighted sum of contributions from P^1, D^1, and D^2. The result is $3.123-4.197p_D$ where p_D denotes the percentage of D state. Thus the magnetic moment favors Case (a) over Case (ab).

Avery and Blanchard[7] have pointed out that an additional condition on the Li^7 wave function is provided by the experimental results[11] on the lifetime and branching ratio for Be^7 K-capture. The absolute square

[9] This is proved immediately by observing that, (a) Q is a one-particle operator, (b) the one-particle integrals vanish for the $1s$ protons because the angular dependence of the operator is given by $P_2(\cos\theta)$.

[10] Rabi, Millman, Kusch, and Zacharias, Phys. Rev. **55**, 526 (1939).

[11] E. Segrè and C. Wiegand, Phys. Rev. **75**, 39 (1949); R. Williamson and H. Richards, Phys. Rev. **76**, 614 (1949).

of the matrix element of the Gamow-Teller interaction operator $\sum_i \tau_1^{(i)}\sigma^{(i)}$ has been inferred[7] from experiment to have the value 1.76. The theoretical value[12] is 5/3 for a P state of symmetry [3]. This value is independent of the detailed properties of the wave function, just as in the case of the magnetic moment, and is unaffected by P state admixture through configuration interaction. The agreement is very good and provides additional evidence in favor of Case (a). Admixture of [3] D states can only decrease the matrix element and impair the agreement, since the absolute square of the matrix element is 3/5 for a [3] D state.

Considering the wide margin of uncertainty in Kusch's estimated value for the quadrupole moment, we may conclude that Case (a) is reasonably consistent with all the data. While Case (ab) provides the possibility of explaining a larger quadrupole moment than can be obtained from Case (a), this can only be secured by sacrificing the good agreement with the other data. It appears from the calculations that the experimental results to date can be understood without assuming large spin-orbit interaction and, especially, without invoking any large departure from partition symmetry.

This problem was suggested by E. Feenberg of Washington University. I wish to record my appreciation for this suggestion and to acknowledge some useful preliminary discussion.

APPENDIX I. CALCULATION OF WAVE FUNCTIONS

The functions needed for the calculation of the quadrupole moment are those with $M=J=\frac{3}{2}$. Hence the P states have $M_L=1$ and $M_S=\frac{1}{2}$, while the D state functions are given by the linear combination: $-5^{-\frac{1}{2}}\Phi(D^1)\cdot\chi_{\frac{1}{2}}+(4/5)^{\frac{1}{2}}\Phi(D^2)\cdot\chi_{-\frac{1}{2}}$ where the superscript is M_L and the subscript M_S. Since we are neglecting spin-spin forces between unlike particles, the neutrons have their own multiplicity and are in a singlet state. The orbital functions Φ for each state are linear combinations of functions ψ with the same total L and M_L and corresponding to a proton orbital angular momentum L_π and a neutron angular momentum L_ν, the coefficients being determined by the symmetry requirement. The ψ-functions are expansible in terms of product functions which assign separate magnetic quantum numbers to protons and neutrons; the coefficients are given by the well-known transformation formulas for angular momentum eigenfunctions.[13] The final step in the decomposition is to express the separate proton and neutron functions in terms of one-particle functions with definite values of n, l, and m_l. The neutron functions for non-equivalent particles require symmetrization. After the decomposition is effected and each ψ expressed in terms of one-particle functions, the coefficients of the ψ's given in Table I are obtained by requiring that Φ be completely symmetrical in all particles. This can be done in the simpler cases by inspection; in others, e.g., the $2p^23p$ configuration, some algebra is required.

The procedure is illustrated in the case of $\Phi_{2p^23p}(P^1)$. The component functions can only be $\psi_{P^1}(F_\pi D_\nu)$ and $\psi_{P^1}(P_\pi \mathfrak{D}_\nu)$, the former corresponding to $2p$ neutrons and the latter to a $2p4f$ pair. The transformation formulas give

$$\psi_{P^1}(F_\pi D_\nu)=35^{-\frac{1}{2}}\{15^{\frac{1}{2}}F_\pi{}^2D_\nu{}^{-2}-10^{\frac{1}{2}}F_\pi{}^1D_\nu{}^{-1}+6^{\frac{1}{2}}F_\pi{}^0D_\nu{}^0-3^{\frac{1}{2}}F_\pi{}^{-1}D_\nu{}^1+F_\pi{}^{-2}D_\nu{}^2\}$$

$$\psi_{P^1}(P_\pi \mathfrak{D}_\nu)=10^{-\frac{1}{2}}\{P_\pi{}^1\mathfrak{D}_\nu{}^0-3^{\frac{1}{2}}P_\pi{}^0\mathfrak{D}_\nu{}^1+6^{\frac{1}{2}}P_\pi{}^{-1}\mathfrak{D}_\nu{}^2\}.$$

The normalized one-particle functions are denoted by

$$(2p^1)\equiv -a,\quad (2p^0)\equiv b,\quad (2p^{-1})\equiv c$$
$$(4f^3)\equiv -d,\quad (4f^2)\equiv e,\quad (4f^1)\equiv -f,\quad (4f^0)\equiv g,\quad (4f^{-1})\equiv h,$$

where the phases have been chosen to agree with the Condon-Shortley convention. The normalized neutron functions are given by

$$D^2=aa,\quad D^1=-2^{-\frac{1}{2}}(ab+ba),\quad D^0=6^{-\frac{1}{2}}(2bb-ac-ca),$$
$$D^{-1}=2^{-\frac{1}{2}}(cb+bc),\quad D^{-2}=cc$$
$$\mathfrak{D}^2=42^{-\frac{1}{2}}\{-15^{\frac{1}{2}}(dc+cd)-5^{\frac{1}{2}}(eb+be)+(fa+af)\}$$
$$\mathfrak{D}^1=42^{-\frac{1}{2}}\{10^{\frac{1}{2}}(ec+ce)+8^{\frac{1}{2}}(fb+bf)-3^{\frac{1}{2}}(ga+ag)\}$$
$$\mathfrak{D}^0=42^{-\frac{1}{2}}\{-6^{\frac{1}{2}}(fc+cf)-3(gb+bg)-6^{\frac{1}{2}}(ha+ah)\}.$$

Hence

$$\psi_{P^1}(F_\pi D_\nu)=70^{-\frac{1}{2}}\{-30^{\frac{1}{2}}dcc-10^{\frac{1}{2}}(ebc+ecb)-8^{\frac{1}{2}}fbb+2^{\frac{1}{2}}(fac+fca)+3^{\frac{1}{2}}(gab+gba)+2^{\frac{1}{2}}haa\}$$

$$\psi_{P^1}(P_\pi \mathfrak{D}_\nu)=140^{-\frac{1}{2}}\{-30^{\frac{1}{2}}(cdc+ccd)-10^{\frac{1}{2}}(bec+bce+ceb+cbe)+2^{\frac{1}{2}}(afc+acf+cfa+caf)-8^{\frac{1}{2}}(bfb+bbf)+3^{\frac{1}{2}}(agb+abg+bga+bag)+2^{\frac{1}{2}}(aha+aah)\}$$

and inspection suffices to give the coefficients of Table I. In the case of $2p^23pP^1$ there are two independent solutions to the equations for symmetrization; these give the orthogonal functions $\Phi_{2p^23p}(P^1)$ and $\Phi^{\times}{}_{2p^23p}(P^1)$ of Table I.

APPENDIX II. CALCULATION OF MATRIX ELEMENTS OF Q

The matrix elements of the one-particle (proton) operator $Q=3z_1{}^2-r_1{}^2$ with respect to the set of functions given in Table I are reduced immediately to integrals of the form:

$$\int\int\int Q\bar{\psi}_a\psi_b d\tau_1 d\tau_2 d\tau_3$$

where ψ_a and ψ_b are the functions of Table I. All integrals of this type, in which the neutron state specified in ψ_a does not exactly match the neutron state specified in ψ_b, vanish by orthogonality. Thus all cross terms in the diagonal matrix elements must vanish. In the next step the ψ-functions are expanded in terms of the product functions with separate quantum numbers for neutrons and protons. All integrals vanish in which the magnetic quantum numbers of the two neutron functions do not match; in the remaining integrals the integration over the neutron coordinates gives unity since the functions are normalized. Thus all integrals have been reduced to the form $\int Q\bar{\phi}_a\phi_b d\tau_1$ where ϕ_a and ϕ_b are one particle functions for the proton with the same magnetic quantum numbers. The one-particle functions of Appendix I contain the normalized associated Legendre functions $\Theta_{l,|m|}$ with the Condon-Shortley phases. Since $Q=2r_1{}^2P_2(\mu_1)$ the preceding integral reduces to the product of an angular integral: $I_{l,|m|;l',|m|}=\int_{-1}^{1}d\mu P_2(\mu)\Theta_{l,|m|}(\mu)\Theta_{l',|m|}(\mu)$ and a radial integral: $(r^2)_{nl,n'l'}$. The eigenfunctions for the isotropic oscillator have been used to evaluate the radial integrals and express them in terms of $(r^2)_{2p,2p}\equiv\langle r^2\rangle_{2p}$. The number of integrals to be evaluated is greatly reduced by observing that, e.g.,

$$\int Q|\psi_{P^1}(P_\pi D_\nu)|^2=\int Q|\psi_{P^1}(P_\pi \mathbf{D}_\nu)|^2=\int Q|\psi_{P^1}(P_\pi \mathfrak{D}_\nu)|^2$$

and that

$$\int Q\bar{\psi}_{P^1}(P_\pi D_\nu)\psi_{P^1}(P_\pi{}^* D_\nu)$$

is obtained from

$$\int Q|\psi_{P^1}(P_\pi D_\nu)|^2$$

by replacing $(r^2)_{2p,2p}$ by $(r^2)_{2p,3p}$.

---

[12] E. Wigner, Phys. Rev. 56, 519 (1939).

[13] E. U. Condon and G. H. Shortley, *The Theory of Atomic Spectra* (Cambridge University Press, London, 1935), p. 76. The phase conventions 14[7] and 4[8] on pp. 78 and 123 have not been used; instead j_2 is taken always to be the lesser angular momentum (when $j_1=j_2$ we use $j_1=L_\pi$, $j_2=L_\nu$ and j_1 for $2p$, j_2 for $3p$ neutrons). The phases of the functions in Table I depend on this convention; the results, of course, do not.

We illustrate by calculating the non-diagonal matrix element Q_{ij} between $2p^24fP$ and $2p^23pD$. After summing over spins this is equal to: $-(1/\sqrt{5})\int Q\bar{\Phi}_{2p^23d}(P^1)\Phi_{2p^23p}(D^1)$. On inserting the expansions of Table I, Q_{ij} further reduces to:

$$-(1/3\sqrt{5})\int Q\bar{\psi}_{P^1}(F_\pi D_\nu)\psi_{D^1}(P_\pi{}^*D_\nu).$$

The decomposition of $\psi_{P^1}(F_\pi D_\nu)$ in terms of product functions was given in Appendix I; the corresponding development for $\psi_{D^1}(P_\pi{}^*D_\nu)$ is: $6^{-\frac{1}{2}}\{-3^{\frac{1}{2}}P_\pi{}^{1*}D_\nu{}^0+P_\pi{}^{0*}D_\nu{}^1+2^{\frac{1}{2}}P_\pi{}^{-1*}D_\nu{}^2\}$. Integration over the neutron coordinates gives

$$\int Q\bar{\psi}_{P^1}(F_\pi D_\nu)\psi_{D^1}(P_\pi{}^*D_\nu)$$
$$=210^{-\frac{1}{2}}\{-3\sqrt{2}\int Q\bar{F}_\pi{}^1P_\pi{}^{1*}-\sqrt{3}\int Q\bar{F}_\pi{}^0P_\pi{}^{0*}$$
$$+\sqrt{2}\int Q\bar{F}_\pi{}^{-1}P_\pi{}^{-1*}\}$$
$$=2\cdot 210^{-\frac{1}{2}}\langle r^2\rangle_{3p,4f}\{-3\sqrt{2}I_{3,1;1,1}-\sqrt{3}I_{3,0;1,0}+\sqrt{2}I_{3,1;1,1}\}$$

where $I_{3,0;1,0}=3\sqrt{21}/35$ and $I_{3,1;1,1}=3\sqrt{14}/35$. Since $\langle r^2\rangle_{3p,4f}=(2\sqrt{14}/5)\langle r^2\rangle_{2p}$, the resulting value of Q_{ij} is $(4\sqrt{21}/15)(\langle r^2\rangle_{2p}/25)$.

PHYSICAL REVIEW VOLUME 80, NUMBER 1 OCTOBER 1, 1950

The Primary Specific Ionization and Intensity of the Cosmic Radiation above the Atmosphere at the Geomagnetic Equator*

S. F. SINGER
Applied Physics Laboratory, Johns Hopkins University, Silver Spring, Maryland
(Received June 9, 1950)

Directional intensities and the primary specific ionization of the charged cosmic-ray flux above the atmosphere were measured by means of a G-M counter telescope in an Aerobee sounding rocket launched at the geomagnetic equator. The intensity at a zenith angle of 45° averaged over all azimuths, was found to be 0.04 particle sec.$^{-1}$ cm^{-2} steradian^{-1}, of which not more than 65 percent can be attributed to primaries, the remainder being due to albedo. The low value (~40 percent) of the observed east-west asymmetry is most directly explainable in terms of positive proton primaries and a large albedo flux at large zenith angles, although a small contribution of negative primaries cannot be excluded.

The primary specific ionization of the radiation above the atmosphere is found to be essentially the same as that of the sea-level radiation, indicating a predominance of singly charged particles of near minimum ionization. This result strongly suggests that the albedo radiation at the equator does not consist of low energy (<100 Mev) protons.

Most of the properties of bursts produced in a small lead block can be accounted for reasonably in terms of known initiating particles and interactions.

I. EXPERIMENTAL ARRANGEMENT

An Aerobee sounding rocket (Round A-11) was fired at the geomagnetic equator about 600 miles off the coast of Peru from the USS Norton Sound on March 22, 1949. The rocket reached an altitude of over 100 km and spent 217 sec. above the appreciable atmosphere. Its trajectory and general flight history were very similar to those[1,2] of Aerobee A-10 which was fired a few days earlier.

This note is mainly concerned with results obtained with an unshielded telescope (Fig. 1) similar to that used in earlier work.[3] In addition to measuring the directional flux of charged radiation, it determined the average primary specific ionization of the radiation, essentially by measuring the efficiency of a low pressure hydrogen-filled counter. This method is not refined enough to determine the ionization of individual particles which traverse the telescope, but does have the advantage of experimental simplicity. All counters[4] were made of relatively thin-walled (0.020 inch) brass tubing with an inside diameter of 2.44 cm. Their effective length was 14.5 cm. As before,[3] the low efficiency counter B' was filled with pure hydrogen, this time to a pressure of only 2.5 cm Hg. Coincidences ABC, $AB'C$, and ACG were telemetered[5] to ground from the

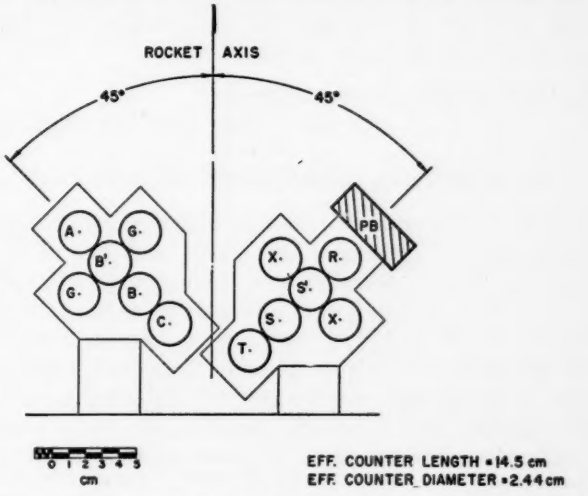

FIG. 1. Disposition in the rocket of telescopes ABC and RST, and lead block.

* Supported by the U. S. Navy, Bureau of Ordnance.
[1] J. A. Van Allen and A. V. Gangnes, Phys. Rev. **78**, 50 (1950).
[2] J. A. Van Allen and A. V. Gangnes, Phys. Rev. **79**, 51 (1950).
[3] S. F. Singer, Phys. Rev. **76**, 701 (1949).
[4] The counters were made up to our specifications by the Nuclear Development Laboratory, Kansas City, Missouri.
[5] G. H. Melton, Electronics **21**, 106 (1948).

TABLE I. High altitude plateau data of telescope *ABC*.

1 Time interval after launching	2 Time (sec.)	3 Number of coincidences (mutually exclusive) *ABC*	4 *ABB'C*	5 *ABCG*	6 *ABB'CG*
65–241[a]	167	61	39	43	29
245–295[b]	50	18	9	8	5

[a] Nine seconds of telemetering record were not read because of noise.
[b] The missile started to turn over at 241 sec. and was pointing nose down after 245 sec.

moving rocket. The experimental efficiency of counter B' was taken as the fraction of coincidences (ABC) accompanied by coincidences ($AB'C$); in terms of mutually exclusive coincidences,

$$\textit{efficiency} = ABB'C/(ABC+ABB'C).$$

The telescope was mounted with its axis at 45° to the missile axis. The solid angle of the telescope was covered only by the 0.040-inch aluminum skin (0.25 g/cm²) of the rocket in the upward direction and by part of a light electronic chassis (~1 g/cm²) in the downward direction. The only major burst producer in the vicinity was a block of lead located off to the side of the telescope ABC (Fig. 1). Most multiple-particle events are believed to have been eliminated by disregarding those cases in which a guard coincidence (ACG) occurred.

II. AVERAGE INTENSITY

The data obtained by telescope ABC are summarized in Table I and compared with sea level results in Table II. Corrections for telescope inefficiency, dead time, and accidental coincidences were negligible. The counting rates given are the net rates; i.e., with guard coincidences subtracted out. The directional intensity (corresponding to an average telescope zenith angle of 45°) was obtained from the net counting rate under the assumption of uniform intensity over the aperture of the telescope of flux incident from above, zero flux incident from the lower hemisphere:[6]

$$j_{av}(45°) = 0.040 \pm 0.003 \text{ particle (sec.}^{-1}\text{-cm}^{-2}\text{-steradian}^{-1}).$$

III. AZIMUTHAL DEPENDENCE OF INTENSITY

A set of 16 photo-cells, together with a magnetometer, were used to determine the aspect and roll of the missile. The roll period during the vacuum trajectory was 1.7 sec.; the angle of the missile axis to the vertical varied from 0° to 15° during the major portion of flight. A histogram of telescope counts *vs.* azimuth angle of the telescope was constructed for the time interval 65–241 sec. and a smooth curve of the form $y = a_0 + R\cos(\phi+\delta)$ fitted to it by least squares technique

[6] In a preliminary account of this experiment given at the Echo Lake Cosmic-Ray Symposium, June 1949, the telescope geometric factor for isotropic radiation was given as 13.5. Subsequently, this factor was corrected to 14.5.

TABLE II. Summary of results (telescope *ABC*).[a]

	1 Sea level (λ =0°)	2 High altitude plateau
(Net) counting rate (sec.$^{-1}$) (at 45° zenith angle)	0.0521 ±0.0028	0.585 ±0.052
Geometric factor (cm²-steradian)	11.9	14.5
(Net) directional intensity (at 45° average zenith angle) (sec.$^{-1}$ cm^{-2} steradian^{-1})	0.00437 ±0.00023	0.0403 ±0.0035 (av.)
Efficiency of counter B'	0.356 ±0.015[b]	0.378 ±0.043 (net) 0.387 ±0.034 (gross)

[a] All errors quoted are standard errors based only on the number of counts.
[b] This measurement made at Silver Spring, Maryland, (λ =50°N) with telescope in vertical position.

(Fig. 2). This procedure was employed to obtain the maximum and minimum intensities and azimuthal asymmetry of column 2 in Table III. A detailed account of the analysis is given in reference 2. Our results are evidently in very good agreement with data obtained by a telescope of different geometry in Aerobee rocket A-10 (column 3 in Table III).[2] *As anticipated, the maximum of the flux of the radiation above the atmosphere occurs in a westerly direction; the absolute value of the azimuthal asymmetry, however, is markedly less than expected.*

IV. PRIMARY SPECIFIC IONIZATION

The measured sea-level efficiency[7] of counter B' corresponds to particles of about minimum specific ionization $J_{p\,\min}$. The efficiency from the data on the cosmic-ray plateau above the atmosphere (Table II)[8] can be compared with the sea-level efficiency after applying the necessary corrections.

As before,[3] a geometrical correction has to be made to the efficiency, since the average path length through counter B' increases in going above the atmosphere as the zenith angle distribution of the radiation changes from a $\cos^2\theta$ dependence to a more nearly isotropic distribution. This additive correction for our particular case is about −0.02. No correction has been made for knock-on electrons, since they are also present in the sea-level case, and the difference can be considered negligible. No correction is made for nuclear bursts, since it can be assumed that most bursts tripped a guard counter and have, therefore, been already subtracted.

The average primary specific ionization of the radiation above the atmosphere is then found to be $1.0 \pm 0.2 J_{p\,\min}$. Essentially the same result is obtained by comparing the counting rate of a low efficiency single

[7] The efficiency of the counter can be computed from the formula eff.$=(1-e^{-J_p LP})$, where $P=2.5/76$ atmos., and the efficiency (Fig. 3) is averaged according to telescope geometry and zenith angle dependence of radiation over all path lengths L; it equals the experimental efficiency for a value of J_p of 6 ion pairs/cm/atmos. H_2. This calculation serves as a check on the reasonableness of our experimental efficiency.

[8] It may be noted that the "gross" efficiency (i.e., multiple particle events not subtracted out) is experimentally equal to the "net" efficiency.

counter[9] (column 1 of Table IV) to the full efficiency counter used[1] in Aerobee A-10 (column 3 of Table IV). The higher efficiency of the single counter, compared to the counter as part of a telescope, can be explained qualitatively as due to the longer path lengths possible in a single counter.

The gross conclusion then is that the *bulk of the ionizing radiation above the atmosphere at the geomagnetic equator* carries a *single charge* and has a *primary specific ionization very close to minimum.* This conclusion may be compared with the result obtained at White Sands, New Mexico ($\lambda=41°$N)[3] where the primary specific ionization of the radiation above the atmosphere was found to be $1.30\pm0.15 J_{p\ \min}$.

V. CHARACTER OF THE PRIMARY RADIATION

The experimental results on the flux, azimuthal asymmetry, and specific ionization can be used for drawing some simple conclusions concerning the character of the charged radiation above the atmosphere at the equator.

It is of interest to find what fraction of particles counted by our telescope is due to albedo; i.e., secondary particles originating in the earth's atmosphere whose directional dependence bears no simple relationship to that of the primaries which produced them. If we take the flux value of 0.028 in the vertical direction[1] as the primary intensity (it is really an upper limit to the primary intensity), the primary intensity at 45° zenith angle, averaged over all azimuths, is about 10 percent less,[10] and is the same for a primary radiation of either sign, or for any mixture of positive and negative particles. Comparing then 0.025 with the experimental intensity of 0.040, we conclude that at least 35 percent of the intensity measured is caused by albedo.

From rocket measurements of the vertical intensity at various latitudes, it may be inferred[11] that a power law spectrum of the form $N(>pc/\mathrm{Ze})=0.48(pc/\mathrm{Ze})^{-1.1}$ relates intensity to magnetic rigidity of the primary radiation for rigidities ranging from 2 to 15 Bv. Extrapolating this spectrum to much higher rigidities, the east-west asymmetry at a zenith angle of 45° at $\lambda=0°$ would be 0.84, much larger than is admissible by our experiment. It is probably more realistic to assume a greater spectrum exponent at these higher energies, which would raise the expected east-west asymmetry still further. To explain our low experimental value of asymmetry it may not be necessary to invoke the existence of negatively charged primaries. Any mixture of negative and positive primaries should still lead to a slight *decrease* of intensity with zenith angle.[10] The increase of intensity with zenith angle, and the low value of azimuthal asymmetry may both be reasonably ascribed to albedo.[12] *Our results are, therefore, consistent with the existence of a primary radiation composed mainly of positive protons.*

VI. CHARACTER OF THE ALBEDO RADIATION

The data on the primary specific ionization, which was found to be $1.0\pm0.2 J_{p\ \min}$ in Section IV, can now be used to draw more detailed, but rather qualitative conclusions about the ionizing radiation above the atmosphere. Purely on the basis of the data of this experiment an upper limit of about 20 percent can be given for the percentage of particles with charge greater than unity; however, it seems most reasonable to assume that they constitute a much smaller percentage of the *total* radiation measured, which includes a large fraction of albedo. We can assume safely that the primary protons have a specific ionization near minimum since their momenta are known from geomagnetic considerations. This is not the case for the albedo. However, for each type of albedo particle, provided this type is assumed to constitute the bulk of the albedo radiation, we can give an approximate range in which the energy lies. We make use of the fact that the primary specific ionization has its minimum value, $J_{p\ \min}$, near a momentum about four times the particle rest mass (Fig. 4). For much higher momenta J_p shows a slow relativistic increase. For lower momenta, however, J_p rises very rapidly. To satisfy our experimental result, which gives for J_p of the radiation above the

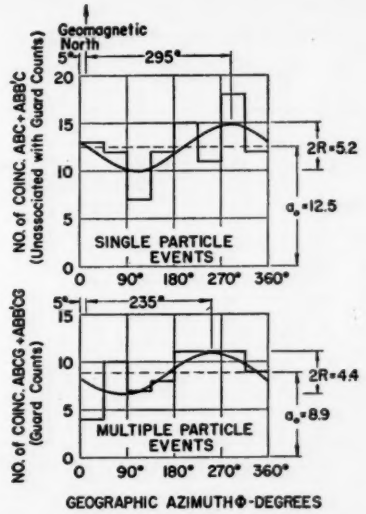

FIG. 2. Histograms of single particle events and multiple particle events respectively, of telescope ABC in 45° segments of azimuth taken for a period of 167 seconds above the atmosphere. The smooth curves are least-square fits to the histogram and are of the form $y=a_0+R\cos(\phi+\delta)$.

[9] Two low efficiency single counters (identical with counter B' of the telescope) were mounted along the axis of the rocket near the tip of the instrumentation nose cone; their counting rates were telemetered to ground.

[10] This result can be deduced from Vallarta's theory of the main cone under the assumption of a reasonable number-spectrum; the zenith angle dependence is very insensitive to the value of spectrum exponent chosen for this computation.

[11] J. A. Van Allen and S. F. Singer, Phys. Rev. 78, 819 (1950).

[12] A similar excess of experimental intensity at large zenith angles over intensity calculated using geomagnetic theory has been observed previously at $\lambda=41°$N and ascribed to albedo by S. F. Singer, Phys. Rev. 77, 729 (1950).

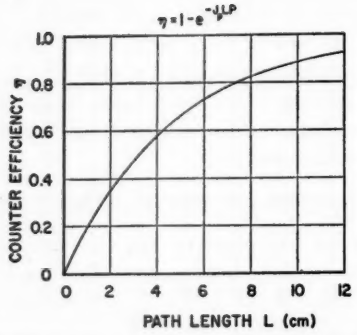

FIG. 3. Efficiency of low pressure (2.5 cm Hg) hydrogen-filled counter B' (or S') *vs.* path length L of a traversing particle of minimum ionization.

atmosphere a value close to $J_{p\,\min}$, we must assume the absence of a large fraction of electrons of energy in excess of 30 Mev, mesons in excess of 6 Bev, and protons in excess of 60 Bev. The last possibility is, of course, extremely unlikely, purely on the basis of energy considerations. Because of the steep rise of the primary specific ionization curve at energies below the minimum, we can exclude with more definiteness even a small percentage of mesons with energies less than 100 Mev, and protons with energies less than about 1 Bev. Electrons of energy less than 10 Mev are excluded as being too soft to pass through the telescope. *These considerations strongly suggest that the bulk of the albedo radiation consists of relatively high energy (>1 Bev) protons and/or 10–30 Mev electrons.* Mesons in the lower ranges of energy can be excluded on the basis of their short lifetimes.

It might be pointed out again that the present data are not consistent with the assumption that a great number of low energy (about 100 Mev) protons[13] are produced in the initial encounters of the primaries, so as to constitute a large fraction of the cosmic-ray flux above the atmosphere *at the equator*. On the other hand, the data on efficiency (Table IV) show a maximum efficiency near the Pfotzer maximum, a phenomenon previously found[14] at $\lambda = 41°$N. This result can be explained reasonably as being due to low energy protons which have been generated some distance below the top of the atmosphere.

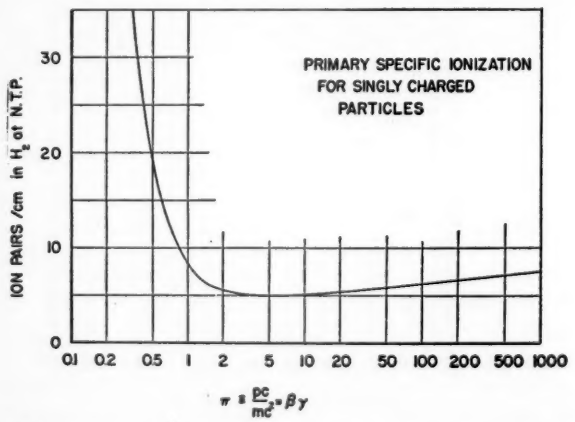

FIG. 4. Primary specific ionization in ion pairs/cm in H_2 at N.T.P. for singly charged particles as a function of their specific momentum $\pi = pc/mc^2$. For particles of charge Ze, the values of the ordinate are multiplied by Z^2.

[13] Assuming 35 percent of the radiation to consist of 100 Mev protons (specific ionization from Fig. 4 of $4J_{p\,\min}$, corresponding to a counter efficiency from Fig. 3 of 0.85), the telescope efficiency would have to be $0.35\times0.85+0.65\times0.38=0.55$, which is clearly much higher than the observed value of 0.38 ± 0.04.

This expedition has been made possible by the continuing support of the U. S. Navy Bureau of Ordnance and by the cooperation of many other branches of the Naval organization; in particular, the Naval Unit of the White Sands Proving Ground, the USS Norton Sound, the USS Agerholm, the USS Richard B. Anderson, and the Naval Ordnance Laboratory.

Special thanks are due Captain T. A. Ahroon, USN, and the other officers and men of the USS Norton Sound for the conduct of the expedition and the rocket firing.

The author is indebted to Professor M. S. Vallarta and to Dr. J. A. Van Allen for discussion of results. Messrs. W. A. Bowen and E. Maple of the Naval Ordnance Laboratory collaborated on the magnetometer phase of the operation. Mr. L. W. Fraser of this Laboratory and Mr. R. F. Ohlemacher of the New Mexico College of Agriculture and Mechanic Arts contributed essentially in the accomplishment of this experiment.

APPENDIX. PROPERTIES OF BURSTS PRODUCED IN LEAD

We wish to present some data of an exploratory experiment which relate to the shielded low efficiency telescope *RST* (Fig. 1)

TABLE III. Angular distribution of intensity.

1 (Net) directional intensity (at av. zenith angle 45°) (sec.$^{-1}$-cm^{-2}-steradian^{-1})	2 Telescope *ABC*	3 A-10 telescope (reference 2)
Average	0.0403±0.0035	λ.0410±0.0021
Minimum	0.032 ±0.005	0.031 ±0.004
Maximum	0.048 ±0.005	0.048 ±0.004
Asymmetry $2R/a_0$	0.42 ±0.28	0.41 ±0.16
Geomagnetic azimuth of maximum	295° ±40°	268° ±15°

TABLE IV. Single counter data on cosmic-ray plateau.

	1 Low efficiency counter	2 Low efficiency counter (shielded with 0.5 cm Pb)	3 Efficient counter (A10)[a]
Counting rate/sec.	4.18±0.16	4.75±0.40	9.7±0.17
Geometric factor (isotropic)	189.5	189.5	185
Av. directional intensity (particles-sec.$^{-1}$ cm^{-2} steradian^{-1})	0.022±0.001	0.025±0.002	0.0525±0.0009
Efficiency	0.42±0.02	0.48±0.04	~1.00
Efficiency at Pfotzer maximum	0.46	0.63	~1.00

[a] See reference 1.

[14] S. F. Singer, Phys. Rev. 77, 730 (1950).

TABLE V. High altitude plateau data of telescope *RST*.

1 Time interval after launching	2 Time (sec.)	3 Number of coincidences (mutually exclusive) *RST*	4 *RSS'T*	5 *RSTX*	6 *RSS'TX*
65–241	167	43	32	48	67
245–295 (rocket pointing nose down)	50	22	8	8	13

TABLE VI. Summary of results (telescope *RST*).

Time interval	Directional flux (av. zenith angle of 45°)—sec.$^{-1}$ cm^{-2} steradian^{-1} Gross (with guard counts)	Net (without guard counts)	Efficiency Gross	Net
65–241	0.079±0.006	0.031±0.004	0.52±0.05	0.43±0.06
245–295	0.070±0.010	0.041±0.007	0.41±0.07	0.27±0.08

and the effects of the lead block on the unshielded telescope *ABC*. Statistics are not good enough to give any more than qualitative ideas, but on the whole they do strengthen the evidence presented by the unshielded telescope. Telescope *RST* was identical in all respects to telescope *ABC*, except for the 2 cm thick lead block covering its aperture. The sea-level calibrations on telescope *RST* (obtained without the lead shield) agreed within the statistical error with those of telescope *ABC* (column 1 of Table II). It can be seen from the data obtained when the rocket was pointing nose down (time interval 245 to 295 sec., Table VI) that, when the lead block is *below* telescope *RST*, the net flux and net efficiency of telescope *RST* agree very well with those of telescope *ABC* (Table II).

The pertinent data are presented in Tables V and VI.

It was originally hoped that the arrangement of lead block and counters would demonstrate two experimental features:

(A) *A directional burst detector:* telescope *RST* (and particularly the shower counts *RTX*) would show a very pronounced east-west asymmetry, much larger than the unshielded telescope *ABC*, for two reasons: (a) the lead would stop soft albedo entering from above and (b) produce bursts predominantly preserving the direction of the primary rays. This was not found to be the case; on the contrary, the azimuthal asymmetries of both net counts and gross counts of telescope *RST* were insignificantly different from zero.

(B) The other purpose was to demonstrate the use of a low efficiency counter as a device to indicate *narrow showers* which could not have been resolved as multiple events by Geiger counters of reasonable diameters.

It appears that the experimental efficiency (Table VI) is considerably higher than in the unshielded telescope indicating that heavily ionizing particles or narrow bundles of lightly ionizing particles, which originate in the lead block, are traversing counter *S'*. This result is supported qualitatively by the high efficiencies of the shielded low pressure counter (column 2 of Table IV).

We may finally note the effect of the lead block on the unshielded telescope *ABC*, i.e., on the guard counts *ABCG* and *ABB'CG*.

(a) The guard counting rate falls to a very low value when the rocket points nose down (Table I), indicating that the lead block produces most of the showers;

(b) A large azimuthal asymmetry, 0.50±0.34, is present (Fig. 2);

(c) The gross efficiency corresponds to particles of about minimum specific ionization (Table II).

We can harmonize results (A) and (B) with (b) and (c) above by assuming that the primary radiation in traversing the lead block produces both showers which preserve the original direction and showers which are mostly isotropic. Telescope *ABC* is not very sensitive to the latter type of event, since it is sufficiently far removed from the lead block to experience fairly low particle densities. It therefore exhibits asymmetry and a lower gross efficiency, whereas telescope *RST* does not. We cannot, however, account simply (i.e., in terms of known processes and known primary particles), for the *sign* of the asymmetry of the shower counts *ABCG*+*ABB'CG* (Fig. 2). With the lead block off to the side of telescope *ABC* (Fig. 1) the maximum of the guard counting rate should occur when telescope *ABC* points east if *positive* primaries produce showers predominantly in the *forward* direction. The precision of the present measurement is too low to allow us to draw any firm conclusions. We hope to be able to investigate this matter further experimentally.

A Determination of the High Altitude Latitude Dependence in Cosmic-Ray Neutron Intensity*

WILLIAM P. STAKER†
New York University, New York, New York
(Received May 1, 1950)

High altitude flights have been made with balloon-borne neutron-detecting equipment at 30.4°N and 54.7°N geomagnetic latitudes. A maximum neutron density was found at an absorption depth of 110 g/cm² at 30.4°N and 100 g/cm² at 54.7°N. The maximum neutron density at 54.7°N is approximately 2.9 times as great as the maximum neutron density measured at 30.4°N. The total integrated neutron density at 54.7°N is approximately 2.4 times as large as that at 30.4°N. These results indicate a greater latitude effect for neutron densities than for total ionization, but less than for primary particles, thus corroborating present theories of neutron formation.

I. INTRODUCTION

A MEASUREMENT of the neutron density as a function of latitude and altitude has been made by means of high altitude balloon-borne equipment at 30.4°N and 54.7°N geomagnetic latitude. As atmospheric neutrons associated with cosmic radiation have been measured by several authors,[1–11] the theory of their origin and vertical distribution is fairly well established. In particular, Bethe, Korff, and Placzek[12] have done much toward this theoretical development which Flugge[13] and Davis[11] have revised by the use of more current experimental data. The latitude dependence for charged cosmic radiation has been studied by several experimenters,[14–16] and the theory has been worked out in great detail by Lemaitre and Vallarta[17] and by Vallarta.[18,19]

II. NEUTRON-DETECTING PROPORTIONAL COUNTERS

Korff and Danforth[20] have described how proportional counters filled with the gas, BF_3, can be used in the detection of neutrons by means of the $B(n,\alpha)Li$ reaction. It should be mentioned that it is only the B^{10} isotope which works, and in normal boron this isotope amounts to 19 percent[21] with B^{11} the predominant isotope.

The capture rate of neutrons in the atmosphere is given in the equation developed by Bethe[12]

$$q=780(n\sigma_a/V_d\sigma_d p_{0d})\ \text{g}^{-1}\ \text{sec.}^{-1}, \qquad (1)$$

where n is the counting rate of the counter; σ_a and σ_d are the cross sections for air and the detector, respectively, for neutrons of the same energy; V_d is the active volume of the detector; and p_{0d} is the pressure in atmospheres of the detecting gas at 0°C.

The number of neutrons per gram per second absorbed in the atmosphere at any altitude can be calculated using Eq. (1). In the middle portion of the atmosphere the capture rate is in equilibrium with the production rate, so that Eq. (1) in such regions also gives the production rate.

In the past, many experimenters[2,3,5–7] have used such BF_3-filled counters in conjunction with cadmium shields in order to obtain an estimate of the neutron density. Since cadmium has an extremely high cross section for slow neutrons, one can assume that the difference in counting rate obtained between a counter when shielded with cadmium and when unshielded will be proportional to the number of neutrons absorbed by the shield. In this way, one can calculate the number of neutrons below 0.4 ev, which is approximately the cadmium cut-off.

In the present experiment, however, it seemed better to use another method of eliminating background counts. During the past year BF_3 has become available in two concentrations of B^{10} other than that found in nature. These available concentrations are 10 percent B^{10} and 96 percent B^{10}. Identical counters were filled to the same pressure, one with BF_3 enriched in the B^{10} isotope and the other with the BF_3 containing only 10 percent B^{10}. It is assumed that if both counters are exposed to the same neutron flux there will be the same amount of background due to recoils, stars, etc., and the

* Assisted by the joint program of the ONR and AEC and by the USAF.

† This report is an abridgment of a dissertation submitted in partial fulfillment of the requirements for the degree of Doctor of Philosophy at New York University, 1950.

[1] C. G. and D. D. Montgomery, Phys. Rev. **56**, 10 (1939).
[2] S. A. Korff, Phys. Rev. **56**, 210 (1939).
[3] S. A. Korff and B. Hamermesh, Phys. Rev. **71**, 842 (1947).
[4] Agnew, Bright, and Froman, Phys. Rev. **72**, 203 (1947).
[5] S. A. Korff and A. Cobas, Phys. Rev. **73**, 1010 (1948).
[6] J. A. Simpson, Phys. Rev. **73**, 1389 (1948).
[7] L. C. L. Yuan, Phys. Rev. **74**, 504 (1948).
[8] Simpson, Baldwin, and Uretz, Phys. Rev. **76**, 165 (1949).
[9] L. C. L. Yuan, Phys. Rev. **76**, 165 (1949).
[10] J. A. Simpson and R. B. Uretz, Phys. Rev. **76**, 569 (1949).
[11] W. O. Davis (to be published).
[12] Bethe, Korff, and Placzek, Phys. Rev. **57**, 573 (1940).
[13] W. Heisenberg, *Cosmic Radiation* (Dover Publications, New York, 1946).
[14] A. H. Compton, Phys. Rev. **43**, 387 (1933).
[15] T. H. Johnson, Rev. Mod. Phys. **10**, 193 (1938).
[16] H. Carmichael and E. G. Dymond, Proc. Roy. Soc. **171A**, 321 (1939).
[17] G. Lemaitre and M. S. Vallarta, Phys. Rev. **43**, 88 (1933); Phys. Rev. **50**, 493 (1936).
[18] M. S. Vallarta, J. Franklin Inst. **227**, 1 (1939).
[19] M. S. Vallarta, Phys. Rev. **74**, 1837 (1948).
[20] S. A. Korff and W. E. Danforth, Phys. Rev. **55**, 980 (1939).
[21] M. G. Inghram, Phys. Rev. **70**, 653 (1946).

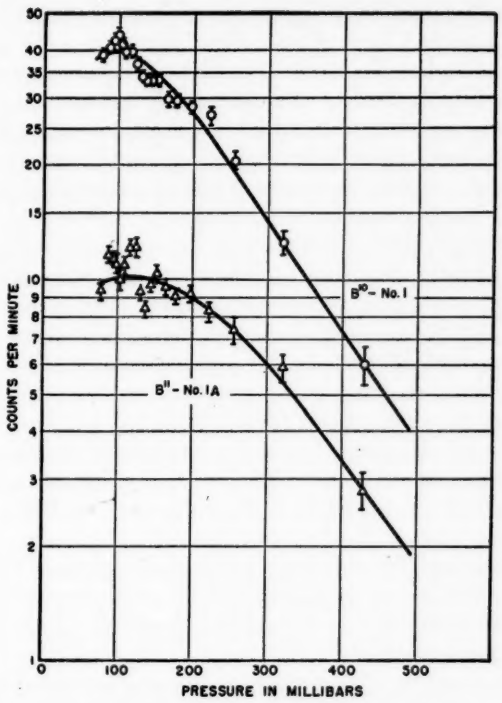

FIG. 1. Individual counting rates. Flight 49, 54.7°N. October 30, 1949.

total counting rate for the enriched counter will be: $A=(0.96N+b)$ c.p.m., while for the isotopically depleted counter it will be: $B=(0.10N+b)$ c.p.m. In each case, N is the expected counting rate for a counter containing 100 percent B^{10} and b is the background. If these equations are solved, we have: $N=(A-B)/0.86$, and $b=B-0.10N$.

It is the value of N which is of most interest here, since this is the neutron density for all neutrons which will cause a count. The dependence of the background, b, upon altitude and latitude also is of interest, since this may give information relative to the cause of this background which we would expect to be caused by large ionizing events such as stars, giant showers, natural contamination alpha-particles, and slow protons.

An additional thing which must be considered is the effect of materials surrounding the BF_3 in the counters. Both copper and aluminum have relatively low absorption cross sections for neutrons, so these surrounding metals should not make a measurable reduction in the counting rates. Actually, both will act as star-producing material, but since the same amount is involved for each counter, counts from this source should cancel out in the background.

III. APPARATUS

The equipment used in these experiments was recently developed at this University especially for the purpose of measuring neutron intensities at high altitudes and has been described by Pavalow, Davis, and Staker.[22]

Two proportional counters filled with gaseous BF_3 were used in each set of apparatus. Other than the filling gases, the counters were identical in construction, and the enriched counters flown at both latitudes were filled simultaneously on the same manifold to the same pressure. Also, the same method of filling was used with the depleted counters, and all possible precautions were taken to make these depleted counters as identical as possible to the enriched B^{10} counters.

The gases used were obtained by heating the BF_3 complex, $BF_3 \cdot CaF_2$. Complex containing the depleted BF_3, as well as complex containing enriched BF_3, was obtained from the Isotopes Division of the Oak Ridge National Laboratory of the AEC.

The counters were checked for contamination background by running them inside a boron shield. This background was less than one-quarter count per minute for each counter used. In addition, a long run was made with each counter in a given geometrical arrangement near a neutron source. In this manner it was possible to see that the counters of the same enrichment were similar in efficiency and that there was the proper ratio between the counting rates of the enriched and depleted counters. No absolute calibration was made of the counters because of the difficulty of obtaining a neutron source with an energy spectrum comparable to that in the atmosphere.

As a result of a number of tests, it was determined

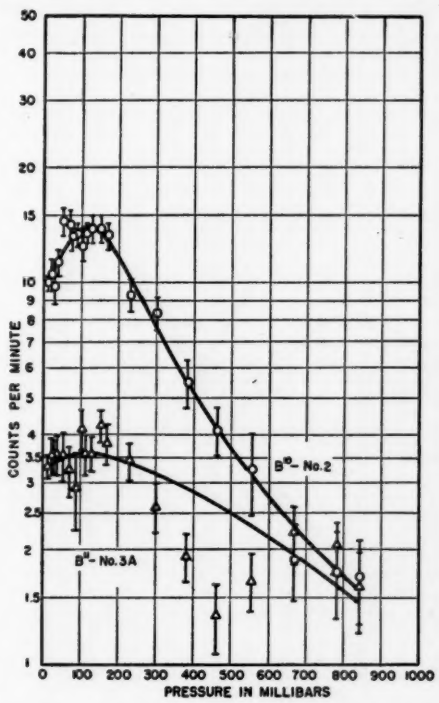

FIG. 2. Individual counting rates. Flight 51, 30.4°N. November 18, 1949.

[22] Pavalow, Davis, and Staker, Rev. Sci. Inst. 21, 529 (1950).

that for consistent results without spurious counts the counters and high voltage system should be pressurized. Lack of such pressurization is evidenced by extra counts at atmospheric pressures corresponding to approximately 40,000 feet or higher. These spurious counts can be traced to a corona discharge taking place between some points of the high voltage system and the frame. In addition, it has been noticed that within the high voltage batteries themselves there appears to be a corona discharge when the pressure of the air surrounding them is less than 185 mb. Therefore, the counters are sealed in aluminum tubes, while the high voltage batteries are located in a welded aluminum box. They are connected by high voltage leads contained in copper tubing sealed by standard flare pressure fittings. The low voltage leads from the central wire of the counter emerge through pressure fittings to the succeeding circuitry.

The flight frame was designed to provide a minimum of star-producing material in the hemisphere above the counter. As a result, all batteries are on a lower shelf of the frame so that all heavy materials are in the center and below the counter. In addition, the counters are mounted with their longitudinal axes in line so that a minimum solid angle is subtended by one counter upon the other.

IV. EXPERIMENTAL RESULTS

For this determination of the latitude dependence of cosmic-ray neutrons at high altitude, one flight was satisfactorily completed at each of two latitudes, namely, 30.4° and 54.7°N geomagnetic latitude.

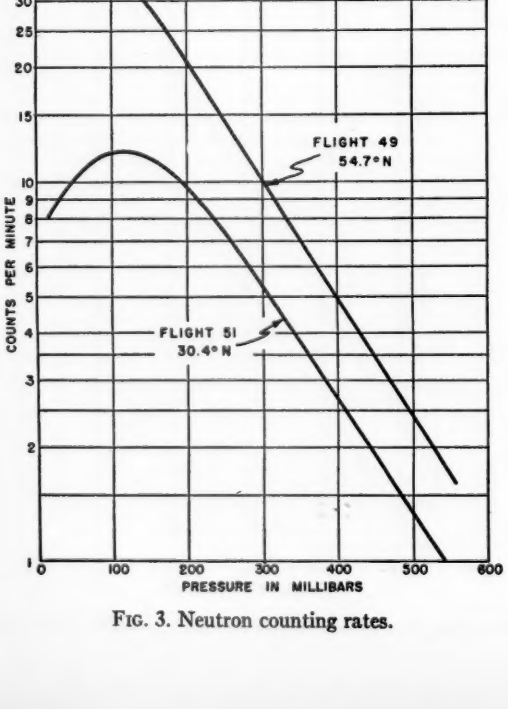

FIG. 3. Neutron counting rates.

The flight at 54.7°N geomagnetic latitude, Flight 49, was launched from Rome, New York, at 7:35 A.M., EST, October 30, 1949. This flight has been reported previously by Davis.[11] A single plastic balloon was used which rose until it reached a maximum altitude of 59,675 feet, where it leveled off. However, instead of remaining stable, the balloon began a slow descent of about 200 ft./min. for some time.

Although the balloon did not stay as long as expected at the maximum altitude, its slow rate of descent proved to be a benefit, because it allowed relatively long counting periods over the range from 60,000 feet down to about 40,000 feet. At this lower altitude, the descent became much more rapid and little worth-while data was received below this point.

The second flight, Flight 51, was launched at 30.4°N geomagnetic latitude, slightly south of Guantanamo Bay, Cuba, at 6:16 A.M., EST, November 18, 1949. The balloon rose at a rate of about 850 ft./min. until it reached equilibrium conditions at approximately 96,000 feet. A relatively large number of counts was recorded at this level, and consequently the statistical accuracy was much improved.

The data for Flight 49 are shown in Fig. 1, and those for Flight 51 are shown in Fig. 2. All of the counting rates are handled as functions of pressure, because pressure is much more significant in diffusion theory than is the physical altitude in feet. The millibar in particular was used because it is the standard meteorological unit and because the Olland cycle modulators were calibrated in these units. In addition, it is quite convenient because the pressure in millibars is approximately equal to the thickness of the absorbing layer in g/cm². That is, 1 mb = 10^3 dynes/cm² = $10^3/980$ g/cm² = 1.02 g/cm².

The neutron counting rates calculated from the individual counting rates of the enriched and the depleted counter, as shown in Figs. 1 and 2, are plotted in Fig. 3. These rates are obtained using the relation, $N=(A-B)/0.86$, which has been derived earlier. Figure 3 shows that the neutron intensity at 54.7°N is approximately 35 counts per minute, while at 30.4°N it is close to 12 counts per minute. This ratio of 2.9 to 1 is comparable to the results of other experimenters at lower altitudes. Although little data existed at the higher pressures for Flight 49, a slope of $\mu=0.007$ mb^{-1} seemed to be as satisfactory for it as for Flight 51, if we assume the relation, $N=N_0\exp(-\mu p)$, where we report p in millibars.

V. DISCUSSION OF RESULTS

The results, as plotted in Fig. 3, clearly show that a maximum counting rate occurred during each flight at an absorption depth of about 100 g/cm². This value is of considerable interest since it is approximately the value that we would expect from calculations based on the work of Bethe, Korff, and Placzek[12] and Flugge.[13] Following their method, we calculate the value of the

mean absorption depth to be less than 100 g/cm², that is, 89 g/cm². This slightly larger measured result is consistent with the fact that the neutrons are not all formed exactly at the top of the atmosphere but throughout a range of depths beginning near the top.

Actually the maximum does not occur exactly at the same pressure for each flight, but the curves show that for the 30.4°N flight it is at 110 g/cm² instead of the 100 g/cm² recorded at 54.7°N. This difference of pressure at which the maximum occurs is in good agreement with the fact that the incoming primary particles are, on the average, more energetic at lower latitudes, which causes the secondary particles to be formed at slightly lower altitudes; i.e., at greater pressures.

It is of interest to compare the results reported here with those obtained by other experimenters. Simpson[6] has reported data obtained in a B29, both as a function of altitude and as a function of latitude. If we extrapolate from his curves to obtain data comparable with ours, we find that at a pressure of 30 cm Hg (400 mb), he obtained 340 counts at 55°N and 200 at 30°N. This would give a ratio of $N_{55}/N_{30}=1.70$. From Fig. 3, we find for 400 mb: $N_{55}/N_{30}=4.8/2.8=1.72$. Actually, the agreement between the author's data and that of Simpson is considerably closer than might be expected. Simpson was measuring only neutrons with energies greater than 0.4 ev because of the arrangement of his experiment. He shielded everything with cadmium and then enclosed his counters with paraffin in order to slow down the neutrons which had penetrated the cadmium to a point where the counter would record them. Consequently, the mean energy of the neutrons whose density Simpson measured was slightly higher than those reported here.

Yuan[23] made measurements of neutron density using a B29 which flew at an altitude corresponding to 28.2 cm Hg (376 mb). Although this is a slightly lower pressure than that of Simpson mentioned above, it is close enough for a good comparison. Yuan's values of counting rates yield a ratio: $N_{55}/N_{30}=23/11.5=2.0$. This is in quite good agreement with the value of Simpson and the author. Again, it should be pointed out that the experiment with which we are comparing is not identical with that reported in this paper. Yuan used a cadmium shield on one counter, so that he was recording the density of neutrons below 0.4 ev, rather than those above 0.4 ev as reported by Simpson, or those of all low energy values as reported herewith.

Some mention should be made of the relation, $N=N_0\exp(-\mu p)$, which was used to relate the neutron densities at different pressures. As mentioned in the previous section, a value of $\mu=0.007$ mb^{-1} was assumed for the data under consideration. This value is probably correct within 10 percent, and from the statistics reported is as close as can be expected. Allowing a 10 percent variation would make it compare quite favorably with the 0.0067 mb^{-1} of Bethe, Korff, and Placzek,[12] the 0.0065 mb^{-1} of Yuan,[24] the 0.0063 mb^{-1} of Simpson[6] and of Agnew, Bright, and Froman,[4] and the 0.007 mb^{-1} suggested by Flugge.[13] Taking the reciprocal of the value given we find that the corresponding absorption thickness is 143 g/cm², or of the order of 150 g/cm², as reported by Bethe, Korff, and Placzek.[12] Bernardini,[24] in discussing the nucleonic cascade, assumes a value of 140 g/cm² for the neutron-producing radiation.

Comparison of these data should be made also with the high altitude data of Yuan.[23,25] At a latitude of 53°N, he obtained a maximum in the neutron counting rate data at 114 g/cm², which is at a point slightly lower (i.e., a higher pressure) than the maximum we report at 100 g/cm² for 54.7°N. This difference can be explained by the fact that, as mentioned earlier, Yuan was measuring neutrons of energies below 0.4 ev. Thus, it can be implied that the neutrons Yuan measured had traveled slightly farther, on the average, than those measured by the technique reported here. Another reason for the discrepancy is that the neutron counters used in this experiment had Pyrex glass envelopes. The use of Pyrex glass would tend to alter somewhat the energy relations of the neutrons counted.

In addition to a comparison of the present results with the neutron density measurements of other authors, we should like to make a comparison with relations obtained in measuring other components of the cosmic radiation. In making this comparison, we will remember that in the present experiment we obtained an absorption depth of approximately 143 g/cm². This value of L, used in the equation $N=N_0\exp(-p/L)$, relates the neutron density to the altitude, and yields a straight line on a semilogarithmic plot, as seen in Fig. 3.

Comparing first with nuclear explosions which cause the stars found in photographic emulsions, we see that Perkins[26] reports that there is an increase in the number of stars with altitude which corresponds to an atmospheric absorption thickness of about 135 g/cm². This value would indicate a close correlation between neutron production and nuclear explosions, as was mentioned earlier.

Another convenient method for obtaining the rate of occurrence of nuclear reactions as a function of altitude is a study of bursts in ionization chambers. Several experimenters have shown that these bursts are well represented by the usual equation if we give a value of 138 g/cm² for the absorption thickness. This value is not significantly different from that mentioned above for stars, and only slightly lower than our value of 143 g/cm² for neutrons. Rossi[27] has plotted the altitude dependence of these ionization bursts with the data of Yuan[7] and Agnew, Bright, and Froman[4] for neutron measurement in order to emphasize the close relation-

[23] L. C. L. Yuan, Phys. Rev. **76**, 1267 (1949).

[24] G. Bernardini (private communication).

[25] L. C. L. Yuan, Princeton University (unpublished data).

[26] D. H. Perkins, Nature **159**, 126 (1947); **160**, 707 (1947).

[27] B. Rossi, Rev. Mod. Phys. **20**, 537 (1948).

ship of bursts with neutrons. As we have mentioned earlier, these neutron data correlate quite well with our neutron data at comparable low altitudes.

Another point which we should discuss is the integral of the area under the curves in Fig. 3. An approximate integration of these values results in a ratio of 2.4 for the area at 54.7°N to that at 30.4°N. This ratio would indicate that approximately 1.4 times as many of the primary particles have energies between 1.0 Bev and about 8.3 Bev as have energies above 8.3 Bev. This point is based on the assumption that the particles causing neutron production are protons, with the energies mentioned being those for vertical incidence, as given by Vallarta.[19] In addition, it is assumed that the multiplicity of neutron production varies but little with primary energy.

From the integrated total of neutrons in the atmosphere obtained at each latitude, one can calculate the total number of neutrons per cm² column at each altitude by means of Eq. (1). This value is 0.98 cm^{-2} $sec.^{-1}$ at 54.7°N, and 0.41 cm^{-2} $sec.^{-1}$ at 30.4°N. The first value is approximately half the value of 1.9 cm^{-2} $sec.^{-1}$ obtained by Yuan[24] at a latitude of 53°N. This difference in value between Yuan's data and that in the present experiment is of the same order of magnitude as the difference in data for neutron production. Yuan obtains 3.6×10^{-3} g^{-1} $sec.^{-1}$ at 20 cm (267 mb), while at the same altitude we obtain 1.45×10^{-3} g^{-1} $sec.^{-1}$. A large fraction of this difference is due to the boron content in the glass of our neutron detectors.

Of interest also is the relation of neutron intensity to total radiation. If we use the information obtained by Bowen, Millikan, and Neher[28] for the total intensity, we find that upon interpolation we obtain a ratio of 1.85 for the maximum of ionization per cm³ per sec. at 55°N to the maximum at 30°N. This ratio can be compared with the value 2.9 for the maximum for neutron densities reported here. Integration of the data of Bowen *et al.* as done by Johnson,[15] leads to a total energy of 2.3 Bev cm^{-2} $sec.^{-1}$ entrant into the atmosphere at 55°N and 1.5 Bev cm^{-2} $sec.^{-1}$ at 30°N. A ratio of 1.5 is obtained from these values, while the integration of our neutron curves yields a ratio of 2.4 for the two latitudes under question. We must be careful to realize that we are not comparing identical relations when comparing the data of Bowen *et al.* with that of the author. However, it does lead one to assume that the variation of the neutron density with latitude is greater than is the variation of the total ionization.

Another comparison besides that with the ionization is that with the number of incoming particles. According to Heisenberg,[13] for protons this curve is represented by the equation, $F=CE^{-1.8}$, so we see that for the latitude dependence, where the energy cut-off is approximately 6 Bev and 2 Bev, we would expect a value of 7.2. This value again is to be compared with our value of 2.4 for the given latitudes. We might also mention the results of Bradt and Peters,[29] who have made a study of the latitude dependence for heavy nuclei of the primary cosmic radiation. These measurements were taken at geomagnetic latitudes 55°N and 30°N, which are essentially identical with those reported herewith. They found a latitude effect of 3.5 for the two latitudes mentioned. This is somewhat larger than the latitude dependence reported for neutrons by the author.

Because we find a greater latitude effect for neutron densities than for total ionization but a lesser effect than for total number of primary particles, the assumption can be made that neutrons are more closely associated with the number of entrant particles than with their energy. For, although the energy does not increase so rapidly with an increase in latitude, the number of particles entering the atmosphere increases more rapidly. The addition of many more low energy particles as we go farther north does not increase the total energy influx appreciably.

All these relationships fit the picture for nucleonic cascades recently suggested by Bernardini[24] in which he breaks these cascades down into three groups. His first group of particles, A, have energies greater than 1 Bev and produce the very penetrating showers. Particles of Class A show an absorption path of about 120 g/cm². Group B, with energies between 10 Mev and 1 Bev, cause the nuclear disruptions such as stars and ionization chamber bursts. As we have discussed earlier, particles causing such nuclear disruptions have an absorption length corresponding to slightly under 140 g/cm². These processes, in turn, yield slow nucleons, both neutrons and protons, with energies less than 10 Mev. From such a picture one would expect that the latitude effect for neutrons would be more than that detected in measuring the total energy but less than that detected when measuring total number of incoming particles, since the processes are not entirely independent of energy.

VI. CONCLUSIONS

Several conclusions can be drawn from the work described.

(1) A maximum atmospheric neutron density definitely occurs at an absorption depth of approximately 100 g/cm² from the top of the atmosphere.

(2) The maximum density of atmospheric neutrons seems to occur at a greater absorption depth the closer to the geomagnetic equator the measurements are made. That is, the absorption depth is near 110 g/cm² at 30.4°N, while it is approximately 100 g/cm² at 54.7°N.

(3) The maximum neutron density at 54.7°N is approximately 2.9 times as great as the maximum neutron density measured at 30.4°N.

(4) An absorption thickness, L, of 143 g/cm² is suf-

[28] Bowen, Millikan, and Neher, Phys. Rev. **53**, 855 (1938).

[29] H. L. Bradt and B. Peters, Phys. Rev. **76**, 156 (1949); **77**, 54 (1950).

ficiently accurate at both of the latitudes under consideration to give the relation for neutrons in the equilibrium region between depths of 225 g/cm² and 800 g/cm², when we use the exponential relationship: $N=N_0 \exp(-p/L)$.

(5) The total neutron density at 54.7°N is approximately 2.4 times as large as that at 30.4°N.

(6) The latitude effect for neutron densities is greater than that for total ionization but less than that for the number of incoming primary particles.

In addition, using the calculations of Vallarta[20] and relation (5) above, we have assumed that there will be 1.4 times as many incoming primary particles in the energy range 1.0 Bev to 8.3 Bev as there are particles exceeding 8.3 Bev in energy, if such particles are protons, and if the multiplicity is not a function of latitude.

A secondary conclusion from (6) is that the neutrons found in the atmosphere are more closely associated with the number of entrant particles than with the energy of the incoming entities.

It seems likely that most of the atmospheric neutrons we measure are formed as a result of nuclear disintegrations which are of a less energetic type than those causing hard showers and very fast neutrons. The reason for believing that neutrons are formed in this manner is the good correlation noted between the absorption thicknesses for bursts and stars and for neutrons.

To summarize the production of neutrons, we might say that apparently the primary positive radiation causes, in the upper atmosphere, large nuclear disruptions which produce fast neutrons, protons, and mesons. These, in turn, cause the soft component and more secondary neutrons and protons. Because of the charged nature of the primary particles, there is a large variation in the density of secondary neutrons with latitude.

In conclusion, the author wishes to express his sincere appreciation for the helpful suggestions given by Professor S. A. Korff. The author wishes also to express his indebtedness to Melvin Pavalow for developing the circuitry and for his special help in connection with the flight from the carrier. The valuable help of L. G. Collyer, W. O. Davis, H. Neuburg, and M. J. Swetnick should also be mentioned, since these flights would not have been possible without the close cooperation of all concerned.

A Floating Double Probe Method for Measurements in Gas Discharges

E. O. JOHNSON AND L. MALTER
RCA Laboratories Division, Radio Corporation of America, Princeton, New Jersey
(Received March 14, 1950)

Measurements with a Langmuir probe in varying or decaying plasmas are defeated by the fact that the plasma potential in these cases follows that of the most positive electrode it can contact. The difficulties can be obviated by the use of a pair of probes joined by a variable potential source. The double probe system "floats" with respect to the discharge system.

From the measurements of probe current *vs.* differential probe voltage, electron temperature and plasma densities can be determined. The method is also applicable to "going" discharges where it has the advantage over the single probe of exerting a negligible influence on the discharge.

I. INTRODUCTION

IN gas discharges either of the stationary or time-varying type it is generally the case that the electrons present in the plasma regions have a Maxwellian distribution. If this is so the concept of temperature can be associated with the electrons. The electron temperature is denoted by T_e.

Knowledge of the electron temperature is of importance in the determination of such quantities as the ambipolar diffusion coefficients. Langmuir and Mott-Smith[1] have described a single probe technique for measuring electron temperatures as well as of other quantities such as electron density and wall and space potentials. Their method can be used for stationary and for certain types of time-varying discharges. However, in any case, unless its area is extremely small, the probe may draw sufficient electron current when operated close to space potential to disturb the discharge conditions which it is designed to measure. As will be made clear below, the single probe method (SPM), is quite unsuited for such cases as the decaying plasma which is present following the interruption of a discharge. A double probe method (DPM) has been developed which exerts a negligible influence on a discharge and which seems to yield accurate temperature data in all types of discharges, including a decaying plasma. Reifman and Dow[2] have described a double probe method for measurements in the ionosphere. Their work will be discussed below.

II. CONSIDERATIONS REGARDING THE SINGLE PROBE METHOD (SPM)

In the Langmuir single probe method,[1] a planar, cylindrical, or spherical electrode is immersed in a discharge plasma and the current to it measured as a function of its potential. Three fairly distinct regions are observed: (1) A region of positive ion current only. In this region the current increases slowly with increasingly negative potential on the probe. (2) A region in which the current passes through zero and then increases rapidly with increasingly positive potentials. A plot of the logarithm of the electron current in this region *vs.* probe potential yields a value for the electron temperature T_e, (3) A region of electron current only in which the current increases slowly with increasingly positive potentials.

In region 2, the current can be expressed as:

$$\ln i_e = -(e/kT_e)V + \ln A j_0, \tag{1}$$

where i_e is the electron probe current, j_0 is the random electron current density, A is the probe area, T_e is the electron temperature.

In Eq. (1) V is the plasma potential measured with respect to the probe. This infers a knowledge of the plasma potential. In practice this need not be known, since it can be replaced by its equivalent $V_S - V_p$, where V_S is the cathode-plasma potential and V_p is the cathode-probe potential. Equation (1) then becomes:

$$\ln i_e = (e/kT_e)V_p + \ln A j_0 - (eV_S/kT_e). \tag{2}$$

Thus it is merely necessary to plot $\ln i_e$ *vs.* V_p in order to secure a value for T_e. An examination of (2) reveals some possible difficulties with the SPM. Equation (2) is significant only if V_S, T_e, and j_0 do not change with V_p. In actual practice, as i_e increases one often observes changes in the discharge patterns, particularly if i_e is an appreciable fraction of the discharge current. Under these circumstances, the probe is disturbing, to some extent, the very quantities it is intended to measure. It would definitely be more satisfying if measurements could be made in a manner less likely to disturb the quantities it is intended to measure. As will be seen, in the double probe method the total current to the probe can never exceed the positive ion current to them. Since this positive ion current is hundreds of times smaller than the electron current to a single probe the DPM appears to be advantageous in this respect.

Langmuir and Mott-Smith[1] have shown how in addition to electron temperature, the probe data can yield values for electron and ion densities; space and wall potentials and for random electron currents. The objections cited above for the use of the SPM in electron temperature determinations are equally applicable here.

[1] I. Langmuir and H. M. Mott-Smith, Gen. Elec. Rev. **27**, 449, 538, 616, 762, 810 (1924).
[2] A. Reifman and W. G. Dow, Phys. Rev. **76**, 987 (1949).

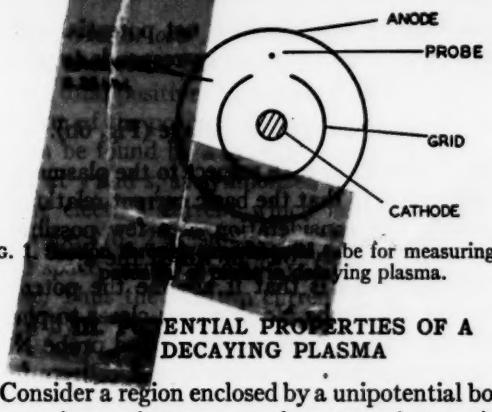

FIG. 1. [illegible] be for measuring floating [illegible]ying plasma.

[illegible]ENTIAL PROPERTIES OF A DECAYING PLASMA

Consider a region enclosed by a unipotential boundary of any shape whatsoever and suppose that at time zero the region is filled with a plasma of arbitrary density distribution. What is the behavior of the plasma at later times if there is no further ionization? It is obvious that, due to their greater velocity, electrons will begin to pour out into the bounding walls. However, as this occurs, the plasma potential will rise. This will, in turn, soon prevent the further loss of all but the fastest electrons, (as determined by the Boltzmann relation). The rate of loss of electrons will diminish to equal that of the rate of loss of positive ions. The plasma now decays while retaining its plasma-like characteristics. In low pressure discharges the losses of charged particles are by the process of diffusion. The plasma potential will be slightly positive with respect to that of the surrounding envelope which will be at the wall potential. As will be seen later the difference in potential between the walls and the decaying plasma will not be more than of the order of tenths of a volt.

Now let some portion of the envelope be increased in potential with respect to the remainder. Then excess electrons will pour into that portion, causing the potential of the plasma to rise until once again the balance between loss of electrons and positive ions is attained. The plasma will now assume a potential slightly positive with respect to the most positive electrode with which it "makes contact." [An exception to this occurs when the area of the most positive electrode is so small that the normal electron diffusion current to it does not exceed the positive ion diffusion current to the entire boundary.] This property of decaying plasmas was demonstrated in a very simple fashion.

A tube was built in the form shown in Fig. 1. The filling was argon at 250μ. It was connected in a circuit as shown in Fig. 2. The tube was fired by impressing a negative pulse on the cathode. The current to the probe as a function of time and E_b, following the interruption of the discharge, was measured by means of the scope across R_b (E_b is the probe battery potential). Two typical oscilloscope traces are shown in Fig. 3. The lower curve is for a case in which the probe is slightly positive with respect to the anode; i.e., $E_b-E_p>0$, (E_p is the anode supply potential). The upper curve is for the case in which $E_b-E_p<0$. At a time t_1, the grid sheath extends across the 1 mm grid opening thus isolating the plasmas on both sides of the grid.[3] In Fig 3, t_1 is the time at which the kinks in the decay curves occur. For any value of E_p, E_b could be set so that at some time $t>t_1$, the current to the probe was zero. Under this condition, the probe is at floating potential E_f. E_p was varied over a range of ± 16 volts on either side of ground potential and E_f was determined in each case for $t>t_1$. The results are plotted in Fig. 4. It is seen that E_f follows E_p very closely.

The plasma potential E_s, is always slightly positive with respect to floating potential. The difference between the two is a function of the electron and ion temperatures. Since (as will be seen) both these temperatures are low for $t>t_1$, it follows that E_s lie close to E_f and therefore close to E_p, i.e., the space potential follows the potential of the most positive electrode, this being the anode in this case. For the case of Fig. 4, when $E_p=0$, E_f appears to be about -0.8 volts. Since the contact difference of potentials between the various electrodes is not known, nothing can be said concerning the significance of this value.

In order to determine how rapidly the plasma potential follows that of the most positive electrode, the potential of the anode was varied by means of steep wave-front signal during the period $t>t_1$. It was found that equilibrium conditions (as observed on the scope) were always re-established within about $\frac{1}{4}$ microsecond. Since this is about the rise time of the pulses employed, it is impossible to estimate the time for equilibrium to be established. Very likely the times involved are deter-

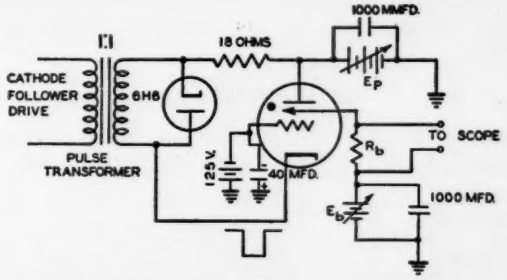

FIG. 2. Circuit for measuring floating potential of probe in decaying plasma.

FIG. 3. Decay currents to probe in tube of Fig. 1.

[3] The phenomenon of splitting of plasmas by the formation of sheaths across aperture openings is described by W. Koch, Zeits. f. Tech. Phys. 17, 446 (1936).

mined primarily by electron mobility considerations and are thus less than 10^{-8} sec. for this particular tube.

IV. THE DOUBLE PROBE METHOD (DPM)

The double probe method makes use of two probes, each similar to the single probe of the SPM. They are interconnected as shown in the circuit of Fig. 5. The potential V_d is termed the differential voltage, and its associated current, i_d the circuit current. The positive sense of these quantities is established by the arrow directions where we define positive current as the rate of flow of positive charge. Unless otherwise noted the circuit of Fig. 5 and its polarity convention will apply to all of the discussion which follows. In brief, the electron temperature will be determined from the way in which i_d varies with V_d.

As with the SPM the DPM is based on the Boltzmann relation and the plasma-sheath properties of a gas discharge. In addition it is based on an application of Kirchhoff's current law which requires in this case that at any instant the total net current of positive ions and electrons flowing to the system from the plasma must be zero.

Qualitative Treatment

As an aid in understanding the mathematical formulation, let us consider qualitatively how the system reacts for several different values of V_d. For simplicity, let us first assume that both probes are equal in area and that no contact potentials or differences in plasma potential from point to point exist. Furthermore, we assume that V_d has no effect on the ion current to the system. This is very closely approximated in practice.

(*a*) $V_d=0$ (Fig. 6a).

Each probe will collect zero net current from the plasma and will ride at the same floating potential. The current i_d must be zero since no net potential acts in the current loop. This condition corresponds to point 0 on the curve of Fig. 7.

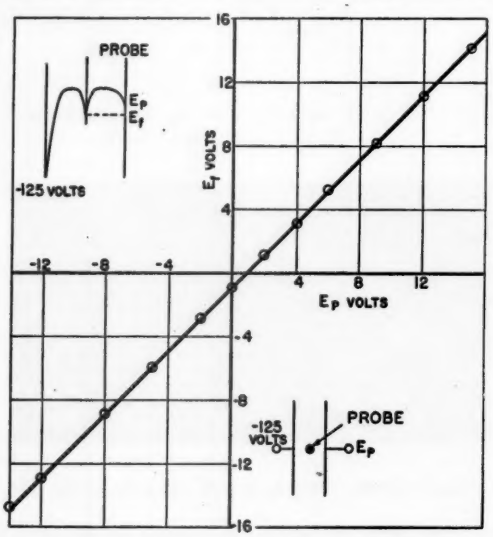

FIG. 4. Probe floating potential as function of anode potential for decaying plasma.

(*b*) V_d=small negative voltage (Fig. 6b).

The probe potentials with respect to the plasma must adjust themselves so that the basic current relations are still satisfied. The consideration of a few possibilities will show that the only way in which the system can satisfy all conditions is that it assume the potentials shown in Fig. 6b. Probe No. 1 moves closer to plasma potential and collects more electrons, and probe No. 2 moves away from plasma potential and collects fewer electrons. The extra electrons flowing to probe No. 1 pass through the circuit to make up the deficiency at probe No. 2. All conditions are again satisfied and the system is located at some point *b* on Fig. 7.

(*c*) V_d=somewhat larger negative voltage (Fig. 6c).

Probe No. 1 moves still closer to space potential and collects the entire electron current to the system since probe No. 2 is now so highly negative with respect to the plasma that no electrons can reach it. Half of the electrons reaching probe No. 1 now pass through the external circuit to probe No. 2. All conditions are satisfied and the system locates at some point *y* on Fig. 7.

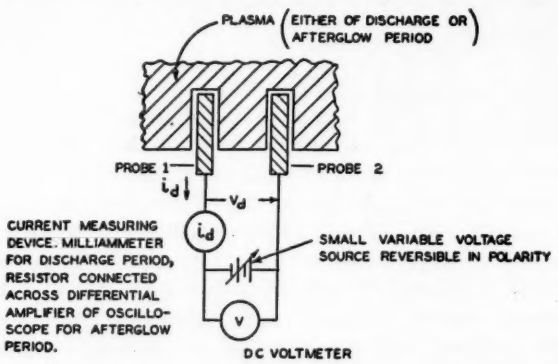
PLASMA (EITHER OF DISCHARGE OR AFTERGLOW PERIOD)
PROBE 1
PROBE 2
i_d
V_d
CURRENT MEASURING DEVICE. MILLIAMMETER FOR DISCHARGE PERIOD, RESISTOR CONNECTED ACROSS DIFFERENTIAL AMPLIFIER OF OSCILLOSCOPE FOR AFTERGLOW PERIOD.
SMALL VARIABLE VOLTAGE SOURCE REVERSIBLE IN POLARITY
V
DC VOLTMETER

FIG. 5. Basic double probe circuit.

Further increase in the negative value of V_d can cause no further change in the current distributions because probe No. 1 already collects a sufficient electron current to balance the entire positive ion current flowing to the system. Consequently probe No. 1 remains fixed with respect to the plasma and probe No. 2 goes negative along with V_d. We can speak of the latter probe as being saturated with respect to positive ions as the system moves along the flat portion *yx* of Fig. 7. In practice one finds that this flat portion has a slight slope as shown by the dotted portion *yx'*. This slow increase is due to an expansion of sheath thickness as the probe goes increasingly negative with respect to the plasma. This will be discussed in greater detail below.

The symmetry of the system will cause it to reverse the previous results when V_d is positive, giving the

portion *ozw* or *ozw'*. The flat portion *zw* or *zw'* corresponds to positive ion saturation current to probe No. 1.

The total positive ion current to the system is simply the sum of the positive ion currents to both probes and so can be found by adding the magnitudes of the currents at *y* and *z*, as symbolized by i_{p_1} and i_{p_2}.

The electron current which flows from the plasma to probe No. 2 is simply the difference between the total space current and the positive ion current to this probe. Thus the electron current i_{e_2} to probe No. 2 is given by

$$|i_{e_2}| = |i_d| - |i_{p_2}|. \tag{3}$$

The value of i_{e_2} which corresponds to a voltage V_d is illustrated graphically in the same figure.

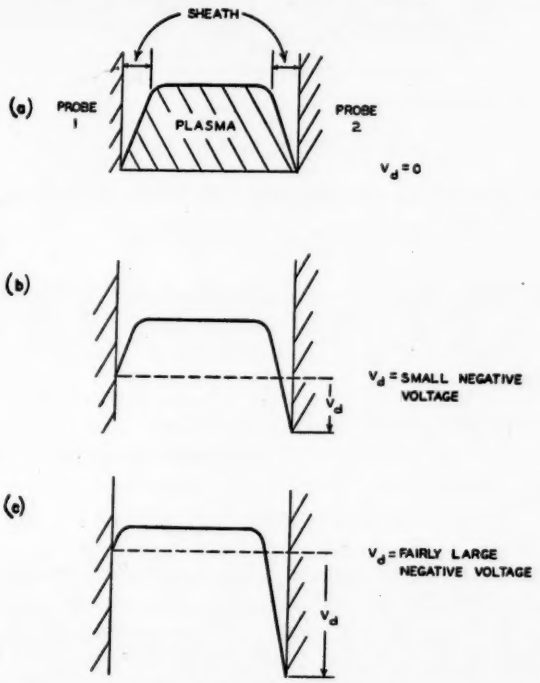

FIG. 6. Sample potential diagrams of the double probe method.

V. TEMPERATURE DETERMINATION

A. Logarithmic Plot Method

The generalized potential diagram for the system of Fig. 5 is shown in Fig. 8. The potentials V_1 and V_2 represent the voltages of the surrounding plasmas with respect to the corresponding probes. The potential V_c represents any small difference in plasma potential which may exist between the regions surrounding the probes, plus the total contact potentials acting in the system. The other symbols are defined in the figure.

Since the net current to the system must be zero

$$i_{p_1} + i_{p_2} = \Sigma i_p = i_{e_1} + i_{e_2}.$$

Substituting the equivalents for i_{e_1} and i_{e_2} in terms of Boltzmann relation, we obtain:

$$\Sigma i_p = A_1 j_{0_1} \epsilon^{-\phi V_1} + A_2 j_{0_2} \epsilon^{-\phi V_2}, \tag{4}$$

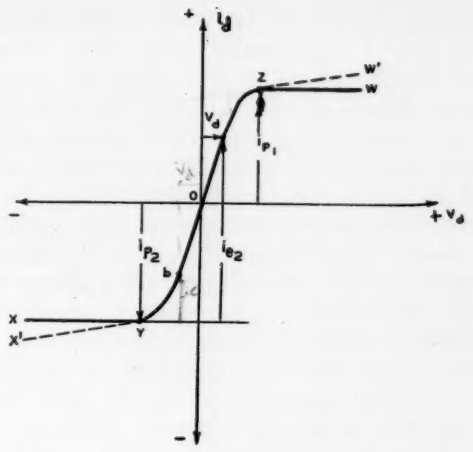

FIG. 7. Voltage-current characteristic of the double probe method.

where

$$\phi = e/kT_e = 11{,}600/T_e.$$

The potential diagram of Fig. 8 yields:

$$V_1 + V_c = V_2 + V_d \quad \text{or} \quad V_1 = V_2 + V_d - V_c. \tag{5}$$

Substituting (5) into (4) and rearranging, we obtain:

$$\ln[(\Sigma i_p/i_{e_2}) - 1] = -\phi V_d + \ln \sigma = \ln \Gamma, \tag{6}$$

where

$$\Gamma = (\Sigma i_p/i_{e_2}) - 1 \tag{7}$$

and

$$\sigma = (A_1 j_{0_1}/A_2 j_{0_2}) e^{\phi V_c}. \tag{8}$$

Thus the plot of ln Γ against V_d should yield a straight line whose slope is a measure of the electron temperature. This equation is seen to be similar in form to that used in the SPM except that in (6) one uses Γ instead of the electron current. It is to be noted that the slope of (6) is essentially unaffected by any of the factors included in σ; *viz.*, probe areas, electron random current densities, difference in plasma potential between probes, and contact potentials. For an unambiguous determination of T_e, the random current densities should not change with probe current. This is much more likely to be the case with the DPM than with the SPM since the current drain can be hundreds of times smaller in the former case. Another important difference between the two cases is seen from Eqs. (2) and (8). We note that the constant term of the latter is free from any restricting dependence on the plasma potential. Thus we see that the DPM is inherently a more general method. It can be used during or after the discharge and even when the plasma potential varies with time.

Possible errors in this method require discussion. The values of i_{p_1} and i_{p_2} used were those at which the curve of Fig. 7 broke away from the saturated regions; (points *y* and *z* of Fig. 7). There are two possible sources of error present. In the first place, there is some uncertainty in the choice of points *y* and *z*. To see how serious

this can be, trial points for y and z were chosen extending over a considerable range away from the obvious "break" points. It was found that when this was done, the end points of the log plot would deviate from the straight line defined by the central points. If one used the slope of the still well-defined straight central portion of the plot for determining the temperature, the values obtained did not vary significantly as the chosen values of i_{p_1} and i_{p_2} were moved around. The reason for this is quite simple. Any change in the selected value of the i_p's, introduces a change (in the same direction) of the estimated value of i_{e_2}. It turns out that (except near y and z) the significant quantity $[(\Sigma i_p/i_{e_2})-1]$ is inappreciably affected. Thus, one can safely say that this method is insensitive to small variations in the choice of i_{p_1} and i_{p_2}.

A second possible source of error lies in the fact, that even in the region between y and z of Fig. 7, the ion current of each of the probes varies slightly due to

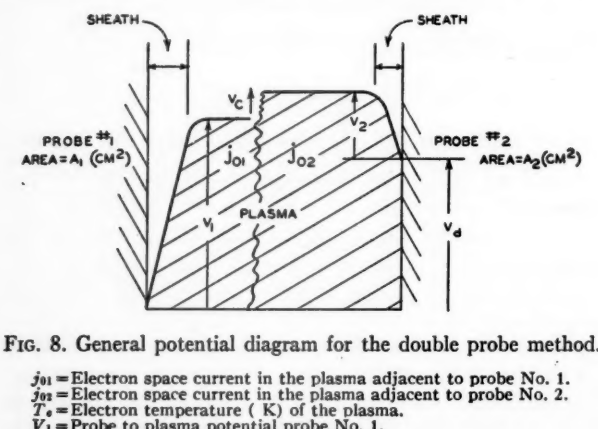

FIG. 8. General potential diagram for the double probe method.

j_{01} = Electron space current in the plasma adjacent to probe No. 1.
j_{02} = Electron space current in the plasma adjacent to probe No. 2.
T_e = Electron temperature (K) of the plasma.
V_1 = Probe to plasma potential probe No. 1.
V_2 = Probe to plasma potential probe No. 2.
V_c = see text.

small changes in sheath thickness.[4] Strictly speaking, one should compute the positive ion current to each of the probes over the range yz and use the sum of these in the log plot. This appears quite unnecessary and is, in fact, inconsequential, for the following reasons: (1) Unless the slope of the saturated ion current regions is considerable, the value of Σi_p can hardly change appreciably over the range yz. In any case, any actual and accepted change must be accompanied by a corresponding value for i_{e_2}. In that case for the reason cited in the second preceding paragraph, the effect on $(\Sigma i_p/i_e)$ will be small, since both Σi_p and i_e change in the same direction in roughly the same ratio, (2) As one moves through the region between the knees, i.e., between y and z, a change in i_{p_1} tends to be compensated for by an opposite change in i_{p_2}, so that the true value of Σi_p remains approximately constant.

[4] The question of sheath thickness change is discussed more fully in the treatment of the "equivalent resistance method" below.

B. Equivalent Resistance Method

Plotting Eq. (6) involves some laborious computation. It turns out that this can be avoided and T_e determined very quickly from i_d *vs.* V_d plots. Equation (6) can be expressed as:

$$i_{e_2}=\Sigma i_p/[\sigma\epsilon^{-\phi Vd}+1]. \tag{9}$$

Taking the derivative of i_{e_2} with respect to V_d and evaluating at $V_d=0$, one obtains:

$$[di_{e_2}/dV_d]_{V_d=0}=(\Sigma i_p\phi\sigma)/(\sigma+1)^2. \tag{10}$$

Solving for T_e and substituting for dV_d/di_{e_2} its practical equivalent, dV_d/di_d, one obtains:

$$T_e=11{,}600\frac{\sigma}{(1+\sigma)^2}\left[\Sigma i_p\frac{dV_d}{di_d}\right]_{V_d=0}. \tag{11}$$

From (6) we can obtain:

$$\sigma=[(\Sigma i_p/i_{e_2})-1]_{V_d=0}.$$

For convenience we introduce the factor G such that:

$$G=[i_{e_2}/\Sigma i_p]_{V_d=0}=1/(1+\sigma). \tag{12}$$

This factor G, which can be obtained directly from the current-voltage characteristic, obviates the need for calculating σ from (8). Substitution of (12) into (11) yields:

$$T_e=11{,}600(G-G^2)[\Sigma i_p dV_d/di_d]_{V_d=0}$$
$$=11{,}600(G-G^2)R_0\Sigma i_p \tag{13}$$

where

$$R_0=[dV_d/di_d]_{V_d=0}. \tag{14}$$

The factor R_0 is denoted as the *equivalent resistance.* This gives the method its name. The simple relation Eq. (13) provides a rapid and convenient means of obtaining the electron temperature directly from the V_d-i_d characteristic. The use of both (8) and (13) will be illustrated in the sets of experimental data which will follow.

Since, in the equivalent resistance method one makes use of the slope of the V_d-i_d curve at only one point, viz. where $V_d=0$, it would be desirable to use the value of Σi_p corresponding to this point when computing T_e from Eq. (13). A simple analysis (presented in the Appendix) indicates that one is usually justified in assuming that the rate of change of ion current along the sloping saturated portions of Fig. 7 is maintained in the regions between the knees. Manipulation of the basic equations of the DPM then yields the necessary relation between probe-space potential and V_d which enables the course of i_{p_1} and i_{p_2} to be followed in the region between the knees. It is found that for all practical purposes, if the V_d-i_d characteristic is reasonably symmetrical, one is safe in extending the lines $x'y$ and $w'z$ (see Fig. 7) 0.8 of the way into the line through $i_d=0$ and then horizontally the rest of the way. The

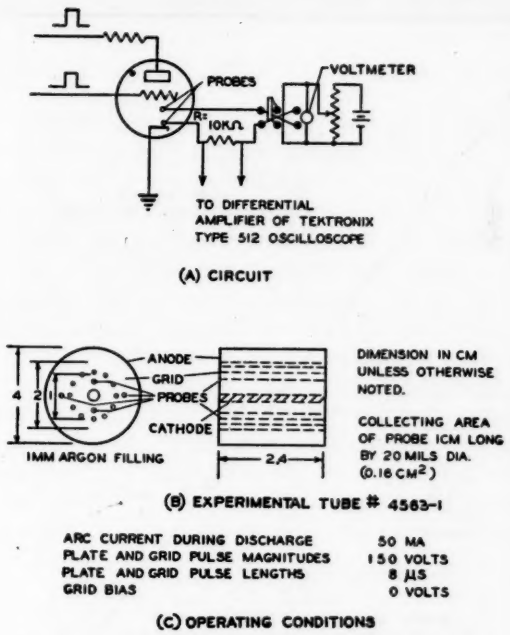

FIG. 9. Tube and circuit for double probe studies of decaying plasma.

choice of this value is explained in the Appendix. From these extended curves one can obtain the value of Σi_p corresponding to $V_d=0$. (An illustration of this procedure is given in Fig. 11.) Experience has shown that if one fails to make this correction for Σi_p when employing the equivalent resistance method, but instead make of the positive ion currents corresponding to points y and z of Fig. 7, then the values for T_e come out to be too large, but virtually never by more than 5 percent. Thus for rapid and approximate temperature determinations one can simply make use of i_{p_1} and i_{p_2} as determined from Fig. 7.

C. The Intercept Method

In some cases the equivalent resistance method cannot be used owing to the fact that when $V_d=0$, one is operating in a region of positive ion saturation to one of the probes (i.e., in region xy or zw of Fig. 7). In that case another rapid method is possible which does not require the laborious computations of the logarithmic plot method.

By simple algebra Eq. (6) can be transformed into:

$$V_d=-\frac{1}{\phi}\ln\left[\left(\frac{1}{\sigma}\frac{\Sigma i_p}{i_{e_2}}-1\right)\right]. \tag{15}$$

Now let V_d'' be the value of V_d which corresponds to $\Sigma i_p/i_{e_2}=D$, and let V_d' be the value of V_d which corresponds to $\Sigma i_p/i_{e_2}=F$. D and F are chosen arbitrarily. Then, substitution of these values in (15) and making use of the fact that $\phi=e/kT_e$, one can solve readily for T_e. The result is:

$$T_e=11{,}600\left[V_d''-V_d'\Big/\ln\left(\frac{F-1}{D-1}\right)\right]. \tag{16}$$

In the case of the intercept method it is found that, unless V_d' and V_d'' are chosen too close to the knees, the value of T_e determined is in excellent agreement with that obtained by the other methods.

In summary we can say that any error in the choice of Σi_p tends to be compensated, with the result that the error registered in T_e will usually be 5 percent or less. It is obvious that the most certain values of T_e are obtained in the cases where the flat portion slopes are a minimum. Comparison of corresponding temperatures obtained with different sets of probes, each set having different values of slopes in the flat portions, indicates that the 5 percent estimate is a reasonable one. This is also borne out by the close correspondence of temperatures as obtained from, (1) the logarithmic plot method based on Σi_p evaluated at the knees, and (2) the other two methods where Σi_p is computed from the interpolated values of i_{p_1} and i_{p_2}.

It will be noticed that the mathematical treatment of the DPM is based on the potential diagram of Fig. 8 which represents an ideal case in which uniform electron densities and probe-plasma potentials exist along the probe surfaces. Such an ideal situation is not achieved in practice. However, it can be shown in a perfectly general and rigorous manner that non-uniform electron densities and probe-plasma potentials introduce no errors into the temperature measurements. Such non-uniformities, even when quite large, only introduce

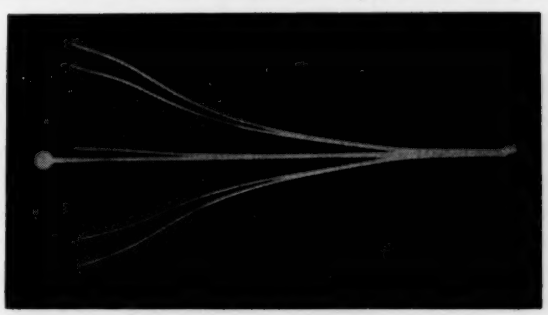

FIG. 10. Double probe current decay curves for tube of Fig. 9.

small corrections in the value of σ as determined by Eq. (7). This deduction is consistent with the observation that the value of σ determined by Eq. (7) is usually in close agreement with its value determined from either the log plot or the factor G.

In the case of probes used in tubes with oxide cathodes it has been found at times the deposition of barium onto the glass probe insulation (with subsequent leakage) causes the flat portions to have considerably increased slopes. A short application of a Tesla coil to the probe leads seems to burn out the barium, elimi-

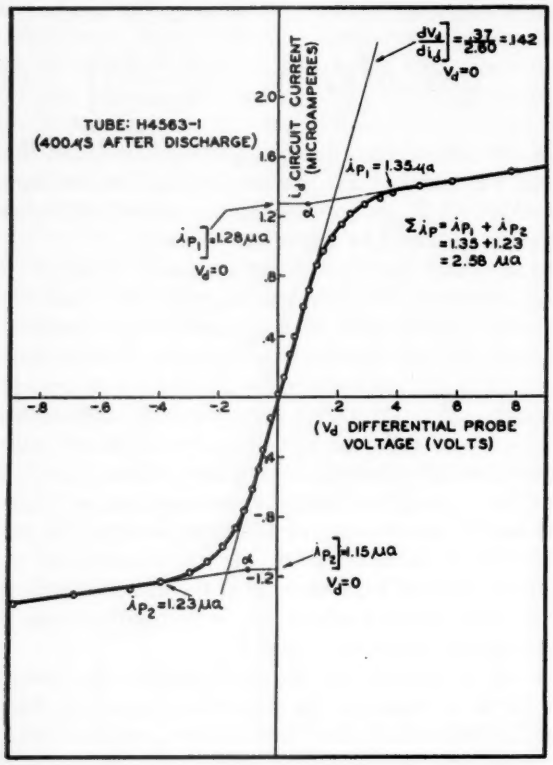

FIG. 11. Double probe current-voltage characteristic.

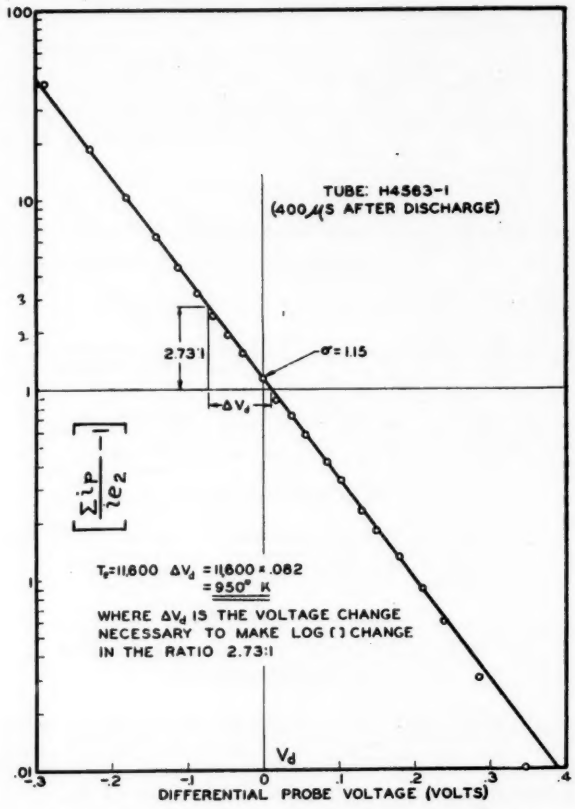
TUBE: H4563-1
(400μS AFTER DISCHARGE)
2.73:1
$\sigma=1.15$
ΔV_d
$\left[\frac{\Sigma i_p}{i_{e_2}} - 1\right]$
$T_e=11,600\ \Delta V_d = 11,600 \times .082$
$=950°\ K$
WHERE ΔV_d IS THE VOLTAGE CHANGE NECESSARY TO MAKE LOG [ ] CHANGE IN THE RATIO 2.73:1
V_d
DIFFERENTIAL PROBE VOLTAGE (VOLTS)

FIG. 12. Double probe temperature determination plot.

nating the leakage. Interestingly enough, the DPM seems to be sufficiently insensitive to error that the measurements made with leakage present (by the methods outlined above) agree within a few percent with those taken after the leakage has been eliminated.

VI. ILLUSTRATIONS OF THE USE OF THE DPM

The presentation of the data which follow is mainly intended for the purpose of illustrating the use of the DPM and not as a detailed study of any particular phenomena which take place in the afterglow period.

The tests were carried out in the cylindrical triode shown in Fig. 9(B). Two sets of double probes were employed, one in the cathode-grid region and the other in the anode-grid region. The measuring set-up is shown in Fig. 9(A). (Only the cathode-grid probes are illustrated.)

The tube (containing Ar at 1 mm pressure) was fired by the simultaneous application of 8 μsec. pulses to grid and anode. The probe current was determined from deflections on a Tektronix No. 512 scope which has a balanced amplifier input. The operating parameters are presented in Fig. 9(C). Various cases illustrating the applicability of the DPM are presented below.

Case 1. Typical probe current decay curves for various values of V_d are shown in Fig. 10. From these curves the current voltage characteristic can be obtained for any time. As an illustrative case, the data for 400 μsec. following the interruption of the discharge are plotted in Fig. 11.

The values of V_d are corrected for the voltage drops in the resistor R. The values selected for the computation of i_p are indicated in the same figure. The plot of the function $[(\Sigma i_p - 1)/i_{e_2}]$ against V_d is presented in Fig. 12. The slope yields an electron temperature of 950°K. The temperature was also computed by means of Eq. (13) (the equivalent resistance method). The factor G is found directly from Fig. 11 and is

$$G=[i_{e_2}/\Sigma i_p]_{V_d=0}=1.12/2.43=0.463.$$

The value of 0.142 volts per μa for R_0 is computed from the slope of the characteristic of Fig. 11 at $V_d=0$. The extensions of the flat portions[5] of the characteristic give the value of Σi_p, at $V_d=0$, as (1.15+1.28) or 2.43 μamp. Substituting the above values into (13) we get:

$$T_e=11,600(0.249)(2.43)(0.142)=1000°\text{K}.$$

This agrees quite well with the 950°K determined from the semilog plot.

The value of σ computed from Eq. (12) and the above value of G is 1.16. This agrees very well with the value of 1.15 determined by inspection of Fig. 12 at the point where $V_d=0$. We can also compute σ from

[5] The reason for this choice is discussed in the Appendix.

(8). Here

$$\sigma=[A_1 j_{0_1}/A_2 j_{0_2}]_{V_d=0}\epsilon^{\phi V_c}=(1)(1.28/1.12)(1.1)=1.24.$$

We assume that $j_{0_1}/j_{0_2}=i_{p_1}/i_{p_2}$ on the basis of the charge neutrality of the plasma. $\epsilon^{\phi V_c}=1.1$ since $V_c\simeq 0.01$ and $\phi\doteq 11.6$ (see Fig. 11). This value of σ agrees reasonably well with the other two.

Case 2. As another illustration of the use of Eq. (8) and (13), for a case wherein the system is more dissymmetrical than in the previous case, we consider a set of data taken from a simple diode filled with 250μ of argon. The probes in this tube were equal in area and identical in size with those of the preceding case. The ar current was 200 ma and all data were collected at 100 μsec. after cessation of the discharge. The current-voltage characteristic is plotted in Fig. 13.

The values of the various factors are found from Fig. 13 and are

$$\Sigma i_p=10.7\ \mu\text{a},\quad [\Sigma i_p]_{V_d=0}=9.95\ \mu\text{a},$$
$$R_0=36{,}700\text{ ohms},\quad G=0.401.$$

Then

$$T_e=11{,}600(0.240)(9.95)(0.0367)=1015^\circ\text{K}.$$

The log plot, shown in Fig. 14 yields a concurrent value of 1055°K. It is interesting to note that the values of σ again check, their values being (*a*) 1.55 from log plot, (*b*) 1.50 from *G*, (*c*) 1.51 from Eq. (7).

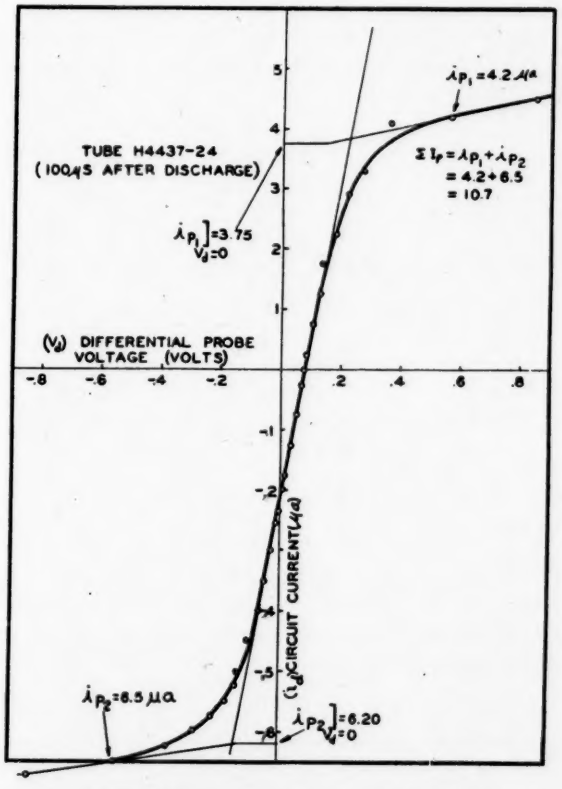

FIG. 13. Double probe current-voltage characteristic.

VII. DISCUSSION O TAL RESULTS

A serious question ar whether or not temperature determinatio s in reality. The concept of an electron ten e is permissible only if the electrons have a Maxwellian distribution. The method here described samples only a small fraction of the electrons present, the electrons collected by the probes being only those which have velocities sufficient to overcome the ever present retarding fields at the probes. The range of electrons sampled can be extended by making tubes with probes of dissimilar size.

It is of interest to determine what fraction of the electrons are sampled in one of the cases studied above. Consider Case 1, whose results are presented in Figs. 11 and 12. An approximate expression for floating potential V_f (with respect to space potential) is given by:[6]

$$V_f=-(kT_e/2e)\ln(T_{em}/T_pM). \qquad (17)$$

Then for the case of Figs. 11 and 12, $T_e=950^\circ$K. For M we use the mass of the argon atom. We assume that T_p is the gas temperature which was about 350°K for this case. Then from Eq. (17) $V_f=0.50$ volts. Since $i_{p1}\simeq i_{p_2}$, the probes must be close to V_f when $i_d=0$. Then from the Boltzmann relation, the ratio of electron

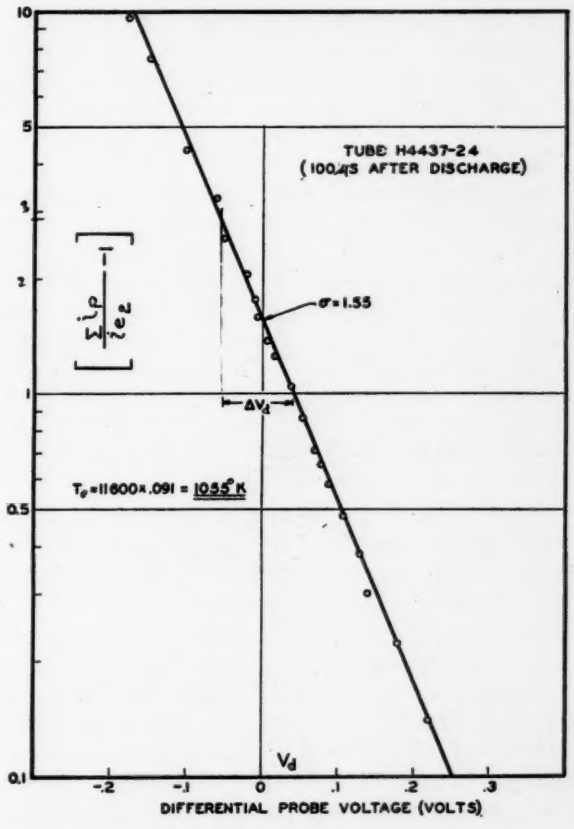

FIG. 14. Double probe temperature determination plot.

[6] L. B. Loeb, *Fundamental Processes of Electrical Discharge in Gases* (John Wiley and Sons, Inc., New York, 1939), first edition, p. 242.

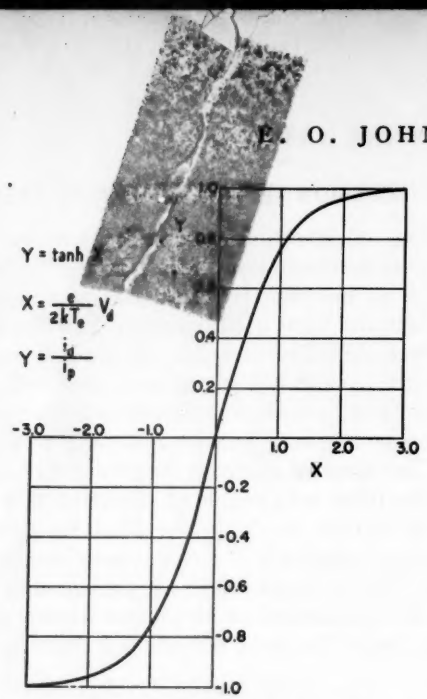

FIG. 15. Ideal double probe current-voltage characteristic.

current density at the probe to the random current density in the plasma near the probe (when the probe potential is V_f) is given by:

$$j_d/j_0 = e^{-(eV_f/kT)} = e^{-(11,600/950)(0.50)} = 0.0021.$$

From Fig. 11 we see that the measurements extend to points where the current to either probe becomes about double the above value. Thus the maximum value assumed by j_d/j_0 in this case is about 0.005. Thus less than the top 1 percent of the electrons are sampled in this case.

In other tubes than those described here, up to 5 percent of the electrons were sampled by means of probes with area ratios of 25. In these cases, too, the results always corresponded to Maxwellian distributions. It may obviously represent a dangerous extrapolation to conclude from the properties of this small sample that the electron velocity distribution is completely Maxwellian.

VIII. FURTHER CONSIDERATIONS OF THE SPM AND THE DPM

It may appear that the single probe can be employed in the fashion of the double probe by considering the single probe as constituting one of a double probe pair and the remainder of the system as constituting the other probe of the pair. This is actually possible only in certain special cases.

From the earlier description of the DPM we see that regardless of the value of V_d (the difference in potential of the probes) the space potential in the plasma is unaffected by changes in V_d. The plasma is dominant in determining its own potential as well as that of the floating probes. The potential of the latter is determined by that of the plasma and the condition of equality of electron and ion currents to the probe system.

This is not the case for the SPM. The probe or electrode potentials for this case can affect the plasma potential in such a way as to alter the quantities being measured. If a hot cathode is present, then the use of a positive probe may give rise to oscillations during the afterglow period. This is an undesirable state of affairs as the measuring device affects the quantity it is designed to measure. If a hot cathode or other copious electron source is not present (as in the case of a cold cathode discharge, or for the isolated anode-grid region plasma of case 3 above), then it is possible to use a single probe combined with the other electrodes as a double probe system.

IX. ANALYTICAL EXPRESSIONS FOR i_d AND i_e

Let us consider a symmetrical double probe system in which: (1) the probes are identical, (2) the random current density at both probes is equal, (3) the contact emf between the probes is zero, and (4) the space potential near both probes is the same. Then from Eq.

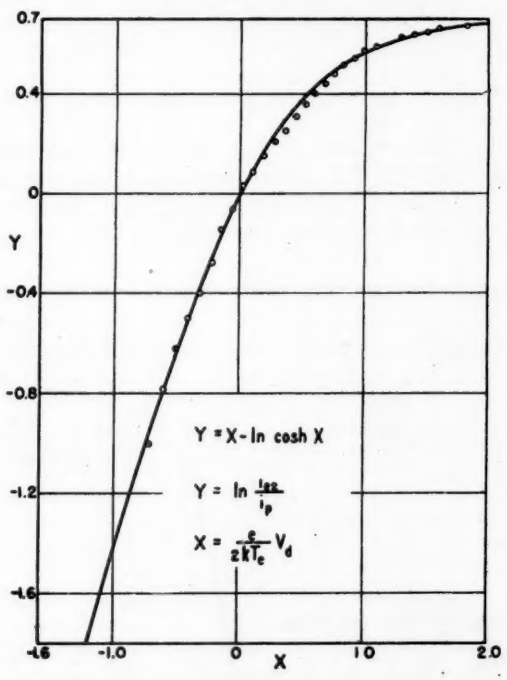

FIG. 16. Theoretical and experimental electron current plots for double probe method.

(8) $\sigma = 1$. Then from Eq. (6)

$$\Sigma i_p/i_{e_2} = 1 + e^{-\phi V_d}. \tag{18}$$

For this symmetrical case, $i_{p_1} = i_{p_2} = i_p$. Then: $\Sigma i_p = 2i_p$, where i_p is the positive ion current to either probe. Making use of this relation and the fact that $i_{e_2} = i_d + i_p$, we can transform Eq. (18) into:

$$i_d/i_p = \tanh(\phi V_d/2). \tag{19}$$

A plot of this function is given in Fig. 15. It is seen to have just the shape of the observed data. (See Figs. 11 and 13.)

Equation (19) above can be written as:

$$2[i_{e_2}/\Sigma i_p]=i_{e_2}/i_p=2/(1+e^{-\phi V_d})$$
$$=\exp(\tfrac{1}{2}\phi V_d)/\cosh(\tfrac{1}{2}\phi V_d).$$

Then:

$$\ln(i_{e_2}/i_p)=\tfrac{1}{2}\phi V_d-\ln\cosh(\tfrac{1}{2}\phi V_d). \quad (20)$$

A plot of Eq. (20) is given in Fig. 16. The values of $\ln(i_{e_2}/i_p)$ were computed for a set of experimental data and the points plotted on Fig. 16. The agreement between theory and experiment is agreeably good.

Reifman and Dow[2] have plotted the quantity $\ln(i_e/i_p)$ for measurements in the ionosphere. Their double probe consisted of the nose and a portion of the body of a rocket. From their curve they conclude that the observed electron distribution is not Maxwellian. Since the shape of their observed curve is similar to ours, it is not possible to account for their conclusion. The shape of the $\ln(i_e/i_p)$ should not be altered qualitatively even for a non-symmetrical structure such as they employed.[7]

X. DETERMINATION OF ELECTRON AND ION DENSITIES AND OF WALL POTENTIAL

Neither the SPM nor DPM are suited for the determination of the electron density n_e in decaying plasmas. This arises from the fact that the plasma potential "rides" with the probe when the latter is run upward (i.e., in a positive direction) in potential. As a consequence, it is impossible to saturate the electron current to the probe unless its area is extremely small. In the Langmuir SPM it is the saturated electron current (corresponding to the bend in the current voltage characteristic) which is used to compute the electron density.

The situation is not completely hopeless, however. In order to determine n_e and n_p, it is merely necessary to set a value on one unknown, the positive ion temperature T_p. This is an exceedingly fortunate situation, since the value of T_p in the decaying plasma is undoubtedly very close to T_g, the gas temperature. This follows from the fact that even though the electron temperature may still (in some cases) be considerably above gas temperature, the kinetics of the impacts of the ions with electrons and gas molecules is such that it is the temperature of the latter which will dominate in determining the ion temperatures. In addition, as will be seen, n_e and n_p vary as the square root of T_p. Thus, errors in selecting a value for T_p will have a much smaller effect on the values of n_e and n_p. We set:

$$j_p=n_p e c_{Ni}, \quad (21)$$

where c_{Ni} is the average drift velocity of the ions. In the decaying plasma, where the space-charge fields are extremely small, c_{Ni} must be due almost entirely to the outward motion from the plasma into the sheath arising from the random motion of the ions. In that case $c_{Ni}=\frac{1}{4}\bar{c}_p$, where $\bar{c}_p$ is the ion velocity averaged over a Maxwellian distribution. Then:

$$n_p=4j_p/e\bar{c}_p, \quad (22)$$

where j_p is the random ion current density, but:

$$j_p=i_p/A_s, \quad (23)$$

where i_p is positive ion current to probe, and A_s is sheath area.

Estimates made by the method of Langmuir and Mott-Smith[1] indicate that at the points y and z of Fig. 4, the positive ion current to the probe is space-charge limited but that the sheath area may be appreciably larger than the probe area.

Making the substitution $\bar{c}_p=1.87\times10^{-8}(T_p/M)^{\frac{1}{2}}$ we obtain:

$$n_p=(1.34\times10^{27}/A_s)i_p(M/T_p)^{\frac{1}{2}}, \quad (24)$$

where M is the mass of a positive ion.

Let us apply this to the case of Fig. 11. For that case, M(argon) $=6.65\times10^{-23}$ g, $i_p=1.35\times10^{-6}$ amp., $T_p=350°$K. Then

$$n_p=(8.0\times10^{8}/A_s)\ \text{ions/cm}^3. \quad (25)$$

To determine A_s we make use of the space-charge-limited current equation for cylindrical diodes:

$$i_p=14.66\times10^{-6}(m_e/M)^{\frac{1}{2}}(LV^{\frac{1}{2}}/\Gamma\beta^2),$$

where V is the difference in potential between the probe and plasma. For this case $L=1$ cm, $\Gamma=0.025$ cm, $i_p=1.35\times10^{-6}$ amp. Then

$$\beta^2=1.62V^{\frac{1}{2}}. \quad (26)$$

To obtain V, we recall first that when the probe is at wall potential ($i_d=0$) its potential with respect to the plasma (as was computed above) is 0.50 volt. As i_d varies from zero in Fig. 11 to the saturation value of i_{p_1}, i_{e_2} changes by a factor of about 2 (this is readily obtained from Fig. 12). The probe-space potential must then decrease by an amount determined from the Boltzmann relation:

$$0.5=\exp[(11{,}600/950°\text{K})\Delta V],$$

or

$$\Delta V=-(950/11{,}600)\times0.693\cong-0.06\ \text{volt}.$$

Then:

$$V=(0.50-0.06)=0.44\ \text{volt}.$$

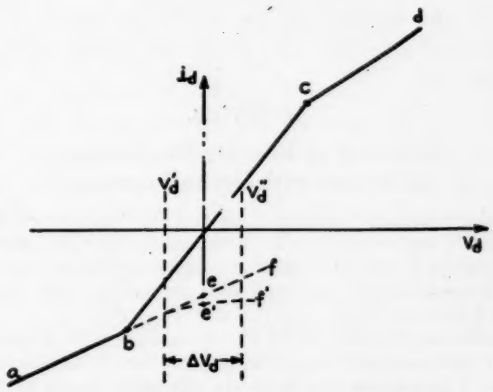

FIG. 17. Idealized double probe characteristic.

[7] Kojima and Takayama, J. Phys. Soc. Japan 4, 349 (1949) have recently described a slightly different method for using double probe data which yields temperature figures very close to those obtained by the methods here described.

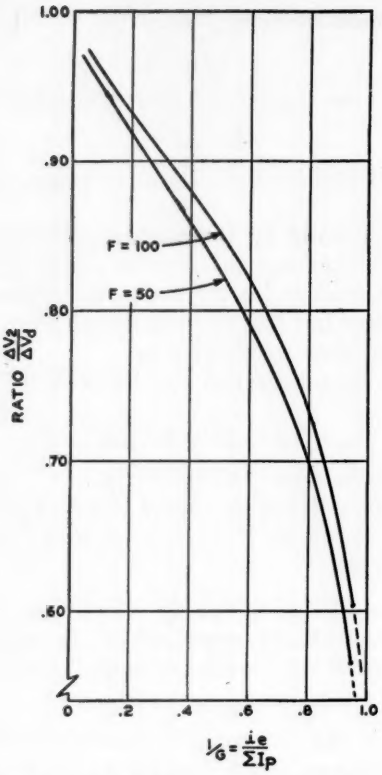

FIG. 18. Relation between space potential and differential potential.

Then from Eq. (26):

$$\beta^2 = 1.62 \times 0.29 = 0.47.$$

Then:

$$\Gamma_s/\Gamma_p = 1.75,$$

where Γ_s and Γ_p are respectively the sheath and probe radii. Then:

$$A_s = 1.75 A_p = 1.75 \times 0.16 = 0.28 \text{ cm}^2.$$

Substituting this value in (25) there results:

$$n_p = 2.9 \times 10^9 \text{ ions/cm}^3.$$

From the equality of electron and ion density, we have immediately

$$n_e = 2.9 \times 10^9 \text{ electrons/cm}^3.$$

The random electron and ion current densities can now be obtained from Eq. (21) using the proper value of $\bar{c}$ in each case.

APPENDIX

Variation of Positive Ion Current to Probes with Probe Potential

In the equivalent resistance method for temperature determination it was necessary to know the value of the ion current to the probes at $V_d = 0$. This cannot be determined directly from the $V_d - i_d$ characteristic. We shall now present a crude analysis showing how the desired quantity may be calculated.

Consider an idealized DPM $V_d - i_d$ characteristic as shown in Fig. 17 with purposely exaggerated slopes for the ion saturation regions. These slopes arise from the change in sheath thickness with change in voltage across the sheath.

Along the saturated portions *ab* (or *cd*) a change in V_d results in an identical change in the value of V_2 (the potential of probe No. 2 with respect to the plasma as illustrated in Fig. 8), since there is no change in the electron and positive ion current distribution as shared by the two probes. This is no longer the case as we move beyond *b* into the electron collection region.

We are interested in how i_{p_2} (the positive ion current to probe No. 2 varies with V_d in the region to the right of *b* in Fig. 17. To a sufficiently good approximation, the positive ion current in this region is given by the well-known space-charge-limited equation for cylindrical diodes:

$$i_{p_2} = c V_2^{\frac{3}{2}} / \Gamma_p \beta^2, \tag{27}$$

where c is a constant, Γ_p is the probe radius. Equation (27) neglects the effect of ion initial velocities, and of the effect of the electrons in the sheath. These cannot have any serious influence, however. A long series of computations for the ranges of current and voltage of interest showed that for the cases we are concerned with, i_{p_2} varies linearly with V_2 to the right as well as to the left of *b*. Thus if changes in V_2 were equal to those of V_d, the i_{p_2} characteristic in the electron flow region would be obtained by simply extending the line *ab* through *e* and *f* as shown in Fig. 17. Actually since V_2 changes less rapidly than V_d in this region, the $i_{p_2} - V_d$ characteristic looks more like the line *abe'f'*. We must determine the value of i_{i_2} at *e'*.

If in Eq. (6) we substitute for i_{e_2} its equivalent value $A_2 j_{0_2} e^{-\phi V_2}$ and solve for V_2 we obtain:

$$V_2 = -\frac{1}{\phi} \ln \frac{\Sigma i_p}{[\sigma e^{-\phi V_d} + 1] A_0 j_{0_2}} \tag{28}$$

Now let V_d take on two values V_d' and V_d'' as shown in Fig. 17. Let the values of V_2 corresponding to these two values of V_d be V_2' and V_2'', respectively. We wish to determine $\Delta V_2 = V_2' = V_2''$. Then:

$$\Delta V_2 = -\frac{1}{\phi} \ln \left[\frac{\sigma e^{-\phi V_d''} + 1}{\sigma e^{-\phi V_d'} + 1} \right]. \tag{29}$$

For the situation corresponding to V_2' and V_d' let

$$\Sigma i_p / i_{e_2} = \Sigma i_p / [A_0 j_{0_2} e^{-\phi V_2}] = F,$$

and similarly let $\Sigma i_p / i_e$ corresponding to V_2'' and V_d'' be denoted by G. Equation (29) then becomes:

$$\Delta V_2 = -(1/\phi) \ln(G/F). \tag{30}$$

From Eq. (6) and the definitions of F and G we can obtain:

$$\Delta V_d = V_d'' - V_d' = -(1/\phi) \ln[(G-1)/(F-1)]. \tag{31}$$

Combining (30) and (31) we obtain:

$$\frac{\Delta V_2}{\Delta V_d} = \frac{\ln(F/G)}{\ln[(F-1)/(G-1)]}. \tag{32}$$

As an origin, we choose a value for F corresponding to V_d close to the point *a* of Fig. 17 where detectable electron current flows. Experimentally it is observed that a definite deviation from the straight line region of the $V_d - i_d$ characteristic is observable when

$$50 < \Sigma i_p / i_{e_2} < 100.$$

As a consequence, the value of $\Delta V_2/\Delta V_d$ was computed from Eq. (32) for $F = 50$, and $F = 100$. The results are plotted in Fig. 18.

For the case of a symmetrical $V_d - i_d$ characteristic,

$$1/G = i_{e_2}/\Sigma i_p = 0.5$$

when $V_d = 0$. It is seen from Fig. 18, that for this condition $\Delta V_2/\Delta V_d \simeq 0.8$. Thus in practice, to find the value of i_{e_2} corresponding to $V_d = 0$, one merely extends the region *ab* of Fig. 17 linearly to a point 0.8 of the way from *b* to *e*. The point α in the figure gives the desired value of i_{p_2} to be used in computing Σi_p in the equivalent resistance method for determining T_e. If the $V_d - i_d$ characteristic is not symmetrical one must make use of Fig. 18 to determine how far beyond the linear region *ab* one must extrapolate in order to determine i_{e_2}.

In the curve of Fig. 11, which is very close to being symmetrical, the figure 0.8 was used.

Scattering of Electrons in Crystals in the Presence of Large Electric Fields

J. BARDEEN AND W. SHOCKLEY
Bell Telephone Laboratories, Murray Hill, New Jersey
(Received June 19, 1950)

By the calculation of transitions between states appropriate to electrons moving in a large uniform electric field superimposed on a periodic crystal field, it is shown the probabilities of scattering by lattice vibrations or imperfections are independent of the uniform field and are given by the usual expressions derived for zero field. This justifies the procedure of treating acceleration by the field and scattering as independent processes.

IN calculations of electrical conduction in solids it is usual to treat acceleration of electrons by the applied field and by scattering as independent processes. The probability of scattering is calculated for the case in which no electric field is present. A question may arise as to the validity of this procedure, particularly when the applied field is so large that the state of the electron changes considerably between collisions. We shall show that although the details of the transition processes may be altered by the electric field, the final expressions for the scattering probabilities are independent of the field.

According to the usual theory the probability per unit time of a transition from a state with crystal momentum $\mathbf{P}=\hbar\mathbf{k}$ to $\mathbf{P}'=\hbar\mathbf{k}'$ is:[1]

$$f(\mathbf{P},\mathbf{P}')=(2\pi/\hbar)|M(\mathbf{P},\mathbf{P}')|^2\delta(E(\mathbf{P})-E'(\mathbf{P}')), \quad (1)$$

where $M(\mathbf{P},\mathbf{P}')$ is the matrix element for the transition and $E(\mathbf{P})$ and $E'(\mathbf{P}')$ are the energies of the initial and final states, respectively. We shall suppose that $E'(\mathbf{P}')$ includes the energy $\hbar\omega$, of the phonon involved in the collision as well as the energy of the electron:

$$E'(\mathbf{P}')=E(\mathbf{P}')\pm\hbar\omega. \quad (2)$$

The upper sign corresponds to absorption and the lower to emission of the phonon.[2] It is convenient to introduce coordinates P_1', P_2', P_3', for $\mathbf{P}'$ such that $dP_2'dP_3'$ lies on the surface of constant energy, $E'(\mathbf{P}')=E(\mathbf{P})$, and dP_1' is normal to this surface. The over-all probability of scattering into $dP_2'dP_3'$ in time Δt is then

$$\rho dP_2'dP_3'\Delta t\int f(\mathbf{P},\mathbf{P}')dP_1'$$

$$=(2\pi/\hbar)|M(\mathbf{P},\mathbf{P}')|^2\rho dP_2'dP_3'\Delta t/(\partial E'/\partial P_1'), \quad (3)$$

where $\rho=h^{-3}$ is the density of states in momentum space. We shall show that (3) still applies when an electric field is present.

The wave equation for an electron influenced by a periodic crystal field, $V_0(\mathbf{r})$, an electric field which produces a force, $\mathbf{F}$, and an interaction operator, H_I, which gives the scattering, can be written as

$$[-(\hbar^2/2m)\Delta+V_0(\mathbf{r})-\mathbf{F}\cdot\mathbf{r}+H_I]\psi=i\hbar\partial\psi/\partial t. \quad (4)$$

We shall solve this equation by the method of variation of constants. The wave function is expanded in a series of functions, $\psi_P(\mathbf{r},t)$, described in Eq. (6), which are solutions of the equation for $H_I=0$ and the coefficients in the expansion are to be determined as functions of time:

$$\psi=\sum_{P'}a_{P'}(t)\psi_{P'}(\mathbf{r},t). \quad (5)$$

The treatment differs from the usual one in that the wave functions used in the expansion are appropriate to an applied electric field, $\mathbf{F}$, rather than for zero field. Such wave functions have been used by Houston[3] to discuss the probabilities of transitions between bands induced by the applied field.

Houston showed that

$$\psi_P(\mathbf{r},t)=U_{P+\lambda t}(\mathbf{r})\exp[(i/\hbar)(\mathbf{P}+\mathbf{F}t)\cdot\mathbf{r}]$$

$$\times\exp\left[-(i/\hbar)\int^t E(\mathbf{P}+\mathbf{F}t')dt'\right] \quad (6)$$

is an approximate solution for an electron in a periodic field on which a uniform force, $\mathbf{F}$, is superimposed. This solution corresponds to a state with momentum increasing uniformly in time as suggested by the motion of a wave packet. The wave function and energy, $E(\mathbf{P})$, corresponding to $\mathbf{F}=0$ are those for zero applied field. The fact that (6) is not an exact solution of (4) with $H_I=0$ corresponds to the possibility of the electron making a transition from one Brillouin zone to another when $\mathbf{P}+\mathbf{F}t$ is near a zone boundary. This is the problem discussed by Houston.[3] Such transitions are important when the force $\mathbf{F}$ is so large that it produces a potential energy difference across one unit cell of the same order as the gap between energy bands. This corresponds to an electric field of the order of 10^7 volts/cm. We shall not be concerned with such large fields and shall neglect the differences between (6) and the exact solution of the time-dependent equation with $H_I=0$.

We are concerned with the effect of the interaction, H_I, which produces transitions between states with

[1] See, for example, F. Sietz, *The Modern Theory of Solids* (McGraw-Hill Book Co., Inc., New York, New York, 1940), p. 521 and following.

[2] If, as in impurity scattering, no phonon is involved, we may set $\hbar\omega=0$.

[3] W. V. Houston, Phys. Rev. 57, 184 (1940).

different $\mathbf{P}$. Initially the electron is in the state $\mathbf{P}$, so that at $t=0$,

$$a_P(0)=1, \quad a_{P'}(0)=0, \quad \mathbf{P}'\neq\mathbf{P}. \tag{7}$$

The equation for $a_{P'}(t)$, obtained by substituting (4) into (3), multiplying by $\psi_{P'}(\mathbf{r},t)^*$ and integrating over space is:

$$i\hbar(da_{P'}/dt)=a_P(t)M(\mathbf{P},\mathbf{P}')$$

$$\times\exp\left[-(i/\hbar)\int_0^t(E(\mathbf{P}+\mathbf{F}t')-E'(\mathbf{P}'+\mathbf{F}t'))dt'\right], \tag{8}$$

where

$$M(\mathbf{P},\mathbf{P}')=\int\psi_{P'}{}^*H_I\psi_P dv. \tag{9}$$

In the derivation of (8) we have treated the $a_{P'}$ with $\mathbf{P}'\neq\mathbf{P}$ as small quantities and have neglected terms which contain both $a_{P'}$ and H_I.

In integrating (8) we shall suppose that the time interval involved is so short that $a_P(t)$ does not change appreciably and may be set equal to unity. We also suppose that the matrix element does not vary appreciably with time during the interval so that it can be treated as a constant. The range of validity of these assumptions shall be discussed later. The integral of (8) from $t=0$ to Δt is then

$$a_{P'}(t)=-(i/\hbar)M(\mathbf{P},\mathbf{P}')$$

$$\times\int_0^{\Delta t}\exp\left[-(i/\hbar)\int_0^t(E(\mathbf{P}+\mathbf{F}t')-E'(\mathbf{P}'+\mathbf{F}t')\right]dt'dt. \tag{10}$$

The exponential is a rapidly oscillating function which integrates to zero except when the rate of change of phase with respect to time vanishes. This latter condition corresponds to the requirement of conservation of energy:

$$E'(\mathbf{P}'+\mathbf{F}t)=E(\mathbf{P}+\mathbf{F}t). \tag{11}$$

The value of $a_{P'}(t)$ is negligibly small unless (11) is satisfied at some time during the interval $0\rightarrow\Delta t$.

To evaluate the integral when this condition is satisfied, we expand the argument of the exponential as a power series in t:

$$\int_0^t[E(\mathbf{P}+\mathbf{F}\tau)-E'(\mathbf{P}'+\mathbf{F}\tau)]d\tau=\alpha t+\tfrac{1}{2}\beta t^2+\cdots. \tag{12}$$

The coefficients have the values:

$$\alpha=E(\mathbf{P})-E'(\mathbf{P}'), \quad \beta=\mathbf{F}\cdot\mathrm{grad}_P(E)-\mathbf{F}\cdot\mathrm{grad}_{P'}E'. \tag{13}$$

If (11) is satisfied at $t=t_0$,

$$\alpha t+\tfrac{1}{2}\beta t^2=\tfrac{1}{2}\beta(t-t_0)^2-\tfrac{1}{2}\beta t_0^2. \tag{14}$$

With use of (12) and (14), Eq. (10) becomes:

$$a_{P'}(t)=-(i/\hbar)M(\mathbf{P},\mathbf{P}')\exp(i\beta t_0^2/2\hbar)$$

$$\times\int_0^{\Delta t}\exp[-i\beta(t-t_0)^2/2\hbar]dt. \tag{15}$$

The integral can be evaluated by the method of stationary phases. Thus if we assume that $\beta\Delta t^2/\hbar$ is a large number and that $0<t_0<\Delta t$, we can replaced the limits 0 and Δt by $-\infty$ and $+\infty$ without appreciable error. Since

$$\int_{-\infty}^{\infty}\exp(ix^2)dx=(1+i)(\pi/2)^{\frac{1}{2}}, \tag{16}$$

we obtain finally

$$|a_{P'}(t)|^2=2\pi|M(\mathbf{P},\mathbf{P}')|^2/|\beta|\hbar \text{ for } 0<t_0<\Delta t \tag{17}$$
$$=0 \text{ otherwise.}$$

We shall next show that the probability of scattering into a certain group of end states given by (17) reduces to the value given by (2). For this purpose we again use coordinates P_1', P_2', P_3' for $\mathbf{P}'$, defined so that $dP_2'dP_3'$ lies on a surface of constant energy. For given P_2', P_3', we suppose that P_{10}' is the value of P_1' which satisfies conservation of energy at $t=0$:

$$E'(P_{10}',P_2',P_3')=E(\mathbf{P}), \tag{18}$$

and that $P_{\Delta t}'\equiv(P_{1\Delta t}',P_2',P_3')$ is the value of $\mathbf{P}'$ which satisfies the equation at $t=\Delta t$:

$$E'(\mathbf{P}_{\Delta t}'+\mathbf{F}\Delta t)=E(\mathbf{P}+\mathbf{F}\Delta t). \tag{19}$$

Transitions are possible for those values of P_1' which lie between P_{10}' and $P_{1\Delta t}'$. The allowed range of values for P_1' for which (19) holds is denoted by

$$\Delta P_1'=P_{1\Delta t}'-P_{10}'. \tag{20}$$

Since Δt is assumed small, $\Delta P_1'$ can be evaluated by expanding both sides of (19) to terms linear in Δt. Using (18) and (20) this gives

$$\Delta P_1'(\partial E'/\partial P_1')+\Delta t\mathbf{F}\cdot\mathrm{grad}_{P'}E'=\Delta t\mathbf{F}\cdot\mathrm{grad}_P E. \tag{21}$$

Solving for $\Delta P_1'$, we find

$$|\Delta P_1'|=\Delta t|\mathbf{F}\cdot\mathrm{grad}_{P'}E'-\mathbf{F}\cdot\mathrm{grad}_P E|/(\partial E'/\partial P_1')$$
$$=\Delta t|\beta|/(\partial E'/\partial P'). \tag{22}$$

Since the probability of scattering is the same for each of the states in the range $|\Delta P_1'|dP_2'dP_3'$, the total probability of scattering into the range $dP_2'dP_3'$ in time Δt is:

$$\rho|a_{P'}(t)|^2|\Delta P_1'|dP_2'dP_3'$$
$$=2\pi\rho|M(\mathbf{P},\mathbf{P}')|^2|\Delta P_1'|dP_2'dP_3'/|\beta|\hbar. \tag{23}$$

With use of (22) for $|\Delta P_1'|$ this becomes

$$(2\pi/\hbar)|M(\mathbf{P},\mathbf{P}')|^2\rho dP_2'dP_3'\Delta t/(\partial E'/\partial P_1'), \tag{24}$$

which is identical with (2). Thus the scattering probabilities are independent of the field.

It remains to discuss the limits of validity of the approximation used in obtaining (2) and (24). Peierls[4] has discussed the applications of (1) and (2) to the theory of conductivity. These equations can be used when the relaxation time, τ, which is the average time between collisions, is sufficiently large so that

$$\tau\Delta E > \hbar, \tag{25}$$

where ΔE is of the order of $\hbar\omega$. If (1) is to be integrated over the distribution function of the electrons, one may take the less stringent condition $\Delta E \sim k_0 T$. Thus (1) and (2) may be used if

$$\tau k_0 T > \hbar. \tag{26}$$

The approximations made in the derivation of (17) and (24) are of a different nature since they depend on the magnitude of the electric field. In the derivation of (17) it was assumed that Δt is sufficiently large so that

$$\beta(\Delta t)^2 > \hbar \tag{27}$$

and at the same time small enough so that $a_P(t)$ and $M(\mathbf{P}, \Delta')$ do not vary appreciably during the interval Δt. Taking $a_P(\Delta t) \sim 1$ implies that

$$\Delta t < \tau. \tag{28}$$

The constancy of the matrix element implies that the state of the electron does not change very much during Δt. Since the momentum changes by $\mathbf{F}\Delta t$, this implies that

$$\mathbf{F}\Delta t < \Delta\mathbf{P}, \tag{29}$$

where $\Delta\mathbf{P}$ is a momentum interval over which the matrix element is substantially constant.

[4] R. Peierls, Zeits. f. Physik **88**, 786 (1934); Helv. Phys. Acta, **7** 24 (1934).

The maximum allowed value of Δt is the smaller of the values determined by the limiting conditions (28) and (29). Condition (29) applies if the electric field is such that the momentum of the electron is changed by a large amount between collisions. Equation (28) applies if $\mathbf{F}\tau$ represents a relatively small change in momentum.

Equation (27) can be written in a somewhat different form by use of the definition (13) for β. It follows from (13) that

$$\beta\Delta t = \Delta E_{\Delta t}, \tag{30}$$

where $\Delta E_{\Delta t}$ is the change in energy of the electrons during Δt. Thus (27) can be written as

$$\Delta E_{\Delta t}\Delta t > \hbar. \tag{31}$$

If (28) applies, (31) may be written

$$\Delta E_\tau \tau > \hbar, \tag{32}$$

where ΔE_τ is now the energy change between collisions. This expression is similar to Peierls' conditions (25) and (26), but may be less stringent if the field, $\mathcal{E}$, is such that $\Delta E_\tau > k_0 T$. If (29) applies, (31) may be written

$$(\partial E/\partial P)(\Delta P)^2 > |eF\hbar|. \tag{32}$$

This equation gives an upper limit for the electric field, but the limiting field is ordinarily quite large. For example, if we set $\partial E/\partial P \sim v \sim 10^7$ cm/sec. and $\Delta P \sim mv$, the limit is:

$$\mathcal{E} < m^2v^3/e\hbar \sim 2\times 10^3 \text{ e.s.v.} \sim 6\times 10^5 \text{ volts/cm}, \tag{33}$$

These arguments show that the usual expressions for scattering probabilities can be used ordinarily when an electric field is present, and, in fact, the range of validity of the expressions may be extended by the presence of an electric field.

* Deformation Potentials and Mobilities in Non-Polar Crystals

J. BARDEEN AND W. SHOCKLEY
Bell Telephone Laboratories, Murray Hill, New Jersey
(Received May 31, 1950)

The method of effective mass, extended to apply to gradual shifts in energy bands resulting from deformations of the crystal lattice, is used to estimate the interaction between electrons of thermal energy and the acoustical modes of vibration. The mobilities of electrons and holes are thus related to the shifts of the conduction and valence-bond (filled) bands, respectively, associated with dilations of longitudinal waves. The theory is checked by comparison of the sum of the shifts of the conduction and valence-bond bands, as derived from the mobilities, with the shift of the energy gap with dilation. The latter is obtained independently for silicon, germanium and tellurium from one or more of the following: (1) the change in intrinsic conductivity with pressure, (2) the change in resistance of an n–p junction with pressure, and (3) the variation of intrinsic concentration with temperature and the thermal expansion coefficient. Higher mobilities of electrons and holes in germanium as compared with silicon are correlated with a smaller shift of energy gap with dilation.

I. INTRODUCTION

THE mobilities of electrons and holes in non-polar semiconductors and insulators are determined by interactions with the acoustical vibrations of the lattice as well as by scattering by impurities or other lattice defects. The former generally predominates in relatively pure materials in which the concentration of carriers is small. Classical rather than quantum statistics may then be applied to the conduction electrons and the wave-length of an electron of thermal energy is large compared with the lattice constant. Such electrons interact only with acoustical vibrational modes of comparably long wave-length whose properties are determined by the bulk elastic constants. The purpose of the present paper is to calculate the magnitude of this interaction on the assumption that local deformations produced by the lattice waves are similar to those in homogeneously deformed crystals. In particular, we shall show that for the case of non-degenerate, spherical energy surfaces in the Brillouin zone the lattice scattering is determined by shifts in the energy bands resulting from dilations associated with acoustical waves.[1]

The discussion of the motion of electrons or holes in semiconductors is usually based on the use of the concept of effective mass. If a gradually varying electrostatic potential is superimposed on the periodic potential of a crystal lattice, it is often a good approximation to neglect the periodic potential and to calculate the motion of an electron of appropriate effective mass in the gradually varying potential. Justifications for this procedure have been given by Peckar,[2] Slater,[3] and James.[4] The criterion is essentially that the change in the gradually varying potential in one period be small compared with the periodic potential. One of our principal aims is to show that this theory can be extended to cover effective potentials which correspond to the position of the energy band boundary as affected by a gradually varying dilation. We shall call effective potentials of this sort, which can be produced by acoustical waves of long wave-length, *deformation potentials*.

The velocity, v, of an electron with energy k_0T (k_0 = Boltzmann's constant) at room temperature is about 10^7 cm/sec. The wave-length, $\lambda=h/mv$, of electron with this velocity is about 7×10^{-7} cm, which is large compared with the lattice constant. The energy of a phonon of corresponding wave-length is

$$h\nu=hc/\lambda=mvc=(c/v)mv^2, \tag{1.1}$$

where c is the velocity of the acoustical wave. Since $c\sim5\times10^5$ cm/sec. as compared with $v\sim10^7$ cm/sec., the energy of the phonon involved in scattering is small compared with k_0T and with the energy of the conduction electrons. This implies that the pertinent acoustical waves can be treated by classical methods, even at fairly low temperatures. In this latter respect the theory for non-polar crystals is simpler than for metals or for polar compounds.

The theory of scattering by acoustical vibrational modes has been discussed by Sommerfeld and Bethe,[5] by Wilson[6] and by Seitz.[7] Making certain assumptions concerning the interaction between electrons and lattice waves, they show that (1) scattering is essentially elastic, (2) scattering is isotropic, and (3) the mean free path is independent of the velocity of the electron and is inversely proportional to the absolute temperature. The mobility then varies as $T^{-\frac{3}{2}}$, as is observed in relatively pure samples of Ge, Si, and Te.

Germanium and silicon have a diamond structure with two atoms per unit cell, so that there are two branches to the vibrational spectrum. Seitz has con-

[1] W. Shockley and J. Bardeen, Phys. Rev. **77**, 407 (1950).
[2] S. Peckar, J. Phys. USSR **10**, 431 (1946).
[3] J. C. Slater, Phys. Rev. **76**, 1592 (1949). Slater's proof is based on a method of G. H. Wannier, Phys. Rev. **52**, 191 (1937).
[4] H. M. James, Phys. Rev. **76**, 1602 (1949).
[5] A. Sommerfeld and H. Bethe, *Handbuch der Physik* (1933), Vol. XXIV.
[6] A. H. Wilson, *The Theory of Metals* (Cambridge University Press, London, England, 1936).
[7] F. Seitz, Phys. Rev. **73**, 549 (1948).

sidered the theory of scattering by the upper branch as well as by the acoustical branch. There is no experimental evidence that scattering by modes in the upper branch plays a role in the conductivity of non-polar semiconductors. Frohlich and Mott, on the other hand, have shown that a major cause of scattering in polar crystals is the interaction with optical modes of long wave-length.. We shall be concerned only with the acoustical branch.

A calculation of the actual magnitude of the mean free path or mobility requires an evaluation of a matrix element of the interaction between electrons and lattice vibrations and some assumption regarding the form and magnitude of this interaction. While some calculations of the matrix element have been given for metals, no explicit calculations have been made previously for non-polar semiconductors. Making use of the deformation potentials, we evaluate the matrix element in terms of certain general properties of the energy band picture in a way which permits correlation with other experimental data. The details of this calculation are given in the Appendix.

The deformation potential is determined by shifts in the energy bands with dilations of the crystal produced by thermal vibrations, and is calculable from the variation in energy band boundaries with lattice constant. The calculation of energy bands has not progressed to the point where these variations can be obtained from first principles. It is possible to check the theory from experimental data, however, because the theory predicts that quantities deduced from the mobilities will be definitely related to effects produced by pressure and by thermal expansion.

II. ENERGY BANDS IN DEFORMED CRYSTALS

In Fig. 1 we give a qualitative diagram showing how the band structure may be expected to vary with lattice constant for a crystal like silicon or germanium.[8] In these crystals a decrease in lattice constant increases the separation between the valence-bond, or filled, band and the conduction band. It should be noted that the energies of the valence-bond and conduction bands, E_v and E_c, may shift in opposite directions as a result of the varying dilation of a lattice wave, thus changing the energy gap, $E_G=E_c-E_v$. In contrast, a varying electrostatic potential, in the absence of distortion, moves the bands up and down together (cf. Fig. 1 of reference 1). We shall shortly consider the effects of more general deformations than pure compressions or dilations and in Section III we shall show how the resulting shifts can be treated as effective potentials.

We shall next consider and dispose of a difficulty in applying curves like those of Fig. 1 to obtain shifts in the energy bands in different parts of a deformed crystal. This difficulty has to do with the fact that deformations may set up electrostatic potentials. When curves like those of Fig. 1 are computed numerically, some arbitrary choice of the zero of electrostatic potential must be made. For example, in calculating curves for diamond, Kimball[8] used a potential which took on the same numerical value near the interior of the atom for all lattice constants; as he points out, this choice is purely arbitrary.

Actually the potential in the interior of the atoms varies with dilation. For example, in the case of semiconductors with large scale deformations the potential is determined as follows: Start with an undeformed crystal of lattice constant a_0. Imagine a deformation which leaves one portion of the crystal unaltered, but, as a result of a continuously varying strain, produces another large region in which the crystal is uniformly dilated to a value a_1. Let the height of the Fermi level corresponding to electrical neutrality and measured relative to the potential energy of an electron at a point fixed near the interior of an atom be U for the undeformed crystal and U' for the deformed crystal. In equilibrium, the potentials will adjust themselves to bring the Fermi levels in different parts of the crystal

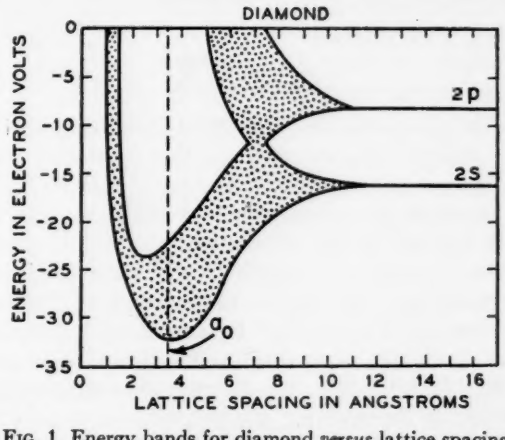

FIG. 1. Energy bands for diamond *versus* lattice spacing (see reference 8).

to the same height. This implies a difference of $U'-U$ in potential energy resulting from the change in electrostatic potential near the interior of an atom. The electrostatic potential difference is produced in part by the space charge of the carriers and fixed impurity ions and in part by polarizations due to relative displacement of the electrons and atomic nuclei in the region of varying strain. As a specific example, in a n-type semiconductor, the requirement of electrical neutrality will lead to approximately the same value of E_c in both parts of the crystal so as to produce the electron densities which compensate the impurity ions.

For the short wave-length lattice waves which contributed to scattering, however, the space charge of the carriers and impurities in the semiconductor is insufficient to set up appreciable potential differences over

[8] The figure is based on calculations of the energy bands in diamond by G. E. Kimball, J. Chem. Phys. 3, 560 (1935). The band structure for silicon has been calculated by J. F. Mullaney, Phys. Rev. 66, 326 (1944).

the relatively short distances involved. In fact, for the wave-length of a thermal electron in germanium of resistivity of 5 ohm-cm, there will be about 10^{-5} electrons on the average in each cube one wave-length on an edge. Even for higher densities, the effect is negligible. Longitudinal lattice waves of wave vector $\mathbf{k}$ produce electrostic potentials of the order $Ne\Delta/k^2$, where N is the concentration of impurity ions and Δ is the dilation of the wave. This effect is negligible compared with the effect of shifting of the bands,[9] except for very small values of k (very long wave-lengths). In addition to the space charge of the carriers, there may be local polarizations and electric fields resulting from relative displacements of neighboring atoms; for non-polar crystals, these will also be negligible. Accordingly, we assume that electric field effects which made the electrostatic potential depend on the strain pattern are negligible for deformation waves of interest for scattering and consider the energies E_c and E_v of the conduction and valence-bond bands each to be a unique function of the local strain.

For a cubic crystal subject to a homogeneous strain ϵ_{ij}, the band energies E_c or E_v can be expressed in the form,

$$E(\epsilon_{ij})=E_0+E_1\Delta, \tag{2.1}$$

where Δ is the dilation

$$\Delta=\epsilon_{11}+\epsilon_{22}+\epsilon_{33}, \tag{2.2}$$

since by symmetry any term containing ϵ_{ij} with $i\neq j$, which changes sign by reflection in a symmetry plane, must have a zero coefficient. The parameter E_1 has the dimensions of an energy, and we shall see that it is closely related to the interaction constant C used in previous theories of scattering.[5,6] If the energy band is degenerate, then relative displacements of the different energy sheets may be produced by shearing strains. It should be possible to extend the treatment of (2.1) and (2.2) to such cases by methods similar to those employed in determining the shape of the energy surfaces.[9a] It is probable that effects associated with complex shapes of the energy surfaces may account for magnetoresistive effects in germanium and silicon. The agreement presented in Table III between the predictions based on (2.1) and experiment suggests that the contributions of scattering due to other terms is relatively small compared to E_1. In this paper we shall neglect the possibility of degenerate energy bands and shall proceed on the basis of spherical energy surfaces in the Brillouin zone.

In a strained crystal a wave function with crystal momentum $\mathbf{P}$ [i.e., having a factor $\exp(i\mathbf{P}\cdot\mathbf{r}/\hbar)$] will have an energy

$$E(P,\epsilon_{ij})=E_0(P)+\Sigma_{ij}\epsilon_{ij}E_{ij}(P). \tag{2.3}$$

For small P, E_{ij} can be expanded in the series:

$$E_{ij}(P)=E_1\delta_{ij}+\Sigma_{kl}\beta_{ijkl}P_kP_l+\cdots. \tag{2.4}$$

Thus the energy for a state with P small is of the form

$$E(P,\epsilon_{ij})=E_0(P)+E_1\Delta+\text{terms in } P^2 \text{ strains}. \tag{2.5}$$

For electrons of thermal energy, the latter terms are generally small compared to $E_1\Delta$ and can be neglected. This is equivalent to neglecting the change in effective mass with strain.

III. THE DEFORMATION POTENTIAL THEOREMS

In the Appendix an analytical treatment is presented showing that the shift in the band edges, which can be written as $E_{1c}\Delta$ for electrons in the conduction band, and as $E_{1v}\Delta$ for holes in the valence-bond band, may be used as varying potentials in calculating the behaviors of electrons and holes. We shall refer to these potentials as *deformation potentials* and write

$$\delta U(r)=E_1\Delta(r), \tag{3.1}$$

supplying the subscripts c and v as required. The first theorem, referred to as the *method of effective mass*, is analagous to the treatments of Wannier, Peckar, James, and Slater.[2-4]. These earlier treatments show that in an undistorted lattice when a perturbation δU_s (s for electro*static*) produced by an electrostatic field is present, the wave function can be obtained by solving the equation

$$[(\hbar^2/2m^*)\nabla^2+\delta U_s(\mathbf{r})]A(\mathbf{r})=EA(\mathbf{r}), \tag{3.2}$$

where $A(\mathbf{r})$ is an amplitude function. (If the crystal is not cubic, $(1/m^*)\nabla^2$ is replaced by $\Sigma\alpha_{ij}(\partial^2/\partial x_i\partial x_j)$ which can be reduced to a principal axis form $\partial^2/m_1\partial x_1^2+\partial^2/m_2\partial x_2^2+\partial^2/m_3\partial x_3^2$. We are not aware of a treatment for the case of degenerate energy bands.) The wave function $A(\mathbf{r})$ is a smoothly varying function which does not vary appreciably over the unit cell; if $\delta U_s(\mathbf{r})$ is so large that $A(\mathbf{r})$ does not satisfy this condition, the method of effective mass becomes inadequate without considerable refinement.

The complete wave function to a good approximation is

$$A(\mathbf{r})\psi_0(\mathbf{r}), \tag{3.3}$$

where $\psi_0(\mathbf{r})$ is the wave function at the band edge and is either periodic with the period of the lattice or simply changes sign from cell to cell. This shows that, except for fluctuations within each unit cell, the probability density is distributed as for a particle of effective mass m^* moving in a potential δU_s. In the Appendix it is shown that if the crystal is deformed a similar theorem applies if a deformation potential

$$\delta U=E_1\Delta(\mathbf{r}) \tag{3.4}$$

is added to δU_s in Eq. (3.2). The suitable modification of (3.3) is introduced in the treatment.

[9] For example, with $N\sim10^{17}/\text{cm}^3$ and $k\sim10^7\ \text{cm}^{-1}$, Ne/k^2 is about 5×10^{-7} e.s.u. or 1.5×10^{-5} volt. This potential contributes a negligible amount compared to E_1 of Eq. (2.1).

[9a] W. Shockley, Phys. Rev. 78, 173 (1950).

The second theorem shows that the deformation potential (3.4) is also suitable for use in a calculation of the matrix element for a transition from a state with crystal momentum $\mathbf{P}$ and wave function

$$\psi(\mathbf{r}, \mathbf{P}) = \exp(i\mathbf{P}\cdot\mathbf{r}/\hbar)U(\mathbf{r}, \mathbf{P}), \tag{3.5}$$

where $U(\mathbf{r}, \mathbf{P})$ has the periodicity of the undistorted lattice, to a state with momentum $\mathbf{P}'$. The matrix element is

$$M = \int \psi^*(\mathbf{r}, \mathbf{P}')\delta U(\mathbf{r})\psi(\mathbf{r}, \mathbf{P})dxdydz, \tag{3.6}$$

where $\delta U(\mathbf{r})$ is $E_1\Delta(\mathbf{r})$ produced by a thermal vibration. The transition from $\mathbf{P}$ to $\mathbf{P}'$ can occur with either absorption or emission of a phonon. Combining the emission and absorption processes gives an effective matrix element for $P \rightarrow P'$

$$|M|^2 = E_1^2\langle\Delta^2\rangle_{Av} = E_1^2 k_0 T/Vc_{ii}, \tag{3.7}$$

where V is the volume of the crystal and $\langle\Delta^2\rangle_{Av}$ is the average dilation of a longitudinal wave with an elastic constant $c_{ii} = \rho v_l^2$ having total energy k_0T, i.e., potential energy $= c_{ii}\langle\Delta^2\rangle_{Av}V/2 = k_0T/2$.

The value of the matrix element can be used in the scattering formula (details in Appendix) to give a mobility of

$$\mu = [(8\pi)^{\frac{1}{2}}\hbar^4 c_{ii}/3E_1^2 m^{*5/2}k_0^{\frac{3}{2}}]T^{-\frac{3}{2}} \tag{3.8}$$

or

$$\mu T^{3/2} = (3.2\times 10^{-5})c_{ii}/E_1^2 \tag{3.9}$$

if m^* is taken to be the free electron mass. In (3.9), μ is expressed in cm²/volt sec. and E_1 in ev.

In the next section we shall discuss experimental values of c_{ii} and in the following section the values of $|E_{1c}|$ and $|E_{1v}|$ obtained by inserting values for μ_n, μ_p, and c_{ii} into (3.9) and solving for $|E_1|$. The results so obtained are compared with the variation of the energy gap E_G, given by

$$E_G = E_{0G} + E_{1G}\Delta, \tag{3.10}$$

where

$$E_{1G} = E_{1c} - E_{1v}. \tag{3.11}$$

If the effect of dilation is to shift the energy bands in opposite directions,

$$|E_{1G}| = |E_{1c}| + |E_{1v}|. \tag{3.12}$$

There are several empirical ways of determining E_{1G}, and estimates of this quantity have been made for Ge, Si, and Te. We shall show in Section V that values of $|E_{1c}|$ and $|E_{1v}|$ obtained from mobility data are in reasonable agreement with values of $|E_{1G}|$ obtained in other ways.

IV. DISCUSSION OF ELASTIC CONSTANTS

The important deformation waves are those which produce dilation by having a large component of atomic displacement parallel to the direction of propagation. Since the waves of interest are long compared with the lattice constant, their velocities can be determined from the elastic constants. In an isotropic solid, the three possible polarizations consist of one purely longitudinal mode and two transverse modes; in a cubic crystal the same situation is true for wave propagating in the (100), (110), and (111) directions, which lie along symmetry axes. For other directions there is a slight mixing of longitudinal and transverse polarizations.

The elastic constants for diamond, germanium, and silicon are given in Table I. Values listed for germanium are from some recent measurements made at the Bell Telephone Laboratories.[10] The only value known for silicon is the compressibility from Bridgman's data[11] on the change of volume with pressure. Values of the compressibilities[12] of diamond, Si, Ge, and Te are given in Table II. Values of the elastic constants of silicon listed in Table I were estimated by assuming that they differ from those of germanium by a constant factor which was obtained from compressibility data. In an isotropic solid,

$$c_{44} = \tfrac{1}{2}(c_{11} - c_{12}). \tag{4.1}$$

It can be seen from Table I that this relation is not well satisfied for these elements. Nevertheless, the velocities of longitudinal waves in the various directions are not very different.

Values of c_{ii} for different directions of propagation can be expressed directly in terms of the cubic elastic constants as shown below:

$$\begin{aligned} &(100)\quad c_{ii} = c_{11}, \\ &(110)\quad c_{ii} = \tfrac{1}{2}(c_{11} + c_{12} + 2c_{44}), \\ &(111)\quad c_{ii} = \tfrac{1}{3}(c_{11} + 2c_{12} + 4c_{44}). \end{aligned} \tag{4.2}$$

For other directions of propagation, the velocities lie between the extremes at (100) and (111), and the waves are not to be strictly longitudinal. However, as can be seen from Table I, differences in c_{ii} in different directions are not large, so that the approximation we have made of treating the material as isotropic will introduce relatively small errors.

V. CALCULATION OF $|E_{1c}|$ AND $|E_{1v}|$ FROM MOBILITY DATA

Data used for the calculation of $|E_{1c}|$ and $|E_{1v}|$ from Eq. (3.9) are listed in Table III which is reproduced with some minor changes from reference 1. Although tellurium is anisotropic, it has been included for purposes of comparison, along with the elements of the fourth group which have the diamond structure. The anisotropy has been neglected. Somewhat arbitrarily we have used the value of c_{ii} in the (110) direction for elements with the diamond structure in place of the

[10] Elastic constants of germanium have been measured by McSkimin, Mason and Bond on a single crystal sample prepared by K. M. Olson.

[11] P. W. Bridgman, Proc. Am. Acad. 76, 187 (1949).

[12] The value for diamond was computed from the elastic constants; values for Si, Ge, and Te are from Bridgman, reference 11.

TABLE I. Elastic constants (units c.g.s.$\times 10^{12}$).

	Diamond	Silicon	Germanium
c_{11}	9.3	(1.67)	1.29
c_{12}	4.1	(0.62)	0.48
c_{44}	4.15	(0.87)	0.67
c_{ii}, (100)	9.3	(1.67)	1.29
c_{ii}, (110)	10.8	(2.0)	1.55
c_{ii}, (111)	11.4	(2.1)	1.64

TABLE II. Compressibilities.

Diamond	0.17×10^{-12} c.g.s.
Si	0.98
Ge	1.26
Te	4.0

appropriate average over all directions of propagation. For tellurium, we have assumed simply that c_{ii} is inversely proportional to the compressibility, and have estimated the value by comparison with diamond and Ge. Values of the mobility in silicon are from the Hall effect measurements of Pearson and Bardeen,[13] in germanium from the drift velocity measurements of Haynes,[14] and in tellurium from Johnson.[15] The mobility of electrons in diamond has been determined by Klick and Maurer[16] but the mobility of holes is unknown. From studies of bombardment induced conductivity, McKay[17] has concluded that the mobility of holes must be greater than 200 cm^2/volt-sec. at room temperature. Values of $|E_{1c}|$ and $|E_{1v}|$ as determined from Eq. (3.9) are listed in the sixth and seventh rows of the table.

Equation (3.9) is based on the assumption that the effective mass is equal to the ordinary electron mass. As the mobility varies as $m_e^{-5/2}$, values of E_{1c} and E_{1v} should be multiplied by $(m/m_e)^{5/4}$ if the effective mass, m_e, differs from the ordinary mass. In the case of silicon, there is evidence that m/m_e is appropximately equal to unity for holes and is greater than unity, perhaps about 1.5, for electrons.[13] Use of the latter value would increase $|E_{1c}|$ from 6.5 to 10.7, and $|E_{1c}|+|E_{1v}|$ from 17.8 to 22. It also would increase the value of $|E_{1G}|$ estimated from concentration data (Section VI) from 33 to 40 ev, in closer agreement with the value deduced from optical data, Values of m/m_e for the other elements listed are uncertain, but are probably not far from unity.

If the conduction and valence-bond bands move in opposite directions with dilation, the magnitude of the shift in energy gap with dilation, $|E_{1G}|$, is given by the sum of $|E_{1c}|$ and $|E_{1v}|$, while if they move the same way, $|E_{1G}|$ is equal to the difference. Estimates of E_{1G} from other data (Section VI), given in the last row of the table, are approximately equal to the sum of $|E_{1c}|$ and $|E_{1v}|$, indicating that the former picture is correct.

TABLE III. Derivation of shift of energy bands with dilation from mobility data and comparison with shift of energy gap with dilation.

	Diamond	Silicon	Germanium	Tellurium
(1) $c_{ii}\times 10^{-12}$ c.g.s., (110)	10.8	2.0	1.55	0.50
(2) μ_n (electrons) (295°K)	900	300	3500	530
(3) μ_p (holes) (295°K)	>200	100	1700	530
(4) $\mu_n T^{\frac{3}{2}}$	45×10^5	15×10^5	180×10^5	27×10^5
(5) $\mu_p T^{\frac{3}{2}}$	$>10\times 10^5$	5×10^5	86×10^5	27×10^5
(6) $\|E_{1c}\|$(ev)	8.8	6.5	1.7	2.4
(7) $\|E_{iv}\|$(ev)	<30	11.3	2.4	2.4
(8) $\|E_{1c}\|+\|E_{1v}\|$(ev)	<39	17.8	4.1	4.8
(9) E_{1G}(ev)	?	~ -30	~ -5	+4.0

The agreement between $|E_{1G}|$ and the sum of $|E_{1c}|$ and $|E_{1v}|$ is good in the cases of germanium and tellurium, and is not as good for silicon. As is discussed in the following section, the value of $|E_{1G}|$ for silicon is obtained by an indirect method which may not be reliable. In any case, *the high mobilities of electrons and holes in germanium as compared with silicon is correlated with a smaller shift in energy gap with dilation.*

VI. SHIFT OF ENERGY GAP WITH DILATION

There are two general methods for obtaining information about energy gaps in semiconductors. One is based on the long wave limit of the fundamental absorption band, and the other on the equilibrium concentrations of electrons and holes, particularly in the intrinsic temperature range.

Absorption of a light quantum in the fundamental band raises an electron from a state in the valence-bond band to a state in the conduction band. One may measure either the absorption coefficient or the photoconductivity (or photo-voltaic effect) of the electrons and holes created by the light as a function of wavelength. At the long wave-length limit the quantum energy is assumed to be equal to the energy gap. Actually, because of thermal fluctuations and possibly also because of local irregularities, the long wave limit is not sharply defined and there is considerable uncertainty in the estimation of the energy gap. If the transition corresponding to E_G is forbidden by selection rules, the long wave limit will correspond to a larger energy than E_G.

Goucher and Briggs[18] have observed the photo-current produced by light absorbed in a p–n junction in silicon as a function of wave-length at different temperatures. They found a change in the long wave limit which corresponds to a shift in energy gap from 1.1 to 1.0 ev

[13] G. L. Pearson and J. Bardeen, Phys. Rev. **75**, 865 (1949).
[14] Pearson, Haynes, and Shockley, Phys. Rev. **78**, 295 (1950).
[15] V. A. Johnson, Phys. Rev. **74**, 1255 (1948).
[16] C. G. Klick and R. J. Maurer, Phys. Rev. **76**, 179 (1949).
[17] Estimated by K. G. McKay from experiments on bombardment induced conductivity in diamond.
[18] F. S. Goucher and H. B. Briggs (unpublished).

between liquid N_2 and room temperature, a difference of about 220°C. This corresponds to a shift of about 4.5×10^{-4} ev/°C. Becker and Fan[19] found a shift of about the same rate from measurements of the absorption coefficient between 77°K and 663°K.

If it is assumed that the temperature variation is entirely due to thermal expansion, the shift of the energy gap with dilation can be obtained by dividing the temperature coefficient by the volume coefficient of expansion. The latter is about 9×10^{-6}/°C for silicon, so that

$$E_{1G}=VdE_G/dV\sim-50 \text{ ev/unit dilation.} \quad (6.1)$$

Similar measurements of Goucher and Briggs[18] on the spectral distribution of the photo-current from an n–p junction in germanium and of Briggs[20] on the absorption coefficient as a function of temperature indicate that the temperature coefficient of E_G is about the same for germanium as for silicon. As the expansion coefficient is about twice that for silicon, the optical data give a value of about -25 ev for E_{1G} for germanium.

As we shall see, methods based on the concentrations of carriers give values of E_{1G} which are smaller than those deduced above from optical data, particularly for the case of germanium; although the values obtained for the energy gaps, E_{0G}, are in reasonable agreement. The source of this discrepancy is not known.[20a] It is believed that values based on concentration data are more reliable because there is less uncertainty in the theoretical interpretation.

In the following paragraphs we shall give the theory of the relationship between concentrations and energy gap and discuss the methods which can be used to determine the energy gap and its variation with volume.

Statistical theory indicates that at any temperature and regardless of impurity concentration as long as the concentrations of carriers are so small that classical statistics may be used, the product of the electron and hole concentrations, np, is[21]

$$\begin{aligned} np&=4(2\pi mkT/h^2)^3(m_nm_p/m^2)^{\frac{3}{2}}\exp(-E_G/kT)\\ &=2.4\times10^{31}T^3(m_nm_p/m^2)^{\frac{3}{2}}\exp(-E_G/kT), \end{aligned} \quad (6.2)$$

where m_n and m_p are the effective masses of the electrons and holes, respectively, and the other symbols have their usual meanings. This relation can be used in several ways to estimate E_G and its change with dilation. These are outlined below.

(*A*) *The variation in intrinsic conductivity with pressure.*—In the intrinsic temperature range, the concentrations of electrons and holes are equal and

$$n_i=p_i=5\times10^{15}T^{\frac{3}{2}}(m_nm_p/m^2)^{\frac{3}{4}}\exp(-E_G/2kT). \quad (6.3)$$

The intrinsic conductivity, being proportional to $n_i\mu\propto n_iT^{-\frac{3}{2}}$ varies as

$$\sigma=\sigma_\infty\exp(-E_G/2kT). \quad (6.4)$$

The energy gap can be estimated from two conductivity measurements σ_1 and σ_2, made at temperatures, T_1 and T_2:

$$E_G=2k\ln(\sigma_2/\sigma_1)(T_1^{-1}-T_2^{-1}). \quad (6.5)$$

This equation has been applied to Bridgman's measurements of the pressure change of resistance of tellurium to estimate the energy gap at different pressures.[22] By combining these results with data on the compressibility of Te, the change in energy gap with dilation can be determined. This gives the value $E_{1G}=4.0$ ev listed in the last row of Table III.

If it is assumed, as is approximately the case for Te, that σ_∞ is relatively independent of pressure and that most of the change in σ comes from the change in E_G, Eq. (6.4) gives

$$dE_G/dP=-2kTd\ln(\sigma/dP). \quad (6.6)$$

The value obtained in this way can be combined with compressibility data to estimate E_{1G}.

A modification of this method has been used by Miller and Taylor,[23] who find $E_{1G}\sim-5.0$ ev for germanium.

(*B*) *The change of resistance of an n–p junction with pressure.*—According to the theory developed by one of the authors,[24] the current flowing across an n–p junction consists of a current of holes, I_p, flowing from the n-region to the p-region and a current of electrons, I_n, flowing from the p-region to the n-region. These currents are proportional, respectively, to the equilibrium concentration of holes in the n-region, p_n, and the concentration of electrons in the p-region, n_p. The net current per unit area flowing at an applied voltage V is:

$$I=I_p+I_n=e\left[\frac{D_pp_n}{L_p}+\frac{D_nn_p}{L_n}\right][\exp(eV/k_0T)-1], \quad (6.7)$$

where D_p and D_n are the diffusion constants for electrons and holes, respectively, and L_p and L_n are the diffusion lengths $(D_p\tau_p)^{\frac{1}{2}}$ and $(D_n\tau_n)^{\frac{1}{2}}$, and τ_p and τ_n are the mean lifetimes for holes and electrons in the n and p regions respectively.

The equilibrium concentrations of holes in the p-region, p_p, and of electrons in the n-region, n_n, are approximately constant, independent of temperature, in germanium in the neighborhood of room temperature. It follows from Eq. (6.2) that p_n and n_p each vary as

[19] M. Becker and H. Y. Fan, Phys. Rev. **76**, 1531 (1949).
[20] H. B. Briggs (unpublished).
[20a] *Note added in proof:*—T. Muto and S. Oyama (to appear in Prog. Theor. Phys.) and H. Y. Fan [Phys. Rev. **78**, 808 (1950)] have shown that a temperature shift of the energy gap can arise from interaction of electrons with lattice vibrations.
[21] See, for example, R. H. Fowler, *Statistical Mechanics* (Cambridge University Press, London, 1936), second edition, Chapter 11. Equation (6.2) follows from expressions for n and p in terms of the Fermi level.
[22] J. Bardeen, Phys. Rev. **75**, 1777 (1949).
[23] P. H. Miller and J. Taylor, Phys. Rev. **76**, 179 (1949) and personal communication from Dr. Miller.
[24] W. Shockley, Bell. Sys. Tech. J. **28**, 435 (1949).

$\exp(-E_G/kT)$, and thus also

$$I \sim \exp(-E_G/kT) \tag{6.8}$$

provided that the effects of pressure on D_p, L_p, D_n, and L_n are negligible. In germanium, E_G increases with decrease in volume, so that a decrease in I and a corresponding increase in resistance with increase in pressure are to be expected.

Measurements have been made by Hall[25] at pressures up to 10,000 p.s.i. on a germanium n–p junction formed by α-particle bombardment and by Pearson[26] on a junction similarly formed and also on one formed by joining together samples of germanium of different compositions. Pearson's measurements extend to about 2000 p.s.i. Both observers found the expected increase in resistance with pressure. The interpretation of the data are complicated by the fact the current does not vary exactly with the applied voltage as is indicated by the theoretical relation (6.7). Such departures from simple theory are often found in rectifying junctions and are usually explained by a non-uniform barrier.[26a] Pearson's data give change of resistance of about 1.75 percent for 1000 p.s.i. for the deuteron junction and 1.25 percent for 1000 p.s.i. for the chemical junction. Hall's data give a change of about 1.3 percent for 1000 p.s.i. at pressures up to 10,000 p.s.i.

In order to estimate E_{1G} we have taken a resistance change of 1.4 percent per 1000 p.s.i., the average of the above measurements. The dilation corresponding to 1000 p.s.i. is about 7×10^{-5}. Thus

$$d(E_G/kT)/d\ln V = 0.014/(7\times10^{-5}) = -200 \tag{6.9}$$

and

$$E_{1G} = 200kT \doteq -5.0 \text{ ev}. \tag{6.10}$$

This value is about the same as that found by Miller and Taylor.[28]

(*C*) *The variation of concentration with temperature.*—The equilibrium concentrations of electrons and holes can be determined from Hall and resistivity measurements in the intrinsic range. It is found that the product of the concentrations fits a law of the form of Eq. (6.2) for both germanium and silicon, but the numerical factors are larger than the theoretical values. Neglecting differences in the effective mass from the ordinary electronic mass, the discrepancy is a factor of about 32.5 for silicon.[13] This has been explained as resulting from a change in the energy gap with temperature. If a linear variation is assumed,

$$E_G(T) = E_G(0) - \beta T. \tag{6.11}$$

A value of

$$\beta = k\ln 32.5 = 3\times10^{-4} \text{ ev/degree} \tag{6.12}$$

accounts for the factor 32.5. The shift in the energy gap with dilation can be obtained if it is assumed that the change with temperature is due entirely to thermal expansion. The volume coefficient of expansion of silicon is about 9×10^{-6} in the intrinsic temperature range, ~500°C. Thus

$$E_{1G} = 3\times10^{-4}/9\times10^{-6} = 33 \text{ ev}. \tag{6.13}$$

The most recent data[27] on the intrinsic conductivity of germanium give

$$np = 8.5\times10^{31}T^3 \exp(-8700/T), \tag{6.14}$$

so that the discrepancy from the theoretical formula is a factor of about 3.5. This gives

$$\beta = k\ln 3.5 = 10^{-4} \text{ ev/degree}. \tag{6.15}$$

The volume coefficient of expansion of germanium[9a] is about 19×10^{-6} in the temperature range of interest (20 to 200°C), so that

$$E_{1G} = 10^{-4}/19\times10^{-6} = 5.25 \text{ ev}, \tag{6.16}$$

in good agreement with the values obtained by the more direct methods.

It is believed that the value for tellurium is most reliable, that for germanium next, and the value for silicon the least. The uncertainty in the case of silicon is due to the fact that there are no direct measurements involving a change of properties with pressure.

In conclusion it may be pointed out that magnetoresistance experiments furnish strong evidence that the energy bands and scattering are far from isotropic in germanium. The anisotropy in scattering which arises from the anistropy in the elastic constants is insufficient to account for these results. It is possible that the bands are degenerate and so are not as simple as those assumed here. However, it seems likely that refinements of this sort will not alter the semiquantitative verification of the consequences of the energy band theory presented above.

APPENDIX: METHOD OF EFFECTIVE MASS AND CALCULATION OF ELECTRON-LATTICE INTERACTION

A. Method of Effective Mass

In this section we show that the effective mass concept may be applied to gradual changes in band structure resulting from lattice distortions, as well as to a gradually varying electrostatic potential. We follow the method of Peckar.[3] The more rigorous theory of James,[4] which is based on a one-dimensional model, can be extended in a similar manner. We have not attempted to use the methods of Wannier and Slater.[5]

An arbitrary distortion can be expressed in terms of a displacement, $\delta\mathbf{R}(\mathbf{r})$, which is a function of the position vector, $\mathbf{r}$. It is assumed that $\delta\mathbf{R}$ is a smoothly varying function so chosen that the displacement of the atom centered at the lattice position $\mathbf{r}_n$ is:

$$\delta\mathbf{R}_n = \delta\mathbf{R}(\mathbf{r}_n). \tag{A.1}$$

[25] H. H. Hall (unpublished).

[26] G. L. Pearson (unpublished).

[26a] *Note added in proof:*—Hall has since made measurements on a junction, prepared by Pearson, which follows the theoretical relation. The relative change of resistance with pressure is in agreement with the earlier measurements quoted above (1.3 percent for 1000 p.s.i.).

[27] From measurements of the intrinsic conductivity of germanium made at Purdue University and at the Bell Telephone Laboratories combined with mobility values of J. R. Haynes quoted.

It is further assumed that the lattice potential in the distorted crystal depends only on the local displacement and strain. Thus if $U_0(\mathbf{r})$ is the periodic potential in the undeformed crystal and U_d is the potential in a crystal subject to the deformation δR, we take

$$U_d(\mathbf{r})=U_0(\mathbf{r}-\delta\mathbf{R})+U_1(\mathbf{r},\epsilon_{ij}), \tag{A.2}$$

where U_1 depends on the strain components

$$\epsilon_{ij}=\tfrac{1}{2}[\partial(\delta R_j)/\partial x_i+\partial(\delta R_i)/\partial x_j] \tag{A.3}$$

and on position. For small strains, U_1 varies linearly with strain.

The wave equation for an electron in the deformed crystal may be written:

$$[(\hbar^2/2m)\nabla^2+E-U_0(\mathbf{r}-\delta\mathbf{R})-U_1(\mathbf{r},\epsilon)]\psi_d(\mathbf{r})=0. \tag{A.4}$$

Both $\delta\mathbf{R}$ and ϵ are assumed to be slowly varying functions of position. We shall obtain an approximate solution for ψ_d in terms of exact wave functions for electrons in a crystal subject to a homogeneous strain.

If the strain ϵ is homogeneous so that $\delta\mathbf{R}$ is a linear function of position, the wave equation for an electron with crystal momentum $\mathbf{P}$ is:

$$[(\hbar^2/2m)\nabla^2+E_h(\mathbf{P},\epsilon)-U_0(\mathbf{r}-\delta\mathbf{R})-U_1(\mathbf{r},\epsilon)]\psi_h(\mathbf{r},\epsilon,\mathbf{P})=0, \tag{A.5}$$

where E_h (h for *homogeneous*, not for *hole*) is of the form of Eq. (2.3).

$$E_h(\mathbf{P},\epsilon)=E_{h0}(\epsilon)+\Sigma_{i,j}\,\alpha_{ij}(\epsilon)P_iP_j, \tag{A.6}$$

and where E_{h0} depends only on the dilation Δ,

$$E_{h0}(\epsilon)=E_0+E_1\Delta. \tag{A.7}$$

The coefficients α_{ij} depend on the effective mass in the deformed crystal. The wave function ψ_h is of the form:

$$\psi_h(\mathbf{r},\epsilon,\mathbf{P})=\exp(i\mathbf{P}\cdot\mathbf{r}/\hbar)u_h(\mathbf{r}-\delta\mathbf{R},\epsilon,\mathbf{P}). \tag{A.8}$$

When $\mathbf{P}$ is small compared to the size of the Brillouin zone, u_h can be expanded in a series of which the first two terms are:

$$u_h(\mathbf{r}-\delta\mathbf{R},\epsilon,\mathbf{P})=u_{h0}(\mathbf{r}-\delta\mathbf{R},\epsilon)+i\mathbf{P}\cdot\mathbf{u}_{h1}(\mathbf{r}-\delta\mathbf{R},\epsilon)+\cdots. \tag{A.9}$$

Following the line of argument used by Peckar, we show that an approximate expression for ψ_d can be obtained by use of the effective mass concept. The wave equation to be used in the method of effective mass is:

$$[\hbar^2\,\Sigma\,\alpha_{ij}\partial^2/(\partial x_i\partial x_j)+E-E_{h0}(\epsilon)]A(\mathbf{r})=0. \tag{A.10}$$

This equation applies to an electron with effective mass given by the tensor α_{ij} moving in an effective potential, $E_{h0}(\epsilon)$, called the deformation potential, where ϵ depends on position. Suppose that a solution of this equation is expressed in the form of a Fourier series or integral:

$$A(\mathbf{r})=\Sigma_P\,a(\mathbf{P})\exp(i\mathbf{P}\cdot\mathbf{r}/\hbar). \tag{A.11}$$

Substitution in (A.10) gives:

$$\Sigma\,a(\mathbf{P})[\Sigma\,\alpha_{ij}P_iP_j+E-E_{h0}(\epsilon)]\exp(i\mathbf{P}\cdot\mathbf{r}/\hbar)=0. \tag{A.12}$$

We shall show that

$$\psi_d=\Sigma_P\,a(P)\psi(\mathbf{r},\epsilon,\mathbf{P}), \tag{A.13}$$

with ϵ now considered to be a function of $\mathbf{r}$, is an approximate solution of (A.4) provided that ϵ varies sufficiently slowly with $\mathbf{r}$.

Substitution of (A.13) into (A.4) gives

$$\begin{aligned}\Sigma_P\,a(\mathbf{P})&[E-E_{h0}-\Sigma_{i,j}\,\alpha_{ij}P_iP_j]\psi_h(\mathbf{r},\epsilon,\mathbf{P})\\&=(\hbar^2/2m)\,\Sigma_P\,a(\mathbf{P})\exp(i\mathbf{P}\cdot\mathbf{r}/\hbar)\\&\quad\left[\sum_{j,k,l}\left\{\frac{\partial u_h}{\partial\epsilon_{kl}}\left(\frac{2iP_j}{\hbar}\frac{\partial\epsilon_{kl}}{\partial x_j}+\frac{\partial^2\epsilon_{kl}}{\partial x_j^2}\right)\right.\right.\\&\quad\left.\left.+2\frac{\partial^2 u_h}{\partial\epsilon_{kl}\partial x_j}\frac{\partial\epsilon_{kl}}{\partial x_j}\right\}+\sum_{kl}\frac{\partial u_h}{\partial x_l}\frac{2\epsilon_{kl}}{\partial x_k}\right].\end{aligned} \tag{A.14}$$

Terms quadratic in ϵ have been omitted. Use has been made of the fact that ψ_h with ϵ constant satisfied (A.5.) The terms on the right-hand side arise from terms in the kinetic energy which depend on a variation of ϵ with position and are small if this variation is sufficiently gradual. The wave function on the left-hand side may be expanded in a power series in P to give:

$$\begin{aligned}\Sigma_P\,a(\mathbf{P})&[E-E_{h0}-\Sigma_{ij}\,\alpha_{ij}P_iP_j]\exp(i\mathbf{P}\cdot\mathbf{r}/\hbar)\\&\times[u_{h0}(\mathbf{r},\epsilon)+i\mathbf{P}\cdot\mathbf{u}_{h1}(\mathbf{r},\epsilon)\cdots].\end{aligned} \tag{A.15}$$

The dominant term vanishes because of (A.12). Thus (A.13) is an approximate solution of (A.4).

Peckar considers the limits of validity of the method as applied to a space variation of potential. Similar considerations apply when the shifts in the energy bands result from lattice deformations.

B. Calculation of the Matrix Element

A calculation of the probability that an electron be scattered from momentum state $\mathbf{P}'$ to state $\mathbf{P}$ as a result of an interaction with a lattice wave depends on an evaluation of the matrix element.

$$M(\mathbf{P},\Delta')=\int\psi(\mathbf{P}')^*V_p\psi(\mathbf{P})d\tau, \tag{A.16}$$

where V_p represents the perturbation produced by the lattice wave. The matrix element vanishes unless

$$\mathbf{P}'=\mathbf{P}\pm\hbar\mathbf{k}\pm\hbar\mathbf{K}, \tag{A.17}$$

where $\mathbf{k}(|k|=2\pi/\lambda)$ is the wave vector of the lattice wave and $\mathbf{K}$ is a lattice vector of the reciprocal lattice space. Since we are concerned with transitions for which both $\mathbf{P}$ and $\mathbf{P}'$ are relatively small, we can set $\mathbf{K}=0$.

We shall show that the matrix element may be calculated by replacing V_p by the deformation potential, $E_1\Delta(\mathbf{r})$, so that

$$\begin{aligned}M(\mathbf{P},\mathbf{P}')&=\int\psi(\mathbf{P}')^*E_1\Delta(\mathbf{r})\psi(\mathbf{P})d\tau\\&=(E_1/V)\int\exp(\pm i\mathbf{P}\cdot\mathbf{r}/\hbar)\Delta(\mathbf{r})d\tau.\end{aligned} \tag{A.18}$$

where V is the volume of the crystal. Although this result follows from the method of effective mass, we shall give a direct proof of (A.18) which shows more directly the relation between the present and previous interaction potentials. It is based on the assumption that V_p is the difference between the potential in the deformed lattice, $U_d(\mathbf{r})$, as given by (A.2) and $U_0(\mathbf{r})$, the periodic potential in the undeformed lattice:

$$V_p=U_d(\mathbf{r})-U_0(\mathbf{r})=U_0(\mathbf{r}-\delta\mathbf{R})-U_0(\mathbf{r})+U_1(\mathbf{r},\epsilon_{ij}). \tag{A.19}$$

The first two terms on the right give the "deformable potential" used by Bloch and Bethe.[5]

We shall show that the error involved in using $E_1\Delta(\mathbf{r})$ in place of V_p is the order of $(P^2/2m)\times$*strains*, which is generally negligible.

The unperturbed wave functions $\psi(\mathbf{P})$ satisfy the wave equation:

$$H_0\psi(\mathbf{P})=[-(\hbar^2/2m)\nabla^2+U_0(\mathbf{r})]\psi(\mathbf{P})=E_0(\mathbf{P})\psi(\mathbf{P}), \tag{A.20}$$

where the energy,

$$E_0(\mathbf{P})=E_0(0)+P^2/2m_e \tag{A.21}$$

and m_e is the effective mass. The Hamiltonian for the perturbed wave function is H_0+V_p.

The proof of the desired theorem is based on use of the wave functions $\psi_h(\mathbf{r},\epsilon,\mathbf{P})$ for electrons in homogeneously strained crystals as defined by Eq. (A.8) and the related functions obtained by assuming that the strain ϵ is a slowly varying function of $\mathbf{r}$. We shall neglect terms which are quadratic in ϵ. We may write

$$\psi_h(\mathbf{r},\epsilon,\mathbf{P})=\psi(\mathbf{r},\mathbf{P})+\delta\psi(\mathbf{r},\epsilon,\mathbf{P}), \tag{A.22}$$

where $\delta\psi$ is of order ϵ.

To prove (A.18), first consider the integral:

$$I=\int\psi(\mathbf{r},\mathbf{P}')[H_0+V_p]\psi_h(\mathbf{r},\epsilon(\mathbf{r}),\mathbf{P})d\tau. \tag{A.23}$$

The result of the operation on ψ_h is

$$\begin{aligned}I=\int\psi(\mathbf{r},\mathbf{P}')&E_h(\mathbf{P},\epsilon(\mathbf{r}))\psi_h(\mathbf{r},\epsilon,\mathbf{P})d\tau\\&+\text{integrals involving }\partial_h/\partial\epsilon\cdot\partial\epsilon/\partial X.\end{aligned}$$

The latter terms, which are similar to those on the right-hand side of Eq. (A.14), are of the order of $[P^2/2m]\times$*strains*, and may be neglected. To terms of the same order,

$$E_k(\mathbf{P}, e)=E_0(\mathbf{P})+E_1\Delta. \tag{A.24}$$

Thus, omitting terms quadratic in the strain, the integral is approximately:

$$I=\int \psi(\mathbf{P}')^*E_1\Delta\psi(\mathbf{P})d\epsilon+E_0(\mathbf{P})\int \psi(\mathbf{P}')^*\delta\psi(\mathbf{P})d\tau. \tag{A.25}$$

We now evaluate I again by expanding the last two terms of Eq. (A.23) and using the fact that $\psi(\mathbf{P})$ and $\psi(\mathbf{P}')$ are orthogonal eigenfunctions of H_0. This gives

$$\begin{aligned} I&=\int \psi(\mathbf{P}')^*V_p\psi(\mathbf{P})d\tau+\int \psi(\mathbf{P}')^*H_0\psi(\mathbf{P})d\tau \\ &=\int \psi(\mathbf{P}')^*V_p\psi(\mathbf{P})d\tau+E_0(\mathbf{P}')\int \psi(\mathbf{P}')\delta\psi(\mathbf{P})d\tau. \end{aligned} \tag{A.26}$$

The second step involves the Hermitian character of H_0. Solving (A.25) and (A.26) for the desired integral gives

$$\begin{aligned} \int \psi(\mathbf{P}')^*V_p\psi(\mathbf{P})d\tau&=\int \psi(\mathbf{P}')^*E_1\Delta\psi(\mathbf{P})d\tau \\ &+[E_0(\mathbf{P})-E_0(\mathbf{P}')]\int \psi(\mathbf{P}')^*\delta\psi(\mathbf{P})d\tau. \end{aligned} \tag{A.27}$$

The last term is the order $P^2/2m\times$*strains* and can be neglected. Thus we have shown that to terms of this order V_p can be replaced by the deformation potential $E_1\Delta(\mathbf{r})$ in computing the matrix element.

With use of $E_1\Delta$ for V_p, the evaluation of the matrix element is relatively simple. The displacement of an atom at $\mathbf{R}_n$ resulting from a lattice wave of wave vector $\mathbf{k}$ is

$$\delta\mathbf{R}(\mathbf{R}_n)=N^{-\frac{1}{2}}\mathbf{l}_k(a_k\exp(i\mathbf{k}\cdot\mathbf{R}_n)+a_k^*\exp(-i\mathbf{k}\cdot\mathbf{R}_n)), \tag{A.28}$$

where $\mathbf{l}_k$ is a unit vector in the direction of the displacement and N is the number of atoms in unit volume. At high temperatures, when the lattice waves are fully excited, the amplitude of the wave is given by

$$|a_k|^2=k_0T/2Mk^2c_l^2, \tag{A.29}$$

where k_0 is Boltzmann's constant, M is the mass of an atom and c_l is the velocity of a longitudinal wave. The dilation resulting from $\delta\mathbf{R}$ for a wave of long wave-length is

$$\begin{aligned} \Delta(\mathbf{r})&=\mathrm{div}\delta\mathbf{R}(\mathbf{r}) \\ &=iN^{-\frac{1}{2}}(\mathbf{k}\cdot\mathbf{l}_k)[a_k\exp(i\mathbf{k}\cdot\mathbf{r})-a_k^*\exp(-i\mathbf{k}\cdot\mathbf{r})]. \end{aligned} \tag{A.30}$$

Only the longitudinal component of the wave contributes to the dilation and thus to the scattering of electrons.

When (A.30) is inserted into (A.18) it is found that the integral vanishes unless the selection rule (A.17) is satisfied, in which case

$$M(\mathbf{P}, \mathbf{P}')=iN^{-\frac{1}{2}}(\mathbf{k}\cdot\mathbf{l}_k)a_kE_1\int u_0(\mathbf{r}, \mathbf{P}')^*u_0(r, P)d\tau. \tag{A.31}$$

Since

$$u_0(\mathbf{r}, \mathbf{P})=u_0(\mathbf{r})+\Sigma\, P_ku_k(\mathbf{r})+\cdots \tag{A.32}$$

and $U_0(\mathbf{r})$ is normalized, the integral is unity to terms of the order P^2. Thus for longitudinal waves,

$$|M(\mathbf{P}, \mathbf{P}')|^2=N^{-1}E_1^2k^2a_k^2. \tag{A.33}$$

The same result is obtained after summing over the three directions of motion in case the waves are not strictly longitudinal and transverse. Inserting (A.29) for a_k^2, we find:

$$|M(\mathbf{P}, \mathbf{P}')|^2=E_1^2k_0T/2NMc_l^2=E_1^2k_0T/2\rho c_l^2, \tag{A.34}$$

where $\rho=NM$ is the density. It should be noted that $|M(\mathbf{P}, \mathbf{P}')|^2$ is independent of $\mathbf{P}$ and $\mathbf{P}'$ if it is assumed that c_l is independent of the direction of propagation of the acoustic wave.

We can replace ρc_l^2 by the elastic constant c_{ii} for longitudinal strain in the direction of propagation of the wave,

$$c_{ii}=\rho c_l^2. \tag{A.35}$$

It should be noted that interaction constant C used by Sommerfeld and Bethe[5] and by Seitz[7] is equal to $(3/2)E_1$; that used by Wilson[6] is equal to E_1.

The reciprocal of the relaxation time for an electron of momentum $\mathbf{P}$ is:

$$1/\tau=(m_eP/\pi\hbar^4)\int_0^\pi |M(\mathbf{P}, \mathbf{P}')|^2(1-\cos\theta)\sin\theta d\theta, \tag{A.36}$$

where θ is the angle between $\mathbf{P}$ and $\mathbf{P}'$. Using (A.34), and assuming c_l to be a constant, we find:

$$1/\tau=m_ePE_1^2k_0T/\pi\hbar^4c_{ii}. \tag{A.37}$$

The mean free path, given by

$$1/l=1/\tau v=m_e^2E_1^2k_0T/\pi\hbar^4c_{ii}, \tag{A.38}$$

is independent of the velocity of the electron. The mobility is

$$\mu=\frac{4el}{3(2\pi m_ek_0T)^{\frac{1}{2}}}=\frac{2(2\pi)^{\frac{1}{2}}e\hbar^4c_{ii}}{3m_e^{5/2}(k_0T)^{\frac{1}{2}}E_1^2}. \tag{A.39}$$

For comparison with experiment it is convenient to express μ in practical units, cm^2/volt-sec., and to express the energy constant, E_1, in electron volts. If the effective mass, m_e is set equal to the ordinary electron mass, and the constant factor is evaluated, it is found that

$$\mu T^{\frac{1}{2}}=(3.2\times10^{-5})c_{ii}/E_1^2. \tag{A.40}$$

Solving for E_1 gives

$$E_1^2=(3.2\times10^{-5})\rho c_l^2/\mu T^{\frac{1}{2}}. \tag{A.41}$$

Equation (47) can be used to determine $|E_{1c}|$ and $|E_{1v}|$ for the conduction and valence-bond bands respectively from observed values for the mobilities of conduction electrons and holes. The values of c_{ii} are obtained in terms of the cubic elastic constants in Section IV.

The Hamiltonian of the General Theory of Relativity with Electromagnetic Field*

PETER G. BERGMANN, ROBERT PENFIELD, RALPH SCHILLER, AND HENRY ZATZKIS
Department of Physics, Syracuse University, Syracuse, New York

(Received April 24, 1950)

In this paper we have given a specific example of a Hamiltonian of a non-linear field theory, a Hamiltonian density completely free of time derivatives. In accordance with the general theory developed previously, this Hamiltonian is one of the constraints between the canonical variables and, therefore, vanishes everywhere. To obtain this function, we have developed methods that will also permit the construction of Hamiltonian densities in any field theory in which the Lagrangian density is quadratic in the first derivatives. Our Hamiltonian differs from the one obtained by Schild and Pirani in that they use Dirac's method to derive a Hamiltonian that is invariant but contains velocities, so that their canonical field equations cannot be solved with respect to the time derivatives of all canonical variables. In our formalism, the canonical equations contain no time derivatives on the right-hand sides, but the adoption of a particular Hamiltonian is equivalent to the adoption of a particular coordinate condition and gauge condition. However, once we have obtained any one Hamiltonian density, we can readily obtain any other one (and thus go over to arbitrary coordinate and gauge conditions) by combination with the other constraints of the theory in question.

1. INTRODUCTION

IN two previous papers,[1,2] it was shown that any set of field equations which can be derived from a variational principle can be cast into the canonical form, with a Hamiltonian which vanishes identically. With the introduction of canonically conjugate variables, the so-called momentum densities, and with the (arbitrary) singling out of some direction at each world point (local "time"-axis), it is possible to reformulate the whole formalism in such a manner that the differential equations are all first-order equations, solved with respect to the "time"-derivatives. On a single "space"-like hypersurface, a small set of equations must be satisfied which do not involve any "time"-derivatives. One of these constraints is the vanishing of the Hamiltonian density. Other constraints are intimately associated with the covariance properties of the theory. If we introduce[2] "parameters," three constraints follow from the invariance of the theory with respect to parameter transformations; if the theory is covariant with respect to general coordinate transformations we shall have four constraints corresponding to coordinate covariance; finally, gauge invariance of the electromagnetic field leads to one constraint of its own. The number of constraints always equals the number of arbitrary functions involved in the transformation group. Once the constraints are satisfied on one hypersurface, the field equations automatically insure that the constraints remain satisfied permanently.

The usefulness of the canonical formalism consists in the relative ease with which the new field equations and their solutions can be discussed. Furthermore, we expect that the quantization of the theories in this form will be a relatively easy and straightforward procedure.

We have given a proof of the existence of the Hamiltonian previously,[2] but did not provide a procedure for its construction. The purpose of this paper is to indicate such a procedure for the large class of theories in which the Lagrangian density is homogeneous and quadratic in the first derivatives. The calculations are then carried through to completion for the best-studied example of a covariant field theory, Einstein's theory of gravitation with an electromagnetic field. The application of the formalism thus obtained to the problem of motion and its quantization will be provided in subsequent papers.

2. THE BASIC FORMS WITH A QUADRATIC LAGRANGIAN

Consider a Lagrangian density which is a homogeneous quadratic function of the first derivatives of the field variables y_A, which, in other words, possesses the form

$$L=\Lambda^{A\rho B\sigma}(y)y_{A,\rho}y_{B,\sigma}. \tag{2.1}$$

For constructing the momentum densities and other pertinent functions, we shall introduce the "parameters" of II, the u^s, t. The modified Lagrangian, JL, will then be homogeneous of the first degree in the "time"-derivatives of all the field variables, including the coordinates. In the special case (2.1), this homogeneous function of the first degree will be a homogeneous quadratic form, divided by a homogeneous linear form. In fact, straightforward calculation shows that JL is given by the expression

$$JL=(l^c\dot{y}_c)^{-1}G^{ab}\dot{y}_a\dot{y}_b, \tag{2.2}$$

where the coefficients G^{ab} and l^a are:

$$\begin{aligned} G^{AB}&=\Lambda^{A\rho B\sigma}Jt_{,\rho}Jt_{,\sigma},\\ G^{A}{}_{\nu}&=\Lambda^{A\rho B\sigma}Jt_{,\rho}y_{B|\sigma}J(u^s{}_{,\sigma}t_{,\nu}-u^s{}_{,t}t_{,\sigma}),\\ G_{\mu\nu}&=\Lambda^{A\rho B\sigma}y_{A|\tau}J(u^\tau{}_{,\rho}t_{,\mu}-u^\tau{}_{,\mu}t_{,\rho})y_{B|s}J(u^s{}_{,\sigma}t_{,\nu}-u^s{}_{,t}t_{,\sigma}), \end{aligned} \tag{2.3}$$

* This work was supported by ONR under Contract 6N-onr-24806

[1] P. G. Bergmann, Phys. Rev. 75, 680 (1949), referred to as I.

[2] P. G. Bergmann and J. H. M. Brunings, Rev. Mod. Phys. 21, 480 (1949), referred to as II.

and

$$l^A=0, \quad l_\mu=Jt_{,\mu}. \tag{2.4}$$

The significance of the indices $a, b, \cdots$ is the same as in II, p. 485. Now we can form without difficulty the expressions for the $(N+4)$ canonical momentum densities π^a and also for the matrix Λ of II, Eq. (3.13), which is closely associated with the algebraic constraints on the canonical field variables y_a, π^a. We obtain the following expressions for the momentum densities, first in the "lumped" notation (in which the original field variables and the coordinates are treated uniformly),

$$\pi^a=(l^d\dot{y}_d)^{-2}(G^{ab}l^c+G^{ac}l^b-G^{bc}l^a)\dot{y}_b\dot{y}_c, \tag{2.5}$$

and then in the "extended" notation,

$$\pi^A=2J^{-1}(G^{AB}\dot{y}_B+G^A{}_\nu\dot{x}^\nu),$$

$$\lambda_\mu=2J^{-1}(G_\mu{}^B\dot{y}_B+G_{\mu\sigma}\dot{x}^\sigma)$$

$$-J^{-2}Jt_{,\mu}(G^{AB}\dot{y}_A\dot{y}_B+2G^A{}_\sigma\dot{y}_A\dot{x}^\sigma+G_{\rho\sigma}\dot{x}^\rho\dot{x}^\sigma). \tag{2.6}$$

The canonical momenta are all homogeneous of the zeroth degree in the dotted variables. The components π^A are fractions in which both numerator and denominator are linear homogeneous forms; the λ_μ are fractions of quadratic forms.

The partial derivatives of the algebraic constraints with respect to the momentum densities are all null "vectors" of the matrix Λ. The components of Λ are

$$\Lambda^{ab}=2(l^i\dot{y}_i)^{-3}$$

$$\times(G^{ab}l^cl^d-G^{ac}l^bl^d-G^{bd}l^al^c+G^{cd}l^al^b)\dot{y}_c\dot{y}_d \tag{2.7}$$

in the "lumped" notation and

$$\Lambda^{AB}=2J^{-1}\Lambda^{A\rho B\sigma}Jt_{,\rho}Jt_{,\sigma},$$

$$\Lambda^A{}_\nu=2J^{-1}G^A{}_\nu-2J^{-2}Jt_{,\nu}\Lambda^{A\rho B\sigma}Jt_{,\rho}$$

$$\times[Jt_{,\sigma}\dot{y}_B+y_{B|s}J(u^s{}_{,\sigma}t_{,\mu}-u^s{}_{,\mu}t_{,\sigma})\dot{x}^\mu], \tag{2.8}$$

$$\Lambda_{\mu\nu}=2J^{-1}G_{\mu\nu}$$

$$-2J^{-2}[Jt_{,\mu}(G^A{}_\nu\dot{y}_A+G_{\rho\nu}\dot{x}^\rho)+Jt_{,\nu}(G_\mu{}^B\dot{y}_B+G_{\mu\sigma}\dot{x}^\sigma)]$$

$$+2J^{-3}Jt_{,\mu}Jt_{,\nu}J^2L$$

in the "extended" notation.

In what follows, we shall denote the algebraic constraints by identifying symbols: the three "parameter" constraints

$$0=y_{a|s}\pi^a, \tag{2.9}$$

by g_s; the four "coordinate" constraints

$$0=F_{A\mu}{}^{B\nu}y_B\pi^AJt_{,\nu}-K_\mu(y_c,y_{c|s},x^\rho{}_{|s}), \tag{2.10}$$

by g_μ; and in the presence of an electromagnetic field, the "gauge" constraint

$$0=Jt_{,\rho}\psi^\rho, \tag{2.11}$$

by ψ. The remaining constraint will serve as the Hamiltonian density and will, therefore, be denoted by H. This last and most important constraint is connected with the homogeneity of the Lagrangian. Inasmuch as the canonical momenta are homogeneous of the zeroth degree in the "time"-derivatives, including the $\dot{x}^\rho$, they must satisfy at least one algebraic identity, and we shall find that this identity is algebraically independent of the constraints (2.9) and (2.10). Our task is to discover this identity.

The algebraic constraints between the canonical variables must hold for any combinations of the field variables consistent with the expression (2.5) for the momentum densities. We shall, therefore, for any combination of parameter values and field variables, construct a symbolic "vector space" in which the time derivatives $\dot{y}_a$ are the coordinates. The functions π^a, (2.5), are then specific zeroth-degree homogeneous functions of the coordinates in that vector space. In any transformation of the $\dot{y}_a$ into new $\dot{y}_a'$ with non-vanishing Jacobian, the "coordinates" of our vector space will undergo a linear transformation, and the momentum densities will transform contragrediently to them. We shall refer to the $\dot{y}_a$ as "coordinates," and we shall call quantities with the same transformation law "contravariant vectors." By the same token, the π^a form a covariant vector, the G^{ab} a covariant symmetric tensor, etc. In attempting to find an algebraic relationship between the momenta (2.5) and the y_a which will serve as our Hamiltonian density, we shall look for combinations which are invariant with respect to the "coordinate transformations" in this symbolic vector space. We are thus led to examine the typical vector-algebraic formations available.

If we look over the "building blocks" that might possibly be used in setting up our desired relation, we find that there are given to us a covariant vector, l^a, and a covariant symmetric tensor G^{ab}, apart from the coordinates $\dot{y}_a$ themselves. But since our relationship is to be a constraint in the y_a and π^a only, satisfied identically in Eqs. (2.5), the coordinates must enter only by way of the functions π^a. In addition, we have the invariant subspaces of the null vectors of the tensors Λ^{ab} and G^{ab}. We know that the π-derivatives of the various algebraic constraints are null vectors of the tensor Λ^{ab}. Some of them are null vectors of G^{ab} as well, as we shall show now.

Take first the derivatives of g_s. We have

$$G^{ab}(\partial g_s/\partial\pi^b)=G^{ab}y_{b|s},$$

$$G^{Ab}y_{b|s}=G^{AB}y_{B|s}+G^A{}_\nu x^\nu{}_{|s}$$

$$=\Lambda^{A\rho B\sigma}Jt_{,\rho}[Jt_{,\sigma}y_{B|s}+y_{B|\nu}J(u^\nu{}_{,\sigma}t_{,\nu}-u^\nu{}_{,\nu}t_{,\sigma})x^\nu{}_{|s}]$$

$$=0, \tag{2.12}$$

$$G_\rho{}^by_{b|s}=G_\rho{}^By_{B|s}+G_{\rho\sigma}x^\sigma{}_{|s}=0.$$

In other words, the "vector" with the components $y_{a|s}$ is a null vector of G^{ab}. Next we shall form the

product of G^{ab} by the π-derivaties of g_μ. In this case, the result is not zero, but proportional to $Jt_{,\rho}$:

$$\partial g_\mu/\partial\pi^B = F_{B\mu}{}^{C\tau}y_C Jt_{,\tau}, \quad \partial g_\mu/\partial\lambda_\rho = 0$$
$$G^{AB}(\partial g_\mu/\partial\pi^B) = \Lambda^{A\rho B\sigma}F_{B\mu}{}^{C\tau}y_C Jt_{,\tau}Jt_{,\rho}Jt_{,\sigma} = 0, \qquad (2.13)$$
$$G_\rho{}^B(\partial g_\mu/\partial\pi^B) = Jt_{,\rho}(\Lambda^{A\nu B\sigma}y_{A,\nu}F_{B\mu}{}^{C\tau}Jt_{,\sigma}Jt_{,\tau}y_C).$$

Thus, while the four vectors $(\partial g_\mu/\partial\pi^B)$ are not themselves null vectors of G^{ab}, there exist three independent linear combinations that are.

The dot product of the "vector" l by any of the seven known null vectors of Λ^{ab} vanishes, as can be proven by a brief computation. Finally, the dot product of these null vectors by the "vector" π^a leads back to the constraints already known. Thus, we require an additional "tensor" to produce the Hamiltonian, and such a tensor would naturally be the inverse of G^{ab}, were it not for the fact that G^{ab} is a singular matrix and therefore possesses no inverse.

3. THE QUASI-UNIVERSE

We can construct a contravariant symmetric tensor by finding the solution of the following conditions:

$$G^{ab}E_{bc}G^{cd} = 0, \quad E_{ab}G^{bc}E_{cd} = 0. \qquad (3.1)$$

These conditions possess a solution, even though G^{ab} is singular, but the solution is not uniquely determined. [Only for a regular matrix G, Eqs. (3.1) will determine uniquely the ordinary inverse G^{-1}.] For a singular matrix G, like the one we have to deal with in our present problem, we shall call E the "quasi-inverse" of G. The significance of E can be ascertained most easily in a "special" coordinate system, in which the null vectors of G are parallel to coordinate axes.[3] In such a special coordinate system, G takes the form

$$G = \begin{pmatrix} g, & 0 \\ 0, & 0 \end{pmatrix}. \qquad (3.2)$$

The most general solution of Eqs. (1.14) in this special coordinate system is

$$E = \begin{pmatrix} g^{-1}, & h \\ h^T, & h^T g h \end{pmatrix}. \qquad (3.3)$$

Here g^{-1} is the inverse of the matrix g, and the rectangular matrix h is completely arbitrary. The superscript ^{T} denotes the transpose. If we set h equal to zero, we get as a solution a matrix which commutes with G and which we obtain by replacing each non-zero eigenvalue of G by its reciprocal value, while retaining the zero eigenvalues unchanged. (Naturally, if there are no zero eigenvalues, i.e. if G is regular, then the quasi-inverse of this form goes over into the inverse.) All possible solutions of (3.1) can be transformed into each other by means of suitably chosen coordinate transformations. In the special coordinate system [in which G has the form (3.2)], the transformation matrix leading from

$$E_0 = \begin{pmatrix} g^{-1}, & 0 \\ 0, & 0 \end{pmatrix} \qquad (3.4)$$

to (3.3) has the form

$$S = \begin{pmatrix} 1, & 0 \\ h^T g, & 1 \end{pmatrix}, \quad y' = Sy, \quad E' = SE_0S^T = E. \qquad (3.5)$$

The transformation law for G is

$$G' = (S^T)^{-1}GS^{-1}, \quad \text{where} \quad S^{-1} = \begin{pmatrix} 1, & 0 \\ -h^T g, & 1 \end{pmatrix}, \qquad (3.6)$$

and if S, (3.5), is applied to G, (3.2), the latter goes over into itself.

For use in the following section, we shall prove the covariant relationship

$$GEl = l. \qquad (3.7)$$

Being normal to all null vectors of Λ and, therefore, *a fortiori*, to all null vectors of G, the covariant vector l must, in a "special" coordinate system, possess the form

$$l = \begin{pmatrix} \lambda \\ 0 \end{pmatrix}. \qquad (3.8)$$

This form is invariant with respect to coordinate transformations (3.5), since the transformation law for l is

$$l' = (S^T)^{-1}l. \qquad (3.9)$$

If we now compute the left-hand side of Eq. (3.7) in a system in which E has the form (3.4), we have the result (3.7) immediately, and since the expression $(GEl - l)$ is a covariant vector, it will vanish in every coordinate system if it vanishes in one.

4. THE HAMILTONIAN DENSITY

If we possess the form E [any one solution of (3.1)], we are able to form additional invariants. Applying matrix notation to (2.5), we can write for the vector π:

$$\pi = \frac{2}{J}G\dot{y} - \frac{1}{J^2}(\dot{y}^TG\dot{y})l, \quad J = l^T\dot{y}, \qquad (4.1)$$

and if we multiply this expression by E to form a contravariant vector, we get

$$E\pi = \frac{2}{J}EG\dot{y} - \frac{1}{J^2}(\dot{y}^TG\dot{y})El. \qquad (4.2)$$

[3] Of course, G does not transform as a matrix, but as a symmetric tensor; but just as in matrix calculus, the existence of null vectors precludes the formation of a "contravariant metric tensor," which would be the precise analog to the inverse in matrix calculus.

Now we can form the scalar $\pi^T E\pi$,

$$\pi^T E\pi=(l^T El)(\dot{y}^T G\dot{y}/J^2)^2 \tag{4.3}$$

and the scalar $l^T E\pi$,

$$l^T E\pi=2-(l^T El)(\dot{y}^T G\dot{y}/J^2). \tag{4.4}$$

Between these two quantities, we can eliminate the $\dot{y}_a$ completely, and we obtain the algebraic relationship

$$(l^T El)(\pi^T E\pi)-[2-(l^T E\pi)]^2\equiv 0. \tag{4.5}$$

The left-hand side of this last constraint is suitable as a Hamiltonian density. In theories which possess coordinate covariance in addition to the trivial parameter invariance, the Hamiltonian simplifies even more. In Section 7, we shall show that the scalar $(l^T El)$ vanishes, and therefore, because of Eq. (4.3), the Hamiltonian density reduces to

$$H=\tfrac{1}{4}\pi^T E\pi=0. \tag{4.6}$$

5. THE FIRST TRANSFORMATION

With the establishment of Eqs. (4.5) and (4.6), the construction of a Hamiltonian density has been reduced to an algebraic problem, namely the determination of the "tensor" E. Instead of merely reporting the result, which can be verified, of course, by substitution into Eqs. (3.1), we shall go through the complete calculations, because they show how the same work may be carried out with a different theory. The guiding idea in these calculations is the continued transformation of G until it is brought as closely as possible into the form (3.2). To find the inverse of the regular matrix g is relatively easy.

The first of this series of transformations isolates the three parameter constraints g_α. Inasmuch as the corresponding three null vectors of the matrix G have the form

$$\partial g_\alpha/\partial\pi^a=y_{a|\alpha}=(y_{A|\alpha}, x^\rho{}_{|\alpha}), \tag{5.1}$$

we shall introduce a new "coordinate system" in the linear vector space of the $\dot{y}_a$ in which these three vectors become coordinate axes. The null vectors of the covariant tensor G are, of course, themselves contravariant vectors. If the three null vectors (5.1) are to become parallel to three particular coordinate axes, then the transformed matrix G (which we shall denote by G') will have only zeros in the corresponding three rows and columns. Naturally, these requirements do not determine the transformation matrix uniquely, though it is clear that the transformation matrix for covariant vectors must contain the three null vectors (5.1) as matrix rows or columns. Calling that matrix A, so that

$$G'=AGA^T, \quad A=(S^T)^{-1} \tag{5.2}$$

[see Eq. (3.6)], and separating for convenience the rows and columns with indices A, B, $\cdots$ from those with indices ρ, σ, $\cdots$, we find that a convenient transformation matrix is

$$A=\begin{pmatrix}\delta^A{}_B, & 0\\ y_{B|r}, & x^\sigma{}_{|r}\\ 0, & v^\sigma\end{pmatrix}, \tag{5.3}$$

where v^σ are four quantities which, for the time being, shall remain undetermined. The determinant of A equals $v^\sigma Jt_{,\sigma}$ and we must, therefore, require that

$$v=v^\sigma Jt_{,\sigma}\neq 0. \tag{5.4}$$

Applying the transformation A, we find that

$$G'=\begin{pmatrix}G^{AB} & 0, & G^A{}_\sigma v^\sigma\\ 0, & 0, & 0\\ v^\rho G_\rho{}^B, & 0, & G_{\rho\sigma}v^\rho v^\sigma\end{pmatrix}, \tag{5.5}$$

$$l'=\begin{pmatrix}0\\0\\v\end{pmatrix}, \tag{5.6}$$

and

$$\pi'=\begin{pmatrix}\pi^A\\0\\v^\rho\lambda_\rho\end{pmatrix}. \tag{5.7}$$

Clearly, the quasi-inverse of the matrix (5.5) can be chosen so that three of its rows and columns consist entirely of zeros, thus:

$$E'=\begin{pmatrix}E_{AB} & 0 & E_A\\ 0 & 0 & 0\\ E_B & 0 & E_0\end{pmatrix}. \tag{5.8}$$

If we make that choice, we have from now on to deal only with covariants in an $(N+1)$-dimensional space, instead of an $(N+4)$-dimensional space. In this reduced space, our covariants will have the forms:

$$\bar{G}=\begin{pmatrix}G^{AB}, & G^A{}_\sigma v^\sigma\\ v^\rho G_\rho{}^B, & G_{\rho\sigma}v^\rho v^\sigma\end{pmatrix}, \tag{5.9}$$

$$\bar{l}=\begin{pmatrix}0\\v\end{pmatrix}, \quad \bar{\pi}=\begin{pmatrix}0\\v^\rho\lambda_\rho\end{pmatrix} \tag{5.10}$$

and

$$\bar{E}=\begin{pmatrix}E_{AB}, & E_A\\ E_B, & E_0\end{pmatrix}. \tag{5.11}$$

6. THE SECOND AND THIRD TRANSFORMATIONS

We shall write the four cooordinate constraints (2.10) in the abbreviated form

$$g_\mu=u_{\mu A}\pi^A-K_\mu, \quad u_{\mu A}=F_{A\mu}{}^{B\nu}y_B Jt_{,\nu}. \tag{6.1}$$

In the $(N+1)$-dimensional space and in the coordinate system denoted by bars ($\bar{G}$, etc.), the gradients of these four constraints take the form

$$\bar{u}_\mu=\begin{pmatrix}u_{\mu A}\\0\end{pmatrix}. \tag{6.2}$$

Because of Eqs. (2.13), we have further

$$\bar{G}\bar{u}_\mu=\begin{pmatrix}0\\U_\mu\end{pmatrix},$$
$$U_\mu=vy_{A,\rho}\Delta^{A\rho B\sigma}Jt_{,\sigma}u_{\mu B}=v^\rho G_\rho{}^B u_{\mu B}. \tag{6.3}$$

Our task is now to further transform the coordinates so that additional rows and columns of the $\bar{G}$-matrix will be filled with zeros. To this end, we shall introduce the transformation matrix D with the components

$$D=\begin{pmatrix}D^{A'}{}_A, & 0\\ u_\mu{}^A, & 0\\ 0, & 1\end{pmatrix}, \tag{6.4}$$

to be used for the transformation of covariant vectors and tensors. The indices A', B', $\cdots$, are to run from 1 to $N-4$, and the coefficients $D^{A'}{}_A$ are to be chosen according to convenience, with the only proviso that the determinant of the matrix D (and that means the N-rowed sub-determinant in the upper left-hand corner) shall not vanish. The resulting covariants shall be denoted by double primes. In the following expressions, each column and row is broken down into three portions, of which the first has $(N-4)$, the second 4, and the third 1 component. For G'' we get

$$G''=D\bar{G}D^T$$
$$=\begin{pmatrix}D^{A'}{}_A G^{AB}D^{B'}{}_B, & 0, & D^{A'}{}_A G^A{}_\sigma v^\sigma\\ 0, & 0, & U_\mu\\ v^\rho G_\rho{}^B D^{B'}{}_B, & U_\nu, & G_{\rho\sigma}v^\rho v^\sigma\end{pmatrix}, \tag{6.5}$$

the vector l remains unchanged,

$$l''=\begin{pmatrix}0\\0\\v\end{pmatrix}, \tag{6.6}$$

and for the vector π'', finally, we have the two alternative expressions

$$\pi''=\begin{pmatrix}D^{A'}{}_A\pi^A\\ u_{\mu A}\pi^A\\ v^\rho\lambda_\rho\end{pmatrix}=\begin{pmatrix}D^{A'}{}_A\pi^A\\ K_\mu\\ v^\rho\lambda_\rho\end{pmatrix}. \tag{6.7}$$

Inasmuch as the vectors $\bar{u}_{\mu A}$ are not null vectors of $\bar{G}$, the second transformation does not make any complete row or column of G'' vanish, as the first transformation did. Of course, it would be an easy matter to find three independent linear combinations of the four numbers U_μ that vanish, and thus, by a further transformation, to produce three further completely empty rows and columns. Presumably, the resulting $(N-2)$-rowed matrix would be non-singular and could be used as the submatrix g of Eqs. (3.2) and (3.4). But such a procedure would destroy the symmetry between the four coordinate directions of physical space, the four directions characterized by Greek indices. That is why we shall adopt a different procedure to find the quasi-inverse.

We shall show that we can define a third transformation matrix T which removes from the matrix G'', Eq. (6.5), the first and third portions in the last row and the last column, which, in other words, reduces G'' to the form

$$G'''=TG''T^T$$
$$=\begin{pmatrix}G^{A'B'}, & 0, & 0\\ 0, & 0, & U_\mu\\ 0, & U_\nu, & 0\end{pmatrix}, \tag{6.8}$$
$$G^{A'B'}=D^{A'}{}_A D^{B'}{}_B G^{AB}.$$

We shall find the quasi-inverse of G''' below. The matrix T has the following form:

$$T=\begin{pmatrix}\delta^{A'}{}_{B'}, & 0, & 0\\ 0, & \delta_\mu{}^\nu, & 0\\ -G_{B'C'}D^{C'}{}_C G^C{}_\sigma v^\sigma, & \beta^\nu, & 1\end{pmatrix}. \tag{6.9}$$

$G_{B'C'}$ is the inverse of the (non-singular) matrix $G^{A'B'}$,

$$G_{B'C'}G^{A'B'}=\delta^{A'}{}_{C'}, \tag{6.10}$$

and β^ν are four quantities subject only to one requirement, that the dot product of β^ν by U_ν has a specified value, namely

$$U_\mu\beta^\mu=\tfrac{1}{2}v^\rho v^\sigma(G_\rho{}^A G_\sigma{}^B D^{A'}{}_A D^{B'}{}_B G_{A'B'}-G_{\rho\sigma}). \tag{6.11}$$

This last condition follows from straightforward computation of the transformation that leads from G'' to G''' in accordance with Eqs. (6.8) and (6.9).

Once we have reduced G''' to the form (6.9), we can obtain its quasi-inverse directly. The matrix E''' has the components

$$E'''=\begin{pmatrix}G_{A'B'}, & 0, & 0\\ 0, & 0, & \sigma^\nu\\ 0, & \sigma^\mu, & 0\end{pmatrix}, \tag{6.12}$$

where σ^μ are four quantities subject to the only requirement that

$$\sigma^\mu U_\mu=1. \tag{6.13}$$

That the matrix (6.12) is really the required quasi-inverse, or, at least, that it is one possible form of the quasi-inverse, can be verified by direct substitution into the defining equations (3.1).

Before we can obtain the expression for the Hamiltonian density, we must apply the third transformation to our two vectors l'' and π''. Again, l'' does not change at all,

$$l'''=l''=\begin{pmatrix}0\\0\\v\end{pmatrix}, \tag{6.14}$$

and for π''' we get

$$\pi'''=\begin{pmatrix}D^{A'}{}_A\pi^A\\ K_\mu\\ v^\rho\lambda_\rho+\beta^\rho K_\rho-v^\rho G_\rho{}^A D^{A'}{}_A G_{A'B'}D^{B'}{}_B\pi^B\end{pmatrix}. \tag{6.15}$$

7. THE HAMILTONIAN

The first and obvious result of our expressions (6.12), (6.14), and (6.15) is that the scalar $(l^T E l)$ vanishes. To obtain the Hamiltonian density, we have, therefore, to evaluate the expression (4.6). Instead of transforming E''' back into E (by applying the three transformations A, D, and T in reverse), we shall determine the Hamiltonian by working out the expression $(\pi^{T'''} E''' \pi''')$. By substituting the appropriate expressions, we get first

$$H=\tfrac{1}{4}G_{A'B'}D^{A'}{}_{A}D^{B'}{}_{B}\pi^{A}\pi^{B}$$
$$+\tfrac{1}{2}K_{\mu}\sigma^{\mu}(v^{\rho}\lambda_{\rho}+\beta^{\rho}K_{\rho}-G_{A'B'}D^{A'}{}_{A}D^{B'}{}_{B}G^{A}{}_{\rho}v^{\rho}\pi^{B}). \quad (7.1)$$

This expression could be used as the Hamiltonian density. Its principal drawback lies in the presence of the four-vectors σ^{μ} and β^{μ} which are arbitrary except for one cumbersome normalization restriction each, Eqs. (6.11) and (6.13), respectively. We shall now show that both of these formations can be eliminated. To this end, we must determine the relationship between U_{μ} and K_{μ}. We have already obtained an expression for U_{μ} in Eq. (6.3). If we now use the constraint (2.10) to get an explicit expression for K_{μ} as well, we find:

$$K_{\mu}=u_{\mu A}\pi^{A}=2J^{-1}u_{\mu A}(G^{AB}\dot{y}_{B}+G^{A}{}_{\sigma}\dot{x}^{\sigma})$$
$$=2u_{\mu A}\Lambda^{A\rho B\sigma}Jt_{,\rho}y_{B,\sigma}=2v^{-1}U_{\mu}. \quad (7.2)$$

This result enables us to use directly the conditions (6.11) and (6.13) to eliminate σ^{μ} and β^{μ}. We have

$$K_{\mu}\sigma^{\mu}=2v^{-1}U_{\mu}\sigma^{\mu}=2v^{-1} \quad (7.3)$$

and

$$K_{\mu}\beta^{\mu}=2v^{-1}U_{\mu}\beta^{\mu}$$
$$=v^{-1}v^{\rho}v^{\sigma}(G_{\rho}{}^{A}G_{\sigma}{}^{B}D^{A'}{}_{A}D^{B'}{}_{B}G_{A'B'}-G_{\rho\sigma}). \quad (7.4)$$

These two expressions, substituted into the Hamiltonian density (7.1) yield the expression

$$H=v^{-2}v^{\rho}v^{\sigma}$$
$$\times[\tfrac{1}{4}G_{A'B'}D^{A'}{}_{A}D^{B'}{}_{B}(Jt_{,\rho}\pi^{A}-2G^{A}{}_{\rho})(Jt_{,\sigma}\pi^{B}-2G^{B}{}_{\sigma})$$
$$+\tfrac{1}{2}(\lambda_{\rho}Jt_{,\sigma}+\lambda_{\sigma}Jt_{,\rho})-G_{\rho\sigma}]. \quad (7.5)$$

In this expression for the Hamiltonian density, the four-vector v^{ρ} remains undetermined, except for the inequality (5.4). However, a short computation shows that the choice of this vector merely affects the manner in which the parameter constraints (2.9) enter into the Hamiltonian. In II, it was pointed out that the choice of Hamiltonian is not unique, but subject to an algebraic combination with the other constraints. The choice of the rectangular matrix $D^{A'}{}_{A}$ has no effect on the eventual form of H, except to permit the addition of linear and quadratic combinations of the coordinate constraints (2.10). Thus, the Hamiltonian (7.5) possesses exactly the degree of arbitrariness required by the general theory.

The canonical field equations take the form

$$\dot{y}_{a}=\partial H/\partial\pi^{a}, \quad \dot{\pi}^{a}=-\delta H/\delta y_{a}. \quad (7.6)$$

In particular, we find that the derivatives of the coordinates x^{ρ} with respect to the parameter t are determined by the expressions

$$\dot{x}^{\rho}=\partial H/\partial\lambda_{\rho}=v^{-1}v^{\rho}=(Jt_{,\sigma}v^{\sigma})^{-1}v^{\rho}. \quad (7.7)$$

The choice of the four-vector v^{ρ} will, therefore, be largely governed by the desired relationship between the coordinates and the parameter.

Finally, we shall show in passing that the relationship (4.4), with vanishing last term, does not lead to a suitable Hamiltonian relationship. By substituting into the scalar $(l^T E\pi)$ the expressions (6.12), (6.14), and (6.15), observing in the process the relationship (7.3), we find that the resulting constraint is a linear combination of the coordinate constraints (2.10) alone and, therefore, not suitable as a Hamiltonian density.

In Section 8, we shall work out the general expression (7.5) for the particular Lagrangian that characterizes the general theory of relativity with electromagnetic terms.

8. THE HAMILTONIAN OF GENERAL RELATIVITY WITH ELECTROMAGNETIC FIELD

The Lagrangian density of the general theory of relativity has the following structure, if the electromagnetic field is included:[4]

$$L=L_{\text{grav}}+L_{\text{el}}, \quad (8.1)$$

where

$$L_{\text{grav}}=[(-g)^{\frac{1}{2}}/16\pi\kappa]g^{\mu\nu}$$
$$\times\left(\begin{Bmatrix}\sigma\\ \rho\sigma\end{Bmatrix}\begin{Bmatrix}\rho\\ \mu\nu\end{Bmatrix}-\begin{Bmatrix}\sigma\\ \mu\rho\end{Bmatrix}\begin{Bmatrix}\rho\\ \nu\sigma\end{Bmatrix}\right) \quad (8.2)$$

and

$$L_{\text{el}}=-[(-g)^{\frac{1}{2}}/16\pi]\phi^{\mu\nu}\phi_{\mu\nu}. \quad (8.3)$$

$\phi_{\mu\nu}$ stands for

$$\phi_{\mu\nu}=\phi_{\mu,\nu}-\phi_{\nu,\mu} \quad (8.4)$$

and

$$\phi^{\mu\nu}=g^{\mu\rho}g^{\nu\sigma}\phi_{\rho\sigma}. \quad (8.5)$$

The ϕ_{μ} are the four electromagnetic potentials. This Lagrangian density contains the field variables and their first derivatives only, but is not a scalar density. Therefore, it belongs to the general class of Lagrangians considered in I. It is also homogeneous quadratic in the first derivatives of the field variables.

We shall now rewrite L to show the coefficients $\Lambda^{A\rho B\sigma}$. Renaming dummy indices and factoring we get:

$$L=\Lambda^{(\alpha\beta)\rho,(\gamma\delta)\sigma}g_{\alpha\beta,\rho}g_{\gamma\delta,\sigma}+Y^{\mu\rho,\nu\sigma}\phi_{\mu,\rho}\phi_{\nu,\sigma},$$

[4] See, for instance, P. G. Bergmann, *Introduction to the Theory of Relativity* (Prentice-Hall, Inc., New York, 1942), p. 193 ff, Eqs. (12.56) and (12.65).

$$\Lambda^{(\alpha\beta)\rho,\,(\gamma\delta)\sigma}=[(-g)^{\frac{1}{2}}/128\pi\kappa]$$
$$\times\{[g^{\alpha\beta}(g^{\gamma\rho}g^{\delta\sigma}+g^{\delta\rho}g^{\gamma\sigma})+g^{\gamma\delta}(g^{\alpha\sigma}g^{\beta\rho}+g^{\alpha\sigma}g^{\beta\rho})]$$
$$+g^{\rho\sigma}(g^{\alpha\gamma}g^{\beta\delta}+g^{\beta\gamma}g^{\alpha\delta}-2g^{\alpha\beta}g^{\gamma\delta})$$
$$-[g^{\alpha\sigma}(g^{\beta\gamma}g^{\delta\rho}+g^{\beta\delta}g^{\gamma\rho})+g^{\beta\sigma}(g^{\alpha\gamma}g^{\delta\rho}+g^{\alpha\delta}g^{\gamma\rho})]\},\tag{8.6}$$
$$Y^{\mu\rho,\,\nu\sigma}=[(-g)^{\frac{1}{2}}/8\pi](g^{\mu\sigma}g^{\nu\rho}-g^{\mu\nu}g^{\rho\sigma}).$$

The coefficients Λ and Y are symmetric in $(A\rho)$ and $(B\sigma)$,

$$\Lambda^{(\alpha\beta)\rho,\,(\gamma\delta)\sigma}=\Lambda^{(\gamma\delta)\sigma(\alpha\beta)\rho},\quad Y^{\mu\rho,\,\nu\sigma}=Y^{\nu\sigma,\,\mu\rho}.\tag{8.7}$$

Λ is, besides, symmetric in each bracketed index pair

$$\Lambda^{(\alpha\beta)\rho,\,(\gamma\delta)\sigma}=\Lambda^{(\beta\alpha)\rho,\,(\gamma\delta)\sigma}.\tag{8.8}$$

In order to substitute into Eq. (7.5), we must determine the null vectors corresponding to the various constraints and, besides, we must make a choice for the reducing matrix $D^{A'}{}_{A}$. There is also a slight complication in that we have, in addition to the parameter and coordinate constraints, the gauge constraint (2.11).

Altogether, we have 14 variables, of which 10 are gravitational and 4 electromagnetic potentials. The matrix G^{AB} with 14 rows and columns actually consists of a 10×10 and a 4×4 matrix, with the rectangular off-diagonal spaces filled entirely with zeros. As a first step, we shall determine the actual expression for G^{AB},

$$G^{AB}=\begin{pmatrix}G^{(\alpha\beta)(\gamma\delta)} & 0\\ 0 & G^{\mu\nu}\end{pmatrix},$$

$$G^{(\alpha\beta)(\gamma\delta)}=[(-g)^{\frac{1}{2}}/128\pi\kappa]$$
$$\times[X(g^{\alpha\gamma}g^{\beta\delta}+g^{\beta\gamma}g^{\alpha\delta}-2g^{\alpha\beta}g^{\gamma\delta})$$
$$+2(g^{\alpha\beta}X^{\gamma}X^{\delta}+g^{\gamma\delta}X^{\alpha}X^{\beta})$$
$$-(g^{\alpha\gamma}X^{\beta}X^{\delta}+g^{\alpha\delta}X^{\beta}X^{\gamma}+g^{\beta\gamma}X^{\alpha}X^{\delta}+g^{\beta\delta}X^{\alpha}X^{\gamma})],\tag{8.9}$$
$$G^{\mu\nu}=[(-g)^{\frac{1}{2}}/8\pi](X^{\mu}X^{\nu}-Xg^{\mu\nu}),$$
$$X^{\alpha}=Jt_{,\beta}g^{\alpha\beta},\quad X=Jt_{,\alpha}Jt_{,\beta}g^{\alpha\beta}.$$

The first of these two submatrices has the four null vectors

$$u_{\mu(\gamma\delta)}=Jt_{,\gamma}g_{\mu\delta}+Jt_{,\delta}g_{\mu\gamma},\tag{8.10}$$

and the second submatrix has the single null vector $Jt_{,\nu}$. These expressions are the null vectors obtainable from the general theory. It is, however, very easy to verify their being null vectors by straightforward computation.

Accordingly, we require two separate matrices suitable for the role designated in the preceding sections by the symbol $D^{A'}{}_{A}$. One 10×6 matrix must reduce the gravitational submatrix to a non-singular 6×6 matrix, while another 4×3 matrix will reduce the electromagnetic coefficients to a non-singular 3×3 matrix. These reducing matrices must have the further property that they are linearly independent of the null vectors indicated above. In an effort to maintain the symmetry between the four (physical) coordinate directions, we chose matrices which, in effect, project four-vectors and four-tensors (in physical space-time) into the three-dimensional space of the parameters u^{a}. And since the matrix elements of D must be independent of t-derivatives, we set:

$$D_{m\mu}=g_{\mu\rho}x^{\rho}{}_{|m},$$
$$D_{(mn)\mu\nu}=\tfrac{1}{2}g_{\mu\rho}g_{\nu\sigma}(x^{\rho}{}_{|m}x^{\sigma}{}_{|n}+x^{\rho}{}_{|n}x^{\sigma}{}_{|m}).\tag{8.11}$$

The resulting expression for $G^{A'B'}$ is

$$G^{A'B'}=\begin{pmatrix}G_{(ab)(cd)} & 0\\ 0 & G_{mn}\end{pmatrix},$$
$$G_{(ab)(cd)}=[(-g)^{\frac{1}{2}}X/128\pi\kappa]$$
$$\times(g_{ac}g_{bd}+g_{ad}g_{bc}-2g_{ab}g_{cd}),\tag{8.12}$$
$$G_{mn}=-[(-g)^{\frac{1}{2}}X/8\pi]g_{mn},$$
$$g_{mn}\equiv g_{\mu\nu}x^{\mu}{}_{|m}x^{\nu}{}_{|n}.$$

We must now find the inverse of this non-singular matrix. We shall first introduce the expressions

$$D^{m}{}_{\mu}=X^{-1}X^{\rho}J(u^{m}{}_{,\mu}l_{,\rho}-u^{m}{}_{,\rho}l_{,\mu})\tag{8.13}$$

with the property

$$D^{m}{}_{\mu}x^{\mu}{}_{|n}=\delta^{m}{}_{n}\tag{8.14}$$

and

$$g^{mn}=g^{\mu\nu}D^{m}{}_{\mu}D^{n}{}_{\nu},\quad g^{mn}g_{ns}=\delta^{m}{}_{s}.\tag{8.15}$$

The inverse matrix must be built up from the g^{mn}.

The inverse electromagnetic matrix can be found by inspection. The determination of the gravitational matrix is only slightly more laborious. There are only two possible combinations of g^{mn} which satisfy all the requirements of symmetry (namely that the matrix $G^{(ab)(cd)}$ be symmetric within each bracketed pair of indices and that it be symmetric with respect to an interchange between the two index pairs as wholes). All that needs to be done is to determine the numerical coefficients of these two possible combinations. The final expression for the inverse is then

$$G_{A'B'}=\begin{pmatrix}G^{(ab)(cd)}, & 0\\ 0, & G^{mn}\end{pmatrix},$$
$$G^{(ab)(cd)}=[32\pi\kappa/(-g)^{\frac{1}{2}}X](g^{ac}g^{bd}+g^{ad}g^{bc}-g^{ab}g^{cd}),\tag{8.16}$$
$$G^{mn}=-[8\pi/(-g)^{\frac{1}{2}}X]g^{mn}.$$

This inverse matrix now must be multiplied by $D^{A'}{}_{A}D^{B'}{}_{B}$. The result of this operation is

$$D^{A'}{}_{A}D^{B'}{}_{B}G_{A'B'}\equiv G_{AB}=\begin{pmatrix}G_{(\alpha\beta)(\gamma\delta)}, & 0\\ 0, & G_{\mu\nu}\end{pmatrix},$$
$$G_{(\alpha\beta)(\gamma\delta)}=[32\pi\kappa/(-g)^{\frac{1}{2}}X](\gamma_{\alpha\gamma}\gamma_{\beta\delta}+\gamma_{\alpha\delta}\gamma_{\beta\gamma}-\gamma_{\alpha\beta}\gamma_{\gamma\delta}),\tag{8.17}$$
$$G_{\mu\nu}=-[8\pi/(-g)^{\frac{1}{2}}X]\gamma_{\mu\nu},$$
$$\gamma_{\mu\nu}\equiv g_{\mu\nu}-Jt_{,\mu}Jt_{,\nu}.$$

The matrix G_{AB} that we have thus defined is, of course, a quasi-inverse of the matrix G^{AB}, Eq. (8.9). In the expression for $G_{\mu\nu}$, we can replace $\gamma_{\mu\nu}$ by $g_{\mu\nu}$, because $Jt_{,\nu}$ is a null vector of that matrix. But the same replacement can be made in the matrix $G_{(\alpha\beta)(\gamma\delta)}$, because the replacement is nothing but the addition of a linear combination of the null vectors (8.10). Thus, the first term in the bracket of Eq. (7.5) has been determined.

The second term can be copied without change. In the last term, we must substitute the correct expression for $G_{\rho\sigma}$. The expressions for $G^{A}{}_{\rho}$, $G_{\rho\sigma}$ are lengthy, but are obtained by routine calculations from the defining equations (2.3). We shall write them down, too, introducing as an abbreviating notation the differential operator

$$y_{A|\sigma}J(u^{s}{}_{,\rho}t_{,\sigma}-u^{s}{}_{,\sigma}t_{,\rho})\equiv y_{A[\rho\sigma]}. \tag{8.18}$$

This differential operator satisfies the product rule of differentiation. With its help, we obtain the following expressions:

$$\begin{aligned}G^{(\alpha\beta)}{}_{\sigma}=&[(-g)^{\frac{1}{2}}/128\pi\kappa]\{(\log g)_{[\tau\sigma]}(g^{\alpha\tau}X^{\beta}+g^{\beta\tau}X^{\alpha})\\&-2g^{\alpha\beta}g^{\rho\tau}{}_{[\tau\sigma]}Jt_{,\rho}-2X^{\tau}[g^{\alpha\beta}{}_{[\tau\sigma]}+(\log g)_{[\tau\sigma]}g^{\alpha\beta}]\\&+2Jt_{,\rho}(g^{\alpha\tau}g^{\beta\rho}{}_{[\tau\sigma]}+g^{\beta\tau}g^{\alpha\rho}{}_{[\tau\sigma]})\},\end{aligned} \tag{8.19}$$

$$G^{\mu}{}_{\sigma}=[(-g)^{\frac{1}{2}}/8\pi](g^{\mu\tau}X^{\rho}-g^{\mu\rho}X^{\tau})\phi_{\rho[\tau\sigma]}$$

and

$$\begin{aligned}G_{\rho\sigma}=&[(-g)^{\frac{1}{2}}/128\pi\kappa]\\&\times\{g^{\iota\kappa}[2g^{\alpha\beta}{}_{[\iota\rho]}g_{\alpha\beta[\kappa\sigma]}-(\log g)_{[\iota\rho]}(\log g)_{[\kappa\sigma]}]\\&-2[g^{\iota\kappa}{}_{[\kappa\sigma]}(\log g)_{[\iota\rho]}+g^{\iota\kappa}{}_{[\iota\rho]}(\log g)_{[\kappa\sigma]}]\\&-4g_{\alpha\beta}(g^{\alpha\iota}{}_{[\kappa\sigma]}g^{\beta\kappa}{}_{[\iota\rho]})\}\\&+[(-g)^{\frac{1}{2}}/8\pi](g^{\mu\kappa}g^{\nu\iota}-g^{\mu\nu}g^{\iota\kappa})\phi_{\mu[\iota\rho]}\phi_{\nu[\kappa\sigma]}.\end{aligned} \tag{8.20}$$

With these substitutions, the final expression for the Hamiltonian density becomes

$$\begin{aligned}H=&v^{-2}v^{\rho}v^{\sigma}\{\tfrac{1}{2}(\lambda_{\rho}Jt_{,\sigma}+\lambda_{\sigma}Jt_{,\rho})-G_{\rho\sigma}\\&+[8\pi\kappa/(-g)^{\frac{1}{2}}X](g_{\alpha\gamma}g_{\beta\delta}+g_{\alpha\delta}g_{\beta\gamma}-g_{\alpha\beta}g_{\gamma\delta})\\&\times(\pi^{\alpha\beta}Jt_{,\rho}-2G^{(\alpha\beta)}{}_{\rho})(\pi^{\gamma\delta}Jt_{,\sigma}-2G^{(\gamma\delta)}{}_{\sigma})\\&-[2\pi/(-g)^{\frac{1}{2}}X]g_{\mu\nu}(\psi^{\mu}Jt_{,\rho}-2G^{\mu}{}_{\rho})\\&\times(\psi^{\nu}Jt_{,\sigma}-2G^{\nu}{}_{\sigma})\}.\end{aligned} \tag{8.21}$$

9. CONCLUSION

The Hamiltonian density which we have obtained is a rather formidable expression, but it is a quantity composed exclusively of the canonical variables and their "spatial" derivatives. The canonical differential equations are of the first differential order and solved with respect to them. Thus, the continuation of a solution of the field equations in the t-direction can be accomplished by a series of iterated integrations. Naturally, the Hamiltonian (8.21) with (8.19) and (8.20) is not the most general expression imaginable that can be used for the Hamiltonian. We can multiply it by an arbitrary (but non-zero) function of the dynamical variables and the parameters (and such a factor will affect the relationship between the parameter t and the coordinates), and we can add arbitrary linear combinations of the coordinate constraints g_{μ}, Eq. (2.10). The addition of parameter constraints g_{s} will have no other effect than would the adoption of particular expressions for the arbitrary v^{ρ}. Thus, having obtained one expression for H, we can easily find all other possible expressions, and we can thus use the equivalent of any coordinate condition and parameter condition desired. As for the gauge constraint (2.11), adding ψ with any factor to the Hamiltonian amounts to the adoption of a particular gauge condition.

The new formalism available will be used to give a new derivation of the equations of motion, which was first achieved by means of an approximation method by Einstein, Infeld, and Hoffmann. We shall obtain the instantaneous acceleration of singularities rigorously by assuming a certain field at a time t_0 in agreement with all the algebraic constraints (including the vanishing of the Hamiltonian density) and then continuing into the future (or past). Later we expect to quantize the theory and to examine problems involving radiative processes.

Letters to the Editor

PUBLICATION of brief reports of important discoveries in physics may be secured by addressing them to this department. The closing date for this department is five weeks prior to the date of issue. No proof will be sent to the authors. The Board of Editors does not hold itself responsible for the opinions expressed by the correspondents. Communications should not exceed 600 words in length.

The Dielectric Constant of Liquid Helium

C. J. GREBENKEMPER AND JOHN P. HAGEN
Naval Research Laboratory, Washington, D. C.
July 20, 1950

THE dielectric constant of liquid helium was measured at frequencies in the vicinity of 9100 Mc using a transmission-type resonant cavity having a high Q. The resonant frequency of the cavity is measured at liquid helium temperatures from 1.6 to 4.2°K with the cavity evacuated. Then liquid helium is admitted into the cavity through a needle valve arrangement, and the new resonant frequency measured over this range of temperature. The frequency shift at 4.20° is about 220 Mc. Since the cavity resonator is completely filled with helium the dielectric constant is given by the expression

$$K=(f_0/f)^2,$$

where f is the resonant frequency with the dielectric in the cavity, f_0 is the resonant frequency without the dielectric in the cavity, and K is the dielectric constant.

This expression is valid as long as the loss tangent is small. The loss tangent of liquid helium was observed during the course of these measurements to be less than 5×10^{-6}.

The cavity used in this experiment was a cylindrical cavity operating in its lowest mode (TE_{111}) made of cast tin. The normal Q (at 4.2°K) was 40,000 and the Q at 1.9°K 1.5×10^6. This cavity was used because it was available from previous investigations on the high frequency resistance of tin. Precautions were taken to insure that the cavity would be filled with liquid helium. The experiment was carried out in an external Dewar flask filled with liquid helium surrounded by liquid nitrogen. The temperature scale used was the 1937 Leiden scale. The resonant frequency of the cavity was measured by means of a high Q wave meter. The maximum error in the determination of the dielectric constant due to an error in the measurement of frequency is ±0.0005.

A plot of the dielectric constant *vs.* temperature is shown in Fig. 1. Wolfke and Keesom's[1] results of 1928, which were done at a frequency of 500 kc, are also shown. Our values are slightly higher than those of Wolfke and Keesom. They quote an accuracy of ±0.001 in °K. Their value at 4.21°K is 1.048; ours at 4.21°K is 1.0492. The value derived from the optical data at this temperature[2] is 1.0491. The agreement appears to be very good. Also shown is a table (Table I) of the polarization per mole computed from our curve of the dielectric constant over the range of temperatures according to the equation:

$$\alpha=3(K-1)M/4\pi(K+2)P,$$

where M is the mass of helium atom and P is the density. The polarization per mole computed for infinitely long waves by Wolfke and Keesom is 0.1234.

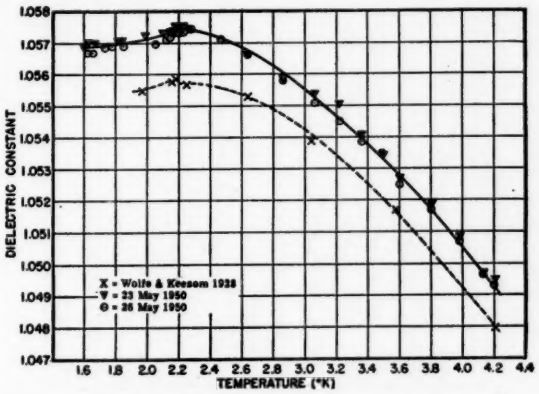

FIG. 1. Dielectric constant of liquid helium.

TABLE I. Dielectric constant and polarization of liquid helium.

Temperature °K	Density[a] g/cm³ ρ	Dielectric constant K	Polarization per mole α
4.21	0.1248	1.0492	0.1236
3.04	0.1405	1.0554	0.1233
2.64	0.1443	1.0568	0.1231
2.25	0.1458	1.0574	0.1231
2.19	0.1458	1.0574	0.1231
1.97	0.1454	1.0571	0.1228
1.62	0.1449	1.0569	0.1228

[a] Densities taken from Table 6.10a, p. 323 of reference 1.

[1] W. H. Keesom, *Helium* (Elsevier Publishing Company, Inc., Amsterdam, 1942), p. 321, paragraph 6.713.
[2] Reference 1, p. 323, paragraph 6.715.

Relativistic Increase in Ionization of Charged Particles in Photographic Emulsions

E. PICKUP AND L. VOYVODIC
Division of Physics, National Research Council, Ottawa, Canada
August 7, 1950

WE have recently started measurements to ascertain whether any increase in ionization for relativistic, singly charged particles can be detected in photographic emulsions. Preliminary results on the few tracks measured so far indicate that there is a minimum value of the ionization at $E/\mu\sim3$ with an increase of about 10 percent to a constant value (or plateau) at $E/\mu\sim20$ up to very high energies.

The photographic emulsion is a special case where ionization can be measured inside a solid material, and we would expect atomic polarization effects to be important in limiting the distant ionizing collisions, which cause the relativistic increase. The polarization effect was first suggested by Swann[1] and treated quantitatively by Fermi,[2] Halpern and Hall,[3] Wick,[4] and Bohr,[5] their theories giving corrections to be applied to the Bethe-Bloch ionization energy loss formula[6] at relativistic energies. The theories, differing in detail, predict some increase beyond a minimum value to a constant value of ionization energy loss. This limiting value, for a given medium, depends only on the maximum value of energy transfer (η) considered. In the present work η was taken[7] as 10 kev.

Figure 1 shows the energy loss curves deduced from the different theories for iron, calculations for this substance being readily available. For E/μ below ~50 the theories disagree somewhat, essentially because of the use of different effective ionization potentials. The different theories agree in giving the same constant plateau value.

The ionization and energies of tracks in two Ilford G5 plates were measured by grain counting and multiple Coulomb scattering, respectively, and the results are shown in Fig. 2. Long tracks were selected so that the probable error in grain counting was about two percent. Since the theories give the same plateau value, the sets of observations for the two plates were normalized

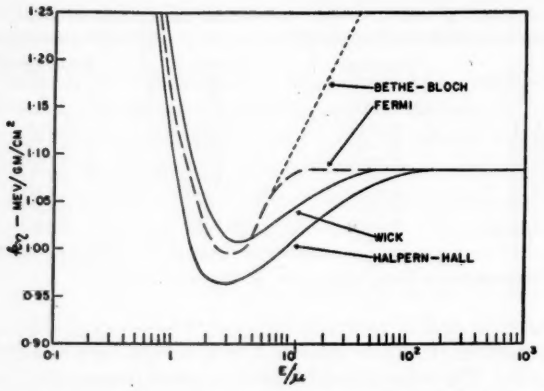

FIG. 1. Theoretical curves for the rate of energy loss in ionizing collisions in iron. Energy transfers less than 10 kev are included. Effective ionization potentials; Bethe-Bloch and Fermi, $I'=26\times13.5$; Wick, $I'=16\times13.5$; Halpern-Hall, $I'=32\times13.5$ ev.

so that the mean grain density for high energy electrons (>20 Mev) in each plate[8] corresponds to the rate of energy loss for AgBr calculated from Fermi's theory for the polarization correction, and the Bethe-Bloch formula, i.e., 1.02 Mev, cm²/g. It is assumed that the production of ions in AgBr crystals only leads to developable grains, and there is no contribution from ionization in the gelatin of the emulsion. The high energy plateau is in agreement with observations by Corson and Keck,[9] who reported the grain density to be constant within two percent for electrons having energies from 10 to 180 Mev; i.e., E/μ from 20 to 360.

To detect a relativistic increase in ionization, it would seem to be necessary that the corresponding energy loss occurs within the AgBr crystal traversed, and is not dispersed in neighboring crystals or gelatin. As is shown by Bohr's treatment,[5] the limiting distance from the path of a particle for ionizing collisions for the plateau will be $\sim c/\nu$; $\nu^2=4\pi ne^2/m$, where n=electron density in the medium, i.e., $\sim10^{-6}$ cm, which is less than the dimensions of the undeveloped AgBr crystal ($\sim3.10^{-5}$ cm).[10] It can also be seen that the plateau sets in at a value of $E/\mu\sim\nu_0/\nu$, where ν_0 is the frequency corresponding to the effective ionization potential, e.g., for iron and AgBr, E/μ (cut-off)$\sim$20 and 30, respectively, in qualitative agreement with the curves in Figs. 1 and 2.

The experimental results seem to indicate the existence of a small increase in ionization beyond minimum up to a limiting plateau. It is hoped to confirm this increase by further observations and it may be possible to compare experimental results with the different theories. If anything, the present results seem to favor that of Wick[11] rather than of Halpern and Hall.[11]

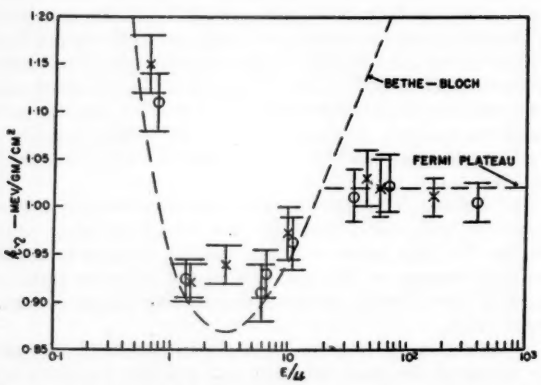

FIG. 2. Dashed curves show Bethe-Bloch energy loss, and Fermi plateau for AgBr. Experimental points, with standard deviations indicated; O—μ-meson decay electrons, and relativistic μ-mesons in sea-level plate. X—high energy electrons, protons, and shower π-mesons in high altitude plate.

We wish to thank Mr. I. B. McDiarmid for assistance with the grain counting and scattering measurements.

[1] W. F. G. Swann, J. Franklin Inst. **226**, 598 (1938).
[2] E. Fermi, Phys. Rev. **57**, 485 (1940).
[3] O. Halpern and H. Hall, Phys. Rev. **73**, 477 (1948).
[4] G. C. Wick, Nuovo Cimento **I**, 302 (1943).
[5] A. Bohr, Kgl. Dansk. Vid. Sels. Math-fys. Medd. **24**, No. 19 (1948).
[6] B. Rossi and K. Greisen, Rev. Mod. Phys. **13**, 240 (1941).
[7] L. Voyvodic, Can. J. Research **28**, 315 (1950).
[8] The actual grain densities were 31.7 and 35.7 grains/100μ, with standard deviations of 0.6 grain/100μ.
[9] D. R. Corson and M. R. Keck, Phys. Rev. **79**, 209 (1950).
[10] J. H. Webb, Phys. Rev. **74**, 511 (1948).
[11] Theoretical curves for AgBr have not yet been calculated, and will probably be a few percent different from those for iron.

Neutron Capture γ-Rays from Cd, Cl, and C

RICHARD WILSON*
Clarendon Laboratory, Oxford, England
August 7, 1950

SPECIMENS of Cd and of CCl_4 were placed in a beam of thermal neutrons from the graphite pile, *BEPO*. The capture γ-rays were measured by measuring the pulse-height distribution of photo-protons from disintegration of deuterium in an ionization chamber counter[1] placed behind the specimen. A small bismuth block in the center of the neutron beam attenuated the direct pile γ-radiation. The background of pile γ-rays was measured by interposing a neutron absorbing shutter of lithium and boron, which had a transmission of about five percent, equal to that of the CCl_4 sample.

Two similar counters were used. The first was filled with 11 atmos. deuterium gas and was operated at 16 kv, and the second was filled with a mixture of 5 atmos. CH_4 and 6 atmos. of H_2, and was operated at 8 kv. Both counters were made of a 1-mm thick aluminium alloy, which did not capture neutrons appreciably. The sensitive volume was enclosed in a sphere of 4 cm diameter.

The first counter had a trace of nitrogen present, and at first trouble was experienced with a large background from the reaction $N^{14}(n-p)C^{14}$. Later, the proton energy[2] of 630 kev from this reaction was used for calibration and to estimate the resolution. The resolution was ±15 percent of the proton energy, being caused partly by ionization chamber defects, which are observable in the $n-p$ reaction distribution, and partly by the influence of the γ-ray momentum on the pulse-height distribution of the photo-protons. This pure deuterium-filled counter had too low a stopping power to detect γ-rays above about 8 Mev. In order to plot the high energy portion of the spectrum, the second counter filled with the methane-deuterium mixture was used. In this counter, however, electron pulses caused too high a background to detect

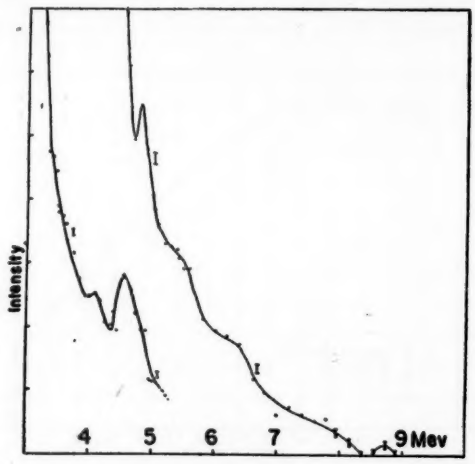

FIG. 1. Neutron capture γ-ray spectrum from cadmium.

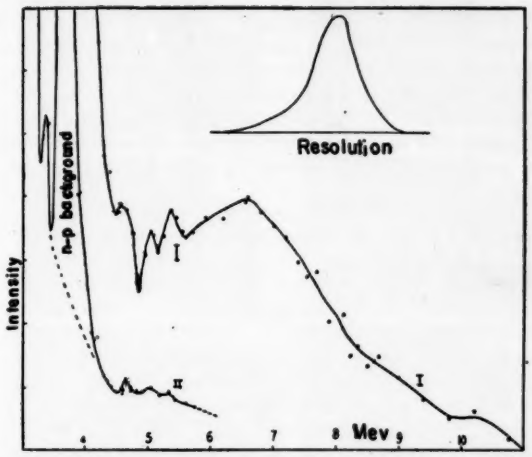

FIG. 2. Neutron capture γ-ray spectrum of carbon tetrachloride. The resolution curve shown is estimated for 8.5-Mev γ-rays; for lower energy γ-rays the resolution is better.

γ-rays below 4 Mev or to detect the $N^{14}(n-p)C^{14}$ reaction. The calibration in this case was made by measuring the saturation characteristics of both counters, and making use of the calibration of the first counter. The way the γ-ray curves overlap in the case of chlorine gives a gratifying justification of this procedure. The overlap for the cadmium spectrum is not so gratifying.

Figures 1 to 3 present the relative intensities of γ-rays of various energies; corrections have been applied to the pulse-height distribution curves for wall effect[1] and for the variation of the photo-disintegration cross section with energy. The statistical standard deviations are not given for each point, but are shown alongside the curves for clarity. The cadmium spectrum is the shape one would expect from the statistics of a many level nucleus. Even here, however, there are distinct signs of a peaked distribution, probably caused by a grouping of levels rather than by single γ-ray transitions. It is not certain, with the low statistics available, whether the slight peak at 8.7 Mev, indicating a direct transition to the ground state, is genuine or not. The chlorine spectrum shows definite signs of level structure. The background $(n-p)$ reaction prevents data being obtained in the energy region shown.

The end points of the spectra can be identified with mass differences and are Cd$\sim$8.5$\pm$0.5 Mev, Cl$\sim$10.5$\pm$0.3 Mev. These figures may be compared with the results of Kubitshek and Dancoff.[3]

The capture in carbon was much smaller, and to avoid background a different arrangement was necessary. The first counter was surrounded with boron to absorb slow neutrons which would otherwise cause an $(n-p)$ reaction, and placed to one side of the neutron beam, shielded from the direct radiation from the pile by the pile wall of cadmium and lead. Large blocks of graphite were placed in the beam, of such a size that the mean free path for Compton scattering of γ-rays in the carbon was approximately the dimensions of the block. The background was measured as before by blocking the beam with a boron lithium shutter. The arrangement was such that appreciable capture could have occurred in surrounding materials, particularly the lead wall of the pile; it is therefore not certain whether the spectrum shown is due to neutron capture in carbon alone, or also to capture in impurities and surroundings. Calibration of the counter was made from the $N^{14}(n-p)C^{14}$ reaction as before. The spectrum shown is corrected as before for wall effect and for variation of photo-disintegration cross section with energy.

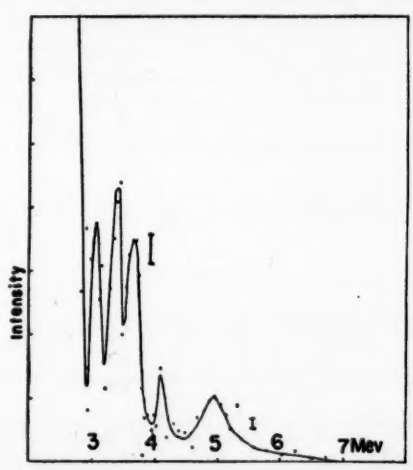

FIG. 3. Neutron capture γ-ray spectrum from graphite.

Gamma-ray peaks were found at 3.05, 3.4, 3.65, 4.1, and 4.95 $\pm$0.05 Mev. The last appears to be a transition direct to the ground state of C^{13}, and agrees well with the value 4.951 Mev found by Kinsey,[4] whose work was published after these measurements were completed. The 4.1-Mev γ-ray is probably a transition[5] to the 0.8-Mev metastable state of C^{13}, and the 3.05-Mev γ-ray may be a transition from the 3.1-Mev excited level to the ground state. The 3.4- and 3.6-Mev γ-rays may come from levels not previously reported, or from impurity capture. The statistics, however, are not good.

No γ-ray of 8 Mev corresponding to capture in C^{13} was found, and it seems probable that 80 percent of the capture in carbon is due to C^{13}.

It is a pleasure to acknowledge the assistance given by Mr. F. W. Fenning and others of the Pile Physics division, and to thank the Director, A. E. R. E. Harwell, for allowing the experiment to be performed. I would also like to thank Dr. H. Halban of the Clarendon Laboratory, for suggesting the experiment.

* Now at the University of Rochester, Rochester, New York.

[1] Wilson, Beghian, Collie, Halban, and Bishop, Rev. Sci. Inst. 21, 699 (1950).
[2] Franzen, Halpern, and Stephens, Phys. Rev. 77, 641 (1950).
[3] H. E. Kubitshek and S. M. Dancoff, Phys. Rev. 76, 531 (1949).
[4] Kinsey, Bartholemew, and Walker, Phys. Rev. 77, 723 (1950).
[5] Fowler, Lauritsen, and Lauritsen, Rev. Mod. Phys. 20, 236 (1948).

A Standard Substance for Precise Electron Diffraction Measurements

F. W. C. BOSWELL*
Department of Physics, University of Toronto, Toronto, Canada
June 29, 1950

DURING the course of some work dealing with the variation of the lattice constants of very small crystals with crystal size, it was necessary to look into the question of a standard reference substance for precision electron diffraction measurements. The conditions to be met are as follows: (1) The recorded pattern should consist of several very sharp rings so that a good average value of the constant to be found can be obtained. (2) When prepared, the material should remain chemically stable and without physical change, such as growth in crystal size, over a period of several days. (3) The lattice constant and crystal structure must be known and be independent of the method of preparation.

Gold has been used as a standard material by several workers. However, Lu and Malmberg[1] have reported thin gold foil to have a lattice constant less than the usual x-ray value, and our results on evaporated gold films corroborate this result. Thin films of alkali halides are unsuitable since, in most cases, the crystals grow on exposure to air. ZnO has been suggested as a standard material. However, both Finch and Wilman[2] and Cosslett[3] have reported that in some cases the lattice constant of ZnO as determined by electron diffraction differs from the x-ray value, and varies with the age of the specimen.

A vacuum-evaporated film of TlCl about 300A thick, deposited on a thin Formvar or collodion substrate was found to provide a satisfactory standard material. A typical transmission electron diffraction pattern is shown in Fig. 1. The angular half-width of

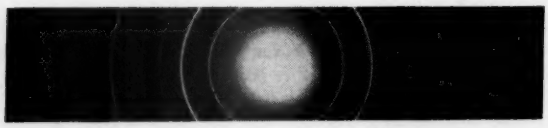

FIG. 1. A typical electron diffraction pattern of an evaporated TlCl film.

the rings (neglecting those which are overexposed) is about 3×10^{-4} radian, and this is thought to be entirely due to an instrumental factor and to the finite sizes of the diffracting crystals. The diameters of these rings can be measured readily with an accuracy of one part in 5000 by means of an optical comparator. No change has been detected in such a specimen left exposed to the air for a number of weeks.

The value which we have taken for the lattice constant of TlCl is the prevision x-ray value given by Jevins and Karlsons.[4] This value was determined assuming the wave-length of the Cu $K\alpha_1$-radiation to be 1.5374A. The lattice constant of TlCl is then 3.834A at 20°C.

We have also found MgO smoke to be useful as a secondary standard. This pattern has the defect that only two recorded rings are sufficiently sharp to allow precise measurement. The specimens were prepared by holding a Formvar-covered wire mesh about 10 in. above a short strip of burning magnesium ribbon. It was found that the lattice constant of MgO smoke did not vary from specimen to specimen. In terms of the TlCl standard mentioned above we found the lattice constant of MgO smoke to be 4.202A. This value is in agreement with the best x-ray determinations for MgO powder.

* Now with the Bureau of Mines, Department of Mines and Technical Surveys, Ottawa, Canada.

[1] Chia-Si Lu and E. W. Malmberg, Rev. Sci. Inst. **14**, 271 (1943).
[2] G. I. Finch and H. Wilman, J. Chem. Soc. **1934**, 751 (1934).
[3] V. E. Cosslett, Nature **136**, 988 (1935).
[4] A. Jevins and K. Karlsons, Zeits. f. physik. Chemie **B42**, 143 (1939).

Pulses in Argon Counters

LAURA COLLI, UGO FACCHINI, AND EMILIO GATTI
Laboratori CISE, Piazzale Cimitero Monumentale, Milan, Italy
July 31, 1950

THE building-up of the discharge in argon counters is due to photons, as pointed out by several authors.[1] The photons generated near the wire during the initial avalanche cause the cathode or the gas to send out a number of photo-electrons which, as soon as they get near the wire, build up a new avalanche, and so on.

No definite results have been obtained from experimental work recently carried out for the purpose of discriminating between the process on the cathode and the photo-ionization in the gas, as both processes seem to lead to results which are quantitatively possible.[2]

Here we give a few experimental observations on this subject.

We have studied α- and β-particle pulses in cylindrical counters of the usual type, filled with argon (previously purified with hot calcium) operating in the proportional and Geiger zones. The brass cathodes range from 60 to 90 mm in diameter; the tungsten wires are 0.2 mm in diameter, and the argon pressure employed ranges from 15 to 100 cm Hg.

A thin layer of uranium has been placed inside the counter.

The circuit consists of a cathode follower, an amplifier mod. 100 (with a rise time of 0.6 μsec.) and a synchroscope-delay line-oscillograph system to observe and photograph the pulses. Different time constants have been employed in the amplification chain and sometimes directly on the counter, in order to differentiate the pulses in a suitable way.

Figure 1 shows the multiplication curves obtained with one of the counters for α- and β-particle pulses, and with two different time constants. Figure 2 shows the pulse forms for increasing voltages.

The interpretation of the curves and of the pulse shapes is as follows. $N(V)$ being the multiplication factor at voltage V due to the ionization process by electron collision (Townsend α-process), and A_0 the number of ion pairs generated by a primary ionizing particle, the first avalanche built up by this particle will contain $Q_0=NA_0$ electrons.

In the multiplication process photons are produced also; if f is the number of photo-electrons extracted from the cathode for each electron of the primary avalanche, the number of electrons extracted from the cathode and which reach the wire will be NA_0f. Here f depends on the nature of the gas, its pressure, the photoelectric efficiency of the cathode for the photons involved, the average solid angle under which the cathode can be seen from the wire, and the wire-to-cathode distance.

After a transit time τ, these photo-electrons reach the high field region in the neighborhood of the wire and are multiplied N times, producing an avalanche containing $Q_1=fN^2A_0$ electrons, *viz.* $Q_1=fNQ_0$.

The following avalanches will be subject to the formula $Q_k=(fN)^kQ_0$.

The foregoing holds good provided $fN<1$, as in this case the convergence of the pulse succession is ensured, and when it is possible to disregard the decrease of N produced by the positive ions which, after a few transit times τ, are still very close to the wire. The succession of photo-electronic pulses originating from every α- or β-particle has been observed by the oscilloscope,

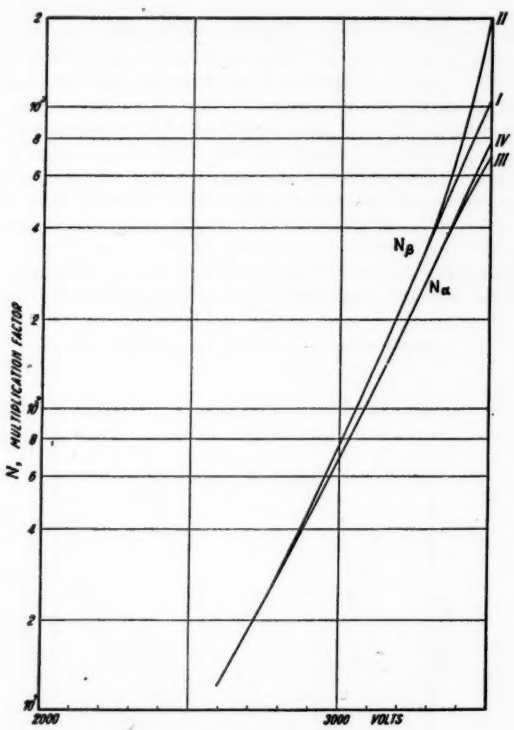

FIG. 1. Multiplication curves. Counter diameter: 90 mm; argon pressure: 76 cm Hg; I. β-particles $RC=1.5\,\mu$sec.; II. β-particles $RC=250\,\mu$sec.; III. α-particles $RC=1.5\,\mu$sec.; IV. α-particles $RC=250\,\mu$sec.; at $N=30$ the space-charge distortion of the multiplication begins for α-particles; at $N=400$ photo-electronic pulses are detectable. The Geiger threshold is at $N\beta=1000$.

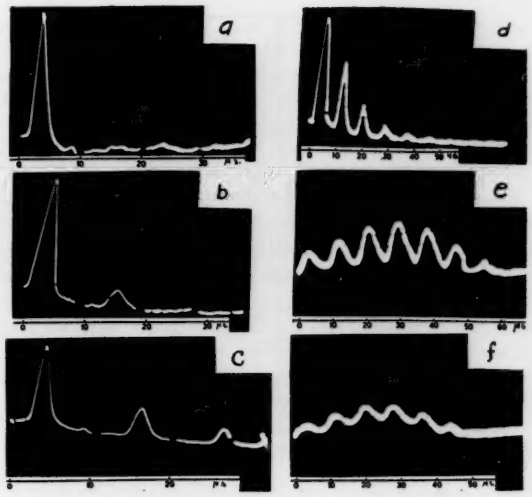

FIG. 2. Pulse shapes. Counter diameter: 90 mm; argon pressure: 76 cm Hg; a, b, c, d, are α-particle pulses. N_α ranges from 50 to 700; and the electron transit time is 12 μsec.; e, f, are β-particle pulses in the Geiger zone. $N_\beta > 1000$. The d pulse in one α-particle in the Geiger zone. Here $Nf\beta$ is >1 but $N_\alpha f$ is still <1.

adopting for the time constant a small value as compared with the transit time. The following pulses appear thus sharply separated from each other.

On the contrary, when a time constant is employed sufficiently large to sum up the whole series, a pulse is obtained whose amplitude is given, with the approximation referred to above, by

$$Q = A_0 N/(1-Nf).$$

The different behavior noted between the α- and β-particle curves at high N values is due to the distortion of the multiplication factor brought about by the large space charge produced by the α-particles, whose action is no longer negligible.

In the case of β-pulses, at a voltage $V > V_s$, where V_s represents such a voltage that $N_\beta f = 1$, an increasing-term succession results. But the ionic charge accumulated on the wire, after a few terms, lowers the field. Consequently the multiplication factor is reduced to such a value that $N_\beta f < 1$; then the succession will go on decreasing till it is exhausted.

This pulse is of the Fig. 2e,f type, its total amplitude is almost independent of the primary ionization of the particle; the Geiger threshold is at voltage V_s.

The sharp separation between the photo-electronic pulses of the succession and the fact that, even at its most remote terms, the rise times are approximately constant and equal to the first rise time, which is determined by the geometry of the primary ionization, prove that in our case the photo-ionization of the gas does not play an important role in the building up of the discharge.

In fact, this is entirely due to the photoelectric effect on the cathode. The f values which can be deduced for the counters employed range from 1/500 to 1/2000.

We thank Professor G. Bolla for useful discussions on the subject.

[1] S. C. Curran and J. D. Craggs, *Counting Tubes* (London, 1949).
[2] C. Balakrishnan and J. D. Craggs, Proc. Phys. Soc. London **63**, Section A, 358 (1950).

Domain Structure of Rochelle Salt

J. FURUICHI AND T. MITSUI
Faculty of Science, Hokkaido University, Sapporo, Japan
August 7, 1950

AS has been shown[1] in investigations on the domain structure of BaTiO, inspection by means of the polarization microscope is the most reliable method for the study of the domain structures of ferroelectric substances if the directions of the optic axes of a domain differ from those of its neighbors. We have found that this method is useful also for rochelle salt, and have verified that in general rochelle salt consists of many domains, between two Curie points.

Thin X-cut specimens of rochelle salt (0.07×0.3 mm thick) have been inspected between crossed Nicols and it has been found that generally the specimens consist of two kinds of regions which have slightly different extinction positions. One of the two extinction positions deviates by a small angle from the c axis to the right, and the other to the left. Generally the region is a band elongated along the c axis (Fig. 1). The band widths which have been observed are from 0.5 to below 0.001 cm. Specimens cut parallel to the b axis and oblique to the a and c axes also show similar structure, consisting of bands perpendicular to the b axis.

These facts show that generally rochelle salt crystal is a repeated twin whose component is a slab perpendicular to the b axis. There are, however, a few X-cut specimens which have groups of bands elongated to the b axis.

When the temperature is increased or decreased from room temperature, the twin structure disappears at about 23° and −18°C (the upper and lower Curie points), and when it is returned to room temperature almost the original structure reappears.

Observations on the effect of an electric field have been performed through pinhole electrodes. When a field is applied in the X direction the structure disappears, and when the field is removed it reappears; however, it is not similar to the initial structure after a strong field is applied for several minutes.

When a stress is applied the structure disappears and when the stress is removed it reappears, but a strong stress applied for several minutes leaves a remanent state.

These properties prove that the component of the twin is itself a domain.

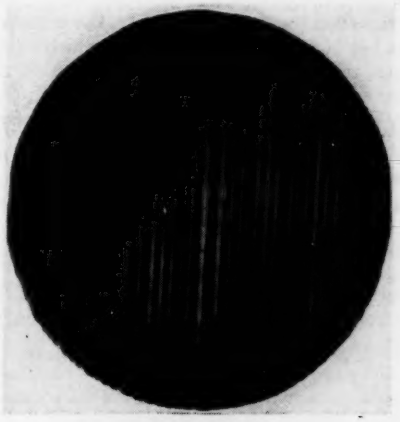

FIG. 1. X-cut specimen observed between crossed Nicols.

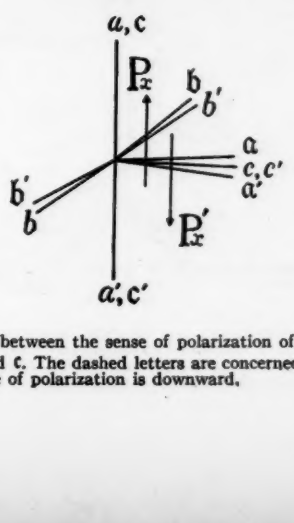

FIG. 2. Relation between the sense of polarization of a domain and its optic axes a, b, and c. The dashed letters are concerned with the domain for which the sense of polarization is downward.

The relation between the sense of the polarization of a domain and its extinction position, or the arrangement of the optic axes, can be determined by observing which of the two extinction positions a specimen possesses after it has been turned into a single domain by the effect of a field applied in one sense. The result is illustrated in Fig. 2, in which the crystallographic axes of domains which are parallel, or almost parallel, to the *a*, *b*, and *c* axes of a large pseudorhombic crystal are called *a*, *b*, and *c*, respectively, for simplicity.

Further investigations are in progress.

The authors are grateful to Dr. H. Kawai for supplying the rochelle salt crystals, and are also much indebted to Mr. Y. Katsui who has given much valuable help and many suggestions in the course of this work.

[1] B. Matthias and A. von Hippel, Phys. Rev. **73**, 1378 (1948). P. W. Forsbergh, Jr., Phys. Rev. **76**, 1187 (1949).

The γ-Ray Spectrum Resulting from Capture of Negative π-Mesons in Hydrogen

WOLFGANG K. H. PANOFSKY, LEE AAMODT, JAMES HADLEY, AND ROBERT PHILLIPS
Radiation Laboratory, Department of Physics, University of California, Berkeley, California

August 8, 1950

PRELIMINARY results concerning the γ-ray spectrum resulting from the capture of π^--mesons in hydrogen have been reported in a previous letter.[1] The purpose of this note is to present more conclusive data and to indicate the resultant mass values for the neutral meson. A more detailed report is in preparation.

The apparatus and geometrical arrangement used are similar to the instrumentation previously reported.[1] The principal improvement is the use of a 32-channel pair spectrometer (Fig. 1). Two sets of spectra are shown: one (Fig. 2) taken with the center of the spectrometer set at 100 Mev and one (Fig. 3) with the center set at 70 Mev. Figure 2 clearly shows that both processes discussed previously coexist, namely:

$$\pi^- + p \rightarrow n + \gamma, \quad (1)$$

$$\pi^- + p \rightarrow n + \pi^0. \quad (2)$$
$$\downarrow$$
$$2\gamma$$

Figure 3 permits a fairly accurate determination of the π^0-mass. We obtain from Fig. 3 and the kinematics pertaining to Eq. (2):

$$M_{\pi^-} - M_{\pi^0} = 10.6 \pm 2.0 \text{ electron masses.}$$

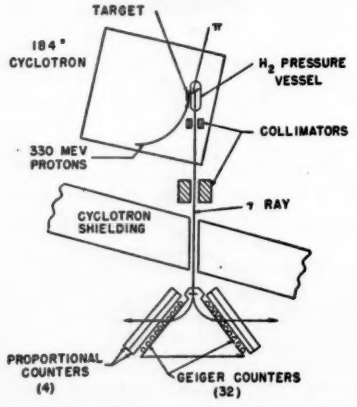

FIG. 1. Geometrical layout (not to scale) of components of the π^--absorption experiment. π^--mesons from the primary target struck by 330-Mev protons are absorbed in the H_2 pressure vessel. The resultant γ-rays are collimated and analyzed in a 90° pair spectrometer.

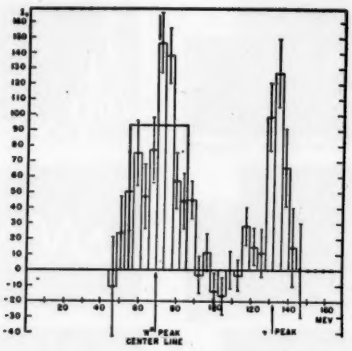

FIG. 2. Gamma-ray spectrum from the absorption of π^--mesons in H_2 with center of spectrometer set near a γ-ray energy of 100 Mev. The center line of the π^0-peak and the γ-peak as computed from a π^--rest energy of 141 Mev are marked. Also the theoretical π^0-spectrum (rectangular contour) is shown to correspond in area to the observed constant and in width to the curve of Fig. 3.

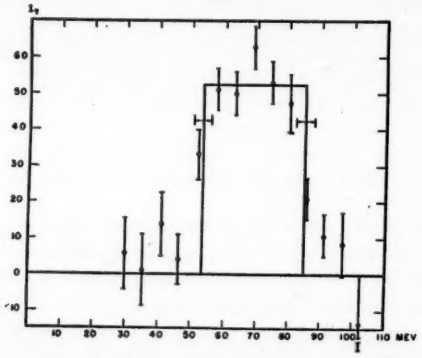

FIG. 3. Gamma-ray spectrum with center of spectrometer set near 70 Mev. The best fit of rectangular contour is shown and the estimate of the probable error of the lower and upper limit of the spectrum is indicated.

Figure 2 permits an estimate of the branching ratio between processes (1) and (2). The result is

$$\Gamma_{\pi^0}/\Gamma_\gamma = 0.96 \pm 0.20$$

and the available momentum space for the π^0 is

$$p/M_{\pi^0}C = 0.23 \pm 0.03.$$

The authors are greatly indebted to Dr. Herbert F. York for cooperation during the early parts of the experiment.

[1] Panofsky, Aamodt, and York, Phys. Rev. **78**, 825 (1950).

Atomic Positions and Vibrations in the Ferroelectric $BaTiO_3$ Lattice

W. KAENZIG
Swiss Federal Institute of Technology, Zürich, Switzerland

July 20, 1950

THE integrated reflections (00*h*) and (0*h*0) from untwinned $BaTiO_3$ single crystals were measured up to high orders ($h=10$) as a function of temperature in the range from 15 to 310°C using MO K_α-radiation and a precision ionization spectrometer.

The influence of extinction could be estimated and taken into account. The investigated crystals were rather perfect and showed considerable primary extinction. Near the transition point of 120°C, fluctuations occur diminishing the primary extinction which lead to a sharp peak of the extinction-sensitive reflections. The transition proper is very sharp and shows a thermal hysteresis of about 2°. Impurities appear to reduce this hysteresis. The

primary extinction in the cubic phase is equal to the primary extinction in the tetragonal phase. Thus the parallel and antiparallel domains are identical with the mosaic blocks.

The fact that the corrections for extinction can be evaluated enables one to determine the variation of the structure factor with temperature from the observed variation of the integrated reflection. The decrease of the mean square amplitude of the lattice vibrations with temperature is found to be quite normal in the cubic region. The variation of the structure factor arising at and below the transition point cannot be accounted for by a mere shift of the atomic positions. It is necessary to assume that considerable changes of the thermal vibrations occur in this temperature range. By a trial-and-error method it was possible to find a single solution agreeing within a few percent with the observed variation of the structure factor. The Ti ions and the oxygen ions lying on the same line along the z axis undergo a sudden displacement along this axis in opposite directions at the transition point, this jump being followed by a continuous change as the temperature decreases (Fig. 1).

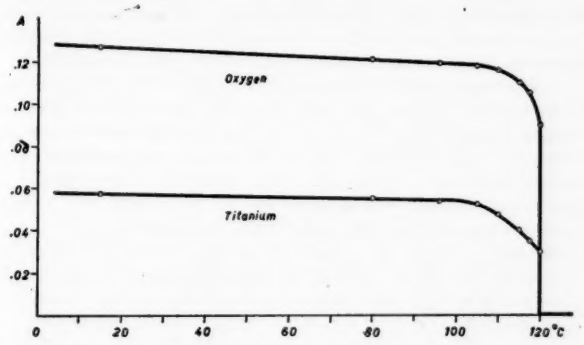

FIG. 1. Variation of the atomic positions (in angstrom units) with temperature.

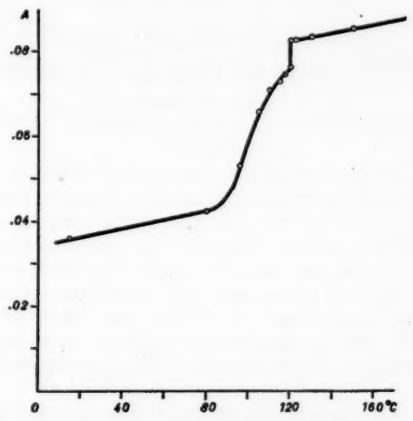

FIG. 2. Variation of the root-mean-square amplitude of the thermal vibration of the Ti ion along the z axis (in angstrom units) with temperature.

The variation of the root-mean-square amplitude of the vibration of the Ti ion along the z axis is shown in Fig. 2. A sudden variation at the transition point is seen to be followed by a continuous rapid decrease below. The Ba ions behave quite normally in the same region. The vibrations in the x direction could not be determined since the reflections $(0k0)$ are too strongly influenced by the anomaly in the extinction. A more detailed study of the lattice vibrations through measurements of the diffuse scattering is being initiated.

The full account of the present investigations will appear in *Helvetica Physica Acta*.

Role of Metastable ($^3P_2$) Hg Atoms in Low Current Discharges in Hg Rare Gas Mixtures

CARL KENTY
Lamp Development Laboratory, General Electric Company, Nela Park, Cleveland, Ohio
August 7, 1950

A POSITIVE column d.c. hot cathode discharge of about 1 ma in a few millimeters of a rare gas (e.g., A, Kr, Xe) plus a few microns of Hg in a 3½-cm tube has been found to have a positive characteristic and ordinary running striations. As the current increases these striations weaken and disappear at 60 to 100 ma. The voltage (V) goes through a broad maximum at about the same current. Decreasing the temperature (Hg density) raises this maximum and displaces it toward lower currents. No ballast is necessary in the region of positive characteristic.

At 1 ma strong illumination with Hg radiation (transmissible through glass) nearly doubles V (Fig. 1), doubles the 2537 output (B_u), nearly doubles the electron temperature (T_e), as shown by probe measurements, and nearly suppresses the striations.

Irradiation with the light of the rare gas concerned has no effect above about 16°C. Above 25°C, the rare gas lines could be seen only with Xe and apparently even here the role of rare gas excitation is negligible.

Absorption measurements with 5461, 4358, and 4047 show high concentrations ($\sim 10^{11}$ cm^{-1}) of $^3P_2$ and $^3P_0$ even at 1 ma; $^3P_2$ in pure gas is nearly twice as populous as $^3P_0$. These concentrations increase relatively slowly, above about 4 ma; $^3P_1$ reaches an appreciable concentration only at higher currents.

A trace of molecular impurity greatly increases V and B_u and also the visible line output (B_v); it further suppresses the striations and destroys $^3P_2$. Thus 4μ N_2 increases V and B_u fivefold, B_v threefold, T_e twofold, and reduces $^3P_2$ to nearly zero (though scarcely affecting $^3P_0$), while completely suppressing the striations. It was found that

$$B_u \cong KV, \tag{1}$$

where K is the same for all impurities tried. The addition of N_2 beyond about 4μ precipitates a new intermittent, or flashing form of discharge, described in the following letter.

These results are explained as arising from the destruction of Hg metastables by irradiatiation, the ionization evidently being mainly two-stage. In pure gas $^3P_2$ furnishes most of the ions, but with impurities $^3P_0$ takes over this role (with more difficulty). The

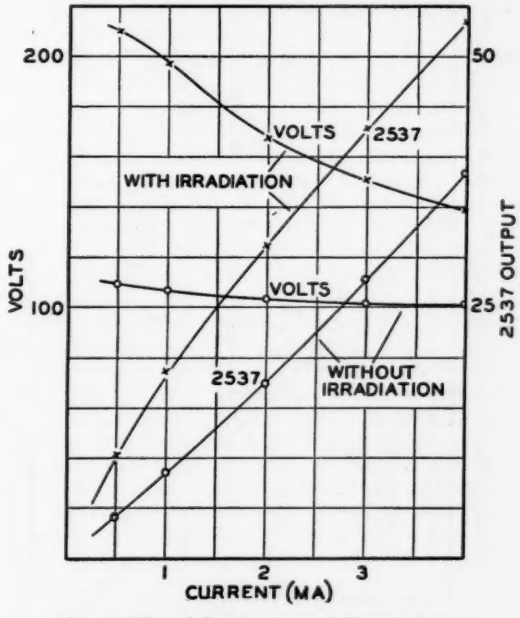

FIG. 1. Effect of illumination with Hg radiation.

quenching of $^3P_2$ by impurities appears to be mainly by $^3P_1$. CO is threefold as effective as N_2. H_2 and CO_2 are comparable to CO, but even at 1 ma, H_2 cleans up rapidly and CO_2 is changed to CO (and HgO). The striations in pure gas evidently depend on the two-stage ionization associated with $^3P_2$.

The apparently small contribution of single-stage ionization may mean that the electron energy distribution is hardly Maxwellian, being deficient at the high speed end and that the cross section for ionization of the ^3P states, especially $^3P_2$, is large[1] compared with that of normal Hg.

Equation (1) indicates that impurities absorb relatively little energy directly from the electrons but act by quenching $^3P_2$ (the main source of ions).

[1] B. Klarfeld, Tech. Phys. U.S.S.R. 5, 913 (1938).

A New Form of Discharge in Gas Mixtures: The Flashing Discharge

CARL KENTY
Lamp Development Laboratory, General Electric Company, Nela Park, Cleveland, Ohio
August 7, 1950

IN the previous letter it was shown that when impurities are added to a 1-ma d.c. hot cathode, positive column discharge in 3-mm A+Hg at 27°C in a 3½-cm tube, the voltage rises markedly and the running striations gradually disappear. At about fivefold normal voltage (with ~4μ N_2 or 0.13μ CO) the discharge suddenly breaks into a "flashing" form which the rotating mirror and the oscilloscope show is both striated and current modulated. A typical wave form is shown by Fig. 1A. The frequency may be from 25 to 10,000 c.p.s., increasing with the N_2/Hg ratio, irradiation with Hg light, current, and decreasing A pressure. The current modulation varies from 25 percent with 10 megohms ballast to nearly 100 percent with 0.2 megohm. The striations are sharp and convex on the cathode side (Fig. 1C) and appear stationary; they are one to one-half tube diameters apart, growing closer with more N_2. The flashes are bright with Hg light, but between flashes the tube appears to be dark. Flashing is favored by a high N_2/Hg ratio, by low current and by irradiation with strong Hg light; it has been an over-all positive characteristic. It is less striking in Kr+Hg and is entirely absent with Xe+Hg.

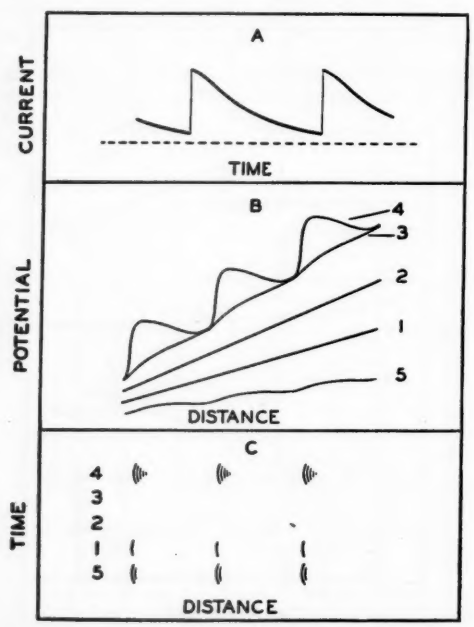

FIG. 1. Characteristics of the flashing discharge.

The following explanation of flashing appears to be in accord with all the observations. At times 1 and 2 (Fig. 1) the gradient is essentially uniform and rising, the brightness (essentially an afterglow) low and the discharge only partly self-maintaining because of net loss of ions by diffusion to the walls. At time 3 the gradient has risen so high as to be unstable, tending to localize. This process takes place extremely rapidly so that at time 4 the gradient is sharply stepped, producing electrons with 12 to 14 volts energy, as indicated by the observed volts per striation. These electrons strongly excite A metastables (and resonance atoms), A′, which quickly ionize Hg. Argon resonance radiation meanwhile diffuses rapidly and the resulting resonance atoms and metastables produce Hg ions by collision in the regions between the striations. The result is that in an extremely short time very high ion densities are built up locally and to a lesser extent throughout the tube. The high stepped gradient meanwhile collapses, while the current rises abruptly. It may be just at the beginning of this time or slightly before that the visible light is mainly produced. In the period just following, few ions are produced but the ionization is decreasing by diffusion to the walls and perhaps recombination. As a result the voltage rises and there is progressively more ionization, probably two stage via $^3P_0$ (since irradiation shortens the time between flashes), but the discharge never becomes self-maintaining till the onset of the next flash.

In the dark period, e.g., at 2, Fig. 1, most of the energy is going into 2537 via $^3P_2$ (quenched by the N_2) and $^3P_1$, ions coming largely from $^3P_0$, while at 4 it is going mostly into Hg ionization via A′. The two processes require such different conditions that both can scarcely occur together. The result is an almost cataclysmic change from one to the other; and a sharp jump in the current is the unfailing sign of flashing.

Flashing does not occur with Xe because Xe′ cannot ionize Hg. A little Xe added to A+Hg+N_2 stops flashing because the Xe absorbs the energy that would otherwise have gone to excite A, Kr+Hg flashes because two of the Kr′ states can ionize Hg.

Grain Counts and Corrected α-Particle Range-Energy Curve for Ilford E-1 Emulsions*

ISADORE B. BERLMAN
Physics Department, Washington University, St. Louis, Missouri
May 29, 1950

IN 1937 Wilkins[1] published a set of curves showing the number of grains in corresponding lengths of proton, deuteron, and α-particle tracks. These tracks were recorded in Ilford R-2 emulsions, now obsolete. This work has now been repeated using Ilford E-1 nuclear emulsions 200μ thick. The emulsions were from the same batch of plates and were developed together after exposure as recommended by Wilson and Venselow[2] for 200μ emulsions. Grains in equivalent lengths of tracks were counted using a Spencer microscope with 120× objective and 10× eyepieces.

The number of developed grains in 10μ intervals, as measured from the end of the track, was counted. Then an average number for each interval was computed from corresponding intervals of all the similar tracks. Figure 1 represents the average number of grains in a given length of track as measured from the end of the track. Curve I was obtained from 110 proton tracks, curve II was obtained from 48 deuteron tracks, and curve III was obtained from 15 α-particle tracks. Occasionally, near the end of the tracks, the grains were too closely packed to be clearly differentiated, therefore an estimation was made. This assumed number per 10μ interval was 16 for protons, 17 for deuterons, and 20 for α-particles.

In the course of analyzing the emulsions in which elastically scattered α-particle tracks were recorded from the bombardment of various thin targets[3] by 20-Mev α-particles from the Washington University cyclotron, it was noted that the predicted ranges

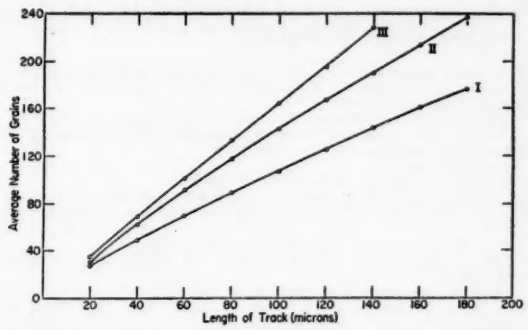

FIG. 1. Average number of grains in a given length of track as measured from the end of the track. Curve I is for protons, curve II is for deuterons, and curve III is for α-particles.

for the α-tracks were greater than the actual measured ranges. The discrepancy was as much as ten percent. In determining the predicted ranges, use was made of the range-energy curve for α-particles as given by Lattes.[4] The curve was verified below 10 Mev but above this value serious departure was found.

The error was assumed to have come from one of two sources. Either the cyclotron beam did not contain 20-Mev α-particles but rather 17.5-Mev α-particles, or the range-energy curve was in error above 10 Mev when applied to Ilford E-1 nuclear emulsions. The first source was eliminated by two considerations; first, it was improbable that a cyclotron producing 10-Mev deuterons would produce 17.5-Mev α-particles, and second, the elastically scattered α-particle tracks from C^{12} and O^{16} at angles greater than 90° to the cyclotron beam were correctly predicted assuming 20-Mev α-particles and using the lower part of the range-energy curve. The curve may be modified as shown in Fig. 2. Curve I is that given by Lattes and curve II is that derived from the Lattes' proton range-energy curve which this author has found to apply to Ilford E-1 nuclear emulsions when various targets were bombarded with 5-Mev protons from the Washington University cyclotron. By assuming that within the experimental limits an α-particle and a proton of the same velocity has the same range, i.e., an α-particle with four times the energy of a proton, loses energy four times as fast due to its double charge, one arrives at curve II. With the modified curve, the ranges of the elastically scattered α-particles are accurately predicted.

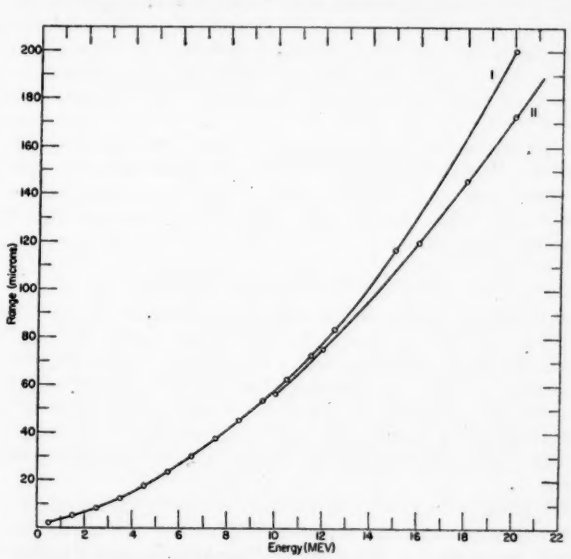

FIG. 2. Alpha-particle range-energy curve. Curve I is that obtained by Lattes (see reference 4). Curve II is a modified curve as applied to Ilford E-1 nuclear emulsions.

I wish to express my gratitude to Messrs. Chia-Hua Chang and Shu-Lung Wang for their careful reading of the plates. I also wish to thank Dr. Robert N. Varney for his many helpful discussions.

* Assisted by the joint program of the ONR and AEC.
[1] T. R. Wilkins and H. J. St. Helens, Phys. Rev. **54**, 783 (1938).
[2] M. J. Wilson and W. Venselow, Phys. Rev. **75**, 1144 (1949).
[3] Results to be published.
[4] Lattes, Fowler, and Cuer, Proc. Phys. Soc. London **59**, 883 (1947).

The Probable Energy Loss of Electrons in Matter*

S. D. WARSHAW† AND JOSES J. L. CHEN
University of Southern California, Los Angeles, California
August 7, 1950

ALTHOUGH the energy degradation of electrons passing through matter is of interest in many experiments, there have been no good measurements of this quantity since the early work of White and Millington.[1] While the average energy loss can be calculated by more or less familiar formulas,[2] Christy has recently emphasized[3] that the use of the *average* rather than the *most probable* energy loss for charged particles can lead to as much as 20 to 30 percent error in the case of moderately energetic electrons. The most probable loss has been calculated most recently by Landau[4] who obtained the energy loss distribution in the form of a universal numerical function, and thereby an expression for the most probable loss. In the result there is a characteristic non-linear dependence of the probable loss on the thickness of the material traversed. This is also true of a classical expression[5] in which, however, the velocity dependence is slightly different and which has a different range of validity. Landau's expression is

$$\Delta E_{\text{prob}}=\xi[\ln(\xi/\epsilon)+0.37], \tag{1}$$

where

$$\xi=nZ(2\pi e^4/mc^2\beta^2) \quad \text{and} \quad \epsilon=[I^2(1-\beta^2)/2mc^2\beta^2]\exp(\beta^2),$$

and n is the number of atoms, with Z electrons each, per cm² of the foil material, β is the velocity of the incident electron in units of the velocity of light c, and m is the electronic mass. The mean excitation potential I is given by Mano.[6] The classical result[5] differs from this only by the introduction of a factor $2(k/K)^2$ in the argument of the logarithm, where $k=1.123$, $K=2v_e/v$ and $v_e=e^2/\hbar$ cm/sec. For $K\ll 1$ Bohr[7] has shown that the quantum treatment is the more appropriate.

The non-linear dependence of the loss on the thickness of stopping material becomes appreciable when foils thicker than some minimum are used, this minimum being defined by the condition of compound scattering.[8] To satisfy this condition while still keeping the thickness much less than the range of electrons in the material is, however, not difficult. For the β-particles from the K-conversion line in Ba 137 (624 kev) traversing aluminum foils, it is required that the thickness be in the middle portion of the range between 0.2 and 260 mg/cm². Hence a direct measurement of the probable loss with a foil thickness from about 5 to 40 mg/cm² of aluminum may be used to verify Landau's expression. The resulting curve of loss *versus* foil thickness should show a small but observable curvature. Our preliminary measurements were made on the shift of the Ba^{137} K-line for various thicknesses of both aluminum and tin. A double thin lens β-ray spectrometer, which is described elsewhere,[9] was used. The stopping material was mounted on a supporting frame which was then placed immediately in front of the conventional thin source holder. With the spectrometer set for 2.1 percent resolution and with 100 microcuries of Cs^{137} as the source, the transmission curve of the K-conversion line was measured as a function of foil thickness and the maxima of these curves were taken to correspond to the most probable final momentum in each case. A comparison of the peak shifts, on an energy scale, with Landau's expression (Eq. (1)) for the cases of both aluminum and tin, is given in Fig. 1, with the

average loss for aluminum, as calculated from the Bethe-Bloch formula,[2] included for contrast. A slight correction for resolution to the apparent peak location has been applied to the experimental values, the correction being about 0.04 to 0.28 kev for aluminum points and 0.26 to 1.02 kev for tin points, in a total loss from 5 to 44 kev. It can be seen that the agreement is excellent; however, other workers[10] report that a similar set of measurements, which appeared while this work was still in progress, show only "reasonable" agreement.

For the resolution used, quantitative measurement of the energy distribution is not possible; however, the line shape as a function of foil thickness (Fig. 2) is in qualitative agreement with Landau's theory.

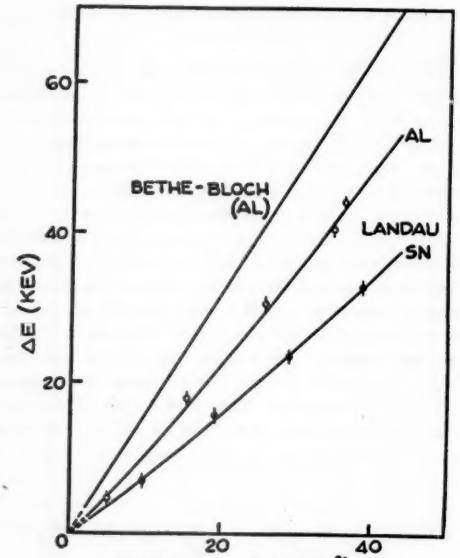

FIG. 1. Probable energy loss *versus* thickness curves for Al(○) and Sn(●) foils. Solid lines are from Landau's theoretical expression. The curve for *average* loss in Al (Bethe-Bloch) is given for comparison.

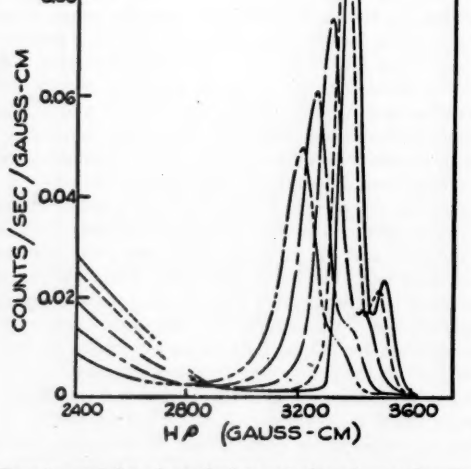

FIG. 2. Experimental line shape (points not shown) as a function of Al thickness (0, 5.2, 15.5, 25.8, 36.2 mg/cm²).

Further work, using lines of different energies, and with other foil materials, is now in progress.

* This work was assisted by the joint program of the ONR and AEC.
† Now at the Institute of Radiobiology and Biophysics, University of Chicago, Chicago, Illinois.

[1] P. White and G. Millington, Proc. Roy. Soc. **A120**, 701 (1928).
[2] W. Heitler, *The Quantum Theory of Radiation* (Oxford University Press, London, 1944), second edition, p. 219 ff.
[3] Unpublished work.
[4] L. Landau, J. Phys. U.S.S.R. **8**, 201 (1944).
[5] See the discussion in Rutherford, Chadwick, and Ellis, *Radiations from Radioactive Substances* (Cambridge University Press, London, 1930), p. 438 f.
[6] M. G. Mano, Comptes Rendus **197**, 319 (1933).
[7] N. Bohr, Kgl. Danske Vid. Seis. Math.-fys. Medd., Acad. Copenhagen **28**, 8, 78 (1948).
[8] E. J. Williams, Proc. Roy. Soc. **A169**, 531 (1939).
[9] Van Atta, Warshaw, Chen, and Taimuty, Rev. Sci. Inst. (to be published).
[10] Birkhoff, Hayes, and Goudsmit, Phys. Rev. **79**, 199 (1950).

Effect of Finite Range Interactions in the (*jj*) Coupling Shell Model

DIETER KURATH
University of Chicago, Chicago, Illinois
August 7, 1950

RACAH has presented as an argument[1] against the *jj* coupling model the statement that for identical particles with Majorana interaction the spin of the ground state is not always that of the odd nucleon. The basis of this statement is the fact that the statistical weight of singlet coupling for particles in equivalent orbits is given by the expectation value of the operator:

$$\Sigma S_{ik}=\Sigma(\tfrac{1}{4}-\mathbf{s}_i\cdot\mathbf{s}_k).$$

This expectation value attains a maximum for minimal I consistent with the exclusion principle, and would thus predict $I=\frac{3}{2}$ for three particles or three holes in a shell.

For identical particles, the Majorana operator is

$$\Sigma P_{ik}=\Sigma(-\tfrac{1}{2}-2\mathbf{s}_i\cdot\mathbf{s}_k),$$

so it leads to the same conclusions. If one chooses the interaction potential of a pair of nucleons as

$$V_{12}=P_{12}\{V_0\exp[-(r_{12}/r_0)^2]\}$$

where r_0 is a parameter giving the range of nuclear forces, one sees that Racah's considerations apply to the case of infinite range, r_0. It is known[2] that with spin-orbit coupling, a δ-function radial dependence gives for the spin of the ground state, the spin of the odd nucleon. Since this is the case of zero range, an investigation has been made to see at what range this level crosses the level $I=\frac{3}{2}$.

Calculations were carried out for three particles in the $1d_{5/2}$ and $1f_{7/2}$ shells, these being the first two cases where the spin of $\frac{3}{2}$ differs from that of the odd nucleon. Spin-orbit coupled functions were used whose radial dependence is the harmonic oscillator function with no nodes,

$$R_l(r)=N_l r^l\exp[-(r/r_l)^2],$$

where l refers to the orbital angular momentum. Energy levels were obtained whose separation depends only on the contribution from the unfilled shell and hence on the ratio (r_l/r_0). These contributions to the energy are plotted in Fig. 1 in units of $(-V_0)>0$. In the $1d_{5/2}$ case, the level $\frac{3}{2}$ is lower for $(r_d/r_0)<0.755$. In the $1f_{7/2}$ case, the $\frac{3}{2}$ level is lowest for $(r_f/r_0)<0.738$, 5/2 is lowest for $0.738<(r_f/r_0)<0.787$, and for greater (r_f/r_0), 7/2 is the ground state.

In order to see at what range these cross-overs occur, the value of r_l may be correlated with empirical nuclear constants. This is done by calculating the square-well problem to give the nuclear radius as $1.48\times10^{-13}A^{\frac{1}{3}}$, and also the experimental binding energy of the last nucleon. The oscillator wave function is then picked

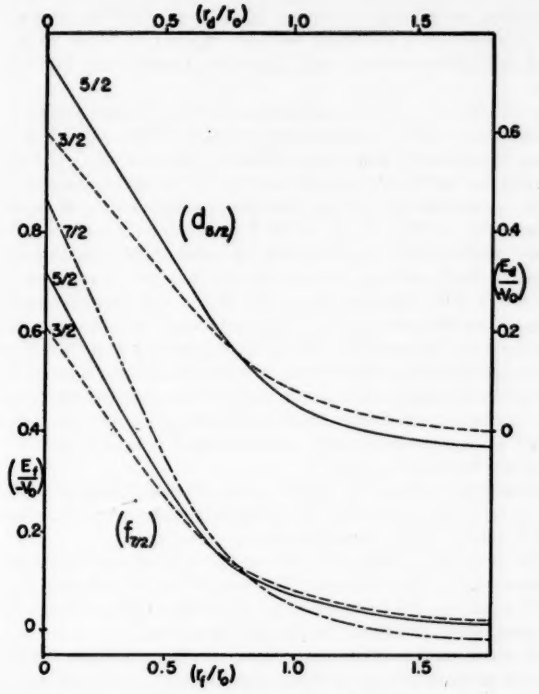

FIG. 1. Energy levels as a function of (r_1/r_0).

to give the closest fit to the square-well function, and as these can be matched quite closely, r_1 can be determined.

The $(d_{5/2})^3$ configuration is expected between $A=19$ and $A=25$. The calculation gives: at $A=19$, 5/2 lower for $r_0<3.5\times10^{-13}$ cm; at $A=25$, 4/1 lower for $r_0<3.8\times10^{-13}$ cm. The $(f_{7/2})^3$ configuration is expected between $A=43$ and $A=55$. The limits are: At $A=43$, 7/2 lowest for $r_0<3.75\times10^{-13}$ cm, 5/2 lowest in the interval 3.75×10^{-13} cm $<r_0<4.0\times10^{-13}$ cm, 3/2 lowest for $r_0>4.0\times10^{-13}$ cm. At $A=55$, 7/2 lowest for $r_0<4.1\times10^{-13}$ cm, 5/2 lowest in the interval 4.1×10^{-13} cm $<r_0<4.35\times10^{-13}$ cm, 3/2 lowest for $r_0>4.35\times10^{-13}$ cm. The usually accepted value for r_0 is about 2.8×10^{-13} cm, so the estimated cross-over points lie close to the region of physical interest, especially for the light elements.

Experimentally one finds a spin of $\frac{3}{2}$ for Na^{23}, and the β-decay scheme for Ne^{23} can be understood[3] with an excited state of 5/2 for Na^{23}. In the β-decay of O^{19} one would like to assume a spin of $\frac{3}{2}$ for its ground state.[4] Also the β-decay of Na^{25} to Mg^{25} (experimental spin of 5/2) shows a smaller ft value for decay to the excited state than to the ground state. These three cases all involve $(d_{5/2})^3$ configurations, which could give a spin of $\frac{3}{2}$ if the cross-over actually lies somewhat lower, and thus account for the experimental results.

In the $(f_{7/2})^3$ case, the experimental spin of V^{51} is 7/2, thus indicating that elements in this part of the periodic table are on the other side of the cross-over region. For heavier nuclei in higher shells, the δ-function approximation is approached, and it seems reasonably certain to conclude that the (jj) model will give the spin of the ground state as that of the odd nucleon. The only remaining exception to the (jj) rule for the spin of odd nuclei is Mn^{55}, which has an experimental spin of 5/2. Since this has a proton configuration of three holes in the $f_{7/2}$ shell, it might be explained by saying that in the $f_{7/2}$ shell elements are still quite close to the cross-over region, and the close-lying 5/2 and 7/2 levels can be inverted by some small perturbation.

The author is indebted to Professor M. G. Mayer for suggestions and helpful discussion.

[1] G. Racah, Phys. Rev. **78**, 622 (1950).
[2] M. G. Mayer, Phys. Rev. **78**, 22 (1950).
[3] V. Perez-Mendez and H. Brown, Phys. Rev. **78**, 812 (1950).
[4] E. Feenberg and K. Hammack, Phys. Rev. **75**, 1877 (1949).

Os^{182} and Os^{183}, New Radioactive Osmium Isotopes*

BETSY JONES STOVER
Radiation Laboratory and Department of Chemistry, University of California, Berkeley, California
August 10, 1950

TWO new neutron-deficient radioactive isotopes of osmium have been produced by proton bombardment of rhenium metal in the Berkeley 184-in. cyclotron and the proton linear accelerator. The half-lives are 12.0±0.5 hr. and 24.0±1 hr. which have been assigned to Os^{182} and Os^{183}, respectively.

To obtain a pure osmium fraction, the bombarded rhenium metal was placed in a small distilling flask, osmium carrier added, then dissolved with nitric acid. Osmium tetraoxide was distilled in a stream of air and collected in 6*N* NaOH as sodium osmate. Both osmium and rhenium were precipitated as the sulfides by bubbling hydrogen sulfide through warm acidified solutions of each to which hydroxylamine hydrochloride had been previously added to reduce the nitric acid. Similar chemistry was employed to determine the osmium-rhenium parent-daughter relationships.

Bombardment of rhenium (Re^{185}, 37.07 percent; Re^{187}, 62.93 percent) with 25-Mev protons in the linear accelerator produced the known[1] 97-day Os^{185} and a 12.0-hr. osmium activity which was shown to be the parent of the[2] 120-day Re^{183}. Magnetic counter and absorption data show that the 12.0-hr. Os^{183} decays by electron capture, and emits conversion electrons of energies 0.15 Mev and 0.42 Mev, and gamma-rays of energies 0.34 Mev and 1.6 Mev. The relative abundances of these radiations, calculated from absorption data, are as follows: 0.15 Mev ϵ^-: 0.42 Mev ϵ^-: *L* x-rays: *K* x-rays: 0.34 Mev γ: 1.6 Mev γ = 0.18 : 0.009 : 0.53 : 1 : 0.18 : 0.10.

With 40-Mev protons in the 184-in. cyclotron, an additional activity of 24-hr. half-life was formed which decayed to the[2] 12.7-hr. Re^{182}. The 24-hr. Os^{182} decays by electron capture, no positrons having been detected. Analysis of the radiations was limited by the growth of Re^{182} and the decay of Os^{183} in the Os^{182} samples.

* This research was done under the auspices of the AEC.
[1] L. I. Katzin and M. Pobereskin, Phys. Rev. **74**, 264 (1948).
[2] H. G. Hicks and G. Wilkinson, Phys. Rev. **77**, 314 (1950).

Sheath Formation in Ion-Neutralized Electron Beams

E. G. LINDER
RCA Laboratories, Princeton, New Jersey
August 7, 1950

BY "ion-neutralized electron beam" is meant an electron beam in which positive ions exist with a density equal to the beam electron density. Such beams may be formed when positive ions are produced, and trapped in the potential depression of a beam until the potential depression disappears by virtue of neutralization of electron space charge. The resulting medium is similar to a plasma except that the electrons are beam electrons and do not exist as an electron gas. The ions, however, do exist as a gas. This type of beam, and associated effects, are discussed in detail in a forthcoming paper by Linder and Hernqvist.[1]

A necessary condition for the existence of such beams is that the surrounding walls be unipotential, or nearly so. Thus, when neutralization is complete, the space is field-free, and the beam potential equals the wall potential. However, if the collector electrode (anode) is varied from beam potential V_0 to potential V, a sheath forms. Within the sheath, ions are swept out, and the beam is unneutralized; outside the sheath, ion-neutralization persists.

A theory of such sheath formation yields for the sheath thickness x,

$$x=\frac{1.5(10^{-6})V_0^{\frac{3}{4}}}{J^{\frac{1}{2}}}\left[\left(\frac{V}{V_0}\right)^{\frac{1}{2}}+2\right]\left[\left(\frac{V}{V_0}\right)^{\frac{1}{2}}-1\right]^{\frac{1}{2}},$$

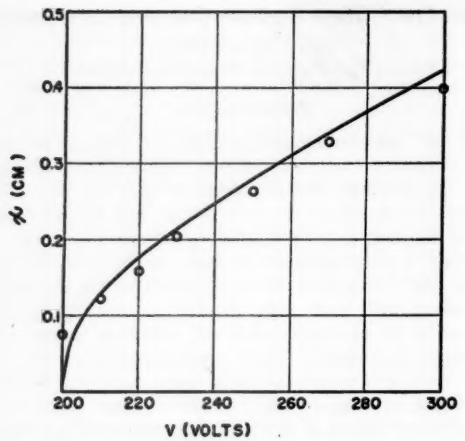

FIG. 1. Sheath thickness as a function of collector voltage for a 200-volt beam.

where J is the current density, V_0 is the beam voltage, and V is the collector potential. This is valid for V either greater or less than V_0. If $V>V_0$ the sheath appears at the collector; if $V<V_0$, the sheath appears at the entrance electrode (grid), in agreement with the theory.

These sheaths are similar to those which form around electrodes and probes in plasmas, but differ in that the electrons are traveling with beam velocity rather than with a velocity characteristic of the temperature of an electron gas. As a matter of fact, if the beam is assumed to have an energy comparable to that of an electron gas in a typical plasma so that $V_0 \ll V$, then the above equation reduces to the Childs-Langmuir space-charge relation, which applies to sheaths in a plasma.

Experimental results are given in Fig. 1. These are for a magnetically collimated beam; 0.70 cm in diameter and 1 cm long, with a current of 35 ma, and a beam potential of 200 volts. More complete data will be published later.

[1] E. G. Linder and K. G. Hernqvist, J. App. Phys. (to be published).

Some Remarks on the Analysis of the First U-Spark Spectrum

J. C. VAN DEN BOSCH
Zeeman Laboratory, Amsterdam, The Netherlands
August 9, 1950

IN a recent letter to the editor[1] McNally has discussed the work on the classification of the first U-spark spectrum. In this connection we wish to make a few remarks.

First of all, McNally makes the statement that the author[2,3] places the low level of Group A, with 3 f-electrons, roughly 20,000 cm^{-1} above the lowest level of Group B (with 4 f-electrons). This is incorrect. Indeed, we searched for a difference of the order of 20,000 cm^{-1} between the two systems. The result was negative, as was described very clearly on page 504 of reference 3. However, 17 high even levels could be added to the system of Group B (with 4 f-electrons) between 51,000 cm^{-1} and 61,000 cm^{-1} above the level $5f^4 7S_{7/2}(0.00)$. On page 505 of reference 3 the ground levels of both system A and system B were put at 0.00, indicating that no connection between the systems was found.

McNally remarks[1] that approximately eleven arc lines were used for determining the 17 high even levels. We do not think this is correct. In fact, among the lines used there are several with an intensity (as given in the M.I.T. table[4]) in the arc a little higher than in the spark. As it is very difficult to separate the U I and U II spectra (the I.P. of U I is just about 4 volts), we do not think that one can conclude that these lines are really arc lines. All intensities are relative numbers, taken from different plates. So the difference of a few units between intensities below 20 is too small to make possible a real separation between arc and spark lines.

As an example, we may use the line λ4285.745 classified in U II in the system with 3 f-electrons as a transition $278_{11/2}-f^3d^2\,{}^6M_{13/2}$.[5] Kiess, Humphreys, and Laun classified this line as a U I line.[6] The line fits very well, however, in the U II spectrum ($\Delta\nu=0.05$).[5]

The intensities given by different authors are—, 6, 2, 6, 3, respectively, arc M.I.T.,[4] spark M.I.T.,[4] Zeeman Laboratory,[6] arc Kiess,[7] spark Kiess.[8] As there are no other data available (e.g., Zeeman effect), one can not decide whether this is really an arc or a spark line. The data given by M.I.T.[4] on one side and by Kiess c.s. on the other are in fact in opposition to each other. Most lines used for determining the 17 high even levels are weak lines with small differences between estimated arc and spark intensities. We think, therefore, that it is of not much value to attach great importance to the differences between the estimated intensities, except when there is a really outstanding intensity either in the arc or in the spark.

In order to confirm the classification of several lines of U II we had often to use our own wave-length measurements, as in the M.I.T. tables[4] many weak lines are missing.

The discrepancy between observed and calculated ν-values[3] is is never higher than 0.12 cm^{-1} for the 78 lines which give the 17 high even levels. Only 7 have a $\Delta\nu$ larger than 0.10 cm^{-1} and they are weak lines for which this is quite possible.

All other lines have a $\Delta\nu$ which is smaller than 0.10 cm^{-1}, and for even 50 of them this value is less than 5 units in the last decimal.

The main reason we thought the configuration with 4 f-electrons to be lower than with 3 f-electrons was that this is the case in the Nd II spectrum, where even only the $4f^4 6s$ configuration has been found. As described in the paper mentioned above[3] from this point of view we made a very careful investigation of well-known real differences between low levels, but without success. So it seems to be more and more probable that the distance between the two systems is very small. Then the interconnecting lines will lie in the infra-red, in which we agree with McNally. We are looking again for the connection between the two systems.

[1] J. R. McNally, Jr., Phys. Rev. **77**, 417 (1950).
[2] J. C. van den Bosch, thesis, Amsterdam (June, 1948).
[3] J. C. van den Bosch, Physica **15**, 503 (1949).
[4] *M.I.T. Wavelength Tables* (John Wiley and Sons, Inc., New York, 1939).
[5] Reference 3, p. 510.
[6] Schuurmans, van den Bosch, and Dijkwel, Physica **13**, 117 (1947).
[7] Kiess, Humphreys, and Laun, J. Research Nat. Bur. Stand. **37**, 57 (1946).
[8] Private communication.

Isotopic Separation due to Settling in the Atmosphere*

JOHN H. MCQUEEN
University of Virginia, Charlottesville, Virginia
August 4, 1950

THE possibility of the separation of isotopes of the atmospheric gases due to settling in the earth's gravitational field was first pointed out by Lindemann and Aston[1] over thirty years ago. However, apparently due to stirring in the atmosphere and to the difficulty of collecting samples at sufficiently high altitudes, this separation has not been previously found. The recent development of methods of collecting air samples with high altitude rockets suggested that this separation should be investigated.

The analogous problem of the separation of the isotopes of gases in a centrifugal field has been investigated thoroughly experimentally and the separations found were in agreement with theory.[2] Also the effects of stirring, temperature variation, etc., on the separation in a centrifugal field have been studied both experimentally and theoretically.[2] Consequently, with this information available it should be possible to determine the

TABLE I. Isotope separation in the atmosphere.

Height of sampling (km)	Date of sampling	Separation (percent)
55.4–58.8	7–21–49	3.9±0.4
53.6–57.7	6–2–49	2.7±0.3
49.0–59.8	7–26–48	2.7±0.5
50.4–53.3	12–6–48	0.4±0.3
48.8–47.6	8–30–49	0.8±0.3
41.4–44.9	12–6–49	Less than 0.3

stirring in the atmosphere by the difference between the measured separation and the calculated separation produced by the gravitational field of the earth. With this in view air samples were obtained from Mr. H. W. Niel of the University of Michigan and the U. S. Army Signal Corps in the altitude range from 40 to 60 kilometers. These samples were analyzed with a 60° Nier-type mass spectrometer. Since the method of sampling was known to reduce the oxygen content of the samples, determinations were made only of the change in the abundance ratio of N^{14} and N^{15}. The method of analysis compared the ratio of the intensity of the $N^{14}N^{14}$ molecular ion beam (mass No. 28) to that of the $N^{14}N^{15}$ molecular ion beam (mass No. 29) in the sample to that in a standard sample collected at ground level. The results of these analyses are given in Table I.

The separations in percent were obtained from the abundance ratio of the mass numbers 28 to 29 in the sample minus that in the standard divided by that in the standard, the quantity multiplied by 100. The deviations indicated are the mean deviations of at least four sets of readings for each sample. The comparatively low precision of the analysis was due to a high background in the instrument at mass No. 29 (seven percent in some cases) which had to be subtracted from the readings.

It is clear from the data that isotopic separation does take place in the atmosphere above 40 km. These separations are less than the calculated values which show a great deal of stirring in the atmosphere especially at 40 km and below. Also the effect of possible "storms" is indicated. However, a large number of air samples collected at both higher and lower altitudes must be analyzed before reliable calculations of atmospheric stirring can be made by this method.

The author wishes to thank Dr. J. W. Beams for suggesting this problem and to express appreciation to Dr. L. B. Snoddy for his interest in and consultation concerning the progress of the work and to thank Mr. F. W. Linke for constructing the spectrometer tube used.

* This work was supported by Naval Ordnance contract.

[1] Lindemann and Aston, Phil. Mag. 37, 523 (1919).
[2] J. W. Beams, J. App. Phys. 8, 795 (1937); Rev. Mod. Phys. 10, 245 (1938). Beams and Skarstrom, Phys. Rev. 56, 266 (1939).

Ionic Mobilities and the Electric Quadrupole Moment of N_2

M. H. JOHNSON
Nucleonics Division, Naval Research Laboratory, Washington, D. C.
July 26, 1950

RECENTLY the electric quadrupole moment of N_2 has been determined from the pressure broadening of a microwave ammonia line on admixing nitrogen to the ammonia gas.[1] If the quadrupole moment is written as qea_0^2 where e is the electronic charge and a_0 the Bohr radius, the value of $q=0.96$ was found. We shall show that this value of q can account for the mobility of positive ions in N_2.

In a collision between an ion (charge e) and an N_2 molecule, separated by a distance r, the quadrupole electrostatic potential energy is of the order $qe^2a_0^2r^{-3}$. When this energy is comparable to the thermal energy, kT, the kinetic energy of the ion can be substantially altered by the quadrupole electric field. The impulse transmitted to the ion by the electric field will not be averaged out by the rotational motion of the molecule because the kinetic energy of rotation, also kT, is insufficient to maintain the rotation against the electrostatic torque. Consequently a collision radius, r_0, can be defined by the equality

$$(r_0/a_0)^3=qe^2(a_0kT)^{-1}. \quad (1)$$

The corresponding ionic mean free path, l, is given by

$$l=(n\pi r_0^2)^{-1}, \quad (2)$$

where n is the molecular density. The diffusion coefficient, D, can be obtained from the familiar formula

$$D=vl/3, \quad (3)$$

where v is an average value for the velocities of ion and molecule. An approximate value of v is

$$v=[1.5kT(m_1^{-1}+m_2^{-1})]^{\frac{1}{2}}, \quad (4)$$

where m_1 and m_2 are the masses of ion and molecule, respectively. For N_2 at NTP we thus find

$$D=0.044(1+m_1/m_2)^{\frac{1}{2}}\ \text{cm}^2/\text{sec}. \quad (5)$$

The corresponding mobility, $eD/(kT)$, is $1.9(1+m_1/m_2)^{\frac{1}{2}}$ cm/sec./volt/cm. Evidently the mobility should be governed by the quadrupole interaction up to temperatures such that r_0 becomes equal to the mean molecular diameter of kinetic theory.

The mobilities of many positive ions have been measured[2] and found to be accurately equal to $2.00(1+28/m)^{\frac{1}{2}}$ cm/sec./volt/cm where m is the molecular weight of the ion. The agreement with the estimate following Eq. (5) indicates that the mobility of positive ions in N_2 is mainly determined by the quadrupole moment of N_2 for temperatures under 900°K.

[1] R. R. Howard and W. V. Smith, Phys. Rev. 79, 132 (1950).
[2] Mitchell and Ridler, Proc. Roy. Soc. (A) 146, 911 (1934).

Microwave Investigation of SCSe

BØRGE BAK,* RAYMOND SLOAN, AND DUDLEY WILLIAMS
Ohio State University,† Columbus, Ohio
August 7, 1950

MICROWAVE investigations of the spectra of the linear molecules[1] OCS and[2] OCSe have yielded many interesting results (isotopic effects, l-type doubling, etc.). Ample reason thus exists for investigating the microwave spectrum of the related linear molecule SCSe, which is richer in naturally occurring abundant isotopic species than are the other two molecules. However, the prospects for a successful investigation were somewhat doubtful, since the dipole moment of SCSe was unknown but was thought to be rather small; to a first approximation the dipole moment would be expected to be equal to the difference between the moments of OCSe and OCS, which is only 0.022 debye unit. Recent tests in this laboratory have revealed, however, that the spectrum can be observed by methods involving Stark-effect modulation at high field intensities.

The SCSe sample was prepared by the usual procedure[3] and was purified by careful fractionation (B.P. 83.85° to 83.95°C at 750 mm). Mass spectroscopic analysis showed the presence of approximately one percent impurity consisting[4] of OCSe, OCS, CSe_2. An attempt to remove the impurity was only partially successful, and the absorption lines of OCSe and OCS appeared on the spectrograms at the expected positions.

The microwave absorption experiments were carried out in a 10-ft. absorption cell containing a Stark electrode. The square-wave modulation technique was employed; the square wave was biased to ground and was applied at a frequency of 5 kc/sec. At a Stark field intensity of 2000 v/cm, absorption lines attributable to SCSe appeared, but the Stark components were not resolved. Resolution of the Stark components was still incomplete when the

TABLE I. Tentative assignment of most intense lines in the $J=5\rightarrow6$ transition of SeCS.

Isotopic species	Ground vibrational state (Mc/sec.)	l-type components (Mc/sec.)	(Mc/sec.)	Moments of inertia (a.m.u.—A²)
$S^{32}C^{12}Se^{82}$	24,021	24,048	24,075	252.49
$S^{32}C^{12}Se^{80}$	24,203	24,214	24,230	250.59
$S^{32}C^{12}Se^{78}$	24,376	24,386	24,406	248.81
$S^{32}C^{12}Se^{77}$	24,508	24,521	24,527	247.47
$S^{32}C^{12}Se^{76}$	24,602	24,614	24,627	246.53

field was increased to 6000 v/cm, at which point arcing between the Stark electrode and the walls of the guide began.

The preliminary frequency measurements for the most intense lines in the $J=5\rightarrow6$ transition are given in Table I along with a tentative assignment. Since the Stark pattern was not completely resolved, the frequencies given in Table I may be in error by as much as 4 Mc/sec.; this is especially true in the case of the l-type components. The moments of the inertia are believed to be correct to ±0.10 a.m.u.—A². Although these preliminary values are not sufficiently precise for accurate determination of internuclear distances, they may be valuable for thermodynamic work.

The present investigation is being extended to include the lines associated with the $J=4\rightarrow5$ and $J=6\rightarrow7$ transitions, some of which have already been observed. It is hoped that improvements in the absorption cell will permit the use of higher Stark fields and that more accurate frequency measurements can be made. At that time, a report on the less abundant isotopic species will be made.

* Now at the Chemical Laboratory of The University of Copenhagen.
† This research has been made possible through support and sponsorship extended by the Geophysical Research Directorate of the Air Force Cambridge Research Laboratories under contract with the Ohio State University Research Foundation. It is published for technical information only and does not represent recommendations or conclusions of the sponsoring agency.
[1] Townes, Holden, and Merritt, Phys. Rev. **74**, 1113 (1948).
[2] Strandberg, Wentink, and Hill, Phys. Rev. **75**, 827 (1949).
[3] Brisco, Peel, and Robinson, J. Chem. Soc. **1929**, 56 (1929).
[4] We are indebted to Mr. S. R. Smith and Miss T. B. Enzer of the Chemistry Department for the analysis.

Isotopic Constitution of Thulium*

C. R. LAGERGREN AND M. E. KETTNER
Department of Physics, University of Minnesota, Minneapolis, Minnesota
August 3, 1950

TO date the only investigation of the isotopic constitution of thulium is that of Aston[1] who reported in 1934 that thulium consists of a single isotope of mass 169. In his report Aston mentioned having difficulty with his apparatus and gave no estimate of upper limits to the existence of other possible isotopes. Recent improvements in mass spectrometry prompted a re-examination of this element.

Our study has verified that thulium is simple to a high degree. The analysis was made with a 60°-type mass spectrometer, described by Leland,[2] incorporating an electron multiplier to give increased sensitivity in ion detection. The sample used was Tm_2O_3, "specure" brand, supplied by Johnson, Matthey and Company, Ltd., London. Ions were obtained by thermionic emission from a tungsten filament coated with a paste made by wetting the sample in distilled water.

A preliminary run at a relatively low emission temperature revealed the presence of ions at all masses in the range 162 to 176. At this temperature all ion intensities were of the same order of magnitude, but with an increase in emission temperature the ratios of all peak heights to that at 169 were found to decrease markedly. This indicated that the presence of peaks other than at 169 was in the main due to impurities rather than to isotopes of thulium. To obtain maximum reduction of the impurity intensities relative to thulium the emitting filament was operated at the highest temperature compatible with stable performance of the spectrometer. The relative ion intensities observed are given in column 2 of Table I.

TABLE I. Ion intensities in the mass range 162 to 176.

Mass No.	Observed intensity	Assumed impurities SmO^+ 0.070 percent	Er^+ 0.48 percent	Yb^+ 0.10 percent	Lu^+ 0.39 percent	Total	Relative abundance of thulium
1	2	3	4	5	6	7	8
162	~0.001		0.0007			~0.001	<0.001
163	0.011	0.011				0.011	<0.002
164	0.016	0.0079	0.0077			0.016	<0.002
165	0.010	0.0097				0.010	<0.002
166	0.166	0.0052	0.160			0.165	<0.02
167	0.115		0.110			0.110	<0.02
168	0.144	0.019	0.130	0.0001		0.149	<0.02
169	100.000						100.00
170	0.087	0.016	0.072	0.003		0.091	<0.01
171	0.015			0.014		0.014	<0.002
172	0.022			0.022		0.022	<0.003
173	0.016			0.016		0.016	<0.002
174	0.032			0.032		0.032	<0.004
175	0.382				0.380	0.380	<0.04
176	0.023			0.013	0.010	0.023	<0.003

Table I also includes a quantitative account which explains the observed intensities in terms of impurities. Assuming the presence of impurity ions, namely SmO^+, Er^+, Yb^+, and Lu^+, in the amounts shown at the heading of columns 3 to 6 respectively and accepting the isotopic constitution of these elements as reported,[3] one arrives at constructed intensities (column 7) which are in good agreement with the observed intensities for all of the small peaks. Consequently it seems reasonable to conclude that the intensities observed at all masses except at 169 can be attributed to impurities. This would then permit isotopes of thulium in amounts not greater than the accuracy with which the observed intensities could be experimentally established. Although the observed and constructed amounts agree everywhere to within five percent, some of the observed intensities may be subject to as much as a 10 percent error. The latter figure was used in arriving at the values in column 8 for the upper limits of possible isotopes of thulium.

We wish to thank Professor A. O. C. Nier for his suggestion of this study and his interest in it. The construction of the apparatus was aided materially by grants from the Graduate School and the Minnesota Technical Research Fund subscribed to by General Mills, Inc., Minneapolis Star-Journal and Tribune, Minnesota Mining and Manufacturing Company, Northern States Power Company, and Minneapolis Honeywell Regulator Company.

* This research was supported by a joint ONR and AEC grant.
[1] F. W. Aston, Proc. Roy. Soc. **A146**, 46 (1934).
[2] W. T. Leland, Phys. Rev. **77**, 634 (1950).
[3] Sm: Inghram, Hess, and Hayden, Phys. Rev. **73**, 180 (1948).
Er and Yb: Same as reference 2.
Lu: Hayden, Hess, and Inghram, Phys. Rev. **77**, 299 (1950).

On Nuclear Quadrupole Moments

R. STERNHEIMER
Los Alamos Scientific Laboratory, Los Alamos, New Mexico
July 17, 1950

IT was pointed out by Rabi that the hyperfine splitting due to the nuclear quadrupole moment includes the effect of an electric quadrupole moment induced in the electron shells. In order to obtain a crude estimate of the moment induced in a core of closed shells we consider the Thomas-Fermi model. For the electrons of maximum energy $E=0$, the momentum p is given by

$$\frac{p^2}{2m}=\frac{Ze^2\chi}{r}+\frac{e^2Q(3\cos^2\theta-1)}{4r^3}, \qquad (1)$$

TABLE I. Effect of the induced quadrupole moment.*

Element	Z	Orbital	R	$\langle V\rangle a_H^3$	$\langle 1/r^3\rangle a_H^3$	$Q/(10^{-24}\ \text{cm}^2)$	$Q_{\text{corr}}/(10^{-24}\ \text{cm}^2)$
B	5	$2p$	0.220	0.860	1.18	0.06[a], 0.03[b]	0.077[a], 0.038[b]
Al	13	$3p$	0.121	1.04	2.57	0.156	0.177
Sc	21	$3d$	0.452	1.89	1.26	——	——
Ga	31	$4p$	0.055	2.21	12.1	0.232[c], 0.146[d]	0.245[c], 0.155[d]
In	49	$5p$	0.038	1.66	13.2	1.144[e], 1.161[f]	1.189[e], 1.207[f]
Eu	63	$4f$	0.405	9.29	6.88	1.2[g], 2.5[h]	2.0[g], 4.2[h]
Lu	71	$5d$	0.125	4.52	10.9	5.9[i], 7.0[j]	6.7[i] 8.0[j]
Ac	89	$6d$	0.116	1.28	3.33	——	——

* In the last two columns of this table the superscripts refer as follows to different sotopes: [a] B^{10}, [b] B^{11}, [c] Ga^{69}, [d] Ga^{71}, [e] In^{115}, [f] In^{113}, [g] Eu^{151}, [h] Eu^{153}, [i] Lu^{175}, [j] Lu^{176}.

where χ is the Thomas-Fermi function at a point in the electron cloud, r is the length of the vector from the nucleus to this point, and θ is the angle included by this vector and the axis of the nuclear quadrupole moment Q. The density of electrons ρ is $8\pi p^3/3h^3$. Let $\Delta\rho$ be the density due to the second term of (1). Thus,

$$\Delta\rho = 8\pi p_0^2 \Delta p/h^3, \tag{2}$$

where Δp is the change of momentum associated with the term containing Q, and p_0 would be the maximum momentum, p, for $Q=0$. We have

$$(p_0\Delta p)/m = e^2Q(3\cos^2\theta - 1)/4r^3. \tag{3}$$

From (1), (2), (3) we obtain

$$\Delta\rho = \pi(2me^2/h^2r^3)^{\frac{1}{2}}(Z\chi/r)^{\frac{1}{2}}Q(3\cos^2\nu - 1). \tag{4}$$

The potential due to $\Delta\rho$ is that of a quadrupole moment ΔQ:

$$\Delta Q = 2\pi\int_0^\pi\int_0^\infty r^4(3\cos^2\theta - 1)\Delta\rho\sin\theta d\theta dr$$
$$= (16\pi^3/5)(2me^2/h^2)^{\frac{1}{2}}QZ^{\frac{1}{2}}\int_0^\infty(\chi r)^{\frac{1}{2}}dr. \tag{5}$$

Upon substituting $r=(0.88534a_H/Z^{\frac{1}{3}})x$, where x is the Thomas-Fermi variable (a_H = Bohr radius), we obtain

$$\Delta Q = [2(1.7707)^{\frac{1}{2}}/5\pi]Q\int_0^\infty(\chi x)^{\frac{1}{2}}dx. \tag{5a}$$

We shall consider the case of a single valence electron; its radial wave function times r will be called v. The energy of interaction E_Q with the nuclear moment can be written:

$$E_Q = -AQ\int_0^\infty(v^2/r^3)dr, \tag{6}$$

where A is a constant. For the interaction $E_{\Delta Q}$ with the induced moment, the penetration of the electron inside the core leads to:

$$E_{\Delta Q} = \frac{2(1.7707)^{\frac{1}{2}}AQ}{5\pi}\int_0^\infty dr v^2\left\{\frac{1}{r^3}\int_0^x(\chi x')^{\frac{1}{2}}dx' + r^2\int_x^\infty[(\chi x')^{\frac{1}{2}}/r'^5]dx'\right\}, \tag{7}$$

where $r'=(0.88534a_H/Z^{\frac{1}{3}})x'$, and the limit x of the x' integrals pertains to r. The difference in sign of E_Q and $E_{\Delta Q}$ reflects the fact that the electrons concentrate in the region where the potential due to the nuclear Q is positive, thus tending to compensate the effect of the nucleus. If we let $R=-E_{\Delta Q}/E_Q$, then Q is $1/(1-R)$ times the value previously obtained without the induced effect. We write

$$R = 0.2998\langle V\rangle/\langle 1/r^3\rangle, \tag{8}$$

where

$$\langle V\rangle = \int_0^\infty dr v^2\left\{\frac{1}{r^3}\int_0^x(\chi x')^{\frac{1}{2}}dx' + r^2\int_x^\infty[(\chi x')^{\frac{1}{2}}/r'^5]dx'\right\}, \tag{9}$$

$$\langle 1/r^3\rangle \doteq \int_0^\infty(v^2/r^3)dr, \tag{10}$$

with: $\int_0^\infty v^2dr = 1$.

Table I gives the values of R for eight elements. The values of $\langle V\rangle$ and $\langle 1/r^3\rangle$ are also listed, together with the quadrupole moments[1] as determined at present and the corrected values, in the cases where data are available. The valence electron functions were obtained by means of the Thomas-Fermi potential,

$$[(Z-1)\chi+1]e/r.$$

A more detailed discussion will be given in a forthcoming paper.

It is a great pleasure to thank Professor Edward Teller, who suggested this problem, for many helpful discussions. I am also indebted to Drs. H. M. Foley and H. Snyder for stimulating discussions.

[1] J. E. Mack, Rev. Mod. Phys. 22, 64 (1950).

Nuclear Magnetic Resonance for K^{39}

T. L. COLLINS
Department of Physics, University of British Columbia, Vancouver, Canada*
July 31, 1950

NUCLEAR magnetic resonance has been found for K^{39} at 1.59 Mc in a field of 8000 gauss using a recording oscillating-detector spectrometer. The sample was 1 ml of saturated aqueous solution of KNO_3. The frequency of the K^{39} resonance was compared with the frequency of the N^{14} resonance in concentrated nitric acid by repeatedly substituting the samples in the oscillator coil without otherwise disturbing the apparatus. The frequencies repeated within the accuracy of a General Radio Type 620-A frequency meter. The result is

$$\nu(K^{39})/\nu(N^{14}) = 0.64580 \pm 0.00006.$$

Using the measurements of Proctor and Yu[1] on N^{14} in nitric acid, we find

$$\mu(K^{39})/\mu(H^1) = 0.13999 \pm 0.00002$$

with no diamagnetic correction or allowance for possible chemical shift. This value agrees with molecular beam measurements.[2]

* Work supported by the National Research Council of Canada.
[1] W. G. Proctor and F. C. Yu, Phys. Rev. 77, 716 (1950).
[2] Kusch, Millman, and Rabi, Phys. Rev. 55, 1176 (1939).

Magnetic Moments of Odd Nuclei

A. DE-SHALIT
E.T.H., Zürich, Switzerland
August 1, 1950

IT has been pointed out by Wangsness[1] that a certain regularity seems to be associated with the magnetic moments of odd nuclei differing by two neutrons. There are, however, certain difficulties with the proposed classification. Besides failing to explain the pair $_{47}Ag^{107,109}$ as mentioned by Wangsness, it fails also in the cases of $_{81}Tl^{203,205}$, $_{55}Cs^{133,135}$, and $_{55}Cs^{135,137}$, not to mention the case[2] of $_1H^{1,3}$. Moreover, by using the argument given by Wangsness as to the effect of the increase and decrease of electric charge density in the nucleus one should expect the inverse effect to take place by the addition of a pair of protons or an alpha-particle instead of two neutrons. This is confirmed by the two pairs $_0n^1 - {}_2He^3$ and $_{78}Pt^{195} - {}_{80}Hg^{199}$, but stands in contradiction to the known cases of: $_{17}Cl^{37} - {}_{19}K^{39}$, $_{55}Cs^{137} - {}_{57}La^{139}$, $_{48}Cd^{113} - {}_{50}Sn^{115}$, $_{36}Kr^{83} - {}_{38}Sr^{87}$, $_{54}Xe^{131} - {}_{56}Ba^{135}$.

A simple and exclusive rule to summarize these data with the exception of the Cs isotopes is the following. An addition of either two protons or two neutrons to an odd nucleus, provided it leaves its spin unchanged, "pushes" its magnetic moment away from a line intermediate to the Schmidt lines.[3]

Except for the cases of $_1H^3$ and $_2He^3$ this actually means that the magnetic moments are pushed toward a better agreement with the naive one-particle model by the addition of such pairs.

Using the above rules inductively one may argue that the nuclei $(Z+2k, N+2m)$ should be closer to the Schmidt lines than the initial (Z, N) nucleus, provided that the spins of the initial,

as well as those of the intermediate ones, are the same. In fact a number of pairs, such as $_{21}Sc^{45}-{}_{23}V^{51}$, $_{31}Ga^{71}-{}_{35}Br^{81}$, $_{31}Ga^{71}-{}_{37}Rb^{87}$, $_{35}Br^{81}-{}_{37}Rb^{87}$, $_{35}Br^{79}-{}_{37}Rb^{87}$, probably show this regularity.

No explanation is offered for this empirical rule; it seems not to be directly connected with the magic numbers which unfortunately do not as yet make their appearance at all in the data of magnetic moments of nuclei.

I should like to thank Dr. D. C. Peaslee for helpful discussions.

[1] R. Wangsness, Phys. Rev. **78**, 620 (1950).
[2] See the table given by J. E. Mack, Rev. Mod. Phys. **22**, 64 (1950).
[3] See, for instance, the graphs given in L. Rosenfeld, *Nuclear Forces* (Interscience Publishers, Inc., New York, 1948), p. 394, or L. W. Nordheim, Phys. Rev. **75**, 1894 (1949).

Natural Spread of the Conic Distribution of the Čerenkov Radiation

YIN-YUAN LI
Department of Physics, University of Illinois, Urbana, Illinois
June 27, 1950

A VISIBLE radiation with remarkable spatial asymmetry was first observed by Čerenkov (1934)[1] during his observations on high speed electrons penetrating transparent materials. Frank and Tamm[2] showed theoretically that the Čerenkov radiation is propagated along the generatrices of a cone that has the direction of the motion of the electron as the axis and a half-angle θ_0 given by

$$\cos\theta_0 = c/\kappa u. \tag{1}$$

u and c/κ are, respectively, the velocity of the fast electron and the phase velocity of the emitted light in the medium, and κ is the refractive index of the medium. They drew this conclusion by simply considering the enforced interference of coherent rays emitted along the electron path. In order to treat the problem in greater detail it is necessary to take into account the fact that the speed of an electron decreases by a small jump whenever a photon is emitted. With this modification we find that the spatial asymmetry of the radiation is given[3] by

$$I(\theta) = I(\theta_0)(\sin^2 y)/y^2, \tag{2}$$

where

$$y = 2\pi(L/\lambda)(c/u\kappa - \cos\theta). \tag{3}$$

λ is the wave-length of the radiation, θ the angle between the direction of the motion of the electron and the direction of the radiation, and L the length of a free path. In the Frank-Tamm theory the finiteness of L is overlooked. By assuming an infinite L we obtain a maximum at $\theta_0 = \cos^{-1}(c/u\kappa)$ as sharp as a δ-function. Since this will not be correct for a finite L, we have a half-breadth $\Delta\theta(\frac{1}{2})$ for the maximum at θ_0 determined by

$$\sin y = y/\sqrt{2}, \tag{4}$$

i.e.,

$$(2\pi\kappa L/\lambda)\sin\theta_0 \Delta\theta(\tfrac{1}{2}) \simeq 160^\circ. \tag{5}$$

We see that $\Delta\theta(\frac{1}{2})$ decreases remarkably with the increase of the free path. It is very interesting to notice that the natural width of the spatial distribution due to the finiteness of the free path of an electron shows quite an analogy to the natural width of a spectral line due to the finite lifetime of an excited atom. In order to estimate the half-breadth which should be actually observed we must substitute the mean free path L_{Av} of the electrons in the medium into (5). From the Frank-Tamm theory we obtain an estimate of $L_{Av} \simeq 10^{-3}$ cm in the case of a medium with $\kappa_{Av} = 1.5$, a transmission region extending from 2000A to 20,000A, and an electron beam with $\frac{1}{4}$ Mev kinetic energy. For the visible radiations the half-breadth is

$$\Delta\theta(\tfrac{1}{2}) \simeq 1^\circ/(1 - c^2/u^2\kappa^2)^{\frac{1}{2}} \simeq 2^\circ. \tag{6}$$

This conservative estimate of $\Delta\theta(\frac{1}{2})$ serves only as a lower limit, since other radiative as well as non-radiative collisions[4] inevitably cause a shorter free path. Consequently, even if a carefully collimated homogeneous beam and a thin plate are used, we still have an observable spread of the visible radiation in its angular distribution.[5] For electrons much faster than those mentioned above ($u \sim c$) both the number of emissions per cm and $\sin\theta_0$ increase slowly with the energy of the incident beam, and so the change of $\Delta\theta(\frac{1}{2})$ from (6) must be very slight. On the other hand, when the velocity of the incident electrons is not far from the threshold c/κ the variation of $\sin\theta_0$, which appears in (5), becomes much greater than that of L_{Av}. The widening of the angular spread with the decreasing of the energy of the incident beam should be noticeable.

The half-breadth of the conic distribution of the Čerenkov radiation is in all cases of the order of several degrees. It is of the same order of magnitude that Ginsburg[6] found theoretically for the angle of separation between two cones of the Čerenkov radiation from a double refractive crystal. His prediction has never been verified, though in recent experiments[5,7,8] mica, with its optical axis in various orientations with respect to the incident beam, has been extensively used. We have made clear that each cone has its natural spread; they closely overlap and cannot be resolved. Probably the double-cone radiation can never be actually observed, even if substances with large deviation among the refractive indices, such as calcite, are used. Furthermore, we can now understand that even if an ideally collimated homogeneous beam and a thin plate of *high dispersive power* are used, no rainbow spectrum with red inside violet (see Eq. (1) and κ increases with frequency) should be observable. Each color has a natural spread of several degrees, and so a close overlap of different colors is inevitable.

In passing we should point out that the Frank and Tamm prediction of the vanishing of radiation when $u \leq c/\kappa$ is merely due to the incorrect assumption of an infinite free path. From Eq. (2) and a finite L we see that when $u < c/\kappa$, it is the distinct maximum of intensity that disappears but not the radiation. The total intensity decreases continuously with the electron velocity decreasing through the threshold c/κ.[9] The non-vanishing radiation intensity when $u < c/\kappa$, as well as the finite spread of radiation also can be easily understood by considering the Huygens construction of coherent rays[10] emitted along a *short* electron free path.

[1] P. A. Čerenkov, Comptes rendus U.S.S.R. **8**, 451 (1934); **12**, 413 (1936); **14**, 102, 105 (1937); Phys. Rev. **52**, 378 (1937).
[2] I. Frank and Ig. Tamm, Comptes rendus U.S.S.R. **14**, 109 (1937).
[3] L. I. Schiff, *Quantum Mechanics* (McGraw-Hill Book Company, Inc., New York, 1949). The derivation of Eq. (2) is given in detail, pp. 261–265.
[4] A quantum theory of the radiative process which produces the photons of the Čerenkov effect will appear in a forthcoming paper.
[5] H. O. Wyckoff and J. E. Henderson, Phys. Rev. **64**, 1 (1943). The observed spread of radiation was interpreted by the authors as *simply* due to the finite width of slits and range of electron energy.
[6] V. L. Ginsburg, J. Phys. U.S.S.R. **3**, 101 (1940).
[7] G. B. Collins and V. G. Reiling, Phys. Rev. **54**, 499 (1938).
[8] J. M. Harding and J. E. Henderson, Phys. Rev. **74**, 1560 (1948).
[9] See Eqs. (36) and (37) of E. Fermi, Phys. Rev. **57**, 485 (1940).
[10] See Fig. 1 of reference 5.

Isomers and Shell Structure

PETER AXEL
*University of Illinois, Urbana, Illinois**
July 26, 1950

THERE are 59 genetically related isomers whose transitions can be classified into the $l=4$ or $l=5$ forbiddenness groups by lifetime-energy considerations.[1] The data that have appeared since the last classification was published[1] have not changed the general conclusions. While the reliable internal conversion measurements are consistent with l assignments, they do not independently define the l values. More internal conversion measurements could both check internal conversion and isomeric transition theory.

The simple spin-orbit coupling shell model, as presented by Maria Mayer,[2] makes specific spin and parity predictions for the

TABLE I. List of isomers. For comparison with shell structure the odd mass number isotopes (odd A) are separated into odd proton and odd neutron.

$l=4$				$l=5$			
Odd A				Odd A			
Odd P	Odd N	Even or unknown A		Odd P	Odd N		Even or unknown A
Rh^{103}	Se^{77}	Sc^{46}	Sb^{124}	V^{91}	Zn^{69}	Te^{131}	Sc^{44}
Ag^{107}	Se^{81}	Co^{58}	Sb^{126}	Nb^{91}	Sr^{87}	Xe^{131}	In^{114}
Ag^{109}	Kr^{79}	Co^{60}	Cs^{134}	Nb^{95}	Sn^{117}	Xe^{135}	Pb^{204}
	Kr^{81}						
Au^{197}	Kr^{83}	Br^{80}	Ta^{182}	Tc^{97}	Sn^{119}	Ba^{133}	Pt
	Sr^{85}	Nb^{94}	Ir^{192}	In^{113}	Te^{121}	Ba^{135}	
	Cd^{111}	Tc^{94}	Er	In^{115}	Te^{123}	Ba^{137}	
	Xe^{127}	Rh^{104}	Yb		Te^{125}	Pt^{197}	
	Dy^{165}	In^{112}	Yb		Te^{127}	Hg^{199}	
	Hf^{179}	Sb^{122}	W		Te^{129}		

energy levels of odd A nuclei. A comparison of these predictions with the lifetime-energy l value assignments demonstrates some major inconsistencies. The presently accepted isomers are arranged in Table I according to l value.

The odd nucleon shells of interest are those from 29 to 50, 51 to 82, and 83 to 126. In agreement with theory, none of these isomers are found below nucleon number 39. From 39 to 50, shell structure predicts both the $p_{1/2}$ and $g_{9/2}$ levels. A mixture of magnetic 2^4 and electric 2^5 pole radiation ($l=5$) is therefore possible. The nearby $p_{3/2}$ level would give electric 2^3 pole radiation ($l=3$). Thus, while the $8l=5$ isomers in this region are consistent with shell theory, the $9l=4$ isomers are not. The $f_{7/2}$ subshell, which could combine with $p_{1/2}$ to give $l=4$, is in the shell below 28 and shell binding energies are much greater than the excitation energy of these $l=4$ isomers (<200 kev).

From 51 to 82 nucleons the available subshells are: $g_{7/2}$, $d_{5/2}$, $d_{3/2}$, $s_{1/2}$, and $h_{11/2}$. At 63 neutrons, the $g_{7/2}s_{1/2}$ combination could give an $l=4$ transition. However, the ground-state spin of Cd^{111} is ½ and the isomeric transition occurs between two excited states. In the upper part of the shell, $h_{11/2}$ can combine with either $d_{3/2}$ or $s_{1/2}$ to give $l=5$; no $l=4$ is predicted. Therefore, Xe^{127} and Au^{197} are inexplicable. The 13 $l=5$ isomers in this region do fit shell theory. However, in 4 cases (Sn^{117}, Te^{121}, Te^{123}, and Te^{125}), the isomeric transition is followed by a gamma-ray. In each case the cross-over transition is absent in contradiction to predictions based on shell theory.

In the final shell, there is consistency for both $l=4$ and $l=5$. At 99 and 107 neutrons, $l=4$ is consistent with the $h_{9/2}p_{3/2}$ or $h_{9/2}p_{1/2}$ combinations. At 119 neutrons, both $l=5$ transitions can be explained by the $i_{13/2}p_{3/2}$ or $i_{13/2}f_{5/2}$ combinations.

To summarize, the simple spin-orbit coupling shell model would predict no $l=4$ transitions below nucleon number 50 and none in the upper parts of higher shells. Of the 14 odd A nuclei only the 2 with nucleon number above 82 are consistent with this prediction. On the other hand, the 23 odd A isomers in the $l=5$ group would fit nicely into this shell model if the absence of cross-over transitions could be explained. Internal conversion measurements can provide valuable additional tests of both isomeric classification and shell structure models.

* This work was assisted by the joint program of the ONR and AEC.
[1] P. Axel and S. Dancoff, Phys. Rev. 76, 892 (1949).
[2] M. G. Mayer, Phys. Rev. 78, 16 (1950).

On the Determination of the P-P Interaction from Scattering Experiments

CARL-ERIK FRÖBERG
Department of Mechanics and Mathematical Physics, Lund University, Lund, Sweden
August 1, 1950

AS is well known[1,2] low energy $P-P$ scattering can be accounted for by several different potential functions. On the other hand, it has recently been proved by Jauho[3] that the nuclear $P-P$ phase shift under certain physically reasonable conditions determines the potential function uniquely. Thus it seems to be of some interest to make a direct attempt at a calculation of the $P-P$ interaction from available experiments.

Starting from the radial equation

$$y''+\left(1-\frac{2\alpha k}{r}\right)y=-V(r)y \tag{1}$$

we can easily prove the relation

$$k\sin\eta(k)=\int_0^\infty uVy\,dr \tag{2}$$

[$y(0)=0$, $y(\infty)\sim\sin(\xi+\eta)$; u is the regular Coulomb wave function, determined by $u(0)=0$, $u(\infty)\sim\sin\xi$, where $\xi=kr-\alpha\ln 2kr+\arg\Gamma(i\alpha+1)$]. Replacing y by u we can solve for V

$$V=-\frac{2}{\pi}\kappa^3\cdot\int_0^\infty\frac{\varphi(\alpha,\beta)\sin\eta}{\alpha^3}\,d\alpha.$$

Here

$$2\alpha=k/\kappa;\quad \kappa r=\beta;\quad kr=\rho;$$
$$\varphi(\alpha,\beta)=\{(d/d\rho)[u(\alpha,\rho)v(\alpha,\rho)]\}_{\rho=\beta/2\alpha};$$

v is the irregular Coulomb wave function, determined by $v(\infty)\sim\cos\xi$.

Since we know practically nothing of $\sin\eta$ for small values of α (i.e., for high energies), it is natural to use a cut-off convention. Choosing the lower limit in the integral (3) proportional to β, which seems to be reasonable, we find that V can be represented very nicely by Yukawa functions, and we obtain the following values of the range r_0 and the strength J using the cut-off radius a:

a	r_0(cm)	J(Mev)
$\beta/2$	$1.21\cdot10^{-13}$	18.2
β	$1.00\cdot10^{-13}$	22.0

A fuller account of the investigation will be published elsewhere (*Arkiv. f. Fysik*) together with a table of irregular Coulomb wave functions.

[1] L. Rosenfeld, *Nuclear Forces* (Interscience Publishers, Inc., New York, 1948).
[2] J. D. Jackson and J. M. Blatt, Rev. Mod. Phys. 22, 77 (1950).
[3] Jauho, Ann. Acad. Sci. Fenn. (to be published).

Theory of Natural Alpha-Radioactivity

BERNARD L. COHEN*
Department of Physics, Carnegie Institute of Technology, Pittsburgh, Pennsylvania
June 21, 1950

RECENT measurements of cross sections of (α,n), $(\alpha,2n)$, and $(\alpha,3n)$ reactions[1-3] give excitation functions which, when compared with Weisskopf's calculation of alpha-capture cross sections,[4] require that the parameter r_0 in the expression for the nuclear radius

$$r=r_0A^{\frac{1}{3}}\times10^{-13}\text{ cm} \tag{1}$$

be taken as 1.5 in the calculation of the Coulomb barrier penetration factor.[5] Using this in the expression for the decay constant, λ,

$$\lambda=\Gamma_\alpha/\hbar=\Gamma_{0\alpha}P(r_0)/\hbar \tag{2}$$

(where Γ_α is the width for alpha-emission, $\Gamma_{0\alpha}$ is the alpha-width without barrier, and $P(r_0)$ is the Coulomb barrier penetration factor which is a very sensitive function of the assumed value of r_0), requires, in order to obtain the observed values for λ,

$$\Gamma_{0\alpha}\sim10^5\text{ ev}. \tag{3}$$

Condition (3) is in considerable disagreement with the value given by Bethe in his many-body theory of alpha-decay[6]

$$\Gamma_{0\alpha}\sim1\text{ ev}. \tag{4}$$

This discrepancy may perhaps be explained as follows. Bethe assumed that neutron widths and alpha-particle widths without

barrier are roughly equal, and calculated the neutron widths from

$$\Gamma_n/E^{\frac{1}{2}}\sim 4\times 10^{-4}(\text{ev})^{\frac{1}{2}}. \quad (5)$$

Which was empirically determined from the available data on neutron capture cross sections. Relation (5) is furthermore in agreement with the expected relation that, all other things being equal,

$$\Gamma \propto E^{\frac{1}{2}} \quad (6)$$

which can be derived from considerations of the momentum space degeneracy of the outgoing particles.

In line with the suggestions of Weisskopf, Feshbach, and Peaslee,[7] Wigner[8] has shown that widths are also proportional to level spacing, D, whence (6) becomes

$$\Gamma \propto E^{\frac{1}{2}}D. \quad (7)$$

Relation (5) must then be considered valid only in cases of neutron capture. Since level spacings in neutron capture are about 10 ev, in general, (5) must be replaced by

$$\Gamma/E^{\frac{1}{2}}D\sim 4\times 10^{-5}(\text{ev})^{-\frac{1}{2}}. \quad (8)$$

Applying (8) to the case of alpha-decay,

$$E^{\frac{1}{2}}\sim 2.5\times 10^{3}(\text{ev})^{\frac{1}{2}}, \quad D\sim 10^{5}\text{ ev}$$

whence

$$\Gamma\sim 10^{4}\text{ ev}. \quad (9)$$

The value of D was obtained from the measured energy differences between various energy groups in natural alpha-decay.[9] Comparison of (9) with (3) indicates that the ratio of neutron width to alpha-width without barrier is about 0.1; and comparison of (3) with the width from the one-body theory (0.8 Mev) indicates that the "probability of formation of an alpha-particle" in a nucleus (i.e., the correction for the many-body theory over the one-body theory) is about one-eighth. Either of these last two values may be in error by a factor of 10 or more.

* Present address: Oak Ridge National Laboratory, Oak Ridge, Tennessee.

[1] I. Halpern, Phys. Rev. 76, 248 (1949).
[2] E. L. Kelly and E. Segrè, Phys. Rev. 75, 999 (1949).
[3] G. M. Temmer, Phys. Rev. 76, 424 (1949).
[4] V. F. Weisskopf, *Lecture Series in Nuclear Physics* LA24, Chapter 36, p. 105.
[5] B. L. Cohen, Carnegie Inst. Tech. Technical Report No. 4, May 20, 1950, unpublished.
[6] H. A. Bethe, Rev. Mod. Phys. 9, 161 (1937).
[7] Weisskopf, Feshbach, and Peaslee, Phys. Rev. 71, 145 (1947).
[8] E. P. Wigner, Am. J. Phys. 17, 104 (1949). T. Teichmann, doctoral thesis, Princeton University.
[9] Reference 6, p. 169.

Ionization by Recoil Particles from Alpha-Decay

RUFUS C. LING AND JULIAN K. KNIPP
Institute for Atomic Research and Department of Physics, Iowa State College, Ames, Iowa
August 8, 1950

SINCE the energy loss of a slow heavy particle is predominantly to recoiling gas atoms, ionization by secondary heavy particles contributes a large fraction of the total ionization resulting from a slow heavy particle that is stopped in a gas.

Let η be the ionization efficiency $\omega^e I/E$ of a primary particle of energy E which gives rise to the number of ion pairs I, where ω^e is the energy loss per ion pair of a particle the energy of which is very high. The ionization efficiency satisfies an equation of the form

$$\frac{d}{dE}(E\eta)=\mu+\lambda\int_0^{E_m'} dE'k(E,E')\eta'(E'), \quad \eta(0)=0, \quad (1)$$

in which $\eta'=\omega^e I'/E'$ is the ionization efficiency of a gas atom of energy E' in its own gas. The functions μ and λ are given by

$$\mu=\omega^e\sigma^e/(b^e+b^r), \quad \lambda=b^r/(b^e+b^r),$$

where σ^e is the cross section for the production of an ion pair in a collision between the primary particle and an atom of the gas including ionization by ejected electrons, and b^e and b^r are the stopping cross sections per atom for the loss of energy by the primary particle to excitation and ionization and to atomic recoil, respectively. The kernel $k(E, E')$ is

$$\sigma(E,E')E'\Big/\int_0^{E_m'} dE'\sigma(E,E')E',$$

where $\sigma(E, E')$ is the cross section per unit energy range for the production of a recoil atom of energy E'; the maximum energy transferred to an atom is $E_m'=4MM'E/(M+M')^2$. The ionization efficiency η' of a gas atom satisfies the differential-integral equation obtained from (1) by regarding the initial particle as identical in nature with the recoil atom; the corresponding functions are designated μ', λ', etc.

We consider a heavy particle ($Z=82$, $M=208$ proton masses) in argon. For velocities less than about $0.4v_0$, where $v_0=e^2/\hbar$, the primary scattering is very nearly spherically symmetrical in the center of gravity system and therefore $k(E, E')\approx 2E'/E_m'^2$. Deviations from spherically symmetrical secondary scattering are unimportant until velocities of the primary particle considerably greater than $0.12v_0$ are attained ($E\gg 78$ kev). Up to these velocities b^r and $b^{r\prime}$ are practically constant,[1] except for negligible linear decrease at very small velocities.

There is evidence[2] to indicate that $\sigma^{e\prime}$ increases very roughly as the square root of the energy in the kev range. Assuming $\mu'\approx a'v'$ and $\lambda'\approx 1$, we obtain $\eta'\approx 10a'v'/7$. Since primary ionization alone gives $(2/3)a'v'$, it is seen that on this basis 53 percent of the ionization due to a gas atom in its own gas is secondary heavy particle ionization.

Assuming, likewise, $\mu\approx av$ and $\lambda\approx 1$, (1) gives

$$\eta\approx[\tfrac{2}{3}a+(16a'\gamma/21)]v, \quad v/v_0\ll 1, \quad (2)$$

where $\gamma=2M/(M+M')=1.68$.

The ionization in argon by single recoil particles from Po, ThC, and ThC′ has been measured by Madsen.[3] His data are well represented by (2) with the proportionality factor

$$\tfrac{2}{3}a+16a'\gamma/21=\omega^e/(15.4\text{ ev})v_0.$$

In order to estimate $\sigma^{e\prime}$, we put a equal to a' and obtain $a'\approx\omega^e/(30\text{ev})v_0$. With[1] $b^{r\prime}\approx 30\pi a_0^2\epsilon_0$, this gives $\sigma^{e\prime}\approx 30\pi a_0^2(v/v_0)$ which at 1 kev is about 10^{-16} cm², in satisfactory agreement with the measurements of Berry,[2] who found $0.7\cdot 10^{-16}$ cm² at 1 kev, and of Rostagni,[4] who found $0.8\cdot 10^{-16}$ cm² at 600 ev. It is found from (2) that about 66 percent of the ionization by a recoil particle from natural alpha-decay is heavy-particle secondary ionization.

[1] N. Bohr, Kgl. Danske Vid. Sels. Math.-fys. Medd. 15, nr. 8 (1948).
[2] H. W. Berry, Phys. Rev. 62, 378 (1942). Neutral N_2, He, and H_2, each in its own gas, showed increasing ionization cross sections at 8 kev. However, A in A showed a decreasing cross section, which effect may be due to the increase with energy in the number of secondaries used to measure the beam although it is difficult to see why it should be so large with A.
[3] B. S. Madsen, Kgl. Danske Vid. Sels. Math.-fys Medd. 21, nr. 8 (1945).
[4] A. Rostagni, Nuovo Cimento 11, 24 (1934).

The Meson Spectrum and Meteorological Variations in Cosmic-Ray Intensity

D. C. ROSE
National Research Council of Canada, Ottawa
August 17, 1950

THE production spectrum of mesons has been derived by Sands[1] from calculations based on the sea-level spectrum and the known behavior of mesons produced in the atmosphere. His results indicate approximately an inverse power law spectrum of the form $dE/E^{2.5}$ over a wide range of energies. Calculations of a similar nature have been made in Ottawa in an attempt to present a physical picture of the meteorological variations in cosmic-ray intensity at sea level. These calculations when compared with measured values of the "barometer effect" give a surprising amount of information about the meson spectrum in the higher momentum range (above about 1.8 Bev/c).

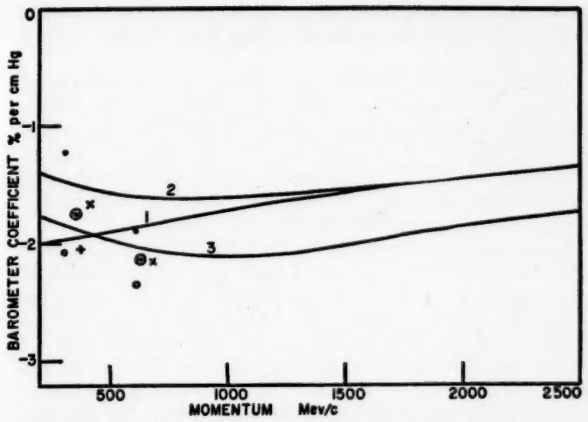

FIG. 1. The integral barometer effect. Curve 1: for the spectrum k/E^3. Curve 2: for the Wilson spectrum. Curve 3: for the Wilson spectrum altered at high energies. Observed points taken simultaneously are marked alike. ⊙ = mean values of the two groups of observed points.

Considering mesons moving downwards in the atmosphere it can be shown that the intensity at sea level N_G can be expressed by the equation

$$N_G = \frac{k}{E^\gamma} \exp\left[-\frac{\mu}{\tau}\int_{p_m}^{p_G} \frac{dp}{\rho\{P_G+\alpha(p_G-p)\}}\right], \qquad (1)$$

where k/E^γ represents the spectral intensity at an effective level of production where the pressure is p_m. μ is the mass and τ the mean life of the meson at rest; p and ρ are the pressure (in grams per cm²) and the density in the atmosphere respectively, and P is the momentum. α is the momentum loss per gram per cm² and is considered constant over any range equivalent to the momentum loss in the atmosphere for values above minimum ionization. The subscript G refers to values at sea level and m to values at the meson production level.

By numerical integration of this equation for a standard atmosphere and again for an atmosphere differing in pressure only, "differential" barometer coefficients were calculated. For comparison with measured values "integral" coefficients were necessary. These were calculated by a further numerical integration.

Continuous recordings with counter telescopes have been taken for over a year at Ottawa and at Resolute (Canadian Arctic, geomagnetic latitude 83) and analyzed with respect to barometric variations. The measurements included herewith were taken from four series of over three months each. During three of the series two counter telescopes were operated together. One was shielded by sufficient absorber so that it would accept mesons above about 300 Mev/c; the second, above about 600 Mev/c.

The points marked in Fig. 1 show the measured barometer coefficients. The most significant feature of these results is that the barometer coefficient is lower in magnitude at lower momentum than at higher momentum. This was consistent in each series of measurements where two counter telescopes were used simultaneously.

The calculations based on Eq. (1) gave a number of unexpected results. If the production spectrum were flat, that is, if $\gamma=0$, the barometer coefficient would be very much smaller in magnitude than that observed, probably too small to measure. The integral barometer coefficient is very sensitive to the value of γ and not very sensitive to the values of the other quantities in the equation.

Curve 1 in Fig. 1 represents the calculated integral barometer coefficient based on a spectrum where $\gamma=3$ over a range of 1.8 to 40 Bev/c. Curve 2 is based on the Wilson spectrum[2] using a smooth curve through the Wilson points shown by Rossi[3] (Fig. 4). For this curve γ is close to 3 above 3 Bev/c but decreases rapidly to a value of about -1 at 1.8 Bev/c. Curve 3 corresponds to a spectrum identical to that of Wilson at the lower energies but for energies above 3 Bev/c $\gamma=3.5$. The production spectra for these three curves are shown in Fig. 2.

A simple power law spectrum such as curve 1 will not make the barometer effect curve upward at low momenta as is required by the experimental results. Though the accuracy is not great the results favor strongly a production spectrum of the type shown by curve 3. At low momenta this is derived from Wilson's measurements but above about 3 Bev/c the curve has a steeper slope than that corresponding to Wilson's spectrum. This greater slope at high momenta is in agreement with the corresponding part of the sea-level spectrum of Caro, Parry, and Rathgeber,[4] but curve 3 would not be as consistent with the lower momenta part of their spectrum.

The details of these calculations and measurements are being prepared for publication at an early date.

[1] M. Sands, Phys. Rev. **77**, 180 (1950).
[2] J. G. Wilson, Nature **158**, 414 (1946).
[3] B. Rossi, Rev. Mod. Phys. **20**, 537 (1948).
[4] Caro, Parry, and Rathgeber, Nature **165**, 688 (1950).

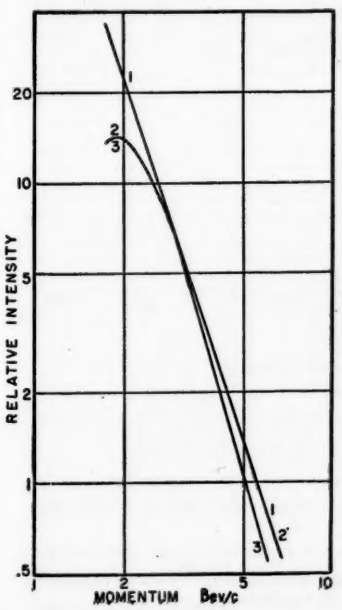

FIG. 2. The production spectrum of mesons. Curve 1: the spectrum k/E^3. Curve 2: computed from the Wilson spectrum at sea level. Curve 3: computed from the Wilson spectrum altered at high energies.

Gamma-Ray Resonances Produced by the Bombardment of Phosphorus with Protons*

G. R. GROVE,† JOHN N. COOPER, AND J. C. HARRIS
Ohio State University, Columbus, Ohio
August 18, 1950

PHOSPHORUS has been bombarded with protons from the Ohio State University electrostatic generator and eleven narrow gamma-ray resonances have been observed for proton energies between 1000 and 1650 kev. Both thick and thin targets of zinc phosphide, evaporated on tantalum disks, have been studied. The excitation curve obtained from a target of approximately 10-kev thickness at 1.3 Mev is shown in Fig. 1. The peaks of the eleven resonances correspond to proton energies of 1.075, 1.105, 1.140, 1.168, 1.270, 1.427, 1.472, 1.500, 1.543, 1.592, and 1.615 Mev, respectively. The relative spacings of the levels are estimated to be accurate within 3 kev and the absolute values of the energies are believed to be not more than 10 kev in error. The energies of the protons were obtained by measuring the current through the coils of the analyzing magnet by use of a standard resistance and a Leeds and Northrup Type K potentiometer. Calibration of the magnet current was made in terms of the accurately known lithium and fluorine resonances.[1]

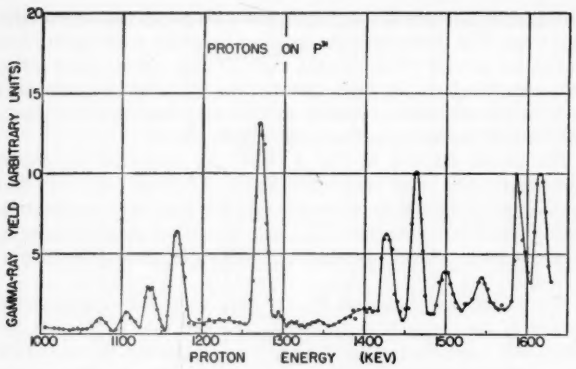

FIG. 1. Gamma-ray yield from a thin (87 micrograms/cm²) zinc phosphide target.

Thick targets both of tantalum and of zinc have been bombarded to make sure that none of the observed peaks can be attributed to either of these elements. Tantalum gave a very small yield which increased slowly with proton energy. The yield from the thick zinc target was much greater than that from the tantalum, but there was no indication that any of the reported resonances could be attributed to zinc.

Absorption measurements of the radiation from the 1.270-Mev resonance have been made with lead, copper, and aluminum. The results are consistent with a gamma-ray of approximately 12-Mev energy. This suggests that the reaction under consideration is $P^{31}(p,\gamma)S^{32}$, since the gamma-rays from $P^{31}(p,\alpha\gamma)Si^{28}$ would be of much lower energy. The proton capture process is 10.7-Mev exothermic; consequently, a 12-Mev gamma-ray is indicated if the excited sulfur nucleus decays to the ground state by a single transition.

The natural half-width of the 1.270-Mev resonance is estimated to be 6.5 kev; this corresponds to a mean life of the excited state of the compound nucleus of approximately 10^{-19} sec. The cross section for this resonance is calculated to be about 6×10^{-28} cm².

Recently calcium phosphide targets have been prepared by vacuum evaporation. With these targets it is planned to repeat measurements in the region covered in Fig. 1 and to extend the energy range downward to overlap the regions previously studied by Curran and Strothers[2] and by Tangen.[3]

The authors are deeply indebted to Professor R. G. Herb of the University of Wisconsin for his generous help and especially for making available to us the results of his unpublished preliminary work on the phosphorus resonances.

* Assisted by the joint program of the ONR and AEC.
† AEC Predoctoral Fellow.
[1] Herb, Snowden, and Sala, Phys. Rev. 75, 246 (1949).
[2] S. C. Curran and J. E. Strothers, Proc. Roy. Soc. London (A) 172, 72 (1939).
[3] R. Tangen, Norske Videnskabers Selskabs Skrifter, 1946 NR1.

New Evidence for the Existence of Positively Charged Particles Appearing near Beta-Ray Emitters*

GERHART GROETZINGER AND DAVID KAHN
Institute for Nuclear Studies, University of Chicago, Chicago, Illinois
August 17, 1950

A SERIES of investigators[1–6] have reported in cloud chambers the appearance of tracks of positively charged particles emerging from beta-ray emitters, which by energy considerations should not decay by the emission of positrons. Two objections against the cloud-chamber evidence of these positive particles have been brought forward,[7–9] which seem, however, not to be valid.[1,2,5,6] The observed momentum loss in foils and the multiple scattering of the particles producing these tracks in cloud chambers have been shown to be consistent with a mass of about twice the electron mass.[3,6]

The fact remained, however, that the existence of these particles could not be ascertained with other means than the cloud chamber. Especially, experiments using beta-ray spectrometers have led to negative results.[10] A tentative explanation that the lack of a production layer—it is customary to mount the radioactive substance in spectrographs on a thin film—might be responsible for the non-appearance of these particles was disproved.[11]

Assuming as another alternative a finite lifetime which does not allow the particles to traverse a path length of a conventional spectrograph, we were led to experiments with a 180-degree (non-evacuated) spectrograph of only 4.4 cm path length. The spectrograph had slits of 2 mm width and was operated with a P^{32} source[12] deposited on aluminum and an Ilford G5 Nuclear Track plate as a detector.[13] The plate to be exposed was wrapped in a layer of paper and placed with one edge against the exit slit so that particles emerging from the spectrograph after being further deflected by the magnetic field outside the spectrograph would hit various parts of the plate at a glancing angle of approximately 17 degrees.

Plate 1 was exposed one minute with a magnetic field of a direction and strength to support the passage of electrons with a momentum corresponding to 1600 gauss-cm. Plate 2 was exposed for 13.5 hours with a field of the same strength but of opposite direction. Plate 3 was exposed for 13 hours under the same conditions as plate 2 with respect to the field, but with a $\frac{1}{16}$-in. thick aluminum plate obstructing the passage of particles through the spectrograph. The three plates were simultaneously developed using the temperature variation method[14] 17 days after their manufacture. They were scanned along three lines (*a*, *b*, and *c*) perpendicular to the direction of the particles at the position of the exit slit. These lines had a distance of 4.2, 8.5, and 11.9 mm respectively from the edge of the plate closest to the exit slit. The points where particles traversing the spectrograph were expected to hit the plates at the position of these lines are indicated by the letters *A*, *B* and *C* respectively.

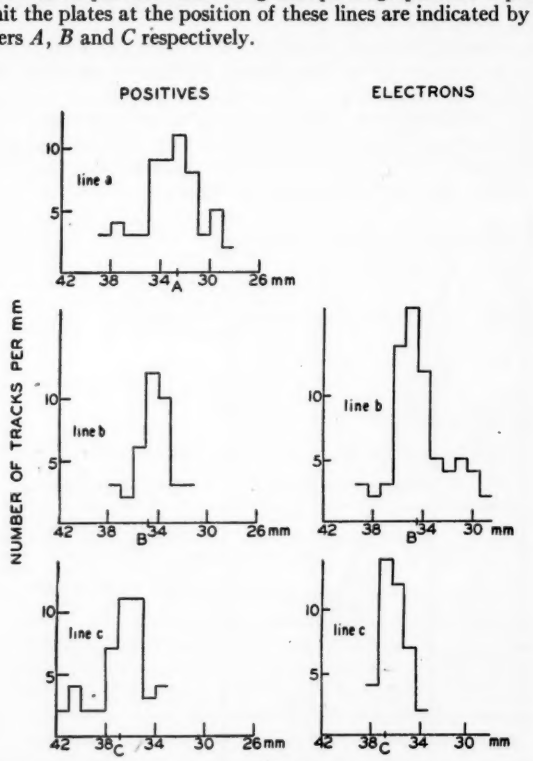

FIG. 1. Distribution of tracks due to electrons (right side) and positive particles (left side) in the photographic plates along three lines (*a*, *b*, and *c*). *A*, *B*, and *C* represent points on these lines where particles traversing the spectrograph are expected to enter the plate.

Due to the fact that the plates did not record electrons of energies exceeding 60 to 70 kev it was not possible, in general, to observe the track of a particle of 1600 gauss-cm entering the emulsion. For this reason tracks of a minimum length of approximately 20 microns were recorded, having at one end the familiar cluster of developed grains corresponding to the stopping of the particle and a decreasing grain density towards the other end where the track is either lost in the background or in some cases comes close to the surface of the emulsions. This criterion should eliminate a large fraction of the electrons due to the x-rays produced by the P^{32} source since these electrons will have in general rather low energies resulting in shorter tracks.

Plate 1 was scanned along the lines *b* and *c*. As can be seen from the two diagrams to the right of Fig. 1, the peaks in the number of tracks per millimeter in the direction of scanning (representing an area of 0.25 mm²) are displaced with respect to each other. From the position of the points *B* and *C* indicated in the figure and the position of each peak it is seen that the displacement of the peaks is approximately that which is to be expected for electrons having traversed the spectrograph (momentum approximately 1600 gauss-cm) and being further deflected by the magnetic field before being stopped in the emulsion. The left column of Fig. 1 shows the results of the scanning along rows *a*, *b*, and *c* of plate 2 in which case the appearance of positive particles was expected. It can be seen that peaks appear which coincide with the points *A*, *B*, and *C*. This indicates that they are due to the passage of positively charged particles through the spectrograph. Plate 3, which was scanned along line *b*, did not show any peak. All the three plates showed about the same number of tracks per millimeter (satisfying our conditions) in regions other than the peaks from which it follows in view of the great difference in the exposure times that the contribution of x-rays due to the P^{32} electrons to this background is negligible. Taking three tracks per millimeter as background and considering the difference in the exposure time, the ratio between positive particles and electrons of around 1600 gauss-cm, averaged for lines *b* and *c*, is found to be $\approx 8\times 10^{-4}$.[15] No attempt was made to find a difference between the tracks obtained with both directions of the field. No difference was apparent by casual observation.

* This research was partly supported by the joint program of the ONR and AEC.

[1] Bradt, Heine, and Scherrer, Helv. Phys. Acta **16**, 491 (1943). (This paper contains an extensive list of the older publications.)
[2] H. G. Heine, Helv. Phys. Acta **17**, 273 (1944).
[3] L. Smith and G. Groetzinger, Phys. Rev. **70**, 96 (1946).
[4] T. H. Pi and C. V. Chao, Phys. Rev. **72**, 639 (1947).
[5] J. S. Barlow and F. T. Rogers, Phys. Rev. **74**, 700 (1948).
[6] G. Groetzinger and F. L. Ribe, Phys. Rev. **79**, 904 (1950).
[7] C. B. A. McCusker, Nature **161**, 564 (1948).
[8] Erdman, Kokotaila, and Scott, Phys. Rev. **76**, 1262 (1949).
[9] J. H. Spaa and G. J. Sizoo, Physica **15**, 316 (1949).
[10] See e.g. K. T. Bainbridge (Account of Harwell Conference) Nature **160**, 492 (1947).
[11] H. Bradt and K. T. Bainbridge, private communication.
[12] The radioactive P^{32} was supplied by the Isotope Branch of the Atomic Energy Commission, Oak Ridge, Tennessee.
[13] The use of a mica window counter as a detector gave inconclusive results due to the difficulty of ascertaining whether particles found to traverse this (evacuated) spectrograph with a field supporting the passage of positive particles were not actually electrons scattered through the spectrograph. Another complication was the sensitivity of the counter to x-rays produced by the P^{32} electrons.
[14] M. J. Wilson and W. Vanselow, Phys. Rev. **75**, 1144 (1949).
[15] In a cloud-chamber investigation by Groetzinger, Ribe, and Kahn, to be published, it was found that the ratio of positives to electrons of all momenta with track lengths in excess of four centimeters is approximately 3×10^{-4} for a P^{32} source on an aluminum backing and approximately 2×10^{-3} for particles emerging from 0.5 g/cm² of lead covering the source.

Neutron Production by Proton Bombardment below the (p,n) Threshold*

B. Jennings, K. H. Sun, and H. A. Leiter
Westinghouse Research Laboratories, East Pittsburgh, Pennsylvania
April 20, 1950

A SMALL neutron yield has been observed when deuterium or beryllium was bombarded by protons at voltages below the established (p,n) threshold. The experimental observations on these yields are shown in Figs. 1 and 2. Several possible experimental causes such as target contamination, beam contamination with deuterons, and gamma-ray sensitivity of the neutron detectors have been considered but are insufficient to explain this "sub-threshold" neutron yield.

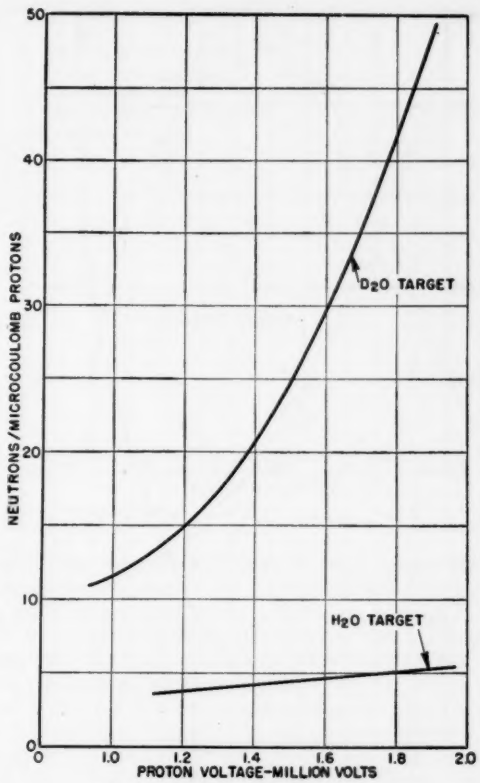

FIG. 1. Neutron yield from deuterium.

We believe that the majority of these neutrons originate from a double process of the (pd, dn) type where the energetic deuterons are formed in the deuterium target by proton-deuteron scattering and in beryllium by the $Be^9(p,d)Be^8$ reaction. These deuterons, in turn, produce neutrons in the deuterium and beryllium targets.

In deuterium, a calculation of the number of neutrons expected from such a double process has been carried out from the known cross section for p–d scattering[1] and for the (d,d) process,[2] and assuming, for comparison with experiment, spherical distribution of the resulting neutrons, good agreement was found with the experimental results shown in Fig. 1.

Neutrons from proton bombardment of Be below the threshold were also reported by Richards[3] but only on thick targets. This suggested a $(p\gamma, \gamma n)$ double process as the origin of these neutrons. The cross section of this (γ,n) process is small[4] and the neutron yield should be proportional to the bulk of Be behind the thick target surface. This dependence was not observed.

The differential cross section multiplied by 4π at 138° of the $Be^9(p,d)Be^8$ and the competing $Be^9(p,\alpha)$ reaction have been measured for proton voltages between 0.2 and 1.4 Mev and found to be[5] between 0.1 and 0.3 barn. Taking 0.17 barn as an average value, an estimate of the deuteron yield can be made, based on 1-Mev proton bombardment of a 200-kv Be target. Assuming the number of neutrons from 1.3-Mev deuterons on a thick Be target is the order of 100 per million, this calculation involving (p,d) and (d,n) processes gives order of magnitude agreement with the number of neutrons observed below the threshold.

If the above explanation for the production of "sub-threshold" neutrons in D and Be is correct, a similar process would not be expected in other elements because beryllium appears to be the only element in which an exothermic (p,d) process is known. It is

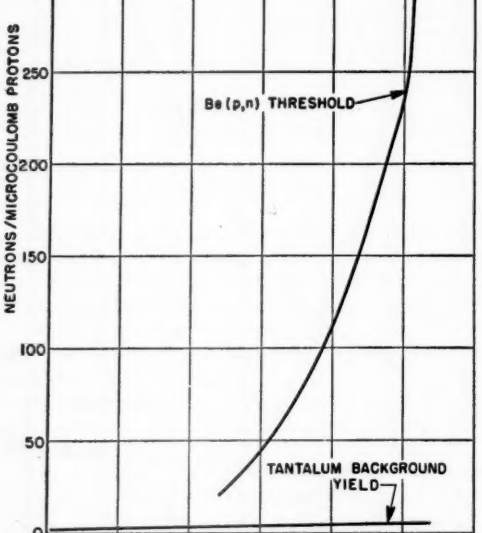

FIG. 2. Neutron yield from beryllium.

true that a $(p\alpha, \alpha n)$ process might contribute a small neutron yield especially where the (p,α) reaction is highly exothermic. However, the neutron yield from $(p\alpha, \alpha n)$ processes would be small compared to the corresponding (pd, dn) reaction because of the higher potential barrier and shorter range of the alpha-particle. From these considerations, it seems unlikely at present that the neutron yield below the threshold would affect the (p,n) studies of other elements.

* Assisted by joint program of the ONR and AEC.
[1] Sherr, Blair, Kratz, Bailey, and Taschek, Phys. Rev. **72**, 662 (1947).
[2] G. T. Hunter and H T. Richards, Phys. Rev. **76**, 1445 (1949).
[3] H. T. Richards and R. V. Smith, Report of Chicago Meeting of American Physical Society, 1949 (Phys. Rev. **77**, 752 (1950)).
[4] W. A. Fowler and C. C. Lauritsen, Phys. Rev. **76**, 314 (1949).
[5] Thomas, Ruben, Fowler, and Lauritsen, Phys. Rev. **75**, 1612 (1949). In Fig. 2 the correct cross-section scale is between 0 and 0.5×10^{-24} cm^2.
Private communication.

Chemical Shifts in the Magnetic Resonance of F^{19}

H. S. GUTOWSKY AND C. J. HOFFMAN
Noyes Chemical Laboratory, University of Illinois, Urbana, Illinois*
August 3, 1950

SEVERAL instances have been reported recently[1-4] of the dependence of nuclear magnetic resonance frequencies on the nature of the chemical compound containing the nuclei. This "chemical effect," or magnetic shielding, has been discussed theoretically[5] but the complexity of the calculations permits their application only to the simplest molecules. We are presently making an experimental survey of the wide variety of existent polyatomic fluorine compounds to determine the influence of structural factors. Initial observations suggest that, in the simpler covalent compounds, the magnetic shielding of an F^{19} nucleus chemically bound to another element is related to the position of that element in the periodic table. For elements in a given period the shielding decreases with increasing atomic number, while for elements in the same group the shielding increases with increasing atomic number. Also, in complex fluorides the shielding depends on the inductive effects of neighboring chemical bonds. Measurements of the influence of temperature on the magnetic shielding in several compounds over a total range of 225° revealed no dependence larger than the experimental error.

Observations were made using conventional equipment,[6] and a permanent magnet with field of 6375 gauss. The magnetic shielding in an "unknown" was determined, at a fixed frequency of 25–54 Mc, by alternately measuring the field biasing current necessary to center the resonance on an oscilloscope, first for the unknown and then for another, reference compound. Only samples were interchanged; the coil containing the samples remained fixed throughout. With field inhomogeneities less than 0.1 gauss, sharp lines in liquids permitted measurements of differences in the resonance field to a probable error of ±0.01 gauss or ±1.5 p.p.m. of the external field. The temperature dependence was investigated by having the sample in a cryostat and a reference sample outside as parts of a dual system excited by the same oscillator. Resonances were viewed on either a dual oscilloscope or a standard oscilloscope with a manual switch. Samples which are gases at room temperature were observed with a similar arrangement.

In Fig. 1(A) are the results for the simpler fluorides, suggesting the periodicity of the magnetic shielding. Data for the N^{14} magnetic resonance[3] in NO_3^-, CN^-, and NH_4^+ and also[7] for B^{11} in BCl_3, BBr_3 and $B(OCH_3)_3$ follow the same rules. Observations on the P^{31} magnetic resonance[7] in PCl_3, PBr_3, PI_3, P_4, and H_3PO_4 follow the period rule but the magnetic shielding in PCl_3 is slightly greater than in PBr_3, counter to the group trend for F^{19}. Figure 1(B) lists the data for various complex fluorides, discussion of which will be given in a later article.

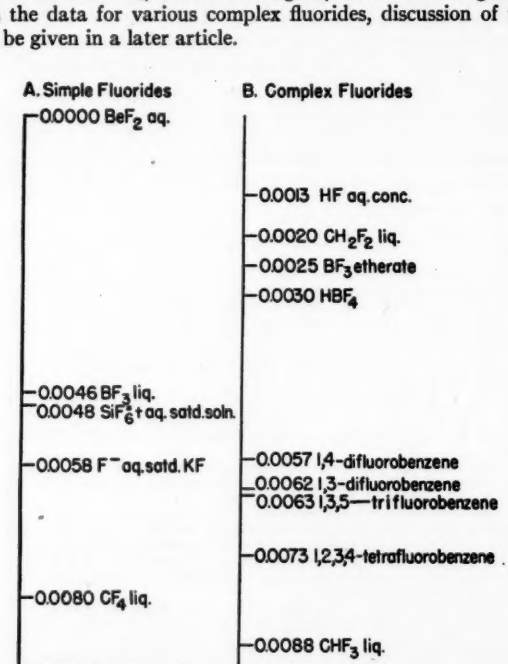

FIG. 1. Magnetic shielding of the F^{19} nucleus. The F^{19} resonance in BeF_2 is at the highest external field, thus exhibiting the largest magnetic shielding. Values given are percentage decrease in resonance field relative to BeF_2. [Except for BF_3 etherate, values in this list for compounds previously reported by Dickinson (reference 2) agree with his values when allowance is made for the difference in external magnetic fields, and a field calibration correction factor (reference 7) of 0.64 is applied to his values. Observations included Co, Cu, Fe, H, (NH_4), Mg, and Zn salts, which differed among themselves only slightly in excess of experimental error.]

Multiple resonances were found in several fluorocarbons containing fluorine atoms in differing structural positions. 2,3,5-trifluorobenzotrifluoride, $C_6H_2F_3-CF_3$, has a double resonance, one with shielding of 0.0115 percent and the other of 0.0047 percent, which in itself is rather broad and may be double. The perfluorolube oil (du Pont) resonance is a triplet with a strong center line at 0.0055 percent and shoulders at 0.0098 and 0.0002 percent. The resonance in $n-C_3F_7CO_2H$ is a doublet at 0.0053 and 0.0095 percent. Several binary mixtures were examined, including $CF_3-CCl=CCl_2$ with 1,4-difluorobenzene, 1,3,5-trifluorobenzene, and 1,2,4,5-tetrafluorobenzene. In these mixtures two resonances appeared at field values identical with those of the separate compounds.

The temperature independence of magnetic shielding was observed in perfluorolube oil from 240 to 400°K, in BF_3 etherate from 175 to 375°K, in CF_3CO_2H from 235 to 370°K, and in a mixture of 1,2,4,5-tetrafluorobenzene and $CF_3-CCl=CCl_2$ from 225 to 400°K. In the mixture only the separation of the resonance lines was followed.

Measurements are in progress on additional simple fluorides to provide more adequate information for detailed theoretical consideration. Also, we wish to report preliminary observations on the magnetic shielding of the proton resonance which in mineral oil apparently occurs at a field 0.02 to 0.05 gauss higher than in benzene, CF_3CO_2H, HBF_4, $CHCl_3$, concentrated HCl and HNO_3.

We wish to thank R. E. McClure and S. B. Yochelson for their assistance with the equipment, and R. L. Poynter for his help with a number of measurements. We are also indebted to Dr. G. C. Finger of the State Geological Survey for many of the compounds.

Equipment was provided largely through a Grant-in-Aid from Research Corporation. We also wish to express our appreciation to the Arnold Engineering Company, Marengo, Illinois, for their cooperation in the design and construction of the large permanent magnet essential to the research.

* Supported in part by the ONR.

[1] W. D. Knight, Phys. Rev. 76, 1259 (1949). This report, while mainly concerned with resonance shifts attributed to conduction electrons in metals, mentions observed chemical effects in phosphorus compounds.

[2] W. C. Dickinson, Phys. Rev. 77, 736 (1950).

[3] W. G. Proctor and F. C. Yu, Phys. Rev. 77, 717 (1950).

[4] J. E. Mack, Rev. Mod. Phys. 22, 64 (1950), Section III C2.

[5] N. F. Ramsey, Phys. Rev. 78, 699 (1950). E. Hylleraas and S. Skavlem, Phys. Rev. 79, 117 (1950).

[6] Bloembergen, Purcell, and Pound, Phys. Rev. 73, 679 (1948).

[7] W. C. Dickinson, private communication; we have confirmed his values for PCl_3, PBr_3, and H_3PO_4 and also observed PI_3 and P_4.

The β-Spectrum of C^{14}

S. D. Warshaw*
University of Southern California,† Los Angeles, California
August 17, 1950

TWO of the most striking contradictions[1] of the predictions of the nuclear shell model are given by the β-spectra of C^{14} and P^{32}. Therefore, although both of these spectra have been extensively investigated, the results are of sufficient interest—and in sufficient doubt—to warrant verification. This communication and one to be published shortly will present a careful repetition of some of these investigations.

Three previous determinations[2] of the C^{14} spectrum have indicated that the shape is allowed. Two other measurements[3] made at about the same time as the former set show at least an indication of a non-linear Fermi plot. Most of these observations had in common the use of an insoluble $BaCO_3$ source, which made the preparation of thin, uniform sources rather difficult. Feldman and Wu (using a helical focusing spectrometer) had probably the best source, since they used an aggregate thickness of only 0.015 mg/cm², and special precautions were taken to ensure that the particle size in the precipitate was small and uniform. However, Cook *et al.* (using a shaped field spectrometer) varied the source thickness from 0.13 to 0.97 mg/cm² and concluded that, since the shape of the spectrum did not depend strongly on the thickness, their observed curvature of the Fermi plot was a real characteristic, rather than an instrumental distortion. Possibly, however, the variation in the *effective* source thickness was less than they supposed; i.e., that much of the distortion was produced not in the source aggregate but rather in the individual grains of the material. However, their result was essentially corroborated by Angus, Cockroft, and Curran, who used a proportional counter technique. In the present investigation, a double thin lens spectrometer was used, with the resolution set at 2.1 percent. Previous work with this instrument[4] has confirmed the negligible amount of purely instrumental distortions. The source material was $NaHCO_3$, converted from the 40 percent enriched $BaCO_3$ obtained from the Isotopes Division at Oak Ridge. It was felt that the danger of losing a small amount of the activity by exchange with CO_2 in the atmosphere[5] would be compensated by the increased accuracy made possible by the ease of deposition of a soluble source material.

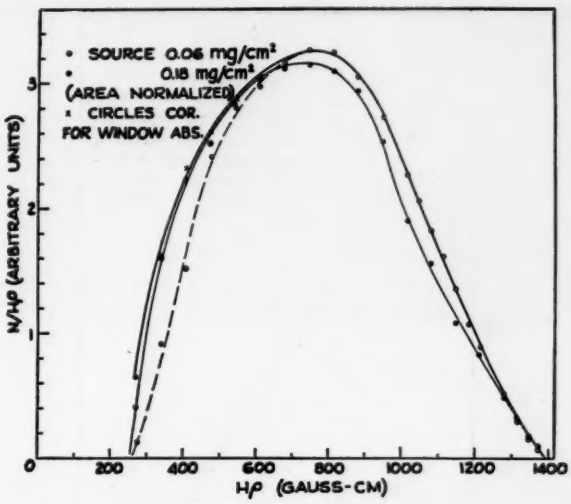

FIG. 1. Momentum distribution for C^{14}.

Thin, uniform sources were deposited on 0.01-mg/cm² Nylon loaded with Aquadag, and immediately placed in the vacuum system to prevent further loss of activity. Figure 1 shows momentum distributions for two of the sources used (0.06, 0.18 mg/cm² approximately) with both curves normalized to the same area. These represent a graphic illustration of the thick source distortion. A window correction (for a 0.05-mg/cm² Nylon window) has been applied to the thin source curve. Figure 2 shows the Fermi plots for these two curves. The thicker source apparently results in a straight line to 80 kev where the curve deviates upward. A still thicker source (0.24 mg/cm², not shown in Fig. 2) was straight only for the last 30 kev of the range. A dashed straight line has been drawn through the thin source points; here, however, there is a distinct indication that the upper solid curve (fitted to the experimental points) is convex to the energy axis, in agreement with reference 3. Below this region the curve is linear to 25 kev, while below this point the (corrected) curve rises. Assuming that the window correction is good, this rise probably is due to source thickness. The maximum (in Fig. 1) occurs at 45 kev, agreeing with Angus *et al.*[3] and the end-point energy is 155±1 kev, in agreement with the previous work.

While, therefore, it would seem that the shape is not quite allowed, this result is not very helpful in explaining the β-transition. The empirical classification is second-forbidden and the spin change is unity. Assuming that the transition is really second-forbidden the only possibility (with no parity change) is the Fermi interaction with the correction factor A_{-}' in Konopinski's notation. This factor however was not applied successfully to the observed plot. Primakoff[6] has suggested that the ground state of N^{14} is an accidental mixture of states in such proportions that the

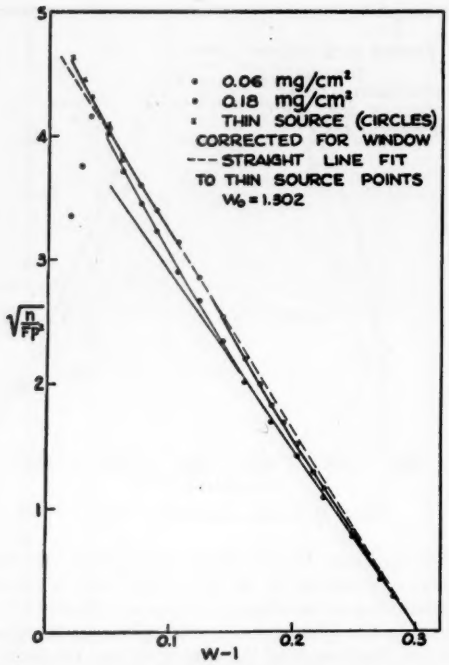

FIG. 2. Fermi plot for C^{14}.

shape may appear to be nearly allowed while the classification is still forbidden. However, Gerjuoy[7] has argued that this explanation is implausible. If the transition is really first-forbidden (unfavored) with a parity change,[7] a much wider latitude in fitting the theory to the observed spectrum shape would be permitted. This would require a modification of the shell model prediction.

I would like to thank Mr. P. S. Magee for performing the chemical conversion.

* Now at the Institute of Radiobiology and Biophysics, University of Chicago, Chicago, Illinois.
† This work was assisted by the joint program of the ONR and AEC.
[1] E. Feenberg and K. C. Hammack, Phys. Rev. **75**, 1877 (1949).
[2] L. Feldman and C. S. Wu, Phys. Rev. **75**, 1286 (1949); L. E. Glendenin and A. K. Solomon, Phys. Rev. **74**, 700 (1948); J. L. Berggren and R. K. Osborne, Phys. Rev. **74**, 1240 (1948).
[3] Cook, Langer, and Price, Phys. Rev. **74**, 548 (1949); Angus, Cockroft, and Curran, Phil. Mag. **40**, 522 (1949).
[4] Van Atta, Warshaw, Chen, and Taimuty, Rev. Sci. Inst. (to be published).
[5] M. Calvin *et al.*, *Isotopic Carbon* (John Wiley and Sons, Inc., New York, 1949), p. 123.
[6] Quoted in reference 1.
[7] E. Gerjuoy (to be published).

A Thermal Mechanism for Residual Latent Image Fading in Nuclear Emulsions

ARTHUR BEISER
Department of Physics, New York University, New York, New York
August 4, 1950

EXPERIMENTS by Mather[1] on fading rates in nuclear emulsions indicate a reduction of approximately 90 percent in the fading of proton tracks when stored prior to development in a vacuum, indicating that at least that proportion of the fading phenomena is chemical in nature, with some constituent of the atmosphere the agent involved. However, it is proposed that some or all of the residual 10 percent of the fading can be explained on the basis of the thermal ejection of electrons from the silver specks of the latent image.

This mechanism would consist in the acquisition by these electrons of sufficient energy to re-enter the conductance band of the crystal, causing an electrolytic current of silver ions to flow from the latent image into the grain. The electrons will recombine with the ions in the interior of the grain where the resulting Ag atoms cannot function as nuclei for development, a redistribution of the latent image similar to that occurring in the Herschel effect. The dissociation energy required to remove an electron from the silver specks comprising the latent image will equal the difference between the work function ϕ of the specks and the energy of the lowest state of the conductance band. The most recent value for this energy has been given[2] as 0.77 ev, and is great enought to assure the comparative stability of such images with respect to thermal decomposition at ordinary room temperatures, corresponding to an energy of approximately 0.7 ev. However, a relatively slight change in one of the factors governing the magnitude of the dissociation energy would be sufficient to alter the rate of thermal regression of a latent image at room temperature. This latter condition is fulfilled in nuclear emulsions to a certain degree, since the size of the silver specks after particle irradiation is much smaller than of those in optical emulsions, leading to a lower value for ϕ and hence to a lower value for the energy needed to release a trapped electron. The smaller size will be due to the rapidity with which a radiation particle traverses the halide grains (about $2 \cdot 10^{-14}$ sec. for 5 Mev alpha-particles). Since the migration of the silver ions through the crystal is considerably slower than that of the electrons, the sensitivity specks will acquire negative charges faster than they can be neutralized and further electrons will be repelled until sufficient silver ions have reached the specks. By that time, however, no further electrons will be available and the repelled electrons will have combined with silver ions in the interior of the crystal. Thus, in a very rapid transfer of energy to the emulsion, the latent image will tend to contain unusually small silver specks, which is generally the case. The small size also may be expected to contribute to the atmospheric instability of the latent image.

[1] K. B. Mather, Phys. Rev. **76**, 486 (1949).
[2] J. H. Webb, J. Opt. Soc. Am. **40**, 3 (1950).

Mechanism of Magnetization in Alnico V

E. A. NESBITT AND H. J. WILLIAMS
Bell Telephone Laboratories, Murray Hill, New Jersey
July 21, 1950

USING magnetic powder pattern technique,[1] new information has been obtained on the mechanism of magnetization in the alloy containing 14 percent Ni, 8 percent Al, 24 percent Co, 51 percent Fe, and 3 percent Cu (Alnico V). This permanent magnet alloy is unique in that it responds to heat treatment in a magnetic field, and the work here reported has been done to try to explain this action.

Figure 1 shows photographs of magnetic powder patterns of polycrystalline Alnico V cooled from 1300°C at 2° to 5°C per second to 810°C and then oil-quenched, a field being present from 900°C to room temperature. Figures 1(a–c) show photographs in which the specimen was magnetized vertically during heat treatment and horizontally during observation. In (a), domains are seen to lie in a vertical direction and as the field is increased from zero to successively higher values (b, c) the domain boundaries either disappear or the domains contract in width and the horizontal lines (splotches), which indicate the direction of magnetization,[1] gradually rotate toward a vertical position. When the specimen is near saturation, the boundaries of the domains disappear and the originally horizontal lines have become vertical. It is evident, therefore, that in this case the mechanism of magnetization is mainly one of rotation and not of boundary displacement.

Figure 2 shows the magnetization curve for the specimen shown in Figs. 1(a–c). The coercive force of this specimen was only 17 oersteds and yet the knee of the magnetization curve occurs in the neighborhood of 450 oersteds. This indicates that the material has a high anisotropy caused by heat treatment in a field. If this material could be divided into fine particles[2] (e.g., by precipitation

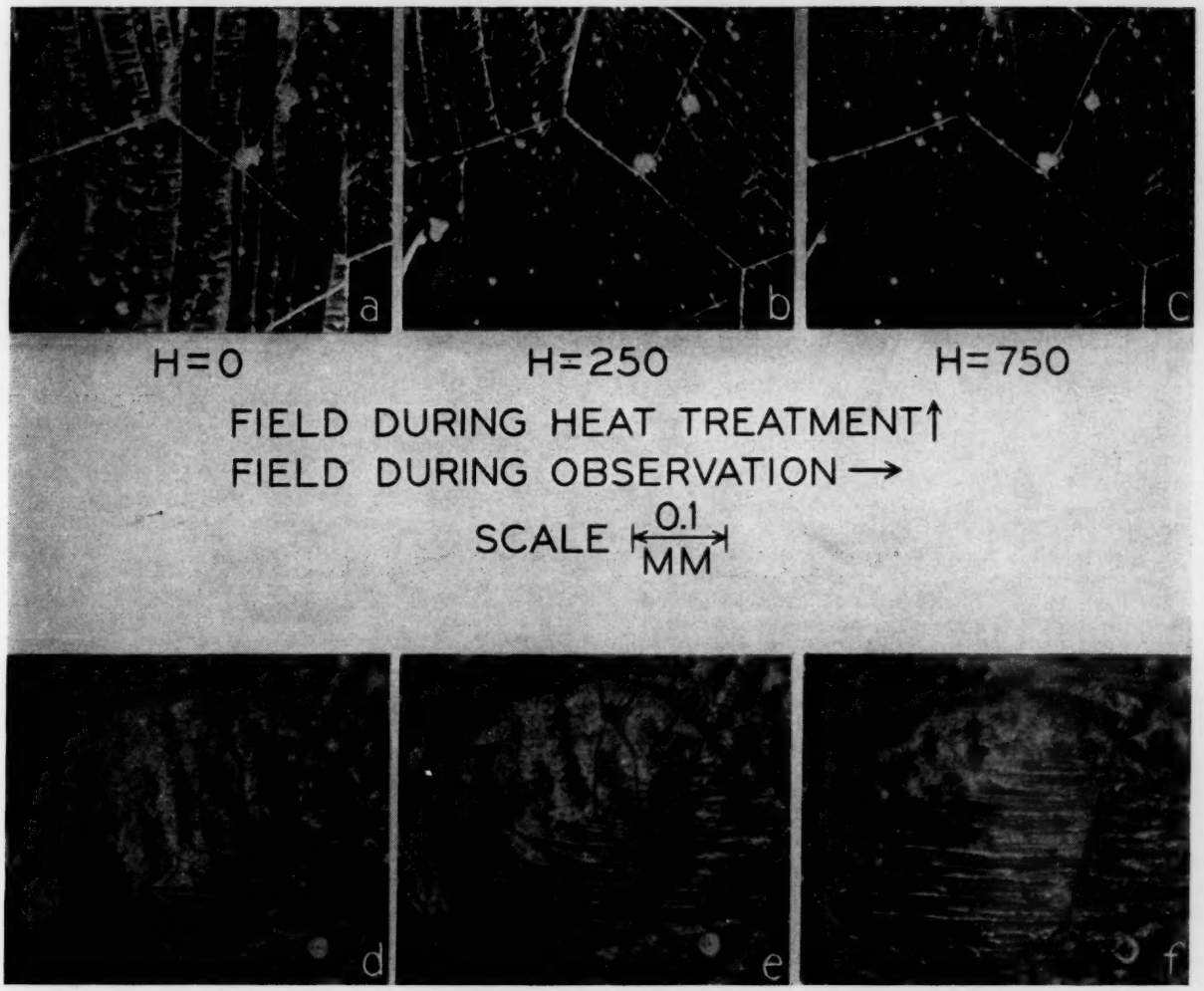

FIG. 1. Magnetic powder patterns on polycrystalline Alnico V; (a), (b), and (c) cooled from 1300°C at 2° to 5° per second to 810°C then oil-quenched a transverse field being present from 900°C to room temperature; (d), (e), and (f) standard Alnico V treatment.

of plates),[3] so that for all orientations the magnetization change would have to occur by rotation, then the anisotropy observed from the magnetization curve could account for coercive forces of the order of 400 to 600 oersteds, as observed for Alnico V.

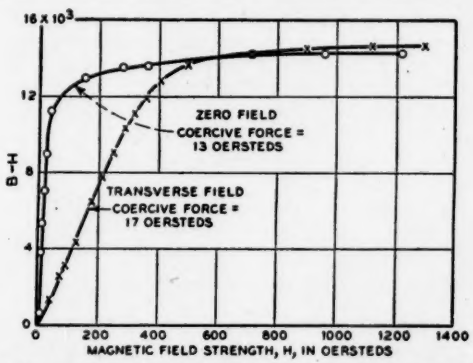

FIG. 2. Magnetization curve on Alnico V cooled from 1300°C at 2° to 5°C per second to 810°C then oil-quenched, a field (indicated) being present from 900°C to room temperature.

If the specimen is heat treated and aged, so as to obtain 600 oersteds coercive force, the domains are visible but much smaller. At residual induction, the domains are not normally visible but as the demagnetizing field is applied in the vicinity of 400 oersteds, spike-like domains appear as in Fig. 1(d). Further increase in the field strength causes these regions of reverse magnetization to grow as in Figs. 1(e) and (f). Finally, however, as saturation is approached they merge and the boundaries again disappear.

At first thought it may seem that the existence of these large spike-like domains in a material of 600 oersteds coercive force is inconsistent with the fine-particle theory of coercive force. This is not necessarily the case since it is entirely possible that these spike-like domains are aggregates of many fine-particle domains which are oriented in the same direction.

The authors are greatly indebted to R. M. Bozorth for valuable discussion and to J. G. Walker for assistance with the photography.

[1] H. J. Williams, Phys. Rev. 70, 106 (1946); Williams, Bozorth, and Shockley, Phys. Rev. 75, 155 (1949).
[2] L. Néel, Comptes Rendus 225, 109 (1947); E. C. Stoner and E. P. Wohlfahrt, Nature 160, 650 (1947).
[3] Kittel, Nesbitt, and Shockley, Phys. Rev. 77, 839 (1950). Drozhjina, Luzhenskaya, and Shur, J. Tech. Phys. U.S.S.R. 19, 95 (1949).

On the Isomerism of Xe^{131}

INGMAR BERGSTRÖM
Nobel Institute of Physics, Stockholm, Sweden
August 18, 1950

FOUR substantially different decay schemes of I^{131} have been reported.[1] Recently it was shown by absorption measurements[2] that the 163-kev γ-ray is due to an isomeric transition in Xe^{131}. It was thought that more detailed information on Xe^{131m} would be of help in deciding between the suggested decay schemes of I^{131}.

The electromagnetic isotope separator of this Institute was used to prepare an extremely thin β-spectrometer sample.[3] Xe^{131m} produced in the decay of 10 mC I^{131} (obtained from Harwell) was mixed with some stable Xe gas to make the Xe spectrum visible on a fluorescent screen. The activity of mass number 131 was collected on an Al foil (0.15 mg/cm), which was used as β-spectrometer sample.[3] The half-life of Xe^{131m} was found to be 12.0 ± 0.3 days. Figure 1 shows the β-spectrum measured with a resolving power of about one percent in the double focusing β-spectrometer and with a 3.9 mg/cm² mica G-M window. The energy of the conversion electrons obtained in this way corresponds to an energy of 162.9 ± 0.4 kev for the γ-ray emitted in the isomeric transition.

In order to search for the conversion lines of the γ-rays of energies 80, 284, and 364 kev as required by the decay scheme of Cork *et al.* a very strong sample was used in a high transmission lens spectrometer with a thin G-M window (cut off $\sim$8 kev). Except the Auger lines no conversion lines with an intensity >0.0005 of the K-line of Xe^{131m} are present. This fact seems to invalidate the decay scheme of Cork *et al.* The 177-kev line found by these authors may be due to a very weak Te^{131m} contamination.

From an analysis of the β-spectrum obtained in the double focusing β-spectrometer, $N_L/N_M=3.4\pm0.4$ was obtained. This value was used to obtain a correct value for the intensity ratio of the K and L conversion electrons obtained from measurements in the lens spectrometer (no window absorption for the K electrons). Thus $N_K/N_L=2.34\pm0.20$. The half-life relation[4] corrected for internal conversion[5] makes $l=5$ most probable. This assignment is also in good agreement with the isomer classification curves of Axel and Dancoff.[6] For $l=5$, $N_K/N_L\approx0.8$ according to the curves of Hebb and Nelson. This would indicate a mixture of 2^5 pole electric and 2^4 magnetic radiation corresponding to a spin difference of 4 and parity change in accordance with nuclear shell theory.[7] The high spin difference associated with the 163-kev γ-ray transition and the spin terms from the coupling theory[7] makes the decay scheme of Owen *et al.* unlikely. Lind *et al.* have also shown[8] by means of precision γ-measurements that this decay scheme is improbable.

The fact that the 163-kev γ-ray seems to decay directly to the ground state of Xe does not fit either the decay scheme of Metzger and Deutsch or that of Kern *et al.* It may therefore be possible that I^{131} decays to Xe^{131m} with a β-ray of about 800 kev to such a small amount that it hardly can be detected because of the strong overlapping 600-kev β-spectrum. This suggestion is also in agreement with the requirements of the nuclear shell theory.[7] Since the spin of Xe^{131} is $\frac{3}{2}$, the ground state of Xe would be a $d_{3/2}$ level and the isomeric state corresponds to the level $h_{11/2}$. The ground state of I^{131} would be $g_{7/2}$. The hypothetical β-transition $g_{7/2}\rightarrow h_{11/2}$ would then be associated with $\Delta L=1$ and $\Delta I=2$. According to Shull and Feenberg[9] the approximate formula $(W_0^2-1)f\cdot t=10^{10}$ is valid in this case. Feister *et al.*[2] showed that about one percent of the I^{131} disintegrations will lead to the metastable state of Xe^{131}. Using this fact and the predicted β-energy 800 kev $(W_0^2-1)f\cdot t=0.6\cdot10^{10}$ is obtained. Even if the ground state of I^{131} is $d_{5/2}$, the transition probability for the 800-kev β^- would be very small, showing that the suggested decay is also plausible from the point of view of the nuclear shell model.

All β-spectrometer investigations of electromagnetically separated rare gases recently performed at this Institute will later appear in detail in Arkiv för Fysik.

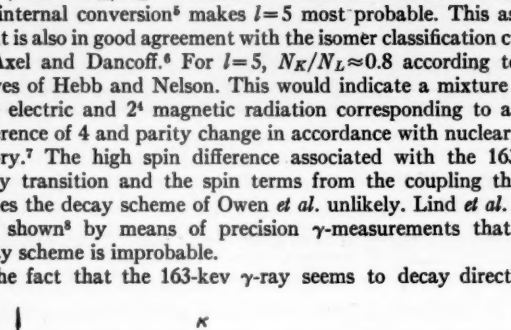

FIG. 1. β-spectrum of Xe^{131m} measured in the double focusing spectrometer with a resolving power of $\sim$one percent.

[1] F. Metzger and M. Deutsch, Phys. Rev. **74**, 1640 (1948); Owen, Moe, and Cook, Phys. Rev. **74**, 1879 (1948); Cork, Keller, Sazynski, Rutledge, and Stoddard, Phys. Rev. **75**, 1621 (1949); Kern, Mitchell, and Zaffarano, Phys. Rev. **76**, 94 (1949).
[2] Brosi, De Witt, and Zeldes, Phys. Rev. **75**, 1615 (1949).
[3] Bergström, Thulin, and Andersson, Phys. Rev. **77**, 851 (1950).
[4] E. Segrè and A. C. Helmholz, Rev. Mod. Phys. **21**, 280 (1949).
[5] Rose *et al.*, Tables of K-shell internal conversion coefficients (privately distributed).
[6] P. Axel and S. M. Dancoff, Phys. Rev. **76**, 892 (1949).
[7] Haxel, Jensen, and Suess, Phys. Rev. **75**, 1766 (1949); M. G. Mayer, Phys. Rev. **78**, 16 (1950).
[8] Lind, Brown, Klein, Muller, and Du Mond, Phys. Rev. **75**, 1544 (1949).
[9] F. B. Shull and E. Feenberg, Phys. Rev. **75**, 1768 (1949).

Microwave Magnetic Resonance Absorption in Nitrogen Dioxide*

J. G. CASTLE, JR.† AND ROBERT BERINGER
Sloane Physics Laboratory, Yale University,‡ New Haven, Connecticut
August 17, 1950

WE have observed the absorption arising from magnetic dipole transitions between magnetic sublevels of rotational states of NO_2. The apparatus is similar to that described previously.[1]

The ground state of nitrogen dioxide has been extensively studied.[2] The state is analogous to a $^2\Sigma$-type with an almost free magnetic moment arising from the spin of the odd electron. There are two magnetic interactions present which give a field-free structure to each rotational level. According to McAfee's observation,[3] the energy of coupling of the electron spin with the spin of the N^{14} nucleus ($I=1$) is of the order of 100 Mc/sec., and is about twice the coupling of the rotational moment (per unit J) to the electronic moment. Therefore, observations at 9360 Mc/sec. would show a rather complete uncoupling of these three magnetic moments.

The observed spectrum at room temperature and a gas pressure of 5 to 15 mm Hg consists of three overlapping lines located at 3303, 3351, and 3398 oersteds. The "free spin" transition[4] with no diamagnetic correction would be located at 3339 oersteds. Outside the triplet there are broad tails which represent the sum of overlapping lines. At lower pressure the spectrum is partially resolved into a large number of lines.

The gas was made by the reaction of oxygen with nitric oxide and separated by condensation. The pressure in the microwave cavity was determined by the temperature of solid NO_2 in a side tube and was read from an extrapolation of Giaque's measurements.

The spectrum is interpreted in terms of a Paschen-Back effect on the three magnetic moments in the molecule. For a particular rotational level, J, K, the energy is approximately

$$W=M_S g_S \mu_0 H+A\,M_S M_I+B\,M_S M_J,$$

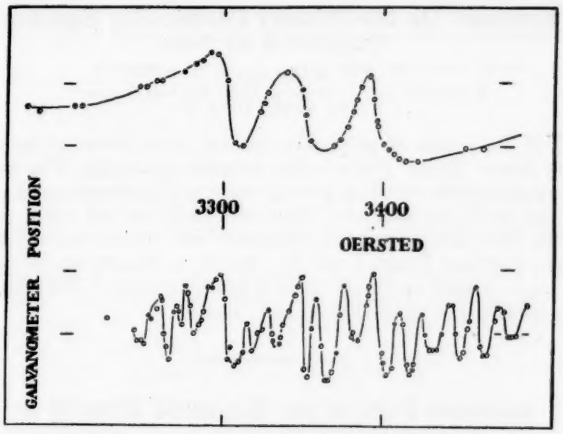

FIG. 1. Magnetic resonance absorption spectra of NO_2 at 9360 Mc/sec. The circles are output galvanometer readings; galvanometer deflections are proportional to the first derivative of the absorption contour. The upper figure shows the three-peaked band at 5.0 mm Hg and 290°K with a modulation amplitude of 8.4 oersteds. The lower figure is for 1.3 mm Hg, 290°K, and 2.1 oersteds.

where the coupling energies A and B may depend on J and K. The magnetic moment generated by the molecular rotation is assumed to be proportional to J, the total rotational angular momentum quantum number. Using the approximation that the rotational energies are given by the symmetric top expression,[3,5,6]

$$F=0.417J(J+1)+5.87K^2 \text{ cm}^{-1},$$

the partition function is 2700 at room temperature. It is evident that several hundred rotational levels contribute lines of low intensity, and that an observed resonance is the sum of a number of such.

Selecting the transition $\Delta J=0$, $\Delta M_s=1$, $\Delta M_I=\Delta M_J=0$, and summing over J, K, M_I, and M_J (with A independent of J and K), one predicts a three-peaked band of absorption lines with the spacings between the peaks equal to A. The envelope of line intensity retains this shape at low pressure.

The general features of the partially resolved spectrum are predicted by this model with B approximately equal to $A/2$. The sharpness of the lines indicates that the spin-rotation term is almost independent of J and K. The coupling of the spin of the odd electron to the spin of the N^{14} nucleus is $A=132$ Mc/sec.

* This study, together with that of reference 1, was part of a dissertation by one of us (JGC) presented for the degree of Doctor of Philosophy in Yale University.

† Du Pont Company Fellow in Physics (1949–50); present address: University of Buffalo, Buffalo, New York.

‡ Assisted by the ONR.

[1] R. Beringer and J. G. Castle, Jr., Phys. Rev. **78**, 581 (1950).
[2] See W. F. Giaque and J. D. Kemp, J. Chem. Phys. **6**, 40 (1938).
[3] K. B. McAfee, Phys. Rev. **78**, 340 (1950).
[4] A. K. Mann and P. Kusch, Phys. Rev. **77**, 435 (1950).
[5] G. Herzberg, *Infrared and Raman Spectra of Polyatomic Molecules* (D. Van Nostrand Company, Inc., New York, 1945).
[6] Claesson, Donahue, and Schomaker, J. Chem. Phys. **16**, 207 (1948).

Angular Correlation of the Gamma-Rays Emitted from the Excited States of A^{38}

ROLF M. STEFFEN
Department of Physics, Purdue University, Lafayette, Indiana*
August 17, 1950

FROM a study of the beta-spectra[1] and the gamma-radiation[2] of the 38-min. Cl^{38} it can be concluded that the two excited states of A^{38} at 2.15 Mev and 3.75 Mev have angular momenta of $J_1=1$, 2, or 3 and $J_2=3$ respectively, the latter having a different parity than the lower excited and the ground state.

In order to obtain more information about the excited levels in A^{38} the angular correlation of the gamma-rays successively emitted from those levels has been measured. The apparatus consisted of two sintillation counters using anthracene crystals as phosphors and RCA 5189 photo-multiplier tubes. To avoid disturbing coincidence counts due to Compton scattering from one counter to the other the crystals were shielded by two lead cones and in addition covered with $\frac{1}{16}$-in. lead foils. The angular resolution of the instrument as determined by observations on annihilation radiation was 10°30′. The resolving time of the coincidence amplifier used was 5.8×10^{-8} sec. The arrangement was tested by a careful measurement of the angular correlation of the gamma-radiation emitted from the excited states of Ni^{60} (decay[2a] of Co^{60+}) and Pd^{106} (decay[2a] of Rh^{106}) (Fig. 1) and was found to be in perfect agreement with the results reported by Brady and Deutsch.[3] The solid line represent the correlation functions

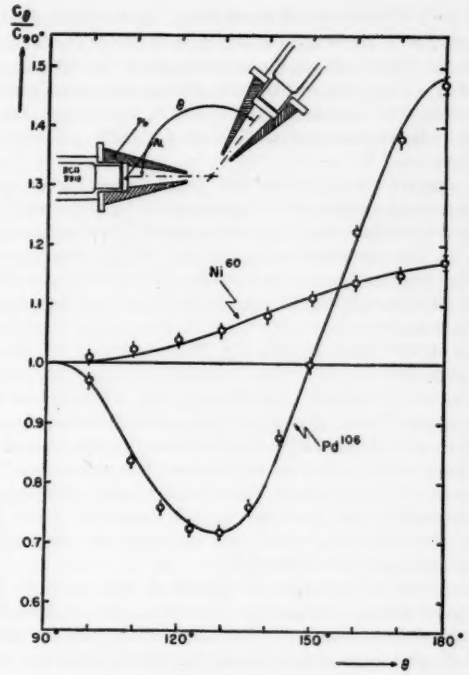

FIG. 1. Angular correlation of Ni^{60} and Pd^{106} gamma-rays.

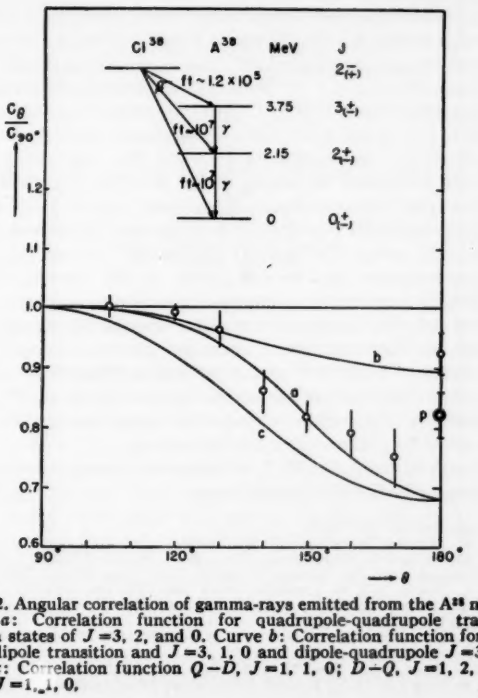

FIG. 2. Angular correlation of gamma-rays emitted from the A^{38} nucleus. Curve *a*: Correlation function for quadrupole-quadrupole transition between states of $J=3$, 2, and 0. Curve *b*: Correlation function for quadrupole-dipole transition and $J=3$, 1, 0 and dipole-quadrupole $J=3$, 2, 0. Curve *c*: Correlation function $Q-D$, $J=1$, 1, 0; $D-Q$, $J=1$, 2, 0; and $D-D$, $J=1$, 1, 0.

$f(\theta)=1+0.125\cos^2\theta+0.042\cos^4\theta$(Ni^{60}) and $f(\theta)=1-1.5\cos^2\theta+2\cos^4\theta$(Pd^{106}), corrected for the finite angular resolution of the instrument. The above angular correlation of the Ni^{60} gamma-rays is to be expected for a quadrupole-quadrupole transition between states of[4] angular momenta $J=4$, 2, and 0. No theoretical explanations for the angular distribution of the Pd^{106} gamma-rays has been given yet.[5,6]

The angular correlation of the gamma-rays of A^{38} has been measured using sources of Cl^{38} produced by bombarding LiCl with 10-Mev deuterons in the Purdue cyclotron. The results are shown in Fig. 2. The measured points follow, within the experimental error, the angular correlation function $f(\theta)=1-\frac{1}{8}\cos^4\theta$. For comparison all the other known correlation functions[4] for quadrupole or dipole transitions are plotted which give smaller emission probabilities at 180° than at 90°. The deviation from the theoretical curve near 180° may be partly due to internal pair production chiefly of the 2.15-Mev gamma-transition. Nevertheless the correction applied (point P in Fig. 2) using Rose's calculations[7] of the coefficient of internal pair production assuming electric quadrupole transition (see discussion below) is not sufficient to bring the point down to the expected place. Part of this effect is probably due to positron annihilation produced by pair formation of the gamma-rays in the absorbers, which are necessary to stop the rather energetic beta-particles from Cl^{38}.

The correlation function $1-\frac{1}{8}\cos^4\theta$ is characteristic for two quadrupole quanta and angular momenta $J=3, 2, 0$ respectively of the A^{38} levels involved. The parity of the two excited states must be equal since otherwise electric dipole radiation would be possible.

Measurements of Myers and Wattenberg[2] indicating that the direct transition from the second excited level to the ground state of A^{38} occurs in less than 3×10^{-4} of the disintegrations make the assignment of the same parity of the second excited level and the ground state of A^{38} necessary. It must therefore be assumed that both transitions are by electric quadrupole radiation and that all three states of A^{38} involved have the same parity. Even if mixtures of different multipole radiations are admitted giving different correlation functions due to interference effects[8] no other assignments can be found which are compatible with selection rules and the abundance of the cross-over transitions.

According to the measurements of Langer[1] the beta-transition from Cl^{38} to the ground state of A^{38} having zero spin is once-forbidden involving a spin change of two units and change of parity suggesting a spin of 2 for Cl^{38} and odd parity if we assume an even parity of the ground state of A^{38}. The intermediate group of electrons has a ft-value of $\sim10^7$ indicating a once-forbidden transition having a spin change of 0 or 1. This indicates an angular momentum of 1, 2, or 3 and even parity in agreement with the results of our correlation measurements ($J_1=2$). The low energy beta-spectrum is allowed according to its ft-value of 1.2×10^5. The selection rules for allowed beta-transitions ($\Delta J=0, 1$, no) give an angular momentum $J_2=2$, 3, or 4 of the second excited state of A^{38} and odd parity. The angular momentum 3 is also found from our measurements, but an odd parity of this level is not compatible with our results, which indicate the same parity for all levels of A^{38}. The interpretation of the angular correlation would suggest therefore that the low energy spectrum in spite of its small ft-value of 1.2×10^5 is once-forbidden. More direct information concerning the parities of the excited levels of A^{38} will be obtained by polarization-correlations experiments which are intended to be performed in this laboratory.

We wish to thank Dr. D. J. Tendam for his help in bombarding the samples in the Purdue cyclotron.

* Supported by the ONR.

[1] L. M. Langer, Phys. Rev. 77, 50 (1950).
[2] V. Myers and A. Wattenberg, Phys. Rev. 75, 992 (1949).
[2a] Obtained from the Isotope Division, AEC, Oak Ridge, Tennessee.
[3] E. L. Brady and M. Deutsch, Phys. Rev. 78, 558 (1950).
[4] D. R. Hamilton, Phys. Rev. 58, 122 (1940). D. L. Falkoff, thesis, Michigan University (1948).
[5] D. S. Ling and D. L. Falkoff, Phys. Rev. 76, 430 (1949).
[6] A. Spiers, Phys. Rev. 78, 75 (1950).
[7] M. E. Rose, Phys. Rev. 76, 678 (1949).
[8] D. S. Ling and D. L. Falkoff, Phys. Rev. 74, 1224 (1948).

Erratum: On the Primary Cosmic-Ray Spectrum

[Phys. Rev. 78, 819 (1950)]

J. A. Van Allen and S. F. Singer
Applied Physics Laboratory, Johns Hopkins University, Silver Spring, Maryland

In the course of publication certain errors occurred in this Letter to the Editor which requires correction. The units of geomagnetic cut-off, as given in terms of the momentum/charge ratio, pc/Ze, are properly billion volts (Bv), and not billion electron volts (Bev) as printed, and should be so understood throughout, including Tables I and II. Line 13 of the text should read "... charged component to geomagnetic latitude." The heading of column 3 of Table II should be "pc/Ze."

Apparent Error in the Measured Mass of S^{32}

A. S. Penfold
Betatron Group, University of Saskatchewan, Saskatoon, Saskatchewan, Canada

August 14, 1950

While attempting to calculate the threshold energy for the reaction S$^{32}(\gamma,d)$P^{30} an apparent anomaly between the measured masses of S^{32} and Si^{30} was encountered.

Discussing mass defects in light nuclei, Rosenfeld[1] states, "In the interval $A=29\cdots34$ there is a large unexplained discrepancy between the values derived from nuclear reaction data and those based on the mass spectrograph measurement of S^{32}." The latter mass was used in Rosenfeld's table of mass defects.

This discrepancy can seemingly be attributed to an error in the measured mass of S^{32}. The following calculations are offered in support of this statement.

The reaction energies of five relevant nuclear reactions are given in the isotopic report of Mattauch and Flammersfeld[2] and in a recent paper on thresholds.[3] These values, together with the reaction energy for the reaction S$^{32}(\gamma,d)$P^{30} which was measured in this laboratory, are listed in Table I.

Seaborg's tables[4] give 3.85 and 3.50 Mev for the β-decay energies of S^{31} and P^{30}. Both values were determined by magnetic spectrometer measurements.

Figure 1 illustrates the situation. The reactions considered are shown by solid arrows and the β-decays by dotted arrows.

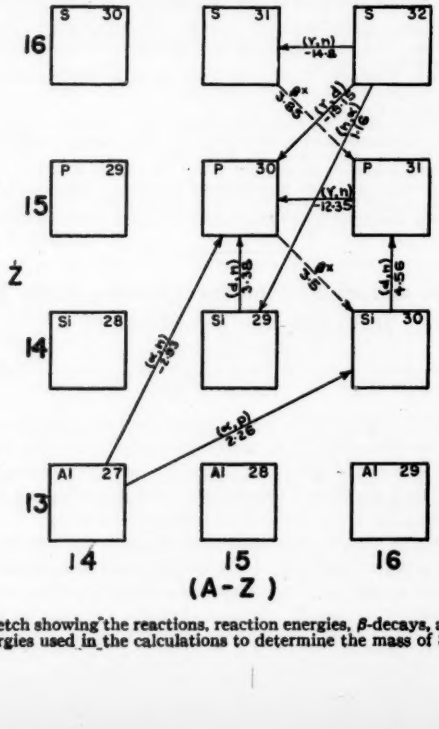

Fig. 1. Sketch showing the reactions, reaction energies, β-decays, and decay energies used in the calculations to determine the mass of S^{32}.

TABLE I. Reaction energies.

Reaction	Reaction energy (Mev)
$S^{32}(\gamma,d)P^{30}$	−19.15
$S^{32}(\gamma,n)S^{31}$	−14.8
$S^{32}(n,\alpha)Si^{29}$	1.2
$P^{31}(\gamma,n)P^{30}$	−12.35
$Si^{30}(d,n)P^{31}$	4.56
$Si^{29}(d,n)P^{30}$	3.38
$Al^{27}(\alpha,n)P^{30}$	−2.93
$Al^{27}(\alpha,p)Si^{30}$	2.26

The mass of Si^{30} is listed by Rosenfeld as 29.98310±0.00032 m.u. A recent measurement by Duckworth[5] giving 29.98290±0.00015 has substantiated this value. The present calculations have been based on the latter value.

The calculations were performed as follows:

$$\left.\begin{aligned} &Si^{30}\rightarrow P^{31}\rightarrow P^{30}\\ &Si^{30}\rightarrow P^{30}\\ &Si^{30}\rightarrow Al^{27}\rightarrow P^{30}\end{aligned}\right\}\rightarrow P_{wm}^{30}\text{ (weighed mean value)},$$

$$\left.\begin{aligned} &P_{wm}^{30}\rightarrow Si^{29}\rightarrow S^{32}\\ &P_{wm}^{30}\rightarrow S^{32}\\ &Si^{30}\rightarrow P^{31}\rightarrow S^{31}\rightarrow S^{32}\end{aligned}\right\}S_{wm}^{32}\text{ (weighed mean value)}.$$

Assuming approximately equal experimental errors in each reaction energy and decay energy used, a one-step calculation was given a weight of one, a two-step calculation a weight of one-half, etc.

The masses of the proton, deuteron, and α-particle were taken from Mattauch and Flammersfeld's tables, while a value of 1.008986 m.u. was used for the mass of the neutron.[6]

The weighed mean value of the mass of S^{32} obtained through these calculations is 31.98199±0.00021 m.u.

This value is in fair agreement with the value 31.98167±0.00017 listed by Mattauch and Flammersfeld, but differs by 0.00110 m.u. (1.02 Mev) from the spectrometric value of 29.98089±0.00007 listed in Rosenfeld's tables.

The calculations also give 28.98568 m.u. for the mass of Si^{29} which is in excellent agreement with the value 29.98567 recently obtained by Duckworth.[7] These values do not agree with the value listed by Rosenfeld.

It is concluded that the measured mass of S^{32} is too low by 0.00110 m.u. and that the correct value is 29.98199±0.00021 m.u.

[1] L. Rosenfeld, *Nuclear Forces* (Interscience Publishers, Inc., New York, 1948), p. 499.
[2] J. Mattauch and A. Flammersfeld, *Isotopenbericht* (1949), Table 3.
[3] McEllhinney, Hanson, Becker, Duffield, and Diven, Phys. Rev. **75**, 542 1949).
[4] G. Seaborg and I. Perlman, Rev. Mod. Phys. **20**, 585 (1948).
[5] Duckworth, Preston, and Woodcock, Phys. Rev. **79**, 188 (1950).
[6] R. E. Bell and L. G. Elliot, Phys. Rev. **79**, 282 (1950).
[7] H. Duckworth and R. S. Preston, Phys. Rev. **79**, 402 (1950).

Detection of Beta-Induced Scintillations from Crystals with a Photo-Sensitive Geiger-Mueller Counter*

C. E. MANDEVILLE AND H. O. ALBRECHT
Bartol Research Foundation of the Franklin Institute, Swarthmore, Pennsylvania
August 16, 1950

IN a previous communication,[1] the writers described experiments in which immediate fluorescent scintillations from crystals of NaCl-Ag were detected in a photo-sensitive Geiger-Mueller counter. The scintillations were produced when the crystals were irradiated by the alpha-particles of polonium. It was also stated that a long period ultraviolet *phosphorescence* was observed when the same crystals were bombarded by beta-particles. All of the above-discussed measurements were carried out with the use of the photo-sensitive scintillation Geiger counter, which was described as "relatively insensitive."

Since the time of the early alpha-particle measurements, the behavior of NaCl-Ag under beta-ray and gamma-ray bombardment has been observed in conjunction with a 1P28 photo-multiplier tube. Contrary to the experience with the scintillation Geiger counter, a copious emission of short decay-time fluorescent ultraviolet was observed when NaCl-Ag was irradiated by both beta-rays and gamma-rays. These pulses were not observed in the early scintillation Geiger counter because of insufficient quantum efficiency. Only the very large light pulses of the polonium alpha-particles could be detected. Consequently, a wire gauze photon counter was sensitized in the manner described by Scherb.[2] By repeated and prolonged discharges at liquid air temperature, an extremely responsive photon counter was obtained. Its sensitivity in the ultraviolet was several orders of magnitude greater than that of the photon counter used for the first alpha-particle detection.

This newly prepared scintillation Geiger counter was found to respond satisfactorily when it was coated with crystals of NaCl-Ag and irradiated by the beta-rays of RaE. The glass sidewalls of the photon counter were sufficiently thick to exclude even the highest energy beta-rays of RaE. Moreover, since the RaE was in equilibrium with its parent and daughter elements, 20 mg/cm² of aluminum were placed between the source and the counter to exclude the possibility of counting any alpha-particles from polonium. Aside from a faint gamma-ray background, coming perhaps from RaD, the entire counting rate arose from the ultraviolet scintillations produced in NaCl-Ag by the beta-spectrum of RaE. Using a relatively crude geometry, an efficiency of ten percent for beta-rays was obtained. This value can be improved upon tremendously. It is thought that an efficiency of one hundred percent can be reached.

To ascertain whether the counter would respond to fluorescent scintillations resulting from gamma-rays on NaCl-Ag, the ultra-sensitive photon counter was placed in a double-walled jacket made of Corning 9741 glass. The space within the concentric cylinders was filled with NaCl-Ag crystals, forming a cylindrical layer of thickness 1.5 cm about the cathode of the counter. Using radioactive Sc^{46} as a source, the counter enclosed by the layer of crystals was irradiated by million-volt gamma-rays. Taking all precautions to maintain a constant geometry, a cylinder of thin black paper was slipped over the counter between the counter and the layer of scintillating crystals. No appreciable change in the counting rate was observed, indicating that even higher quantum efficiencies in the ultraviolet must be obtained before scintillations resulting from gamma-ray bombardment can be detected.

* Assisted by the joint program of the ONR and AEC.
[1] C. E. Mandeville and H. O. Albrecht, Phys. Rev. **79**, 117 (1950).
[2] M. V. Scherb, Phys. Rev. **73**, 86 (1948).

The Scattering Lengths of the Deuteron

D. G. HURST AND N. Z. ALCOCK
Atomic Energy Project, National Research Council of Canada, Chalk River, Ontario, Canada
August 14, 1950

THE angular variation of neutron scattering by deuterium gas has been measured. A new spectrometer, especially designed for such work, was used instead of earlier equipment.[1] Neutrons, of wave-length 1.063A, were selected by crystal diffraction from a well-collimated beam leaving the Chalk River reactor. They passed through a cell containing deuterium gas at liquid nitrogen temperature and 21 atmospheres pressure. Scattered neutrons were measured by a BF_3 proportional counter every eight degrees in the angular range 11.2° to 67.2°. Sixteen angular sweeps were made with gas in the cell, 1000 counts being taken at every stop so that 16,000 counts were taken at each angle. Background, which ranged from 10 percent to 15 percent, was determined with the cell evacuated.

The experimental counting rates were corrected for background, for hydrogen content of the deuterium, and for double scattering. The resulting quantities were transformed to relative differential cross sections by dividing by the effective scattering volume. Com-

parison with theoretical cross sections calculated by the methods of Hamermesh and Schwinger[2] and Spiers[3] but with allowance for the ground-state vibration, gave

$$(a_{\frac{1}{2}}-a_{\frac{3}{2}})^2/(2a_{\frac{1}{2}}+a_{\frac{3}{2}})^2=0.173\pm^{0.028}_{0.022}$$

where $a_{\frac{1}{2}}$ and $a_{\frac{3}{2}}$ are the scattering lengths of the deuteron. Two values of the ratio $a_{\frac{1}{2}}/a_{\frac{3}{2}}$ are consistent with this result.

These are $a_{\frac{1}{2}}/a_{\frac{3}{2}}=3.2\pm0.3$ or 0.12 ± 0.04. In combination with a total cross section of 3.44 ± 0.06 barns for a free deuteron[4] and the known fact[5] that $2a_{\frac{1}{2}}+a_{\frac{3}{2}}>0$ these yield

$$\left.\begin{matrix}a_{\frac{1}{2}}=(0.26\pm0.02)10^{-12}\text{ cm}\\ a_{\frac{3}{2}}=(0.826\pm0.012)10^{-12}\text{ cm}\end{matrix}\right\}\text{ or }\left\{\begin{matrix}(0.638\pm0.006)10^{-12}\text{ cm}\\ (0.07\pm0.03)10^{-12}\text{ cm}\end{matrix}\right\}.$$

These values lie outside the results of Fermi and Marshall.[5] They lead to a coherent scattering cross section of 5.8 ± 0.2 barns which is consistent with the Oak Ridge value[6] of $5.2\pm^{1.0}_{0.5}$ barns, but is more closely defined. A full account of this investigation is being submitted to the *Canadian Journal of Research* for publication.

It is a pleasure to acknowledge the work of Mr. A. J. Pressesky in the design of the spectrometer and to thank Dr. N. K. Pope for discussions on theoretical points.

[1] N. Z. Alcock and D. G. Hurst, Phys. Rev. **75**, 1609 (1949).
[2] M. Hamermesh and J. Schwinger, Phys. Rev. **69**, 145 (1946).
[3] J. A. Spiers, Phys. Rev. **75**, 1765 (1949).
[4] E. Fermi and L. Marshall, Phys. Rev. **75**, 578 (1949).
[5] C. G. Shull *et al.*, Phys. Rev. **73**, 842 (1948).
[6] Wollan, Davidson, and Shull, Phys. Rev. **75**, 1348 (1949). The limits of error have been privately communicated.

Angular Correlation: A General Proof of the Method of D. R. Hamilton

STUART P. LLOYD*
Physics Department, University of Illinois, Urbana, Illinois
August 14, 1950

THE relative probability for a (randomly oriented) nucleus $N'(j')$ of total angular momentum j' to decay to a nucleus $N(j)$ by emitting a system S_1 with properties A_1 and then for $N(j)$ to decay (quickly) to $N''(j'')$ by emission of S_2 with properties A_2 is given by second-order time-dependent perturbation theory as:[1]

$$W(A_1,A_2)=\Sigma_{m'}\Sigma_{m''}|\Sigma_m(m''|A_2|m)(m|A_1|m')|^2$$
$$=\Sigma_{m'}\Sigma_{m''}\Sigma_{m_1}\Sigma_{m_2}(m''|A_2|m_1)(m_1|A_1|m')^*\times(m''|A_2|m_2)(m_2|A_1|m'). \quad (1)$$

Explicitly, the matrix elements are:

$$(m|A_1|m')=\int\psi_j{}^{m*}(X)H(X,A_1)\psi_{j'}{}^{m'}(X)dX, \quad (2)$$

where $\psi_j{}^m(X)$, $\psi_{j'}{}^{m'}(X)$ are wave functions of states with total angular momentum quantum numbers (j,m), (j',m'), X is the set of nuclear coordinates, and $H(X,A_1)$ is the term in the Hamiltonian that leads to the creation of S_1; similarly for the others. If one is using unpolarized detectors for particles P_1 of S_1, P_2 of S_2, one is interested in the directional correlation function

$$\bar{W}(\mathbf{p}_1,\mathbf{p}_2)=\mathcal{S}_1\mathcal{S}_2W(A_1,A_2)$$

where $\mathbf{p}_1$, $\mathbf{p}_2$ are the momenta of P_1, P_2 and $\mathcal{S}_1$, $\mathcal{S}_2$ denote averaging over irrelevant directions in A_1, A_2 (spins, polarizations, and neutrino directions). If (1) is used to express (2) in terms of the matrix elements it is seen that interference terms $m_1\neq m_2$ appear in $\bar{W}(\mathbf{p}_1,\mathbf{p}_2)$; it has been shown in particular cases that these are removed if either $\mathbf{p}_1$ or $\mathbf{p}_2$ is taken to be along the axis of quantization. If $\mathbf{p}_1=\mathbf{p}_1{}^{(0)}$ is along the axis of quantization, $\bar{W}$ becomes:[1,2]

$$W(\mathbf{p}_1{}^{(0)},\mathbf{p}_2)=\Sigma_m[\mathcal{S}_1\Sigma_{m'}|(m|A_1{}^{(0)}|m')|^2]\times[\mathcal{S}_2\Sigma_{m''}|(m''|A_2|m)|^2]. \quad (3)$$

We shall show, using group-theoretic methods, that (3) holds for any S_1, S_2.

Let $(M'|\mathrm{P}|M)^J$ be a $(2J+1)$-dimensional unitary irreducible representation of the unimodular unitary group $\{\mathrm{P}\}$ on two variables, the spin group. If the set of quantities $f_J{}^M$ belongs to the representation, the transformation P:

$$\xi_i=\Sigma_j\xi_j'\mathrm{P}_{ji}\quad i,j=1,2$$

induces the transformation

$$f_J{}^M=\Sigma_{M'}f'_J{}^{M'}(M'|\mathrm{P}|M)^J \quad (4a)$$

with Hermitian conjugates

$$\bar{f}_J{}^M=\Sigma_{M'}(M|\mathrm{P}^{-1}|M')^J\bar{f}'_J{}^{M'}. \quad (4b)$$

With the correspondence: $f_1{}^{\pm1}=(-if_y\mp f_x)/\sqrt{2}$, $f_1{}^0=f_z$, P induces a rotation: $\mathbf{r}'=R\mathbf{r}$ on $\mathbf{r}=(x,y,z)$ where $R=R(\mathrm{P})$ is the dyad of a rotation. Assume that the nuclear wave functions belong to the representations, and use (4) to rotate the nuclear coordinate system; there obtains:

$$(m|A_1|m')=\Sigma_\mu\Sigma_{\mu'}(m|\mathrm{P}^{-1}|\mu)^j(\mu|\mathrm{P}A_1|\mu')(\mu'|\mathrm{P}|m')^{j'}. \quad (5)$$

This is straightforward if one has one-component nuclear wave functions, but the formula is the same with spinor wave functions. Substitution from (5) and similar equations and repeated use of the unitary and group properties of the $(M'|\mathrm{P}|M)^J$ give:

$$W(A_1,A_2)=W(\mathrm{P}A_1,\mathrm{P}A_2)=W(RA_1,RA_2), \quad (6)$$

since W can be a function only of vectors. The $\mathcal{S}_1$, $\mathcal{S}_2$ procedures are invariant under rotation, so that one has also:

$$\bar{W}(\mathbf{p}_1,\mathbf{p}_2)=\bar{W}(R\mathbf{p}_1,R\mathbf{p}_2). \quad (7)$$

$\bar{W}(\mathbf{p}_1,\mathbf{p}_2)$ is thus a rotational invariant and as such can be a function only of $p_1{}^2$, $p_2{}^2$, and $\mathbf{p}_1\cdot\mathbf{p}_2=p_1p_2\cos\theta$, so that one may write

$$\bar{W}(\mathbf{p}_1,\mathbf{p}_2)=W(\mathbf{p}_1,\mathbf{p}_2,\theta).^3$$

If one takes $\mathbf{p}_1=\mathbf{p}_1{}^{(0)}$ to be along the z axis, $\bar{W}(\mathbf{p}_1{}^{(0)},\mathbf{p}_2)$ must be independent of the azimuth of $\mathbf{p}_2$, so that

$$\bar{W}(\mathbf{p}_1{}^{(0)},\mathbf{p}_2)=\bar{W}(\mathbf{p}_1{}^{(0)},R^{(0)}\mathbf{p}_2), \quad (8)$$

where $R^{(0)}$ is any rotation around the z axis. If the equations for such a rotation are (in spherical coordinates):

$$\varphi'=\varphi-\alpha,\quad\theta'=\theta,\quad r'=r$$

there are two $\mathrm{P}^{(0)}$ to which it belongs:

$$\mathrm{P}_\pm{}^{(0)};\quad\xi_1=\pm e^{i\alpha/2}\xi_1',\quad\xi_2=\pm e^{-i\alpha/2}\xi_2'$$

and either one gives, if $(M|\mathrm{P}_\pm{}^{(0)}|M')^J=(\pm)^{2M}e^{iM\alpha}\delta_{MM'}$,

$$(m''|A_2|m)=\exp[i\alpha(m-m'')](m''|\mathrm{P}^{(0)}A_2|m). \quad (9)$$

Expansion of the members of (8) and use of (9) gives

$$\mathcal{S}_1\mathcal{S}_2\Sigma_{m'}\Sigma_{m''}\Sigma_{m_1}\Sigma_{m_2}(m''|A_2|m_1)^*(m_1|A_1{}^{(0)}|m')^*\times(m''|A_2|m_2)(m_2|A_1{}^{(0)}|m')$$
$$=\mathcal{S}_1\mathcal{S}_2\Sigma_{m'}\Sigma_{m''}\Sigma_{m_1}\Sigma_{m_2}(m''|\mathrm{P}^{(0)}A_2|m_1)^*(m_1|A_1{}^{(0)}|m')^*\times(m''|\mathrm{P}^{(0)}A_2|m_2)(m_2|A_1{}^{(0)}|m')$$
$$=\mathcal{S}_1\mathcal{S}_2\Sigma_{m'}\Sigma_{m''}\Sigma_{m_1}\Sigma_{m_2}\exp[-i\alpha(m''-m_1)]\times(m''|A_2|m_1)^*(m_1|A_1{}^{(0)}|m')^*\exp[i\alpha(m''-m_2)]\times(m''|A_2|m_2)(m_2|A_1{}^{(0)}|m').$$

This last must be independent of α; the interference terms $m_1\neq m_2$ must vanish, and what is left gives Eq. (3), which thus holds in the general case.

Equation (6) is stronger than this, though; it suggests that one should be able to write

$$W(A_1,A_2)=\Sigma_L\Sigma_M(-)^MU_L{}^M(A_1)V_L{}^{-M}(A_2),$$

where $U_L{}^M(A_1)$, $V_L{}^M(A_2)$ belong to the $(2L+1)$-dimensional irreducible representation of the rotation group. Such U, V have been constructed and simplified, using properties of the vector-addition coefficients obtained by Racah,[4] and should be of assistance in studying the cases in which one detects the polarization of one or both of the particles. The directional correlation function is obtained for the general case in the form

$$W(\theta)=\Sigma_L\Sigma_M(-)^M\mathcal{S}_1U_L{}^M(A_1)\cdot\mathcal{S}_2V_L{}^{-M}(A_2)$$
$$=\Sigma_L\gamma_LP_L(\cos\theta),$$

where $P_L(\cos\theta)$ is the Legendre polynomial and the γ_L are in what amounts to closed form, i.e., free of magnetic quantum number sums.

I wish to thank Professor S. M. Dancoff for criticism and encouragement.

* AEC Predoctoral Fellow.
[1] D. R. Hamilton, Phys. Rev. **58**, 122 (1940).
[2] D. L. Falkoff and G. E. Uhlenbeck, Phys. Rev. **79**, 323 (1950). Section II contains discussion and references.
[3] H. Weyl, *The Classical Groups* (Princeton University Press, Princeton, 1939), pp. 52–53.
[4] Giulio Racah, Phys. Rev. **62**, 438 (1942).

Quantum Effects in the Interaction of Electrons with High Frequency Fields

J. C. WARD
Clarendon Laboratory, Oxford, England
July 18, 1950

IN a paper with the above title, Smith[1] has calculated the interchange of energy between a beam of electrons and a microwave field inside a resonator. An experiment to observe the quantum nature of the energy transfer will be performed shortly in this laboratory. In order to detect this effect it is clear that the energy of the electrons must be defined with an uncertainty which is less than the quantum energy, and it is this condition that produces the experimental difficulties. By means of a time-of-flight velocity focusing tube it is hoped to produce 1000-ev electrons with a spread of 10^{-5} v.

The approximation made in Smith's treatment is essentially to treat the electron as classical and the field as quantized. It would seem, however, more appropriate to the experimental conditions to treat the electron as quantized and the field as classical. Under these conditions the phase integral approximation should give an accurate prediction of the probabilities of energy transfer. Assuming an electric field $E_0 \sin\omega t$ across the resonator gap of width a, it is found that the probability of an electron gaining or losing r quanta in passing through the field is $J_r^2(z)$, where $J_r(z)$ is the Bessel function of rth order, and $z=(eaE_0/\hbar\omega)(\sin\frac{1}{2}\theta/\frac{1}{2}\theta)$. θ is the transit angle defined by $\theta=a\omega/v$, with v the electron velocity.

This result may be understood from the fact that the Broglie waves of the electron are phase-modulated as they pass though the gap. In the limit of large numbers of quanta transferred, this distribution tends to the classical distribution.

[1] L. P. Smith, Phys. Rev. **69**, 195 (1946).

Self-Diffusion in Cobalt

FOSTER C. NIX AND FRANK E. JAUMOT, JR.
Randal Morgan Laboratory of Physics, University of Pennsylvania, Philadelphia, Pennsylvania*
August 18, 1950

RADIOACTIVE Co^{60}, obtained from the AEC[1] was used as a tracer element in the study of self-diffusion in cobalt. This isotope has two gamma-ray spectra of energies 1.30 and 1.16 Mev, and a beta-ray spectrum of energy 0.31 Mev, necessitating a careful determination of the absorption coefficient which is essential in the method used for calculating the self-diffusion coefficient. In the present work this quantity was determined directly, in such a way as to approximate as nearly as possible the conditions present in the diffusion samples.

Samples of pure cobalt were coated with radioactive Co^{60} and placed in pairs, with active faces together, into a furnace which was evacuated to a pressure of less than 10^{-5} mm of Hg. Diffusion runs were made at temperatures of 1050°C, 1150°C, and 1250°C for 18 hours.

The mathematical analysis given by Steigman, Shockley, and Nix[2] relating the fraction of counts remaining after diffusion to the diffusion coefficient, D, was used to determine D. A plot of $\ln D$ *versus* $1/T$ gave the activation constant, A, and the activation energy, Q, where

$$D=Ae^{-Q/RT}.$$

The data indicate that the self-diffusion coefficient for cobalt is given approximately by

$$D=0.367e^{-67000/RT}\ \text{cm}^2\ \text{sec.}^{-1}.$$

Good agreement was found between the value of Q obtained from the plot of $\ln D$ *versus* $1/T$ and the value obtained from the Langmuir-Dushman equation

$$D=(Qd^2/Nh)e^{-Q/RT},$$

where N is 6.06×10^{23} mole^{-1}, h is Planck's constant, and d is the lattice constant.

* This work was supported by the ONR.
[1] AEC, Isotopes Branch: Catalog and Price List No. 3, July, 1949.
[2] Steigman, Shockley, and Nix, Phys. Rev. **56**, 13 (1939).

A New Method of Integration of Weak Nuclear Magnetic Resonance Signals

G. SURYAN
Department of Physics, Indian Institute of Science, Bangalore, India
June 28, 1950

SUBSTANTIAL increases in our knowledge of nuclear magnetic resonance and its application to the study of the crystalline state of matter could be achieved if it were possible to obtain a high signal-to-noise ratio for nuclear magnetic resonance signals. The method employed heretofore to attain high signal-to-noise ratio consisted in reducing the band width of the detecting system. This, however, necessitates a scanning of the nuclear magnetic resonance signals point by point. High discrimination against noise could be effected if it were possible to add algebraically the signals obtained in individual observations. One method of doing this has been attempted by Bloch[1] and others who made use of the integrating property of photographic materials. However, this method is quite tedious as it requires taking several thousand photographs, and ultimately depends on the contrast qualities of the photographic materials. The limitation imposed by this method is due to the fact that photographic materials integrate positive quantities only, whereas to get true discrimination against noise, algebraic addition is necessary.

A method of doing this based on the principle of magnetic recording of sound has been developed in this laboratory. The method is as follows. A hollow steel cylinder is mounted coaxially on the shaft of an alternator which supplies the a.c. required to modulate the nuclear magnetic resonance. By means of a small magnetic recording head similar to those used in sound recording, nuclear magnetic resonance signals are recorded in a close spiral on the steel cylinder by slowly traversing the length of the cylinder as it rotates. The pick-up head covers the whole length of the cylinder. In this, the noise being random, it mostly gets canceled whereas the signal adds up. It is also possible that a direct addition of magnetism takes place at the place where signals are close. This, however, is small. Thus on the whole, recordings of nuclear resonance signals over a period of time taken to fill the steel cylinder are averaged and large discrimination against noise is possible. The equivalent number of observations for a period of one minute is about 1500 using an alternator giving 25≈. It is possible to see the signal on an oscilloscope separated out from noise as the time of integration increases. This method also gives a fair idea of the shape of the resonance signal.

In this connection, it is suggested that magnetic recording may be helpful in investigating the transient effects in nuclear magnetic resonance.

[1] F. Bloch and D. H. Garber, Phys. Rev. **76**, 585 (1949).

Proceedings of the American Physical Society

MINUTES OF THE MEETING AT MEXICO CITY, JUNE 21–23, 1950

THE 300th meeting of the American Physical Society was held at Mexico City on Wednesday, Thursday, and Friday, June 21, 22, and 23, 1950. This meeting was unique. Never have we enjoyed such hospitality. The great and beautiful opera-house in the Palacio de Bellas Artes was placed at our disposal for the Inaugural Session on the Wednesday morning; and in this splendid setting our meeting was opened by the Minister of Public Education (Sr. Lic. Manuel Gual Vidal) representing the President of the Republic of Mexico. Dr. Luis Garrido, Rector of the Universidad Autonoma de México, gave an address of welcome, to which the President of the American Physical Society responded. Immediately afterward the Ministry of Public Education gave a luncheon for the members of the Society and for their wives in a distinguished restaurant, with music by the orchestra of the Ministry. On the Saturday following the meeting, the members of the Society received the signal honor of being declared distinguished visitors of the City of Mexico at a ceremony held in the Municipal Palace; six of us, as representatives of the rest, received badges and scrolls from Sr. Lic. Alejandro Carrillo, representing the Governor of the Distrito Federal. Thereupon the authorities of the Distrito Federal brought the Society to Xochimilco and entertained us all at luncheon. On the Thursday afternoon, the Ambassador of the United States (the Honorable Walter Thurston) entertained the members of the Society and their wives at a cocktail party in the Embassy. A fuller account of these magnificent events and of the meeting generally will be published in *Physics Today*.

The scientific sessions were held in buildings of the University of Mexico, to wit, the Palacio de Minería and the Anfiteatro Bolívar, the latter being the large auditorium allotted to the Symposium on Cosmic Rays and to the other invited papers. The programme of these sessions is republished here in full just as it stood in the Bulletin. A correction is necessitated by the lamentable death of H. L. Bradt; the work which he would have described as part of the Symposium was presented by his colleague and collaborator B. Peters. J. A. Van Allen presented a paper in the Symposium; the invitation to him was unfortunately made too late to permit of inclusion of the title in the Bulletin. Only one other of the invited papers was omitted; several authors of contributed papers found themselves unable to be present.

The banquet of the Society was held on the Friday evening in the Salón de los Candiles of the Hotel del Prado. The after-dinner speakers were the Ambassador of the United States; Sr. Ing. Alberto J. Flores, Director of the School of Engineering of the University of Mexico; Dr. Manuel Sandoval Vallarta; Dr. E. U. Condon and Dr. W. V. Houston.

Very special words of gratitude are due the Comisión Impulsora y Coordinadora de la Investigación Científica which bore the *entire* expense of the meeting (apart from the luncheons at which we were entertained by other departments of Government) as well as attending to all of the innumerable details necessary to the operation of so great and unprecedented a meeting. Several ladies of Mexico served at the various registration-desks; we are much indebted to them. The number who registered amounted to 207; there were perhaps others who failed to register. At the banquet and at the luncheons we had the pleasure of the company of many Mexicans, who should be described as our hosts rather than as our guests.

The Council met on the Friday afternoon and again on the Saturday morning. The terrible problem of finding a successor to the late John Torrence Tate as Managing Editor of the American Physical Society (and Editor of *The Physical Review*) was solved for the period extending to the next Annual Meeting (February, 1951), through the willingness of E. L. Hill to accept appointment to these offices for the period in question. To him, and to his colleagues at the University of Minnesota who will assist him, our thanks are expressed. For the period beginning at the end of the next Annual Meeting, the duty of finding a candidate devolves upon the 1950 Nominating Committee; the name of the candidate will appear on the next election ballot. At this meeting of the Council one hundred and twenty-seven candidates were elected to Membership in the Society; their names are printed below.

At the banquet the following Resolution was adopted by a standing vote by all members of the Society who were present:

"John Torrence Tate was Managing Editor of the American Physical Society and Editor of *The Physical Review* for twenty-four years. The task was great from the beginning, and soon became enormous. From decisions of policy down to the most minute details, he discharged his manifold

duties with unique skill, perfect care and incessant diligence. His journal was the channel by which the physicists of the United States disclosed their work to each other and to the world, and physicists of many other nations shared its pages. It was his proud achievement and the culmination of his lifework. Mindful of its immeasurable debt to its good and faithful servant, the American Physical Society assembled in Mexico records its undying gratitude, and sends its condolences to the wife and son of its departed friend."

Elected to Membership: Henri Amar, George W. Anderson, Jr., Donald R. Baker, Paul E. Baker, I. Bergstrom, Abraham L. Berlad, Robert Betchov, Henry A. Blumenfeld, Max A. Bredig, Lawrence E. Brennan, John A. Brinkman, Philip L. Browne, Merle E. Bunker, Giorgio Careri, Rose A. Carney, E. Paul Carter, Randall S. Caswell, S. Chapman, Arthur C. Christman, Jr., Borisas Cimbleris, Richard W. Cole, Carl C. Cowen, Kenneth C. Crebbin, William H. Culver, Juan de Oyarzabal, Arthur H. Dexter, Ernest J. Dieterich, Theodore L. Ether, Lawrence W. Fagg, Franklin L. Fillmore, Gerhard E. Fischer, Zygmunt Fonberg, Simon Foner, Stuart G. Forbes, Kenneth W. Ford, Rudolf Frerichs, Sherman Fried, Edward J. Fuller, Charles W. Galloway, Herbert Gelernter, Earl H. Gilmore, Stephen J. Goldsack, Raymond F. Goodrich, Richard H. Graham, Gerard M. Grosof, Robert M. Hale, Haven B. Hall, Charles L. Hammer, Milton Hansburg, Norman F. Harmon, Isadore Harris, Earl E. Hays, A. Hedgran, Phyllis Hersh, Jerald E. Hill, Edward L. Hubbard, Gordon C. Hunt, Thomas J. Hurley, Jr., S. Johansson, Dale R. Jones, Allan N. Kaufman, Clefas H. Killian, Robert W. King, Jr., Bennett Kivel, David A. Kleinman, Robert T. Knapp, Henry H. Kolm, Michael Komich, Thomas E. Kristofferson, Samuel W. Kurnick, Victor A. Lewinson, Glenn G. Lorch, P. David Luckey, Jr., Allen Lurio, Leonard C. Maier, Jr., Heinz Maier-Leibnitz, Manfred Mannheimer, David E. Matthews, Robert C. McBryde, James McC. McCampbell, Sherman C. McGarry, William C. Meecham, Jr., Alan G. Mencher, Herman L. Miller, Kyuichiro Miyamoto, Robert G. Moorhouse, William G. Myers, William S. O'Hare, Jesse Oroshnik, Paul Owen, Robert H. Parmenter, Armin R. Perry, Jr., David A. Rich, Dominique C. Rivier, Frank Roberts, Clemens Roothaan, Herbert N. Royden, Lawrence Ruby, Roberto A. Salmeron, Jacob Savitt, Hans Schaffner, Wilbur W. Schoof, Galen B. Schubauer, Walter G. Schweitzer, Jr., Peter M. Sherk, Sol R. Silverman, Ronald Smelt, Carroll E. Smith, Robert J. Spotz, James H. Stein, Irving Stein, James C. Stelyn, Wolfram G. Stenzel, George W. Stuart, Jr., Harry S. Thomas, Jr., Wilma Thompson, Marvin A. Van Dilla, Jun-chuan Wang, Orville H. Weddle, Erich S. Weibel, Loring C. White, Lowell D. White, Kenneth Whitham, Thurlow C. Wilfong, Jr., Boyd A. Wise, Jr., Charles E. Wood, and Alan H. Woodcock.

KARL K. DARROW, *Secretary*
American Physical Society
Columbia University
New York 27, New York

Erratum Pertaining to Paper N9

N9, by B. Smaller, E. Yasaitis, and H. L. Anderson. The by-line should read "Argonne National Laboratory and University of Chicago." The equation in the last line should read $\mu_H/\mu_D = 3.25720013 \pm 0.00000037$.

PROGRAMME

WEDNESDAY MORNING AT 11:00

Palacio de Bellas Artes

(I. I. RABI presiding)

Inaugural Session

A1. Opening of the meeting by DR. MIGUEL ALEMÁN, *President of the Republic of Mexico.*

A2. Address of welcome on behalf of the Universidad de México by LUIS GARRIDO, *President of the Universidad de México.*

A3. Response by I. I. RABI (*Columbia University*), *President of the American Physical Society.*

WEDNESDAY AFTERNOON AT 15:00

Anfiteatro Bolívar

(C. C. LAURITSEN presiding)

Invited Papers on Accelerators and Artificial Mesons

B1. Report on the Cyclotron at Nevis. E. T. BOOTH, *Columbia University.* (40 min.)

B2. The Experimental Programme of the Institute for Nuclear Studies at the University of Chicago. S. K. ALLISON, *University of Chicago.* (40 min.)

B3. Artificial Production of Mesons. E. M. MCMILLAN, *University of California, Berkeley.* (40 min.)

WEDNESDAY AFTERNOON AT 15:00

Minería

(F. SEITZ presiding)

Solid-State Physics

C1. Superconducting Niobium Nitride at Microwave Frequencies.* MAX BODMER, JEAN V. LEBACQZ, AND D. H. ANDREWS, *The Johns Hopkins University.*—The operation of a NbN bolometer as a detector of radiofrequency signals has been reported in a previous paper.[1] The work has now been extended to frequencies in the 10,000-mc band using a cryostat which maintains the operating temperature, −259°C, for about seven hours. The impedance of the bolometer is only about one ohm, and a special tuner, adjustable inside the vacuum, matches this impedance to that of a standard 3-cm wave guide. Because of the high transformation ratio, the band width of the tuner is only about 10 mc. With this equipment, both a bolometer action and a detection action were observed in demodulating the microwave energy.

* Assisted by the ONR.

[1] Lebacqz, Clark, Williams, and Andrews, Proc. I. R. E. **37**, No. 10, 1147 (1949).

C2. Perturbation Treatment of Heisenberg's Model of Ferromagnetism.* H. EKSTEIN, *Armour Research Foundation.*—The Slater-Bloch equations for the exchange interaction between N atoms of spin $\frac{1}{2}$ can be written under the form of a wave equation describing the distribution of r fictitious particles (the reversed spins) over N lattice sites. The Hamiltonian includes repulsive and attractive forces. For consistency, in order to obtain the correct number of eigenvalues, it is necessary to prescribe Fermi-statistics for the "particles." At the same time, this convention takes into account rigorously the repulsive forces, i.e., the impossibility of two reversed spins occupying the same lattice point. When the energies obtained by first-order perturbation calculus are introduced into the partition sum, they yield an implicit equation for the magnetization as a function of temperature and field, similar to the Weiss equation. For low temperatures, Bloch's $T^{\frac{3}{2}}$ law is obtained, but the slope of the M-T curve becomes infinite at the Curie point. For a simple cubic lattice, the Curie point is at $kT_c \sim 2J$. For the linear chain, the relative number of reversed spins at $T=0$ is of the order $\frac{1}{r}$, contrary to Bloch's result $r \to \infty$. For the two-dimensional lattice, one obtains ferromagnetism.

* Work supported by ONR.

C3. Further Observations on Domain Fringe Fields. L. MARTON, J. A. SIMPSON, AND A. VAN BRONKHORST, *National Bureau of Standards.*—The previously reported fringe field observations on a single cobalt crystal were continued and extended. Identification of the domain boundaries by means of

powder patterns allows us to orient the crystal in the proper direction for optimum observation of the electron optical shadow pattern. Quantitative data on the field distribution in the equatorial planes between domain walls in the 100 plane of the crystal shall be communicated. Experiments were carried out also on colloidal Ni and Fe particles. For the purposes of that type of work, the instrument was modified to operate at higher magnifications. In the case of such colloidal particles, no attempt was made to measure the field quantitatively. The effort was directed towards resolving the problem of whether such particles contain one, two, or four domains.

C4. Anomalous Diamagnetism of Graphite. S. MROZOWSKI, *University of Buffalo.*—The relation of the diamagnetism of aromatic molecules to the diamagnetism of graphite is explained in terms of a variable energy gap between the filled and empty (conduction) bands. Experimental data show that the anomalous component of the molar susceptibility of aromatic molecules due to a quantized motion of electrons around the benzene rings is roughly proportional to the number of benzene rings in the molecule. The diamagnetic contribution of these filled energy levels is independent of temperature, and represents only a small part (1/13.5) of the susceptibility of large graphite crystals. In large aromatic molecules the energy gap becomes small enough for electrons to be activated into the conduction band thus giving rise to a diamagnetism of free electrons and holes. This temperature dependent component increases with increase of molecular dimensions (increase of the effective number of electrons) up to the value corresponding to an infinitely large graphite crystal. The susceptibility of graphite can be explained quantitatively in terms of Landau diamagnetism as was done by Ganguli and Krishnan, modifying however their assumptions in accordance with Wallace's analysis of electronic motions in the graphite lattice.

C5. The Self-Diffusion of Cobalt in Gelatin as Measured with Co^{60}.* HERMAN BRANSON AND WOODFIN LEWIS, *Howard University.*—The self-diffusion coefficient of cobalt in gelatin gel was measured at 5°C by permitting the gelatin blocks with equal concentration of $Co(NO_3)_2$ to lie in contact for different times ranging from 72 to 600 hours. The lower block contained a trace of Co^{60}. The self-diffusion coefficient was found to vary slightly with time averaging 1.73×10^{-6} cm²/sec. The analyses were made on 1 mm sections of the blocks into which the Co^{60} diffused. The experimental values are discussed in terms of the models for diffusion in binary alloys presented by Seitz and Bardeen. It is shown that the values are consistent with a mechanism which assigns a "brush-heap" structure to the gel with the Co ions moving from position to position by a place-exchange process. The Einstein-Stokes equation gives an abnormally small value for the radius of the diffusing particle. The activation energy with the above value of D according to the Frenkel theory is $q\sim2kT$.

* Assisted by the ONR and Research Corporation of New York.

C6. Frequency Factor and Activation Energy for the Volume Diffusion of Metals.* G. J. DIENES, *North American Aviation, Inc.* (Introduced by M. M. Mills).—The theoretical equations proposed for calculating D_0 of the diffusion-constant-temperature relation $D=D_0e^{-E/RT}$ are critically discussed in the light of presently available data. It is concluded that none of the relations gives satisfactory agreement with experiment. Empirical analysis of experimental data covering a wide range of D_0 and E values showed that the quantity E/T_m, where T_m is the melting point in °K, is the main factor in determining the value of D_0, and that D_0 depends approximately exponentially on E/T_m. In addition to many other diffusion constants, it is shown that the anisotropic diffusion of zinc and the widely differing diffusion constants for self-diffusion in α- and γ-iron are included in the proposed empirical correlation. A possible theoretical basis for the empirical correlation is described based on the idea of local melting or disordering. The quantity E/T_m is identified with the entropy of activation.

* This document is based on work performed under Contract for the AEC.

C7. The Rate of Diffusion of Gold into Copper at Low Gold Concentrations.* A. B. MARTIN AND FRANK ASARO, *North American Aviation, Inc.*—The rate of diffusion of small concentrations of gold into copper has been measured by the radioactive tracer method. Radioactive gold was electroplated on the ends of small polycrystalline copper rods and the samples annealed at temperatures between 750°C and 1000°C. The penetration of gold was determined by sectioning in a lathe, the chips from each cut being collected, weighed, dissolved in acid, and the activity measured with an immersion Geiger counter. The data have been analyzed assuming D to be independent of concentration. The variation of D with temperature is described by $D=Doe^{-Q/RT}$, with $Q=44{,}900\pm1300$ cal./mole and $Do=0.1\pm0.06$ cm²/sec. (least squares fit). Although the data are not sufficient at the present time to permit a detailed quantitative analysis of the various factors which influence the measured values of the diffusion coefficients, it appears that Q and Do are constant within the statistical reliability of the results for (1) gold concentrations from 0.001 to 1.0 atom percent, (2) copper purity from 99.999 percent to 99.95 percent, and (3) grain sizes having mean linear dimensions up to 1.0 mm.

* This paper is based on work performed under Contract for the AEC.

C8. Effect of High Energy Neutron Bombardment on Crystal Lattice of Beryllium, Graphite, Diamond, and Aluminum.* S. S. SIDHU AND C. O. HENRY, *University of Pittsburgh.*—Powdered samples of beryllium, graphite, diamond, and aluminum were bombarded for periods of about 10, 20, and 30 hours with neutron flux of 6.4×10^8 neutrons/sec./cm²/microampere of deutron current. The flux was obtained from Be(d,n) reaction with deutron energy of 15 Mev from the University of Pittsburgh Cyclotron. The energy corresponding to the maximum intensity in the hetrogeneous beam of neutrons was approximately 3 Mev. X-ray diffraction patterns of the samples were made before and after the bombardment, and the diffraction data obtained from these patterns were compared. Marked changes were observed in some of the lattices. These results will be reported.

* This research was supported in part by ONR.

C9. The Photography of Atoms in Crystals.* In the ordinary simple microscope, the same light is permitted to flow through the entire system. A more general microscope can be devised in which light of one wave-length is permitted to flow as far as the diffraction image of the object, then light of a second wave-length is substituted at this plane, and continues to flow through the rest of the optical system. It is shown that for such a generalized microscope, the magnification depends not only on the ordinary image-to-object distance ratio, but also on the ratio of wave-lengths used. Utilizing x-rays and visible light, this second factor is about 10^4 diameters, and the whole magnification is of the order of 3×10^5. This is enough to permit one to see an atom. Apparatus has been built which realizes this theory. A most important characteristic of any such system is that a loss of phase occurs at the first diffraction image, where the wave-length substitution takes place. This phase must be supplied by the apparatus. It is accomplished with the aid of phase shifters prepared from a large uniform mica cleavage fragment. The apparatus and the results achieved with it are described.

* Author unknown. This is presumed to be a case in which the author put his name and address only in the covering letter, which was destroyed before the omission of these data from the abstract was perceived.

C10. X-RAC and the Feasibility of Automatic Crystal Structure Analyses.* RAY PEPINSKY, *The Pennsylvania State College.*—X-RAC, the analog computer for crystal structure analysis, generates a two-dimensional density function involving up to 820 Fourier coefficients in less than one second. All centro-symmetric functions corresponding to complete permutations of 20 phases, e.g., or 2^{20} syntheses, can thus be generated and recorded in a few hours. These syntheses can be automatically examined for maximum and minimum excursions, number of maxima, molecular symmetry, possible knowledge of the density function in certain regions, etc., and acceptable syntheses and corresponding phases recorded in this time. Guidance as to choice of terms for such phase permutation can be obtained from phase-limiting equalities and inequalities arising from positiveness, upper limits, atomicity, etc. The number of terms required for a synthesis is reducible through application of artificial temperature factors of various strengths, and choice of most significant coefficients can be made through examination of correspondence between Patterson syntheses formed from a restricted number of terms and from the complete array of terms. Further approaches to automatic determination are possible via the X-RAC structure-factor computer. Atomic coordinates are established in this by d.c. voltages. These can be modulated until agreement between calculated and observed factors is simultaneously obtained at a number of reciprocal lattice nodes.

* Development supported by ONR.

C11. Low Temperature X-Ray Diffraction Goniometer.[1] B. C. FRAZER AND RAY PEPINSKY, *The Pennsylvania State College.*—A low temperature x-ray goniometer has been constructed for single crystal studies at temperatures of liquid air and below, and specifically for investigations of ferroelectric crystals below their Curie points. The instrument is similar in its basic features to a design by Helmholtz,[2] but the incorporation here of an adjustable arc goniometer and convenient translatory adjustments permits ordinary single-crystal techniques. Standard oscillation, Weissenberg, or precession camera methods may be used. The crystal is cooled by conduction through a copper mount at the base of the liquid air chamber of a demountable stainless steel Dewar. Surrounding the crystal and completing the outer wall of the Dewar is a removable glass bulb drawn down to a thin-walled tube in the immediate vicinity of the crystal. The crystal is irradiated through the thin-walled tube and is rotated in the beam by rotation of the Dewar. Vacuum is maintained during operation by continuous pumping. Details of construction and operation of the instrument and the modifications necessary for use with liquid hydrogen are discussed.

[1] Development supported by Signal Corps Engineering Laboratories.
[2] L. Holmholtz, J. Chem. Phys. 3, 740 (1935).

C12. Performance of Cadmium Sulphide as a Detector of X-Radiation. JOHN E. JACOBS,* *General Electric X-Ray Corporation* (Introduced by Richard W. Jones).—CdS crystals were irradiated with 1.54A pulsating x-radiation and the a.c. component of crystal current was measured. The very long delay in reaching steady state conditions observed when the d.c. component is measured was eliminated by this means. When a secondary illumination of constant magnitude is applied to the crystal while it is irradiated with pulsating X-rays it is found that the characteristics of the crystal are altered greatly. Green light increases the yield while red and blue light decreases the yield. Crystals having lattice defects as evidenced by asterism in Laue patterns were found to have random noise currents as well as to exhibit erratic multiplication processes. Crystals have been subjected to total quanta exceeding 10^{12} with no apparent change in characteristics. It is necessary to irradiate the region adjacent to the negative electrode to achieve maximum output currents. If the x-ray beam is confined to a narrow region adjacent to the negative electrode, blocked for a period and suddenly applied, a current in excess of the steady state value is observed. This effect is modified by use of a secondary illumination.

* Work carried out at Northwestern University.

WEDNESDAY EVENING AT 21:00

Anfiteatro Bolívar

(MANUEL SANDOVAL VALLARTA presiding)

El átomo desde Lucrecio hasta ahora. KARL K. DARROW, *Bell Telephone Laboratories.*

(Conferencia popular)

THURSDAY MORNING AT 10:00

Minería

(A. C. G. MITCHELL presiding)

Nuclear Instrumentation; Beta-Emitters

D1. Electrostatic Direct Current Transformer of 300 Kilovolts.* JOSE MIRELES MALPICA, *Instituto Politecnico Nacional.*—A search for a source of d.c. high voltage for the acceleration of electrified particles led to the Direct Current Electrostatic Transformer. A rotating dielectric transfers electrical energy from a primary to a secondary circuit. A

pair of metallic brushes with the moving dielectric between them and connected to a d.c. source of high voltage, constitutes the primary circuit. The charging current is passed to the surface of the dielectric by corona. When the charged region reaches the secondary brushes, a potential difference approaching the primary voltage is set up between them. In the 1 to 1 d.c. electrostatic transformer the secondary current is given by the following relationship: $i=S(E_p-E_s)\times C_s dA/dt$, where: S is a function of the corona conduction conditions, E_p primary voltage, E_s secondary voltage, C_s capacity per unit area, dA/dt rate of change of area per unit time. Since the primary and secondary circuits are conductively independent, several disks can be placed on a shaft with the primaries in parallel and the secondaries in series, raising the voltage. The 1 to 9 ratio experimental 300 kilovolt electrostatic transformer is used for industrial radiography and is a step in the construction of a one million volt transformer.

* This paper will be given as an invited paper in Session I.

D2. Synchrotron-Oscillation Resonance. NELSON M. BLACHMAN, *Brookhaven National Laboratory.**—Although detrimental betatron-oscillation resonances in a synchrotron have been studied,[1] synchrotron-oscillation resonance has received less attention. The latter's frequency is much lower than the former's, varying from 2620 to 1800 c.p.s. in the Brookhaven proton synchrotron, and resonance may occur with power-supply harmonics. The Brookhaven magnet is powered by a nominally 60-cycle generator and 12-phase rectifier having significant output components at multiples of 720 c.p.s.; the third gives cause for concern. The corresponding ripple of the magnetic field is extremely small because of the magnet's inductance; yet a large synchrotron oscillation may result, losing much of the beam. An extremely small ripple or noise modulation in the accelerating frequency, if present, would have a similar effect; the synchrotron is less sensitive to amplitude modulation. The effect of the magnetic-field ripple, if not filtered out, may be corrected by introducing compensatory a-m or f-m. Such f-m will be introduced by the system which continuously produces the proper frequency for the magnetic field, though some error may be present. The fall in the synchrotron-oscillation frequency with increasing amplitude also helps by its detuning effect.

* Work done under the auspices of the AEC.
[1] E. D. Courant, J. App. Phys. **20**, 611 (1949); D. M. Dennison and T. H. Berlin, Phys. Rev. **69**, 542, and **70**, 764 (1946); N. M. Blachman and E. D. Courant, Rev. Sci. Inst. **20**, 596 (1949).

D3. The Axial Motion of an Electron in a Constant Wave Velocity Section of a Linear Accelerator. DAVID CAPLAN AND EDWARD AKELEY, *Purdue University.*—The relativistic differential equations for the axial motion of an electron in a wave guide, excited by a progressive sinusoidal longitudinal electric wave of constant $\beta \leq 1$, have been integrated. The first integral yields the results of Slater, and gives the energy phase relationship, which is periodic. A second integration yields the phase-distance relationship, and thus completes the determination of the orbits. All separatrices, and the special case of $\beta=1$, are exactly integrable in terms of trigonometric and hyperbolic functions, while the general case requires elliptic integrals of the first and third kind. The former are obtainable from tables, while the latter are evaluated by series expansions, or in the case of particles near the crossing point of the separatrices where the convergence is slow, by the use of the addition theorem for elliptic functions of the third kind. Families of complete orbits in the form of energy-distance and time-distance graphs will be shown for $\beta=0.7$ and 0.97. These are applied to the proposed new Purdue accelerator, which is to consist of three constant wave velocity sections corresponding to $\beta=0.7$, 0.97, and 1, respectively.

D4. The Longitudinal Motion of Electrons in a Linear Accelerator. THOMAS KEENAN and EDWARD AKELEY, *Purdue University.*—Using a modification of a method previously reported,* the energy and phase of electrons moving on the axis of an accelerator have been determined as a function of the distance along the axis. A synchronous particle is defined for the progressive wave case, and the deviations of the energy and phase of an actual electron for both the progressive and standing wave cases from that of the synchronous are expressed as power series in the initial values of these deviations. The coefficients in these expansions are power series in the amplitude of the force acting on the particle. Both expansions have been computed through second-order terms. The computations have been made for a class of accelerators in which the initial energy of the synchronous particle is 50 kev, while its phase relative to the wave is variable. Graphs have been drawn in the progressive wave case for various values of (1) phase of synchronous particle relative to wave, and (2) initial deviation of phase of actual particle relative to synchronous one. In certain cases, corresponding standing wave graphs have been made.

* Hoffman and Akeley, Phys. Rev. **77**, 761, 1950.

D5. Krypton Bombardments: Radioactive Rb 84. WALTER C. BECKHAM* AND M. L. POOL, *Ohio State University.*—Krypton, in an internal gas container, was bombarded with 20-Mev alpha-particles and 10-Mev deuterons. The interior of the container was washed after bombardment with dilute HCl to recover transmutation products. The Rubidium fraction from the deuteron bombardment showed a 38-day half-life. The same activity was obtained by the α+Br reaction. Histograms show that β^+ and β^- are both emitted by this 38-day activity with the number of $\beta^+/\beta^-=6.2$. An end-point energy of 1.3 Mev was obtained by absorption measurements. A gamma-ray of 0.8 Mev is also present. K-capture is inferred from the observed X-rays. Based upon the mode of production and the characteristic radiations emitted the 38-day activity is clearly assigned to Rb 84. The strontium fraction of the Kr+α bombardment shows three position emitting activities which have not yet been assigned mass numbers.

* Lt. Col. U. S. Air Force.

D6. Characteristic Radiations of Rhodium (105).* C. E. MANDEVILLE AND E. SHAPIRO, *Bartol Research Foundation.*—The 36.8-hr. rhodium (105) was grown from its short-lived ruthenium parent when metallic ruthenium was irradiated by neutrons in the Oak Ridge pile. The target material was purified prior to irradiation by the distillation of RuO_4 from a perchloric-sulfuric acid solution of $RuCl_3$. Chemical separations for the removal of ruthenium and technetium were carried out subsequent to exposure. The beta-rays have a maximum energy of ~0.6 Mev as measured by aluminum absorption, and the gamma-rays were found to have an energy of 0.30 Mev when absorbed in lead. The beta-gamma coincidence rate is independent of the beta-ray energy, and the magnitude suggests that the harder beta-rays are coincident with soft quanta of the x-ray region. Very few beta-rays are coincident with the gamma-ray at 0.30 Mev. No beta-beta coincidences were detected for ranges exceeding 6 mg/cm^2. No gamma-gamma coincidences were found.

* Assisted by the joint program of the ONR and the AEC.

D7. Excitation Function for the 6.7-hr. Cd^{107} by (p,n) and $(d,2n)$ Reactions from Ag^{107}. D. N. KUNDU AND M. L. POOL, *Ohio State University.*—A stack of Ag foils (each 0.3 mil thick) was bombarded with 5-Mev protons and 10-Mev deuterons within a special target. The stack was shielded on all sides except for a small slot for the entry of the beam. From the activities measured up to thicknesses far beyond the range of the bombarding particle, the excitation function for the 6.7-hr. Cd^{107} was constructed. The thresholds for the $Ag^{107}(p,n)$ and $Ag^{107}(d,2n)$ reactions were at 3.15 and 4.50 mils respectively. The (p,n)-curve dropped steeply by a factor $\sim 10^{-6}$ from the first to the 10th foil beyond which it could not be traced. The proton resonance peaks expected in the light of recent reports[1] are, therefore, not observed. The resonance peaks for the 6.7-hr. activity reported from secondary protons in deuteron bombardments, were also looked for but not found. The presence of proton resonance peaks should have been observed more clearly in this straight proton bombardment than in one where the protons have to result from a primary deuteron reaction. In the deuteron bombardment, the 13-hr. Pd^{109} was again quite high in the front foils as compared to that resulting from the (n,p) reaction alone.

[1] C. Chamie, J. de Phys. et Rad. 11, 77 (1950).

D8. Gamma-ray Spectrum of the 2,3 Day Isomer of Cadmium 115*. E. BROCK DALE AND J. D. KURBATOV, *Ohio State University.*—Cadmium metal was activated by neutrons in Oak Ridge National Laboratory and was studied with a thin lens gamma-spectrometer. In addition to K and L photoelectron-peaks produced by the 336 ± 1 kev gamma-ray, photoelectrons of energies of 434 ± 1 kev and 506 ± 2 kev were found. These photoelectrons correspond to a gamma-ray, 522 ± 2 kev. It has been observed that the 522 kev gamma-ray, prompt transition in indium 115, follows the 2.3 day isomer of cadmium 115.[1] The 336 kev gamma-ray is emitted by the metastable state, $T_{\frac{1}{2}}=4.5$ hr., of indium 115 as had been established previously. Less intense peaks of photoelectrons of lower energy than 0.5 Mev were also found in the 2,3 day cadmium 115. The scheme of disintegration of cadmium 115 will be discussed.

* Supported by a grant of The Development Fund of the Ohio State University.

[1] J. M. Cork and others. Bull. Am. Phys. Soc. 25, 47, V10 (1950).

D9. Forbidden Shape Beta Spectrum of Sb^{124}.* L. M. LANGER, R. D. MOFFAT, AND H. C. PRICE, JR., *Indiana University.*—By means of improved techniques and higher specific activity sources, the beta-spectra of $Sb^{124}(60.d)$ have been reinvestigated in greater detail and with greater accuracy than was possible previously.[1] The 40 cm radius of curvature, shaped field spectrometer was used for the measurements. It is now found that the highest energy group has a spectrum shape of different from that of an allowed transition. The observed distribution is satisfactorily explained by means of the factor a, characteristic of a once forbidden transition involving a spin change of two units and a parity change. The twice forbidden factor c does not fit the data. The ft value is $\sim 10^{10}$. According to the nuclear shell model, the transition from $_{51}Sb_{73}^{124}$ to the ground state of $_{52}Te_{72}^{124}$ is expected to have a parity change. Because of the forbidden shape, the end-point values for the two highest energy groups are changed to $2.291\pm.005$ and $1.69\pm.01$ Mev. A gamma-ray corresponding to this energy difference was reported earlier.[1] A search was made for possible positron emission to Sn^{124} and also for Auger electrons following possible K-capture. No indication was found that these processes compete in measurable amounts with the observed negatron emission to Te^{124}.

* Assisted by a grant from the Frederick Gardner Cottrell Fund of the Research Corporation and by the Joint Program of the ONR and AEC.

[1] C. S. Cook and L. M. Langer, Phys. Rev. 73, 1149 (1948).

D10. Re182 and Re183 by Relative Cross Sections. H. TALMAN DYBVIG AND M. L. POOL, *Ohio State University.*—It has been determined through relative cross-section measurements that a $14H$ activity which decays by K-capture with a 0.92 Mev γ-ray is located in Re182 and a $2.8D$ activity decaying by K-capture with a 1.75 Mev γ-ray is to be found in Re183. In addition, the $3.79D$ activity of Re186 was confirmed. These activities were produced by deuteron bombardments on tungsten in which enriched isotopes from Oak Ridge were used. The enriched isotopes ($W182$ and $W183$) which were received in the oxide state were reduced to the metallic state before bombardment; and after bombardment, the tungsten and rhenium fractions were chemically separated. The relative cross-section calculations which give the above results were made using the $3.79D$ activity of Re186 and the $24.1H$ activity of $W187$ as monitors.

D11. Radiations from Os^{185}, Os^{191} and Os^{193}.* MERLE E. BUNKER, ROBERT CANADA, AND ALLAN C. G. MITCHELL, *Indiana University.*—The radiations from Os^{185} (97 days), Os^{191} (32 hr.) and Os^{193} (15 days) have been investigated with the help of a magnetic lens spectrometer. Os^{185} decays by orbital electron capture accompanied by two gamma-rays of energy 0.648 and 0.878 Mev. The number of gamma-ray quanta of 0.648 Mev is six times that of 0.878 Mev. Os^{191} decays by the emission of beta-rays of maximum energy 1.10 Mev and does not appear to be accompanied by any gamma-rays. Os^{185} decays by beta-particle emission accompanied by two gamma-rays of energy 0.128 Mev and 0.041 Mev. The beta-ray spectrum is obscured by internal conversion and Auger lines. The end point is approximately 0.135 Mev.

* Assisted by the joint program of ONR and AEC.

D12. Los Espectros Continuous de los β-Rayos de los Gases Radioactivos en la Cámara de C. T. R. Wilson. MARGUERITE M. ROGERS* Y F. T. ROGERS, JR.,* *University of North Carolina.*—Los espectros de los β-rayos, por ejemplo de[1] Hídrogeno 3 y[2] Bismuto 210, han sido deducidos por las medidas de la distribución, $H(p)$, de las proyecciónes de las trayectorias (por H^1H^3O y $Bi^{210}(CH_3)$ respectivamente) en una cámera de Wilson. Permitimos $H(p)=\Sigma a_i \exp(-b_i p^2)$ ó $\Sigma c_{2i} p^{2i}$; pues la relación

$$H(p)\sim\int_x\int_\phi G(p\csc\phi)dxd\phi$$

de la distribución, $G(l)$, de las longitudes; aquí $\mathbf{x}$ es el eje de observación y ϕ es el ángulo con $\mathbf{x}$. Desués de corrección de la estadística por las longitudes y los torcimientos, la distribución de las energías cinéticas se obtienen esencialmente por multiplicación con la raíz cuadrada del alcance. Este método, primeramente intendado por A. Leigh-Smith y H. O. W. Richardson, parece superior en ciertas investigaciónes con el espesor minimo del soporte por la materiál radioactiva.

* Ahora en U. S. Naval Ordnance Test Station, Inyokern, California.

[1] W. J. Byatt, F. T. Rogers, Jr., y A. W. Waltner, Phys. Rev. 75, 909 (1949).

[2] A. W. Waltner y F. T. Rogers, Jr., Phys. Rev. 75, 1445 (1949).

THURSDAY MORNING AT 10:00

Anfiteatro Bolívar

(I. I. RABI presiding)

Symposium on Cosmic Rays

E1. Geomagnetic Analysis of the Primary Spectrum. MANUEL SANDOVAL VALLARTA, *El Colegio Nacional y Instituto de Física. Universidad de Mexico.* (20 min.)

E2. Geomagnetic Effects at the Top of the Atmosphere. J. R. WINCKLER, *University of Minnesota.* (20 min.)

E3. The Magnetic Field of the Sun. D. H. MENZEL, *Harvard University.* (20 min.)

E4. The Energies and Nuclear Interactions of Heavy Primary Rays. E. P. NEY, *University of Minnesota.* (20 min.)

E5. On the Nature of the Primary Cosmic Rays. H. L. BRADT, *University* of *Rochester.* (20 min.)

E6. Disintegrations and Meson Production by Relativistic Particles at Different Latitudes. E. O. SALANT, *Brookhaven National Laboratory.* (20 min.)

THURSDAY AFTERNOON AT 15:00

Anfiteatro Bolívar

(C. C. LAURITSEN presiding)

Symposium on Cosmic Rays, Concluded

F1. Nuclear Collisions Between High Energy Cosmic-Ray Particles. MARCEL SCHEIN, *University of Chicago.* (20 min.)

F2. The Abundance and Masses of Cosmic-Ray Particles at Low Elevations. R. B. BRODE, *University of California, Berkeley.* (20 min.)

F3. The Particles in Penetrating Showers. C. D. ANDERSON, *California Institute of Technology.* (20 min.)

F4. Penetrating Showers from Carbon and Lithium. W. B. FRETTER, *University of California, Berkeley.* (20 min.)

F5. Neutrons in the Cosmic Rays. S. A. KORFF, *New York University.* (20 min.)

F6. Some Properties of the New Unstable Cosmic-Ray Particles. R. B. LEIGHTON, *California Institute of Technology.* (20 min.)

THURSDAY AFTERNOON AT 15:00

Minería

(E. S. AKELEY presiding)

Invited Paper

G1. Theories of Gravitation. H. P. ROBERTSON, *California Institute of Technology.* (40 min.)

G2. A Perfectly Symmetrical Universe in Flat Space-Time. CARLOS GRAEF FERNÁNDEZ, *Institute of Physics of the University of Mexico.* (20 min.) (Absrtact underneath.)

Gravitation, Relativity, Theoretical Physics

G2. A Perfectly Symmetrical Universe in Flat Space-Time. CARLOS GRAEF FERNÁNDEZ, *Institute of Physics of the National University of Mexico.* (Introduced by M. S. Vallarta).—A cosmology is developed in the flat space-time of Einstein's theory of special relativity as an extension of Birkhoff's theory of gravitation to cosmical scale. It is assumed that the metagalaxy is perfectly symmetrical; i.e., that the mass-density measured at all galaxies is the same function of the age of the universe. A consequence of this type of symmetry is a universe with a finite volume and an infinite mass. The distribution function for the velocities of the galaxies is obtained, and so is the total number of galaxies for a given apparent magnitude.

G3. Potentials of a Rotating Spherical Shell in Birkhoff's Theory of Gravitation. FERNANDO ALBA, *Institute of Physics of the National University of Mexico.*—Starting with the potentials of Birkhoff's theory due to a moving particle, the gravitational potentials of a rotating spherical shell are obtained for the interior and for the exterior of the sphere. These potentials can be expressed exclusively in terms of zonal harmonics of the orders zero and two. The equations of

motion of a particle moving in the interior or in the exterior of the spherical shell are established. The exterior potentials for a rotating sphere can be easily obtained if the density is a function of the radius alone.

G4. Vector Boundary Value Problems and Their Applications. J. ADEM AND M. MOSHINSKY, *Institutos de Geofísica y Física, Universidad de México.*—Some problems in the field of heat conduction and in vibration phenomena have suggested the formulation of a special type of boundary value problem. For example, the problem of heat conduction in a cross, is a complex one when one considers the surface of the same as a boundary. If, on the other hand, we define the vector $\theta=(\theta_1, \theta_2, \theta_3, \theta_4)$ in which each of the components $\theta_i(x, t)$ correspond to the temperature associated with a corresponding branch of the cross, the problem reduces to that of conduction of heat in 4 bars with appropriate boundary conditions at the end points, and it can be completely solved. We have discussed the general mathematical formulation of these problems, in which the vector function satisfies both, a matrix differential equation in the interval [0, 1] and general boundary conditions at the boundary of the interval. The method has been applied to the conduction of heat in interconnected rings, in a reel, in a wheel, etc., and to problems of vibrations of plates that interact through an elastic medium, etc. The methods developed suggest interesting analogies for some nuclear physics problems.

G5. Un Cero de una Cierta Función de las Funciónes de Bessel. F. T. ROGERS, JR., *U. S. Naval Ordnance Test Station,* Y H. L. MORRISON, *North Carolina State College of Engineering.*—Permitimos $\nu(R)=+(1+1/R^2)^{\frac{1}{2}}$, $u(R, r, \rho)=+(1/rR-\rho/R^2)^{\frac{1}{2}}$, y $c=\exp(-\pi R)$. El cero primero de $J_\nu(u)J_{-\nu}(cu)-J_\nu(cu)J_{-\nu}(u)$ con respecto á $\rho<0$, por $R>0$ y $r>0$, se requiere[1] en problemas ciertas de la estabilidad critica dinámica de los fluidos. Este cero se identifica por los ν-valores positivos de los enteros medios nones, de $\rho=R/r-M(R)$. Hemos computado de un método numérico que $M(R)=2.25+7.17R+10.71R^3$ por $0\leq R\leq 0.9$; estimamos en $M(R)$ incertidumbres menor de 0.05 de la desviación promedia.

[1] Esto determina, por ejemplo, la cercanía térmica circa de la estabilidad critica en el fluido real (en otras palabras, con un coeficiente $\neq 0$ por la dilatación termal) que es impidiendo según la ley de Darcy.

THURSDAY AFTERNOON AT 15:00

Minería

(L. MARTON presiding)

Mostly Electron Physics and Optical Physics

H1. Effect of Space Charge on Pulsed Electron Beams. SURINDRA N. KALRA, AND WILLIAM J. FRY, *University of Illinois.*—The effects of space charge on the definition of pulsed electron beams is investigated. Three types of pulses are considered, namely, plane parallel pulses of infinite extent, coaxial cylindrical pulses of infinite length, and concentric spherical pulses. By considering the expansion of surfaces of the same geometry as the pulses, the expansion of the set of pulses due to space charge forces alone can be studied. A uniform initial charge density inside each pulse is assumed. In case of a single pulse of any of the three geometrics described above, the time, τ, needed for the pulse to double its initial dimensions is independent of the initial dimensions. The current density, J, such that in time, τ, the pulses just double themselves in dimensions for zero initial velocity is given by: $J_0=5.96\times10^{-17}\phi^{\frac{1}{2}}/\tau^2$ for plane parallel pulses, $J_\tau=4.64\times10^{-17}\phi^{\frac{1}{2}}/\tau^2$ for spherical, and $J_0=1.37\times10^{-16}\phi^{\frac{1}{2}}/\tau^2$ for cylindrical pulse; where ϕ is the beam potential in m.k.s. units. It can be shown that during the expansion of the pulses under space charge forces the separation between successive infinite plane parallel pulses remains constant and the charge density at any time is uniform insider every pulse, and τ is the same for all pulses. In the cases of spherical and cylindrical pulses, successive pulses catch up with one another.

H2. Generation of Coherent Electromagnetic Radiation. LLOYD T. DEVORE, SURINDRA N. KALRA, AND WILLIAM J. FRY, *University of Illinois.*—Possible limitations on the generation of coherent e.m. radiation are considered with respect to a coupling system fed by a pulsed electron beam. After a certain length of time, an equilibrium is reached in the coupling and radiating device such that the energy radiated plus that lost because of resistance of the walls, etc., in a unit time is equal to the energy input. At equilibrium, the product of energy and frequency in the coupling device is $P=(QJ^2A^2l^2)/(\pi f\epsilon V)$, where J is the current density, A the area and l the length of the path of the current beam through the device, f the frequency, ϵ the permitivity and V the volume. If the volume of the device is large compared to one wave-length, then the noise power is given by $P_n=(8\pi kTVf^4)/(QC^3)$. If γ is the signal to noise ratio required, then $P=\gamma P_n$ yields the minimum value of Q needed at any frequency or for a given value of Q, it yields the maximum frequency that can be generated with a given value of γ. For spherical metal cavities, this relation reduces to $f^6=1.97\times10^{73}J^2/\gamma$. The limitations on J are discussed in the preceding paper.

H3. Space Charge Distribution in a D.C. Cut-Off Magnetron. D. REVERDIN AND L. MARTON, *National Bureau of Standards.*—The elementary magnetron was investigated by sending an electron beam axially through the tube. From the complicated shadow patterns cast by two wire screens, one can determine the change of direction of individual trajectories of the exploring beam due to the electric space charge field in the magnetron. The conclusions of the study are that the space charge distribution does not conform to Hull's predictions. Three different shapes of space charge distribution were observed. One has a sharp maximum near the cloud radius. The second falls off gradually toward the cathode. The third is time variant. The shape of the space charge distribution is closely related to the symmetry of the magnetron. The experiments seem to confirm Haeff's theory of noise amplification in a dense space charge cloud. The presence of a double stream of electrons is very probable.

H4. Electrostatic Charging of Aircraft Glass During Flight. E. STICKLEY, *Pittsburgh Plate Glass Company,* M. M. NEWMAN AND J. D. ROBB, *Lightning and Transients Research Institute.*—Loss of radio communication occurs when flying through serious precipitation static conditions. The role of the glass portions of the aircraft surface in this phenomenon has been investigated. It has been established that streamering

discharge across the glass surface, as a result of triboelectrification, is a major cause of radio interference. The resultant electrical transients and their interaction on radio receiving equipment were recorded by high speed oscillography. In contrast to earlier corona oscillograms which were distorted and lengthened by amplifier time constants, the steep impulsive nature of streamer and corona transients was brought out by new wide-band amplifier techniques.

H5. General Theory of Voltage Stabilizers. J. J. GILVARRY AND D. F. RUTLAND, *Rand Corporation and Institute for Numerical Analysis, N. B. S.*—The standard theory of voltage stabilizers,[1] which characterizes a stabilizer by three parameters (the stabilization ratio, internal resistance, and equivalent bleeder conductance), requires an approximation in general application, since an active four-terminal network requires four parameters for its specification. A fourth parameter can be obtained by a generalization of the equivalent bleeder conductance to yield two parameters. Defining the four-performance parameters as independent of load, one can construct an equivalent circuit of four elements (which are functions of the performance parameters) for the general voltage stabilizer. The general solution of the problem of expressing the over-all performance parameters of a stabilizer in terms of parameters of the stabilizer itself and the load and supply resistances then follows directly. As compared to previous results[1] (which now refer strictly to an identifiable special case only), no change in the general formula for the over-all stabilization ratio S occurs, but the formula for the over-all internal resistance R requires a correction. Confirmatory experimental results will be presented.

[1] F. V. Hunt and R. W. Hickman, Rev. Sci. Inst. 10, 6 (1939).

H6. Gyroscopic Stabilization of a Free Body.* J. K. TYSON, *Armour Research Foundation.*—The orientation of a free body may be stabilized by the use of three gyroscopes pointing in mutually perpendicular directions only if the gyroscopes are free to precess about mutually perpendicular axes. The equations of motion of the system are the Lagrange-Euler equations, which may be extended to bodies having internal degrees of freedom, and three equations for the precession of the internal gyroscopes. Solution of the linearized equations for the system demonstrates the approximate stability of the orientation against small torque impulses, while an approximate solution of the non-linear equations provides a description of the behavior under torques of long duration. The initial motion of the body is a uniform rotation at a rate governed by the frictional torques resisting precession of the gyros, while approximate stabilization is maintained for a torque impulse equal to the total angular momentum change of the gyros during their precession.

* Work sponsored by Equipment Laboratory, Air Materiel Command.

H7. Mass Spectrometric Studies of Two Series of Organic Compounds.* ANTHONY DONFOR, WEBSTER KENDRICK, AND HERMAN BRANSON, *Howard University.*—The two series (1) methane, methyl chloride, dichloromethane, chloroform and carbon tetrachloride, and (2) methyl amine, dimethyl amine, and trimethyl amine have been studied in a 60° Nier-type mass spectrometer. The electron intensity was 50 volts. Appearance potentials have been obtained for the molecular fragments. The data are viewed as additional information on the forces operating in the molecules.

* Assisted by the ONR and Research Corporation of New York.

H8. Raman Spectra at Low Temperatures. The Raman Spectrum of Tetramethyl Diborane. BERNARD RICE, J. M. GONZALEZ-BARREDO, AND T. F. YOUNG, *University of Chicago.*—Apparatus for the production of the Raman spectrum of a substance at a low temperature and in the absence of air has been designed and constructed. The Raman tube is encased in the upper part of a drilled copper rod the lower end of which is immersed in a Dewar flask containing a coolant, e.g., liquid nitrogen. Windows in the copper jacket admit the exciting light. The Raman spectrum of liquid tetramethyl diborane at a temperature below 0°C was photographed. The lines observed included none with frequencies characteristic of terminal boron-hydrogen stretching. This fact is evidence for a hydrogen-bridge structure in the tetramethyl diborane molecule:

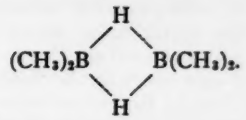

It also constitutes further evidence for a bridge structure in diborane. In the frequency range characteristic of bridge-hydrogen stretching two lines exist, instead of the one strong one found in the spectrum of diborane, B_2H_6.

H9. The Detection of Soft X-Rays with a Scintillation Counter.* LYMAN A. WEBB, RONALD S. PAUL, AND FRANCIS E. DART, *University of Oregon.*—Using a tube having a pure tungsten filament and an aluminum anode, x-rays in the range 5.6A to 15.5A (800 to 2200 ev) have been detected with a scintillation counter. The phosphor screen of wurtzite or other material protected from light by films of plastic and aluminum about 0.0002 cm thick is exposed to the x-rays within the tube. Scintillations are detected by an IP21 photo-multiplier tube and the signals passed through a linear amplifier and pulse height discriminator before they are counted with a conventional scaler. It is assured by means of grids placed in front of the screen that the scintillations observed cannot be due to electrons or ions. Counting rates are measured successively at various discriminator levels, the discriminator level being raised by 5 percent of the maximum pulse height at each successive measurement. The integral bias curves thus obtained are used to plot differential pulse height curves. These are able to detect the Al K line at 8.32A. Data will be presented on the effect of protecting film thickness on the wave-length threshold for detection of x-rays, on the results obtained with different phosphors, and on results obtained with different target materials in place of aluminum.

* Research supported in part by Geophysical Research Directorate, Air Force Cambridge Research Laboratories.

H10. Scintillation Properties of Solutions.* G. T. REYNOLDS AND F. B. HARRISON, *Princeton University.*—Experiments reported previously[1] have been extended to include a systematic study of many solutions, the effect of concentration of the solution, and the emission spectra of various solutions. Results show that terphenyl in *m*-xylene, *p*-xylene, or thiophene-free benzene give pulses about 0.4 the height of anthracene crystal pulses when observed with a 5819 photo-multiplier. Other solutions will be compared. A noticeable scintillation effect is observed with as little as 3 parts by weight of terphenyl in 100,000 parts of solvent. The response of various solutions to the cesium 600-kilovolt electron will be shown and compared to the response of an anthracene crystal. The emission spectra of solutions irradiated with ultraviolet light or x-rays contain significantly shorter wave-lengths than the corresponding spectra of crystals. The spectra of terphenyl and anthracene will be discussed in detail, as will the problem of matching the various scintillators with appropriate photomultipliers.

* This work was supported by the joint program of the ONR and AEC.
[1] Reynolds, Harrison, and Salvini, Phys. Rev. 78, 488 (1950).

H11. Probability of Auto-Ionization in Light Atoms. TA-YOU WU AND L. OUROM, *National Research Council, Canada.*—With the view of testing the adequacy of the method of treat-

ing such problems, the probability of radiationless transition of the $1s^22p3s\ ^1P$ state of Be to the continuum $1s^22s$+ejected p electron has been calculated according to the usual perturbation theory. The discrete wave functions are obtained by the variational method and the continuous wave function is obtained by numerical integration of the Schrodinger equation. The transition probability so obtained is $\sim 5\times 10^{13}$ per second, leading to a width of ~ 250 cm^{-1} for the level $1s^22p3s\ ^1P$. This is at least 10^3 times larger than what is indicated by the widths of the spectral lines observed. This result, together with similar earlier calculations for the He atom, shows that the perturbation theory is inadequate for the light atoms. It is also pointed out that in these calculations and those on the Auger effect in the literature, there is an inconsistency in the use of the perturbation, since the use of variational or "screened" wave functions implies that a part of the electron-electron interaction has already been included in the initial approximation and it is hence incorrect to treat this whole interaction as the perturbation causing the transition.

H12. Isotope Shift in the C^{14} Atomic Spectrum for $2p^1S_0 - 3s^1P_0$.* JOHN R. HOLMES, *University of Southern California.*—A measurement has been made of the wave number difference between the above line of C^{12} and that of C^{14} in order to compare it with the previous measurement of isotope shift in C^{13}.[1] It was thought that because of some change in nuclear structure there might be an anomalous shift in the spectrum of C^{14} such that the splitting between the lines of C^{12}, C^{13}, and C^{14} would not be due solely to the change in nuclear mass. The change in the Rydberg constant between C^{12} and C^{14}, the normal mass effect, would predict an isotope shift in this line of plus 0.261 cm^{-1}. The experimental measurement gave a shift of minus 0.294 cm^{-1}, indicating a "specific mass effect"[2] of minus 0.555 cm^{-1}. Comparing this with C^{12},[1] there seems to be no anomaly since the observed shifts are proportional to the percentage change in mass. This is the result expected from any effect depending solely on a change in nuclear mass, as contrasted with the nuclear volume effects found in heavy elements.[3]

* Supported by ONR.
[1] John R. Holmes, Phys. Rev. 77, 745 (1950).
[2] D. S. Hughes and Carl Eckart, Phys. Rev. 36, 694 (1930).
[3] M. F. Crawford and A. L. Schawlow, Phys. Rev. 76, 1310 (1949).

H13. A New Mounting for an Echelette Diffraction Grating. W. F. C. FERGUSON AND J. H. GREIG, *New York University, Washington Square.*—With this mounting a single ruled echelette grating may be used "in the blaze" over a very wide range of wave-lengths. This is accomplished by tilting the grating with respect to the incident light as in a Littrow mounting, and then rotating the grating about an axis perpendicular both to the grating elements and the incident beam. By this rotation the path difference between beams of light reflected from successive elements of the grating may be varied from a maximum value, the ordinary blaze wavelength, to zero. The spectrum reflected from the grating may then be reflected from a plane mirror, rotating with the grating, to produce a constant deviation mounting. The image of the slit is found to be tilted as the grating rotates. This can be compensated by a rotation of the slit. In a trial, using an echelette designed for the near infra-red, all orders of the sodium D-lines from the fifth to the first were caused to pass an observing telescope, successively in the blaze, by a 55 degree rotation of the grating mounting.

THURSDAY EVENING AT 21:00

Anfiteatro Bolívar

(MANUEL SANDOVAL VALLARTA presiding)

El sol y el universo. D. H. MENZEL, *Harvard University.*

(Conferencia popular ilustrada con la espectacular película "Explosiones en el Sol," que muestra gráficamente las protuberaciones gaseosas en la atmósfera solar)

FRIDAY MORNING AT 10:00

Anfiteatro Bolívar

(I. I. RABI presiding)

Invited Papers

I1. Electrostatic Direct-Current Transformer of 300 Kilovolts. JOSE MIRELES MALPICA, *Instituto Politecnico.* (15 min.) (Abstract printed under D1).

I2. Evolution of Modern Physics. R. A. MILLIKAN, *California Institute of Technology.* (40 min.)

I3. Low Velocity Layers in the Earth's Interior, the Ocean and the Atmosphere. BENNO GUTENBERG, *California Institute of Technology.* (40 min.)

I4. Lattice Imperfections and Plastic Flow in Metals. FREDERICK SEITZ, *University of Illinois.* (30 min.)

FRIDAY MORNING AT 10:00

Minería

(C. C. LAURITSEN presiding)

Gamma-Rays and Neutrons

J1. Gamma-Neutron Cross Section of Some Isotopes for γ-Ray Energies up to 27 Mev. L. KATZ, H. E. JOHNS, R. A. DOUGLAS, AND R. N. H. HASLAM, *University of Saskatchewan.*—Using the Schiff formula for bremsstrahlung in the forward direction[1] from a thin target and the computed response of an "*r*" meter to high energy γ-rays, it has been possible to calculate (γ, n) cross sections from the yield curves of these reactions induced by γ-rays from a betatron. We find the $Cu^{63}(\gamma, n)Cu^{62}$ cross section to have its maximum at 17.5 Mev and a value of 0.10 barn. The curve is fairly symmetric about this energy having a half width of 6 Mev and area of 0.6 Mev-barn between 11 and 24 Mev. This width is very much greater and is centered around a lower energy than that reported by Baldwin and Klaiber.[2] Our absolute value for the cross section is in good agreement with that obtained using Li γ-rays. The values for other reactions examined were

$Cu^{65}(\gamma,n)^{64}$	19 Mev	0.02 Barn	6 Mev	0.12 Mev barn
$Sb^{121}(\gamma,n)Sb^{120}$	14.5	0.20	6	1.2
$Sb^{123}(\gamma,n)Sb^{122}$	14.5	0.28	6	1.5
$Ta^{181}(\gamma,n)Ta^{180}$	13.5	0.05	5	0.26

[1] H. W. Koch and R. E. Carter, Phys. Rev. **77**, 165 (1950).
[2] G. C. Baldwin and G. S. Klaiber, Phys. Rev. **73**, 1156 (1948).

J2. Gamma-Rays Induced by the Proton Bombardment of Phosphorus.* G. RICHARD GROVE,† JOHN N. COOPER, AND J. C. HARRIS, *Ohio State University.*—Phosphorus has been bombarded by protons from the Ohio State Van de Graaff generator and a number of narrow (p, γ) resonances observed. The gamma-ray yield as a function of generator voltage reveals distinct intensity maxima at approximately 1.08, 1.11, 1.14, 1.17*, 1.27*, 1.43*, 1.47*, 1.50, 1.54, 1.59*, and 1.62* Mev, where the asterisks indicate the more intense peaks. The energies of the protons were obtained from the analyzing magnet current, which was calibrated in terms of the fluorine resonances. The cross sections for all these resonances are low; for the most intense, that at 1.27 Mev, the cross section is estimated to be of the order of 0.0004 barn by comparison with the fluorine 340 kev resonance. Thick and thin targets of zinc phosphide, evaporated on nickel and tantalum, have been studied. The thinnest target had a thickness of roughly 10 kev at 1.3 Mev.

* Assisted by the joint program of the ONR and the AEC.
† AEC Predoctoral Fellow.

J3. Gamma-Resonances in Magnesium Bombarded with Protons.* JOHN N. COOPER, WARREN E. TAYLOR, J. C. HARRIS, AND G. RICHARD GROVE.† *Ohio State University.*—Protons from the recently completed Ohio State University Van de Graaff generator have been used to bombard thin magnesium targets, prepared by evaporation on tantalum in a vacuum. A large number of gamma-resonances are observed in the voltage region between 0.35 and 1.5 Mev. In the vicinities of 450 and 720 kev there is considerable activity over a broad region; this activity has not yet been resolved. At proton energies of about 0.88, 1.03, 1.06, 1.11, 1.22, 1.26, and 1.35 Mev very distinct resonance yields of gamma-rays are observed. Near the 1.03 Mev resonance there is good evidence for the presence of two incompletely resolved "satellites." The contours of several other resonances suggest that they are not due to single levels. The complex nature of gamma-ray yield as a function of proton energy is not surprising in view of the fact that all three stable isotopes of magnesium were present in the targets.

* Assisted by the Joint Program of the ONR and the AEC and by the Ohio State University Development Fund.
† AEC Predoctoral Fellow.

J4. Measurement of Gamma-Ray Energies With Crystals of NaI(Tl). R. HOFSTADTER AND J. A. MCINTYRE, *Princeton University.*—A monoenergetic gamma ray (Energy $E_0 > 2mc^2$), on impact with a crystal of NaI(Tl) produces three pulse distributions according to the three possible interactions (a) Compton effect, (b) Photoelectric effect, (c) Pair production. The Compton effect results in a wide distribution of recoil electron energies, while the latter two interactions produce very narrow electron energy distributions. The photoelectric "line" has the energy $E_0 - E_K$ and the pair "line" $E_0 - 1.02$ Mev where E_K is the binding energy of the K electron in iodine. We have succeeded in observing all three distributions simultaneously in the same crystal. A single gamma-ray line therefore produces three peaked distributions two of which are sharp lines. Because of this multiplicity, careful consideration must be given to assignments in a complex gamma-spectrum. The two crystal coincidence spectrometer previously described[1] eliminates the photoelectric line but leaves the pair line along with the desired Compton peak. The pair line arises because an annihilation quantum is captured in the gate detector crystal. Results with Na^{24}, Co^{60}, Sb^{124} will be shown. This work was supported by the U. S. Army Signal Corps and by the joint program of the ONR and AEC.

[1] Bull. Am. Phys. Soc., Washington Meeting, 1950, paper G2.

J5. Angular Distribution of Gamma-Rays from Fluorine. R. B. DAY, C. Y. CHAO, W. A. FOWLER, AND J. E. PERRY, JR., *California Institute of Technology.*—Investigations are being made of the angular distribution of the γ-rays from the reaction $F^{19}(p, \alpha\gamma)O^{16}$. The detecting apparatus, which is similar to that used by Devons and Hine,[1] consists of Geiger counters mounted on a frame work that can be rotated about the target chamber. Coincidences between the front and back counters are recorded and provision is made for varying thicknesses of aluminum absorber to be placed between the counters. The target chamber and detecting equipment are surrounded by a large housing of lead bricks to reduce background radiation. Preliminary results indicate that the distribution is of the form $1 + a\cos^2\theta$. The values of a at various resonances are tabulated below.

E_p (kev)	873	935	1290	1355	1381
a	0.14	0.02	0.69	0.30	−0.03

This work was assisted by the joint program of the ONR and AEC.

[1] Devons and Hine, Proc. Roy. Soc. **199A**, 56 (1949).

J6. Neutron Capture Gamma-Ray Spectra. BERNARD HAMERMESH, *Argonne National Laboratory.*—The D_2O-soaked plate technique[1] has been applied to the neutron capture γ-ray[2] spectra of Al, Cl, Fe, Br, Cd, La, W, Au, and Hg. The method is limited to energies above 3 Mev and the energy resolution is approximately ±0.25 Mev. The spectra may be classified as follows: 1) Cd and Hg. The intensity is probably still rising below 3 Mev. The intensity decreases steadily up

to the high energy cut-off of the spectrum. There is no evidence of line structure. 2) Fe, Br, La, and W. The intensity is a maximum near 5 Mev. There is evidence of line structure. 3) Al, Cl and Au. The intensity is nearly constant over a wide range of energies. There is evidence of line structure. The spectra of the heavy elements W, Au and Hg might be expected to be similar on the basis of a statistical nuclear model. It is suggested that the differences may be due to the different odd-even character of the compound nuclei that probably emit the γ-rays, i.e., W^{187}, Au^{198}, and Hg^{200}.

[1] G. Goldhaber, Phys. Rev. 74, 1725 (1948).
[2] B. Hamermesh, Phys. Rev. 76, 182 (1949).

J7. Polarization Effects of Scattered Neutrons. W. E. MEYERHOF, D. B. NICODEMUS, AND FELIX BLOCH, *Stanford University.*—When a neutron is scattered from a nucleus ($I \neq 0$) there exists a finite probability Q of spin flip of the neutron, which permits a calculation of the spin scattering lengths.[1] We are measuring the spin flip probability by the change in polarization of a polarized beam of slow neutrons due to single scattering from various substances. Two $\frac{1}{2}$ in. thick iron blocks magnetized to saturation are used as polarizer for the neutron beam and analyzer for the scattered neutrons respectively. The cyclotron producing the neutrons is pulsed to reduce the fast neutron background. The experiment is complicated by the smallness of the singly scattered neutron intensity (20–50 slow neutrons/min.). To check the method we have measured Q for carbon ($I=0$) and found $Q=0.15\pm0.25$, the expected value being $Q=0$. Other results will be presented.

[1] O. Halpern and M. H. Johnson, Phys. Rev. 55, 898 (1939).

J8. Variation of High Energy Neutron Collision Cross Sections with Energy. J. DEJUREN AND B. J. MOYER, *University of California, Berkeley.*—An investigation of the variation of nuclear total cross sections for neutrons between 90 and 270 Mev has been made using bismuth fission for detection. The bombardment of a 0.5 in. Be target with protons in the 184 in. cyclotron produces a neutron flux of mean energy approximately 70 Mev less than the incident proton energy for bombarding energies between 160 and 350 Mev. The total cross sections of carbon, aluminum, copper, and lead approach constant values in the neutron energy interval between 180 and 270 Mev. The total hydrogen cross section decreases less rapidly than $1/E$. At 95, 160, 220, and 270 Mev, its values are respectively 73 ± 1.5, 51 ± 2.6, 41 ± 2.4, and 38 ± 1.5 millibarns.

J9. Experiments Upon Anisotropic and Inelastic Scattering with a Highly Collimated Neutron Beam. ALEXANDER LANGSDORF, JR., *Argonne National Laboratory.*—Neutrons are collimated by a tapered hole on the axis of a truncated conical shield whose apex is located at the source, the target of an electrostatic generator. The usual detector consists of nine BF_3 proportional counters on each of seven circles at increasing radii. The counters are embedded in a paraffin ring (17 in. O.D., $2\frac{3}{4}$ in. I.D., 13 in. long) 50 in. from the target and inside a cylindrical shield in back of the cone. The beam (of 10^{-3} steradian) only reaches the ring detector when scattered by a sample. Anisotropic scattering is measured by locating the scatterer before, in, or beyond the ring. For one Mev neutrons, and isotropic scattering, over-all efficiency of counting reaches 20 percent at the central position, and backgrounds are about 10 percent for scatterers of 90 percent transmission. Shielding is still adequate up to at least 1.5 Mev. Anisotropy associated with resonance scattering is particularly interesting. An "age" distribution is obtained from the radial counting distribution; once calibrated this gives information on neutron energy and hence inelastic scattering. Anisotropy effects complicate interpretation. These techniques give low resolution data very rapidly. Higher resolution may be obtained using the same equipment in other ways with lower counting rates. Transmission cross section data is readily obtained with small samples.

FRIDAY MORNING AT 10:00

Minería

(R. B. BRODE presiding)

Cosmic Rays, I

K1. Camaras para Rayos Cosmicos. R. RICHARD-FOY, *Comision Impulsora de la Investigacion Cientifica, Mexico.*—Construímos seis cámaras chicas de Wilson trabajando en paralelo con propósito de medir la variación de ionisación a través de placas de plomo puestas entre cámaras. La expansión esta regulada automáticamente en función de la temperatura por un dispositivo de control de la presión detrás del pistón. Las cámaras quedan así ajustadas mas de una semana y se modifican solamente por la evaporación de la humedad. Tres grupos de dos contadores puestos en coïncidencia, y un grupo de cuatro en anticoïncidencia seleccionan las particulas que se paran. El dispositivo electrónico de seleccion tiene solamente cuatro tubos y un thyratron, y funcionó satisfactoriamente durante un año. Las fotografías se sacan por dos cameras cuyos obturadores estan syncronisados con la luz, lo que permite observar al mismo tiempo que se fotografía. Tenemos 20 cm de profundidad de campo a 80 cm de distancia con apertura $f/16$ y una dirección de toma a 25° de haz luminoso El consumo total, incluyendo producción de aire comprimido es menor de 500 w siendo así possible trabajar en altura. Las experiencias siguen y daremos oportúnamente informe de los resultados.

K2. A Proportional Counter Technique. LEO R. DAVIS, C. W. KISSINGER, AND G. J. PERLOW, *U. S. Naval Research Laboratory.*—A method has been devised for making simultaneous range and ionization measurements on charged cosmic rays by use of a proportional counter and Geiger counters. The latter form a telescope defining a beam through the former. The proportional counter pulse is registered only when the Geiger tube telescope furnishes an appropriate trigger. To investigate the fluctuations in the ionization determination, an experiment was performed using as test particles the sea-level mesons capable of penetrating 10 cm Pb. The distribution curve (number *versus* pulse height) obtained was relatively broad. The effect of geometrical variation in path length through the proportional counter has been shown to be unimportant. The fluctuation due to the statistics of the multiplication process was worked out by analogy with the Furry model of a cascade shower. This also accounts for a

small fraction of the observed width of the curve. Finally, the theory of Landau on the fluctuation of the energy loss in the gas, coupled with the wide spread in energy of the mesons, fits the observed data reasonably well. Mesons of very high energy contribute significantly to the width through the logarithmic increase of ionization with speed.

K3. Rocket Measurement of Cosmic-Ray Ionization and Range. G. J. PERLOW, T. A. BERGSTRALH, C. Y. JOHNSON, AND J. D. SHIPMAN, JR., *U. S. Naval Research Laboratory.*—A V-2 rocket was launched in February at White Sands, New Mexico with a counter telescope containing two proportional counters in a threefold set of Geiger tubes. Below this were absorbers of ~1, 3 and 11 cm Pb. Counter trays below each absorber interrogated as to range and showers each particle accepted by the threefold set. Simultaneously each proportional counter was sampled. The system was calibrated with mesons on the ground. As in previous flights, the soft component above the atmosphere was detected. Almost all of the particles which stop in 1 cm Pb are unequivocally identified as electrons. The larger part of those which penetrate 4 cm but produce no count below 15 cm are also electrons including possibly some primaries. Of the particles which penetrate all the lead the larger number have the properties of primary protons. An alpha-particle group also appears. The best values of the intensities will be presented. Some possible ambiguity in these figures remains due to the bursts always found in rocket experiments.

K4. On the Albedo of Cosmic Radiation.* A. ROMERO JUÁREZ, J. DE OYARZÁBAL, C. GÓMEZ, AND F. MEDINA, *Instituto de Física, Universidad de México.*—The equations of motion of a charged secondary particle in the earth's magnetic field are solved by numerical integration. The secondary particle is produced by impact of a primary at some point of the earth's atmosphere and arrives at some other point. Both dipole and quadripole terms of the earth's field are taken into account, because the secondary particle is never more than an earth's radius away from the earth's surface. Preliminary numerical integrations show that—particles of energy 0.3 Störmer arriving at geomagnetic latitude 40° and geographic longitude 120°W, in the direction given by zenith-angle 60° and azimuth 0° (north) depart from points located very far away in latitude and longitude. The work is being continued for other energies, latitudes and directions of arrival.

* Work done under the auspices of C.I.C.I.C.

K5. On the Primary Cosmic-Ray Spectrum.* J. A. VAN ALLEN AND S. F. SINGER, *Applied Physics Laboratory, Johns Hopkins University.*—Based on recent rocket flights and further analysis, improved experimental values of the vertical intensity of cosmic rays *above* the atmosphere at geomagnetic latitudes 0°, 41°, 50°, and 58° will be presented. The intensities obtained in the range of magnetic rigidities from 2.6 to 15 Bev: (i) are markedly higher than the intensities deduced from ionization integrals, and (ii) follow a considerably flatter spectrum than hitherto believed. Data on the zenith angle dependence of intensity at various latitudes and on the east-west asymmetry at the equator make possible some assessment of the contribution of albedo to the experimental intensities above the atmosphere. However, it still appears that a large fraction of the energy brought in by the primary radiation disappears into forms other than ionization.

* Supported by the Navy Bureau of Ordnance.

K6. The Knee in the Primary Cosmic-Ray Spectrum.* S. F. SINGER AND J. A. VAN ALLEN, *Applied Physics Laboratory, Johns Hopkins University.*—Extending our rocket measurements of the vertical intensity above the atmosphere at $\lambda = 0°$, 41°, 50°, and 58°N by means of the balloon experiment of Pomerantz at 69°, we find a marked flattening of the form of the spectrum for magnetic rigidities below 1.5 Bev ($\lambda = 56°$). The expected diurnal variation calculated in the manner of Dwight, but with the flatter spectrum based on our rocket measurements, turns out to be still very substantial. In the light of recent astrophysical evidence (Thiessen) and absence of an *observed* diurnal variation (Pomerantz, Bergstrahl, Stroud), causes other than the sun's magnetic field should be considered for the existence of a knee: (a) intrinsic scarcity of low energy primary cosmic rays due to the manner of generation and propagation, (b) possible effects of geomagnetic penumbra, resulting in a larger effective cut-off energy at higher latitudes than obtained from the simple Störmer and shadow cones.

* Supported by the Navy Bureau of Ordnance.

K7. The Relative Intensities at 3.4 Kilometers and Sea Level of the Cosmic-Ray Proton Component.* JOSEPH E. HENDERSON, CHARLES E. MILLER, DAVID S. POTTER, AND JAY TODD, JR., *University of Washington.*—Measurements have been made at an altitude of 3.4 kilometers in which magnetic cloud-chamber photographs were taken of those particles stopping in 5 cm of lead absorber. The distribution in momentum of the negatively charged non-shower particles shows a sharp maximum which can be identified as due to negative mesons. The corresponding distribution of positive particles shows two sharp and well-resolved maxima which can be identified as positive mesons and protons. This type of measurement has been repeated at sea level. To date the number of tracks photographed at sea level is statistically inadequate to give accurately the intensity ratio for the two altitudes. Within the present accuracy the meson intensity corresponding to the range 0 to 5 cm lead has decreased by a factor of about 3 and the corresponding proton intensity by a factor of about 10 in going from 3.4 kilometers to seal level. The relative meson intensities are in line with other measurements of the intensity of lower energy mesons, while the relative proton intensities are those to be expected from indirect measurements of the relative intensities at these altitudes of the nuclear cosmic-ray component from studies of star production, slow neutrons and other nuclear phenomena.

* Supported in part by the ONR.

K8. Large Meson Showers Produced by Primary Cosmic-Ray Particles. E. PARKER and B. PETERS, *University of Rochester.*—In photographic emulsions exposed to cosmic radiation one observes occasionally a large number of tracks due to singly charged relativistic particles emanating from a star. These events have usually been interpreted as meson showers. If the plates are exposed at high altitudes (<20 g/cm^2 of air) one finds that most showers of multiplicity $N \gtrsim 10$ are produced by primary particles of charge $Z > 1$. Of the twelve largest showers observed (ranging in multiplicity from $N = 10$ to $N = 56$) only two ($N = 11$ and 13 respectively) were produced by singly charged particles. Of the remaining 10 large showers five were due to helium nuclei, four to particles of charge $Z = 6$ to 8 and in one case the primary could not be identified. Thus primary particles heavier than helium account for a large fraction of the large showers although they constitute only one percent of the incident radiation. The relative contribution to the large showers made by protons and heavier nuclei depends very critically both on their respective energy spectra and on the way in which multiplicity of meson production depends on the energy of the colliding nucleons. This relation will be discussed.

K9. On the Abundance of Light Nuclei (Li to Si) in the Primary Cosmic Radiation. B. PETERS AND H. L. BRADT, *University of Rochester.*—The determination of the charge Z

of relativistic nuclei has been improved so that up to $Z\sim12$ to 14 neighboring elements are resolved. In stacks flown at $\lambda=30°$ geomagnetic latitude below 20 g/cm² air tracks are traced through electron sensitive plates which alternate with strongly underdeveloped insensitive plates, in which grain counting permits a more accurate charge determination than previously obtained. Among the primary nuclei (heavier than hydrogen and helium) carbon, oxygen, nitrogen (?), magnesium, silicon, and neon, roughly in this order, are the most abundant. Most, if not all of the small number of lithium, beryllium and boron nuclei observed must be attributed to high energy fragments resulting from the collision of heavier primary particles with nuclei of the air above the balloon. Since fast nuclei of charge $Z=3$, 4, or 5 are produced with high probability in nuclear collisions involving fast heavy ions, the absence (or low abundance) of these light nuclei in the primary radiation implies that the heavy nuclei, before hitting the earth, have not traversed an amount of matter sufficient to establish equilibrium with their collision products. Thus if ρ is the average number of atoms per cm³ of interstellar matter along the orbits of the cosmic rays, their age t must be less than $3\times10^6/\rho$ years.

FRIDAY AFTERNOON AT 15:00

Minería

(C. D. ANDERSON presiding)

Cosmic Rays, II; Atmospheric Physics

L1. Penetrating Showers in Carbon.* JOHN R. GREEN AND W. B. FRETTER, *University of California at Berkeley.*—Penetrating showers produced in carbon in a cloud chamber containing carbon and lead plates[1] have been analyzed and compared to the penetrating showers produced in lead in the same cloud chamber when it contained only lead plates.[2] Similarity in angular distribution of lightly ionizing secondary particles indicates that the events observed in the two experiments are of the same average energy. When necessary geometrical corrections are made, a value of 3.2 to 3.6 penetrating particles per event is obtained from carbon; the corresponding value from lead is 3.8. Multiplicities of observed penetrating particles up to ten were obtained for single events in carbon plates. The similarity of events in carbon and in lead suggests multiple production of mesons. Associated production of electronic cascade showers can be explained by assuming that they are produced by high energy gamma-rays originating near the parent event. The mean free path of lightly ionizing secondaries of the penetrating showers for subsequent production of nuclear events is found to be 237 ± 29 g/cm² of carbon.

* Assisted by the joint program of the ONR and AEC.
[1] John R. Green and W. B. Fretter, Phys. Rev. **78**, 92 (1950).
[2] W. B. Fretter, Phys. Rev. **76**, 511 (1949).

L2. Improved Calculations on Cascade Shower Theory. IRA BERNSTEIN, *Brookhaven National Laboratory.**—Snyder[1] has recently given solutions of the diffusion equations of cascade shower theory of such a nature that accurate numerical calculations of the average number of particles at a given depth in an absorber are readily derivable therefrom. He used, however, the so-called completely screened cross sections for pair production and bremsstrahlung. These assign too large a value to the elementary processes associated with low energy particles, though they are accurate for high energy particles. By writing the diffusion equations as a single integral equation an iteration scheme has been developed, which permits introduction of more accurate cross sections. The first approximation is taken to be the Snyder solution. The first iteration on this yields a correction to the Snyder result which indicates that the shower maximum is decreased by ten or more percent, and that there is a decrease in the average number of particles at small depths, with a corresponding increase for large. The results are quantitatively accurate only for light elements and moderate initial energies.

* Work performed at Brookhaven National Laboratory under contract with AEC.
[1] H. S. Snyder, Phys. Rev. **76**, 1563 (1949).

L3. Neutron Production by Cosmic Rays at Three Depths.* R. D. SARD, *Washington University.*—Further measurements by the Washington University cosmic-ray group on neutrons associated with charged cosmic-ray particles will be reported. With apparatus of the type previously described,[1] measurements have been made at Climax, Colorado[2] (3400 m), St. Louis (160 m), and in the sub-basement of a St. Louis skyscraper under 1000 to 1500 g cm^{-2} of material. The changes of the various coincidence rates with depth are used to separate neutron production by μ-mesons from neutron production by nucleons (or their π-meson secondaries). The sea-level-mountain comparison indicates that most, but by no means all, of the sea-level $(AB\text{–}C:N)$ events are due to the stopping of μ-mesons, in the Pb absorber. The $(ABC:N)$ events can be ascribed to the nucleonic component. The sea-level-underground comparison indicates either that the nucleonic component is hardly more attenuated than the mesonic component at the underground site used or that there is production of low energy neutrons by fast μ-mesons. Numerical results will be presented.

* Research partially supported by the joint program of the ONR and AEC.
[1] Sard, Conforto, and Crouch, Phys. Rev. **76**, 1134 (1949).
[2] W. B. Fowler, Phys. Rev. (to be published).

L4. Cosmic-Ray Diurnal Effect Measurements. T. A. BERGSTRALH AND C. A. SCHROEDER, *U. S. Naval Research Laboratory.*—In two balloon flights at Minnesota a search was made for diurnal effects in the cosmic radiation at altitudes above 50,000 feet. Measurements were made simultaneously at the total ionizing radiation, γ-radiation in the energy range of approximate 0.08 to 5 Mev; and fast neutrons. The ionizing radiation and γ-radiation was measured by means of a central horizontal counter tube surrounded by a closely packed ring of horizontal counters. Coincidences between the central counter and the outer ring determined the ionizing radiation, while anticoincidences gave the intensity of the γ-radiation. The neutron flux was measured by two BF_3 counters, one filled with enriched BF_3, mounted side by side in a vertical paraffin cylinder eight inches in diameter surrounded by Cd, One flight was launched at 12:30 A.M. CST and remained aloft until 8:00 A.M. The other flight was launched at 6:20 P.M. and landed at 10:10 P.M. No diurnal effects were observed. The statistical accuracy of this measurement is on the order of one percent for the total ionizing radiation and on the order of 3.5 percent for the γ-radiation and neutron measurements.

L5. Barometric and Out-Door Temperature Coefficients of Frequency of Small Cosmic-Ray Bursts. JAMES W. BROXON, *University of Colorado.*—Multiple linear regression coefficients (b) and partial correlation coefficients (r) and the normal significance ratios (t) of r, have been computed for the frequency of occurrence of a class of small cosmic-ray bursts with respect to barometric pressure ($_{12\cdot3}$) and out-door temperature ($_{13\cdot2}$), for 19 individual months. This class of bursts represents (1.2 to 1.9)$\times 10^6$ ion pairs collected in a very heavily shielded spherical ion chamber of 13.3 liters effective volume containing argon at 20 atmospheres and 25°C at Boulder, Colorado, geomagnetic latitude 49°N. These occurred at an average rate of about 10 per hour. Eighteen of the 19 months displayed negative barometric coefficients. The average $b_{12\cdot3}$ for all 19 months was −1.54 percent/mm, while the average for the 10 months with $t_{12\cdot3}$ above the two percent level was −2.44 percent/mm. (The barometric coefficient for the background cosmic-ray ionization in the same chamber has a lower order of magnitude.) Fifteen of the 19 months displayed negative temperature coefficients. The average $b_{13\cdot2}$ for all 19 months was −0.98 percent/°C, while the average for the 7 months with $t_{13\cdot2}$ above the two percent level was −1.66 percent/°C.

L6. The Change of Intensity of the Nucleonic Component during Magnetic Storms. J. A. SIMPSON, *University of Chicago.*—Several measurements of the latitude dependence of the neutron and star intensities under 312 g-cm^{-2} of air between 40° and 65°N geomagnetic latitude show a flattening of the intensity curves in the region above 50°N. Two sets of these measurements followed closely the commencement of moderately severe or severe magnetic storms. In each case the intensity above 50°N showed a characteristic increase with increasing age of the storm. Following the commencement of one of the storms it was found that in a period of five days the knee of the intensity curve had shifted northward approximately 3° with a fast neutron intensity increase of six percent. No changes of intensity were observed below 47° geomagnetic latitude. It may be shown that these intensity changes were not due to longitude or temperature effects. The data indicate that the low energy cut-off for the primary radiations was decreasing with the increasing age of the magnetic storm.

L7. Correlation of Auroral Observations in the Northern and Southern Hemispheres. D. E. LITTLE AND G. M. SHRUM, *University of British Columbia.*—Studies have been made of observations of the Aurora Borealis and the Aurora Australis with a view to establishing a correlation between them. The degree of this correlation gives some indication of the effect of atmospheric conditions upon the occurrence of aurorae. The work has brought out the need for more detailed records of observations, especially in the Southern Hemisphere.

L8. Surface Ozone in Arctic Regions.* W. S. WILSON, *University of Alaska.*—The author's use of the indirect oxidation of sodium arsenite as an agent for the determination of daily average values of the concentration of ozone in the atmosphere near the surface is described. Values obtained at College, Alaska, for the first three months of 1950 are shown. These show large variations from day to day, often rising to many times the maximum value. Except for a few unusually high values which are apparently associated with special conditions in the Arctic atmosphere, the values for the concentration are on an average rising with increasing altitude of the sun. As a rule these values are less uniform and higher than those reported from stations in lower latitudes.

* This work was supported in part by contract with the U. S. Air Force, through sponsorship of the Geophysical Research Directorate, Air Materiel Command.

Post-Deadline Papers

FRIDAY AFTERNOON AT 15:00

Anfiteatro Bolívar

(R. A. MILLIKAN presiding)

Invited Papers

M1. Soil Mechanics of the City of Mexico. NABOR CARRILLO, *Comisión Impulsadora y Coordinadora de la Investigación Científica.* (20 min.)

M2. Forces on a Supraconductor in a Magnetic Field. W. V. HOUSTON, *Rice Institute.* (30 min.)

M3. Modern Developments in X-ray Crystal-Structure Analysis. RAY PEPINSKY, *Pennsylvania State College.* (40 min.)

FRIDAY AFTERNOON AT 15:00

Minería

(E. M. MCMILLAN presiding)

Artificial Mesons; Miscellany in Nuclear Physics

N1. Photo-Mesons from Carbon. J. M. PETERSON, R. S. WHITE, AND W. S. GILBERT, *University of California, Berkeley.*—The energy spectrum of negative and positive π-mesons produced in carbon by x-rays from the 330-Mev electron synchrotron in Berkeley has been measured at angles of 45°, 90°, and 135° to the beam axis using C-2 nuclear emulsions. The carbon target was a sphere of 0.620-inch diameter, approximating a point source. The meson detection system employed completely poor geometry; the nuclear plates were imbedded in a massive cylinder of copper surrounding the target. The minus-plus ratio has no statistically significant variation with energy; the average over energy appears to be independent of angle and equal to about 1.35 (±0.15 at 90° and 135°, ±0.2 at 45°). The energy spectra characteristically have broad

maxima in the region from 30 to 70 Mev and fall to zero in the region from 100 to 150 Mev, the exact behavior depending on the angle. More mesons are emitted at 135° and at 90° than at 45°. The total cross section is about 3×10^{-28} cm² per nucleus per quantum. This work was supported by the United States AEC.

N2. Photoproduction of Mesons from Hydrogen. A. S. BISHOP, J. STEINBERGER, AND LESLIE J. COOK, *University of California, Berkeley.*—Using the delayed coincidence technique[1,2] for detection of artificially produced mesons, we have measured the energy distribution of π^+-mesons from hydrogen. These mesons are formed when the x-ray beam from the 335-Mev electron synchrotron strikes a liquid hydrogen target. Since the photons are completely absorbed in the process of meson creation, there is an exact relationship (for a given angle of emission of mesons) between the energy of the meson and the energy of the photon responsible for its creation. Thus, using the measured energy distribution of the mesons at 90°, and the energy distribution of the photons from the synchrotron, we have determined the excitation function for photoproduction of mesons at 90°. This function increases rather slowly and flattens off for photon energies above about 280 Mev. This work was performed under the auspices of the AEC.

[1] F. Rasetti, Phys. Rev. 60, 198 (1941).
[2] J. Steinberger and A. S. Bishop, Bull. Am. Phys. Soc. 25, 11 (1950).

N3. Positive Mesons Produced by 345-Mev Protons in Liquid Hydrogen. VINCENT Z. PETERSON, *University of California, Berkeley.*—The production of mesons in proton-proton collisions has been studied directly using the photographic technique by bombarding a liquid hydrogen target with 345-Mev protons. A "point" source having 0.002-in. Al walls contains the hydrogen, and plates imbedded in copper absorbers are placed at various angles with respect to the beam. Earlier experiments[1] having shown that only positive mesons are produced, a bending magnet has been interposed between target and detector to separate mesons from elastically scattered protons. Exposures made at $30\pm1\frac{1}{2}°$ show an improvement in mesons-to-background of about 100. The sharp peak near the higher end of the meson energy spectrum,[1] indicating a strong interaction between the outgoing nucleons, has been obtained with much better statistics. However the energy resolution was still insufficient to determine whether or not a real deuteron is formed in the process. Further experiments at $15\pm\frac{1}{2}°$ designed to improve the energy resolution at the upper end of the spectrum, until limited only by the energy spread of the primary beam (~2 Mev), are now in progress and will be reported. This work was performed under the auspices of the AEC.

[1] Post-deadline paper by the author at the Washington, D. C. meeting.

N4. D−He⁴ Interaction for 10.3-Mev Deuterons. JOHN C. ALLRED, DAROL FROMAN, ALVIN HUDSON, AND LOUIS ROSEN, *Los Alamos Scientific Laboratory.*—A multiple nuclear plate camera[1] has been utilized to make simultaneous observations of the range and intensity distribution of the products of the D−He⁴ reaction for 10.3-Mev deuterons from 18.4° to 158.6° (center of mass). The externally focused beam from the Los Alamos cyclotron was used for these experiments. There is evidence for a sizable cross section for the reaction $D+He^4\rightarrow He^4+n+p-2.2$ Mev. The differential elastic scattering cross-section curve shows marked anomalies. The elastic scattering cross section in millibarns for some of the CM angles investigated are: 22.0°, 371±13; 29.4°, 192±7; 43.8°, 57±2; 51.0°, 22±1; 55.4°, 10.5±0.4; 58.4°, 9.8±0.4; 69.4°, 21.7±0.9; 78.8°, 39.6±1.4; 85.4°, 58±2; 97.7°, 69.1±2; 110.6°, 58.7±2; 120.6°, 41.8±1.5; 124.6°, 37.8±1.3; 129.3°, 37.0±1.6; 137.8°, 40.0±1.4; 147.4°, 52.2±2.6; 155.4°, 73±7; 157.4°, 82±8.

[1] J. C. Allred and Louis Rosen, Bull. Am. Phys. Soc. 25, No. 3, 36 (1950), abstract Q4.

N5. Transmutation of N¹⁵ by Protons. A. W. SCHARDT, W. A. FOWLER, AND C. C. LAURITSEN, *California Institute of Technology.*—Measurements have been made from 0.2 to 1.6 Mev of the cross sections of the reactions (1) $N^{15}(p\alpha)C^{12}$, (2) $N^{15}(p\alpha')C^{12*}(\gamma)C^{12}$, and (3) $N^{15}(p\gamma)O^{16}$. The second reaction involves the well-known level in C¹² at 4.5 Mev. The gamma-rays from (2) and (3) were separated by coincidence absorption measurements. All three reactions show marked resonances. Preliminary results for the resonance widths and for the cross sections (10^{-24} cm²) are tabulated.

E_R (Mev)	Γ (kev)	σ_1	σ_2	σ_3
0.36	~100	0.1		
0.429	<0.8		0.2	
0.899	2		0.6	
1.0	~160	0.5	0.002	0.0005
1.21	20	0.6	0.2	

This work was assisted by the joint program of the ONR and AEC.

N6. A Study of the $N^{14}(p,\gamma)O^{15}$ Reaction.* D. B. DUNCAN† AND J. E. PERRY, JR., *California Institute of Technology.*—The cross section for the transmutation of nitrogen by protons has been investigated using an electrostatic generator. Excitation curves have been obtained up to 2.7 Mev from the bombardment of thick Be_3N_2 targets, nitrogen gas targets of various thicknesses, and a thin target formed by proton bombardment of a copper foil in a nitrogen atmosphere. Properties of the observed resonances are tentatively summarized.

E_R (Mev)	0.277[1]	1.065	1.550	1.748	1.815	2.356	2.489	
$Y_{max}(\infty)$	0.4	6	1	1.5	4	15	20	all $\times10^{-10}$
$\omega\gamma$ (ev)	0.02	0.6	0.2	0.2	0.5	2	3	
Γ (kev)	<2[1]	5	50	11	7	14	11	
σ_R (cm²)	—	3.5	0.06	0.3	1	2	3.5	all $\times10^{-28}$

These resonances are superimposed on a non-resonant yield whose cross section is 0.4, 3, 6×10^{-29} cm² at 1, 2, and 2.5 Mev respectively. Extrapolation of these yields to low energies indicates that the non-resonant reaction is dominant in the Bethe sun cycle.

* This work was assisted by the joint program of the ONR and AEC.
† AEC Predoctoral Fellow.
[1] Tangen, Kgl. Nord. Vid. Sels. Skr. No. 1 (1946).

N7. Excited States of N¹³ and C¹³. R. G. THOMAS,* *California Institute of Technology.*—If *nn* and *pp* nuclear forces are equal, corresponding excited states should be found in light mirror nuclei. In comparing low energy levels of C¹³ with those of N¹³ it must be considered that the levels in N¹³ are in the continuum, and that the amount of time the proton spends outside of the nucleus with a diminished Coulomb interaction depends on the reaction width. The states at 2.37 and 3.52 Mev in N¹³ are compared with those at 3.10 and 3.91 Mev in C¹³. The large width-without-barrier of the first state in N¹³ suggests an *s*-wave reaction[1] and a large level shift. By applying Green's theorem to the neutron wave function in C¹³ and the proton wave function in N¹³ and using the resonance theory of Feshbach, Peaslee, and Weisskopf or Wigner and Eisenbud, the level shift can be calculated in terms of logarithmic derivatives at the nuclear surface and the reaction width. Taking into account nuclear expansion with excitation, level shifts are calculated which are in reasonable agreement with observation.

* AEC Predoctoral Fellow.
[1] Fowler, Lauritsen, and Lauritsen, Rev. Mod. Phys. 20, 236 (1948).

N8. The Fission Yield Curve of Th^{232} with Pile Neutrons.* J. NIDAY AND A. TURKEVICH, *Argonne National Laboratory* and the *University of Chicago.*—The relative yields of nineteen products of thorium fission with mass numbers between 72 and 144 have been determined radiochemically. The thorium was irradiated in the center of the Argonne heavy water pile,

the effective neutrons probably having not much more than the threshold energy. Most of the yields determined were on the light side of mass 116. A complete fission yield curve was drawn assuming all the fissions are binary and assuming, arbitrarily, that two neutrons are emitted. Thorium fission is similar to slow neutron fission in being highly asymmetric. The peak yields occur 120±20 times as frequently as symmetrical products. As has been noted previously, the main effect of varying the mass of the fissioning nucleus (e.g. Pu^{239} cf. Th^{232}) appears to be to shift the light peak, the heavy peak tending to occur in the same mass region.

* A few of these results were presented before the Chicago meeting of the AAAS (December, 1947).

N9. Precise Determination of the Ratio of the Deuteron to Proton Magnetic Moment. B. SMALLER, E. YASAITIS, AND AND H. L. ANDERSON.—A precision determination has been made of the ratio of the deuteron to proton nuclear magnetic moment utilizing the Purcell method of resonance nuclear induction. A unique method of synchronization has resulted in high stability of both H and D patterns with respect to each other, and has minimized the need for ultra-precision in oscillation frequency and stability. Simultaneous measurements of ν_H and ν_D on the same D_2O–H_2O sample have removed the need for high field homogeneity over a region greater than the sample area. The widths of the H and D resonance lines were 0.018 gauss and 0.048 gauss respectively in a field of 7200 gauss. The relative error in frequency ratio determination that could be achieved was less than 5×10^{-8}. Measurements on 5 different samples having different Mn^{++}/D^+ concentration ratios ($10^{-4}\rightarrow0$) gave $\mu_H/\mu_D=3.25720037\pm0.00000056$.

N10. Production of Deuterium-Zirconium Targets. J. J. MOORE AND R. N. LITTLE, *The University of Texas.*—Deuterium-Zirconium targets[1] for use in the reaction D_2 on D_2 have been produced in which two different methods of heating the zirconium metal target to outgas it have been used. By one method the target was heated by electrical conduction through the metal and in the second method by direct bombardment of the metal target with electrons, using the target as the plate of a vacuum tube. An attempt is being made to put the production of these targets on a semimass production basis. Tritium targets will also be produced in the same manner upon the receipt of tritium gas. Results concerning yield of neutrons and decay in yield of neutrons due to use will be given.

[1] Graves, Rodrigues, Goldblatt, and Meyer, Rev. Sci. Inst. 20, No. 8, 579–582 (1949).

FRIDAY AFTERNOON AT 15:00

Minería

(L. I. SCHIFF presiding)

Nuclear Theory

O1. The Energy Levels of Atomic Nuclei. H. A. WILSON, *Rice Institute.*—Nearly 200 energy levels, between 0 and 5 Mev, have been reported for about 40 different nuclei. These levels have been arranged in order of magnitude and a graph drawn showing the magnitudes against the order numbers. The graph shows a series of rounded off steps showing that there is a series of levels each belonging to several different nuclei. The levels at the steps are 4.80, 4.40, 4.00, 3.65, 3.50, 3.30, 3.00, 2.80, 2.55, 2.40, 2.00, 1.65, 1.25, 0.80, 0.65 Mev. Eleven of these 15 levels are nearly equal to values of $E_n=0.387((n-1)(n+2))^{\frac{1}{2}}$ Mev with n equal to the integers from 12 to 2. These values of E_n are 4.80, 4.41, 4.02, 3.63, 3.24, 2.84, 2.45, 2.05, 1.64, 1.22, 0.77 Mev. According to the spherical shell nuclear model proposed by the writer all nuclei should have vibration levels equal to E_n. The graph shows that only a few of the nuclei have each value of E_n. This means that when nuclear levels are observed usually only a few of the possible levels actually appear. The levels 3.50, 3.00, 2.55, 0.65 are probably rotation-vibration levels.

O2. Nuclear Saturation and Magic Numbers in Terms of a Non-Linear Meson Theory. L. I. SCHIFF, *Stanford University.*—A non-linear term corresponding to contact repulsion between mesons is expected to: (1) provide a many-nucleon interaction that leads to nuclear saturation without repulsive interactions in odd l states; (2) provide a sounder physical basis for the single-nucleon model that leads to shell structure and magic numbers. The relatively slow increase of meson density with increasing nucleon density causes: (1) the kinetic energy per average nucleon to increase more rapidly than the potential energy for high density; (2) the potential energy of a nucleon to depend less on its immediate neighbors than on the average nucleon density in its vicinity. For such a neutral scalar meson in free space, plane wave solutions of the classical field equation are found, but localized static solutions do not exist. The meson source functions associated with nucleons must be extended in space; the divergent parts of the total energy (nucleon self-energy) are additive and can be eliminated. A variation principle gives an upper bound for the energy, and is being used to calculate the two-nucleon interaction. A crude model of a heavy nucleus, in which the source density is constant, gives reasonable results for the binding energy and volume per nucleon.

O3. Boundary Conditions for the Description of Nuclear Reactions. M. MOSHINSKY, *Institutos de Física y Geofísica, Universidad de México.*—A phenomenological description of nuclear reactions by means of appropriate boundary conditions, will be proposed. The several stages of the reaction (initial particles, compound nucleus, etc.) are described in their respective configuration spaces, and the state representing the nuclear reaction is given by a wave function of the type introduced by Fock.[1] The wave equations satisfied by the Fock wave function, are deduced with the help of an analogy with vibration problems. We find that the interactions leading to the nuclear reaction can be expressed as boundary conditions between the different components of the Fock wave function taken at the point of coincidence of the particles. A discussion is given of elastic scattering and two particle nuclear reactions, showing that this procedure gives the same dependence of the cross sections on energy as the Breit-Wigner resonance formula and its generalizations. With the help of appropriate wave functions in n-particle configuration space, the present procedure can be be extended to the description of multiple particle nuclear reactions. The energy distribution between the particles produced in the reaction has been investigated, and the results

are compared with known multiple particle disintegrations such as β-decay.

[1] Fock, Zeits. f. Physik 622, 75 (1932).

O4. Normal Modes of Vibration of Nuclei. I. BLOCH, *Vanderbilt University.*—The force between two nuclear particles is idealized as a linear function of the particles' separation. In the absence of spin-orbit interaction, the Hamiltonian can then be separated by transformation to normal coordinates; the Schrödinger equation for a nucleus containing A particles is equivalent to $3A$ separate equations, one for each of the $3A$ normal modes of vibration. Three of these equations together have a plane-wave solution which describes the motion of the center of mass. The parameters in the remaining $3(A-1)$ equations depend on the spins and isotopic spins of the nucleons; each equation is of the type which applies to a linear harmonic oscillator. The nucleus described by such a set of equations has infinite binding energy, but may nevertheless behave in some ways like actual nuclei. Furthermore, for the lowest energy levels, the linear forces may be "cut off" at some finite distance by means of a perturbation calculation.

O5. Scattering of Mesons by Nucleons. ALEJANDRO MEDINA, *Universidad Nacional de México.*—The scattering of mesons by free and bound nucleons is considered and the scattering cross section determined assuming different types of coupling and including radiative corrections. Using fundamentally Schwinger's methods, a procedure is devised whereby the cross section can be directly obtained.

O6. On the Self-Energy of Mesons. FERNANDO PRIETO, *Universidad Nacional de México.*—Using Schwinger's well-known method, the self-energy of a meson in interaction with a nucleon field has been considered, extending Matthews calculations[1] to other types of coupling. Mass renormalization factors are in each case determined and following Dyson[2] the elimination of the self-energy terms is effected.

[1] P. T. Matthews, Phys. Rev. 76, 1657 (1949).
[2] F. J. Dyson, Phys. Rev. 75, 486 (1949).

O7. Polarization of Vacuum by Meson Fields. JUAN DE OYARZABAL, *National University of Mexico.*—Calculations have been performed on the polarization of a matter vacuum due to a meson field. Using Schwinger's method,[1] the induced current in vacuum has been evaluated assuming different types of coupling. The effect of vacuum polarization on the interaction between mesons has also been considered. This work is an extension of Case's[2] calculations.

[1] J. S. Schwinger, Phys. Rev. 75, 651 (1949).
[2] K. M. Case, Phys. Rev. 76, 1 (1949).

O8. Spin-Orbit Interactions and Nucleon-Nucleon Scattering. K. M. CASE AND A. PAIS, *Institute for Advanced Study.*—It will be shown that the Berkeley data on n-p and p-p scattering may be interpreted in a charge independent theory utilizing a spin-orbit (LS) interaction of the kind familiar from atomic physics. An LS coupling does not affect low energy phenomena. The contribution to the cross-section is proportional to $\sin^2\theta$ and thus favors 90° scattering. At this angle the LS scattering is four times as large for p-p as it is for n-p. A strongly singular spatial dependence suffices for a simultaneous description of the 30 and 350 Mev p-p experiments. It is important for the n-p case that the P scattering caused by the LS term does not interfere with S scattering due to central forces. Hence the interpretation of n-p scattering by Christian and Hart is essentially unaffected. General considerations on the bound state of the deuteron fix the sign of the coupling so that for given orbital angular momentum the state of largest j lies lowest. This, as well as the magnitude, is suggestive in connection with Goeppert-Mayer's interpretation of the shell model for heavy nuclei.

FRIDAY EVENING AT 20:00

Salón de los Candiles, Hotel del Prado

(I. I. RABI presiding)

Banquet of the American Physical Society

After-Dinner Speakers

Scientific Cooperation in Action. MANUEL SANDOVAL VALLARTA, *El Colegio Nacional e Instituto de Física, Universidad de México.*

Title to be announced. E. U. CONDON, *National Bureau of Standards.*

SUPPLEMENTARY PROGRAMME

SP1. Motion of Charges in Magnetic Fields. A. ROMERO JUAREZ, *Instituto de Física, Universidad de México.*—The motion of a charged particle in a static purely magnetic field is characterized by the fact that the curvature κ of the orbit at every point is proportional to the magnitude of the force. Plane motion is considered. If the field H depends only on the distance r to a fixed point, the trajectory can be obtained in a simple manner. To do this we notice the following property of a plane curve: if κ depends only on r, the polar equation of the curve can be found by means of quadratures only. The results are applied to the following cases: (a) Superposed dipole and constant fields. The solution involves automorphic functions of genus 2, When the constant field vanishes, one gets the equation of the orbits in the equatorial plane of a magnetic dipole and it is possible to express it in terms of elliptic functions. (b) Magnetic field proportional to $1/r$. Only elementary functions appear in this case. The more general case in which H varies as $1/r^n$ is examined and values of n are determined for which the problem is soluble in terms of given functions.

* To be given at the end of Session H if the Chairman rules that time permits.

SP2. Multipole Order of the 3.1-Mev Gamma-Ray from Carbon 13.* R. G. THOMAS,† *California Institute of Technology.*—There is evidence that the radiation from the 2.37-Mev state in N^{13} is electric dipole. A determination of the

multipole order of the radiation from the state at 3.1 Mev in the mirror nucleus C^{13} is of interest as a check on the possible correspondence of these two levels. A magnetic lens spectrometer was used to measure the intensity of the gamma-radiation and internally formed positrons from this state produced in the reaction $C^{12}(d, p)C^{13*}$. Gamma-ray intensity was determined from photoelectric conversion in thorium and Compton conversion in thin and thick aluminum foils; polarization effects and straggling in energy loss were considered in calculating the electron stopping cross section required for the thick converter method. The observed pair formation could be compared with the theoretical energy distribution given by Rose only over the high energy portion of the positron spectrum which was free from the effects of extraneous radiations. For electric dipole radiation the agreement is within 10 percent, the estimated experimental error; the deviation would be greater than 60 percent for other radiation multipoles. This work was assisted by the joint program of the ONR and AEC.

* To be given after Session N if the Chairman rules that time permits.
† AEC Pre-doctoral Fellow.

SP3. The Interaction of Birkhoff's Gravitational Field with the Electromagnetic and Pair Fields.* M. MOSHINSKY, *Institutos de Física y Geofísica, Universidad de México.*—The flat space-time theory of gravitation proposed by G. D. Birkhoff is discussed from the standpoint of a field theory, and in particular, the interaction of Birkhoff's field with other fields is developed. This interaction is shown to take place through the interaction Lagrange function $h_{\mu\nu}\Theta_{\mu\nu}$ where $h_{\mu\nu}$ is the symmetric tensor potential describing the gravitational field and $\Theta_{\mu\nu}$ is the symmetric energy momentum tensor of the external field. With the help of this interaction Lagrange function, the action of the gravitational field on the electromagnetic and pair fields can be established, and shown to lead to a modification of Maxwell and Dirac equations. These modified equations determine a change in the index of refraction and a shift of the energy levels of the atom, which account for the bending of light and the red shift, respectively, in gravitational phenomena. Furthermore, the effect of an external gravitational field on the Dirac equation leads to a gravitational correction to the magnetic moment associated with the spin and orbital motion of the electron. The correction of the spin magnetic moment of the electron, due to the gravitational field of the star or planet on whose surface it is found, is $-M/R$ Bohr magnetons, where M is the mass of the star in relativistic units, and R the radius in cm. On the surface of the earth the correction is therefore $\simeq 10^{-9}$.

* To be given after Session G if the Chairman rules that time permits.

Author Index to Papers Presented at the Mexico Meeting

Adem, J. and M. Moshinsky—No. G4
Alba, Fernando—No. G3
Aleman, Miguel—No. A1
Allison, S. K.—No. B2
Allred, John C., Darol Froman, Alvin Hudson, and Louis Rosen—No. N4
Anderson, C. D.—No. F3
Beckham, Walter C. and M. L. Pool—No. D5
Bernstein, Ira—No. L2
Bergstralh, T. A. and C. A. Schroeder—No. L4
Bishop, A. S., J. Steinberger, and Leslie J. Cook—No. N2
Blachman, Nelson M.—No. D2
Bloch, I.—No. O4
Bodmer, Max, Jean V. Lebacqz, and D. H. Andrews—No. C1
Booth, E. T.—No. B1
Bradt, H. L.—No. E5
Branson, Herman and Woodfin Lewis—No. C5
Brode, R. B.—No. F2
Broxon, James W.—No. L5
Bunker, Merle E., Robert Canada, and Allan C. G. Mitchell—No. D11
Caplan, David and Edward Akeley—No. D3
Carillo, Nabor—No. M1
Case, K. M. and A. Pais—No. O8
Cooper, John N., Warren E. Taylor, J. C. Harris, and G. Richard Grove—No. J3
Dale, E. Brock and J. D. Kurbatov—No. D8
Davis, Leo R., C. W. Kissinger, and G. J. Perlow—No. K2
Day, R. B., C. Y. Chao, W. A. Fowler, and J. E. Perry, Jr.—No. 15
DeJuren, J. and B. J. Moyer—No. J8
Devore, Lloyd T., Surindra N. Kalra, and William J. Fry—No. H2
Dienes, G. J.—No. C6
Donfor, Anthony, Webster Kendrick, and Herman Branson—No. H7
Duncan, D. B. and J. E. Perry, Jr.—No. N6
Dybvig, H. Talman and M. L. Pool—No. D10
Ekstein, H.—No. C2
Ferguson, W. F. C. and J. H. Greig—No. H13
Fernandez, Carlos Graef—No. G2
Frazer, B. C. and Ray Pepinsky—No. C11
Fretter, W. B.—No. F4
Garido, Luis—No. A2
Gilvarry, J. J. and D. F. Rutland—No. H5
Green, John R. and W. B. Fretter—No. L1
Grove, G. Richard, John N. Cooper, and J. C. Harris—No. J2
Gutenberg, B.—No. I3
Hamermesh, Bernard—No. J6
Henderson, Joseph E., Charles E. Miller, David S. Potter, and Jay Todd, Jr.—No. K7
Hofstadter, R. and J. A. McIntyre—No. J4
Holmes, John R.—No. H12
Houston, W. V.—No. M2
Jacobs, John E.—No. C12
Juarez, A. Romero—No. SP1
Juarez, A. Romero, J. de Oyarzabel, C. Gomez, and F. Medina—No. K4
Kalra, Surindra N. and William J. Fry—No. H1
Katz, L., H. E. Johns, R. A. Douglas, and R. N. H. Haslam—No. J1
Keenan, Thomas and Edward Akeley—No. D4
Korff, S. A.—No. F5
Kundu, D. N. and M. L. Pool—No. D7
Langer, L. M., R. D. Moffat, and H. C. Price, Jr.—No. D9
Langsdorf, Alexander, Jr.—No. J9
Leighton, R. B.—No. F6
Little, D. E. and G. M. Shrum—No. L7
McMillan, E. M.—No. B3
Malpica, J. M.—No. D1, I1
Mandeville, C. E. and E. Shapiro—No. D6
Martin, A. B. and Frank Asaro—No. C7
Marton, L., J. A. Simpson, and A. Van Bronkhorst—No. C3
Medina, Alejandro—No. O5
Menzel, D. H.—No. E3
Meyerhof, W. E., D. B. Nicodemus, and Felix Bloch—No. J7
Millikan, R. A.—No. I2
Moore, J. J. and R. N. Little—No. N10
Moshinsky, M.—No. O3, SP3
Mrozowski, S.—No. C4
Ney, E. P.—No. E4
Niday, J. and A. Turkevich—No. N8
de Ouarzabal, J.—No. O7
Parker, E. and B. Peters—No. K8
Pepinsky, R.—No. C10, M3
Perlow, G. J., T. A. Bergstralh, C. Y. Johnson, and J. D. Shipman, Jr.—No. K3
Peterson, J. M., R. S. White, and W. S. Gilbert—No. N1
Peters, B. and H. L. Bradt—No. K9
Peterson, V. Z.—No. N3
Prieto, F.—No. O6
Rabi, I. I.—No. A3
Reverdin, D. and L. Marton—No. H3
Reynolds, G. T. and F. B. Harrison—No. H10
Rice, Bernard, J. M. Gonzalez-Barredo, and T. F. Young—No. H8
Richard-Foy, R.—No. K1
Robertson, H. P.—No. G1
Rogers, F. T., Jr. and H. L. Morrison—No. G5
Rogers, Marguerite M. and F. T. Rogers, Jr.—No. D12
Salant, E. O.—No. E6
Sard, R. D.—No. L3
Schardt, A. W., W. A. Fowler, and C. C. Lauritsen—No. N5
Schein, M.—No. F1
Schiff, L. I.—No. O2
Seitz, F.—No. I4
Sidhu, S. S. and C. O. Henry—No. C8
Simpson, J. A.—No. L6
Singer, S. F. and J. A. Van Allen—No. K6
Smaller, B., E. Yasaitis, and H. L. Anderson—No. N9
Stickley, E., M. M. Newman, and J. D. Robb—No. H4
Thomas, R. G.—No. N7, SP2
Tyson, J. K.—No. H6
Vallarta, M. S.—No. E1
Van Allen, J. A. and S. F. Singer—No. K5
Webb, Lyman A., Ronald S. Paul, and Francis E. Dart.—No. H9
Wilson, H. A.—No. O1
Wilson, W. S.—No. L8
Winckler, J. R.—No. E2
Wu, Ta-You and L. Ourom—No. H11